Impact of interocean exchange on the Atlantic overturning circulation

Wilbert Weijer

2000

Impact of interocean exchange on the Atlantic overturning circulation

Invloed van uitwisseling tussen oceanen op de Atlantische omwentelingscirculatie
(Met een samenvatting in het Nederlands)

PROEFSCHRIFT

ter verkrijging van de graad van doctor aan de Universiteit Utrecht op gezag van de Rector Magnificus, Prof. dr. H.O. Voorma, ingevolge het besluit van het College voor Promoties in het openbaar te verdedigen op maandag 8 mei 2000 des middags te 16.15 uur

door

WILBERT WEIJER

geboren op 15 augustus 1971, te Enschede

Promotor:

Prof. dr. W.P.M. de Ruijter

Co-promotoren:

Dr. ir. H.A. Dijkstra

Dr. P.J. van Leeuwen

Faculteit Natuur– en Sterrenkunde, Universiteit Utrecht

Dit proefschrift is mede mogelijk gemaakt door financiële steun van het Nederlands Onderzoek Programma (NOP-II).

ISBN: 90-393-2373-9

"...to live on the land we must learn from the sea..."

John Denver, Calypso, 1975

Contents

1 Introduction **1**
- 1.1 Ocean circulation and climate variability . . . 1
- 1.2 The thermohaline circulation . . . 3
- 1.3 NADW renewal paths . . . 7
- 1.4 Importance of interocean exchange for the thermohaline circulation . . 9
  - 1.4.1 The strength of the thermohaline circulation . . . 9
  - 1.4.2 The stability of the thermohaline circulation . . . 11
- 1.5 The problems addressed in this dissertation . . . 12

2 Estimates of Atlantic interocean exchange **15**
- 2.1 Introduction . . . 15
- 2.2 Bering Strait . . . 16
- 2.3 The Southern Ocean and the ACC . . . 17
- 2.4 The Weddell Gyre . . . 18
- 2.5 Agulhas Leakage . . . 19
  - 2.5.1 Geostrophic calculations of direct Agulhas Leakage . . . 19
  - 2.5.2 Interocean exchange by ring translations . . . 20
  - 2.5.3 Estimates of Agulhas Leakage: inversion studies . . . 23
  - 2.5.4 Estimates of Agulhas Leakage: model studies . . . 26
- 2.6 Conclusion . . . 28

3 Atlantic interocean exchange in an OGCM **31**
- 3.1 Introduction . . . 31
- 3.2 The sections . . . 33
  - 3.2.1 The OCCAM General Circulation Model . . . 33
  - 3.2.2 The thermohaline fields . . . 34
  - 3.2.3 The flow fields . . . 36
  - 3.2.4 The subsections . . . 39
- 3.3 Net fluxes of volume, heat and salt . . . 39
  - 3.3.1 Calculating the fluxes . . . 39
  - 3.3.2 Volume fluxes . . . 41
  - 3.3.3 Heat fluxes . . . 42
  - 3.3.4 Salt fluxes . . . 43

3.4 Vertically integrated fluxes . . . 45
3.4.1 Heat fluxes . . . 45
3.4.2 Salt fluxes . . . 45
3.5 Horizontally integrated fluxes . . . 48
3.5.1 Volume fluxes . . . 48
3.5.2 Heat fluxes . . . 50
3.5.3 Salt fluxes . . . 52
3.6 Discussion . . . 54
3.6.1 NADW route . . . 54
3.6.2 Possible return paths . . . 57
3.6.3 Estimating the return transports and associated heat and salt fluxes. . . . 58
3.7 Conclusions . . . 61

4 Sensitivity of the overturning circulation to lateral fluxes of buoyancy 63
4.1 Introduction . . . 63
4.2 Fluxes of heat and salt across 30°S . . . 66
4.3 The model . . . 70
4.3.1 Domain and configuration . . . 70
4.3.2 Equations and scaling . . . 71
4.3.3 Boundary conditions . . . 72
4.3.4 Integral characteristics . . . 76
4.4 Results . . . 79
4.4.1 Symmetric vs. non-symmetric basin: Comparison of two NPP states . . . 79
4.4.2 Realistic lateral fluxes . . . 80
4.4.3 Thermohaline forcing and overturning strength . . . 85
4.5 Discussion . . . 87
4.5.1 Scaling relations . . . 87
4.5.2 Thermohaline component of the lateral salt flux . . . 89
4.5.3 The model . . . 91
4.5.4 Implications for the impact of Agulhas Leakage . . . 93
4.6 Summary and Conclusions . . . 95
4.A Appropriate values for T_0 and S_0 . . . 97
4.B Potential energy and the reference depth . . . 97

5 Remotely induced stability of the thermohaline circulation 99
5.1 Introduction . . . 99
5.2 Model set-up . . . 102
5.2.1 The model . . . 102
5.2.2 The sources . . . 103
5.3 Results . . . 104
5.3.1 The basic experiment (no Bering Strait) . . . 104
5.3.2 Impact of Agulhas Leakage . . . 107

5.3.3 Uniqueness of the basic solution . . . 109
5.3.4 Multiple equilibria in the presence of Bering Strait inflow . . . 114
5.4 Summary and discussion . . . 117
5.4.1 Importance of NADW renewal paths . . . 117
5.4.2 Northern sinking preference . . . 118
5.4.3 Possible implications for climate switches . . . 118
5.5 Conclusion . . . 120
5.A The sources . . . 122

6 Response of the overturning circulation to South Atlantic buoyancy sources 129
6.1 Introduction . . . 129
6.2 The model . . . 131
6.2.1 The Hamburg LSG model . . . 131
6.2.2 The equations . . . 132
6.2.3 The source distribution . . . 133
6.2.4 The spin-up . . . 134
6.3 Slow source modification . . . 139
6.3.1 Overturning response . . . 139
6.3.2 The linear response . . . 141
6.3.3 Nonlinear response . . . 143
6.3.4 Energy conversions . . . 148
6.4 Fast source modification . . . 156
6.4.1 Dispersion of the perturbation . . . 157
6.4.2 Overturning response . . . 160
6.5 Summary and discussion . . . 163
6.5.1 Summary . . . 163
6.5.2 Response of the overturning circulation . . . 166
6.5.3 Comparison with freshwater studies . . . 168
6.5.4 The source/sink parametrisation of Agulhas Leakage . . . 169
6.5.5 The role of surface forcing . . . 170
6.6 Conclusions . . . 170
6.A The components of the pressure work . . . 172
6.B Convective adjustment as a density source . . . 173

7 Conclusion 175
7.1 Discussion . . . 175
7.2 Recommendations . . . 177

References 179

Summary 191

Samenvatting 195

Dankwoord 197

Chapter 1

Introduction

1.1 Ocean circulation and climate variability

The present day concern with global warming has increased public awareness that human activity might influence the global climate system. This concern has also greatly raised the scientific interest in the functioning and stability of the climate system. Paleoclimatic records show that, although global climate has been remarkably stable during the Holocene, large climate instabilities characterised the Pleistocene era of ice ages (e.g., Dansgaard et al. 1993). During the last glacial period, climate not only was colder than today, but also oscillated between warm and cold periods in a rather regular fashion, the so-called Dansgaard/Oeschger events (Dansgaard et al. 1982). Furthermore, the end of the last glacial was characterised by a significant rapid climate change event, the Younger Dryas. It caused a severe return to glacial conditions after the ice-age was followed by the considerably warmer Alleröd period.

More alarming than those of the glacial period are the abrupt climate fluctuations that occurred during the last interglacial ($\sim$ 125 to 115 kyr B.P.), the Eem. This period is considered a "prime target" for paleoclimatic reconstruction (GRIP members, 1993), since it was characterised by a slightly warmer climate than at present, and thus provides a possible analogue for future climate evolution. Ice cores have indicated that several cold periods, lasting between 70 yr and 5 kyr, interrupted the warm climate of this period. "The most pressing question", according to GRIP members, "is why similar oscillations do not exist today".

Despite the relative stability of climate during the Holocene, paleoclimatological records show that climate fluctuations took place in the near past as well (Stocker and Mysak 1992). These fluctuations were not as catastrophic as the instabilities that occurred during the Pleistocene; they may have been related to oscillations, rather than to drastic reorganisations of the climate system. Nevertheless, periods like the Medieval Warm Period and the Little Ice Age of the 17th century, strongly influenced nature and society.

It has been recognised that the ocean's thermohaline circulation may have played an important role in generating the Pleistocene and Holocene climate fluctuations

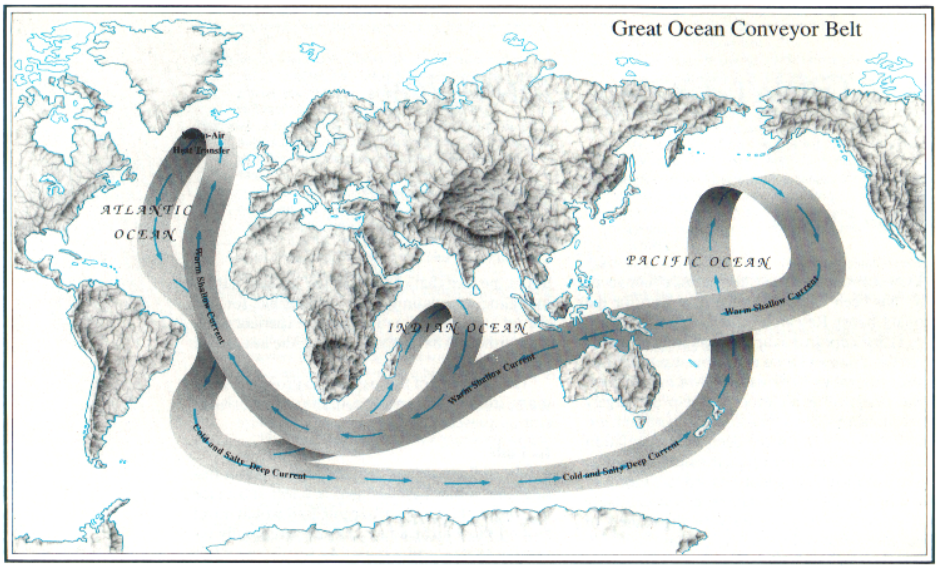

Figure 1.1: *Cartoon of the global ocean conveyor belt circulation, as depicted by Broecker (1987).*

(e.g., Broecker et al. 1985; Keigwin et al. 1991; Stocker and Wright 1991a). This circulation, driven by buoyancy fluxes at the surface, has been popularly depicted by Broecker (1987, 1991) as a conveyor belt (Fig. 1.1), spanning the World Ocean. It transports large amounts of heat northward in the Atlantic, and is to a large extent responsible for the relatively mild North Atlantic climate. A critical chain of this global circulation pattern is the process of deep convection and downwelling in the northern North Atlantic, that produces the North Atlantic Deep Water (NADW). At the end of the last ice age, when the ice caps retreated and discharged their freshwater into the North Atlantic, convection may have ceased. The reduction of NADW formation reduced the northward heat flux, causing a return to cooler conditions (Keigwin et al. 1991). Variations in the (relatively fresh) Pacific-Atlantic throughflow through the Bering Strait have been invoked to explain the climate fluctuations during the last interglacial. Shaffer and Bendtsen (1994) argued that the higher sea-level during the Eem allowed for a stronger throughflow, making the overturning circulation more sensitive to fluctuations in the hydrological cycle than today.

One of the challenges of present-day climate research is to determine to what degree the present climate system is stable to anthropogenic (or natural!) perturbations. Will climate instabilities arise as a result of global warming? Will there be quantitative changes in the strength of the thermohaline circulation, comparable to

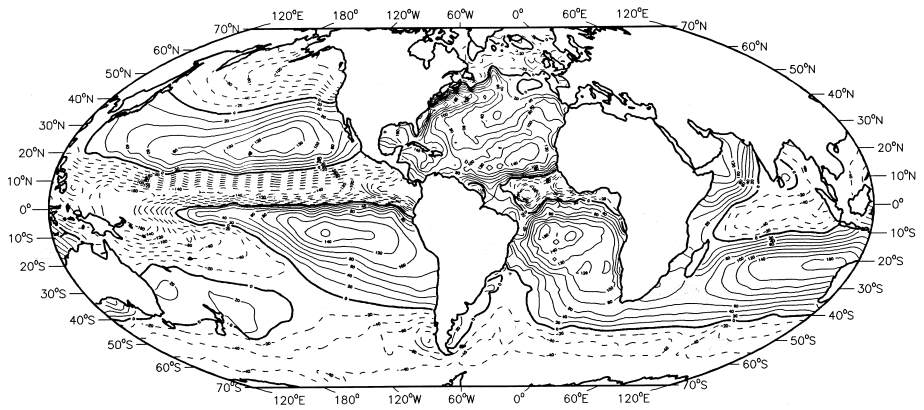

Figure 1.2: *Evaporation minus precipitation over the global oceans (Schmitt 1994). Contour interval is 20 cm* yr^{-1}*. Negative contours are dashed, and denote excess precipitation over evaporation. This map is a composite of Schmitt et al. (1989) for the Atlantic, and Baumgartner and Reichel (1975) for the other oceans.*

those that have taken place during the Medieval times or the 17th Century? Or can the thermohaline circulation be destabilised, so that more dramatic climate changes may be expected, like the Younger Dryas?

1.2 The thermohaline circulation

The thermohaline circulation is driven by surface buoyancy fluxes. These fluxes set up density gradients on a global scale. The resulting gravitational imbalance generates pressure gradients that drive the large-scale motion. One component of these buoyancy fluxes is the surface freshwater flux. This flux is the imbalance between evaporation, precipitation and continental run-off ($E - P - R$), and generates gradients in the ocean's salinity field. Figure 1.2 shows that the subtropics are dominated by evaporative freshwater loss, whereas in the tropics and at high latitudes precipitation prevails.

The other component of the surface buoyancy fluxes is the ocean's surface heat budget (Fig. 1.3). The surface heat flux is an imbalance between the radiative heat balance (incoming solar radiation minus emitted long-wave radiation), and the sensible and latent heat flux (e.g., Gill 1982). In general, the ocean gains heat at tropical and subtropical latitudes, whereas it loses heat at higher latitudes. Figure 1.3 shows that large regional variations exist, and that especially western boundary currents of subtropical gyres often display excessive heat loss.

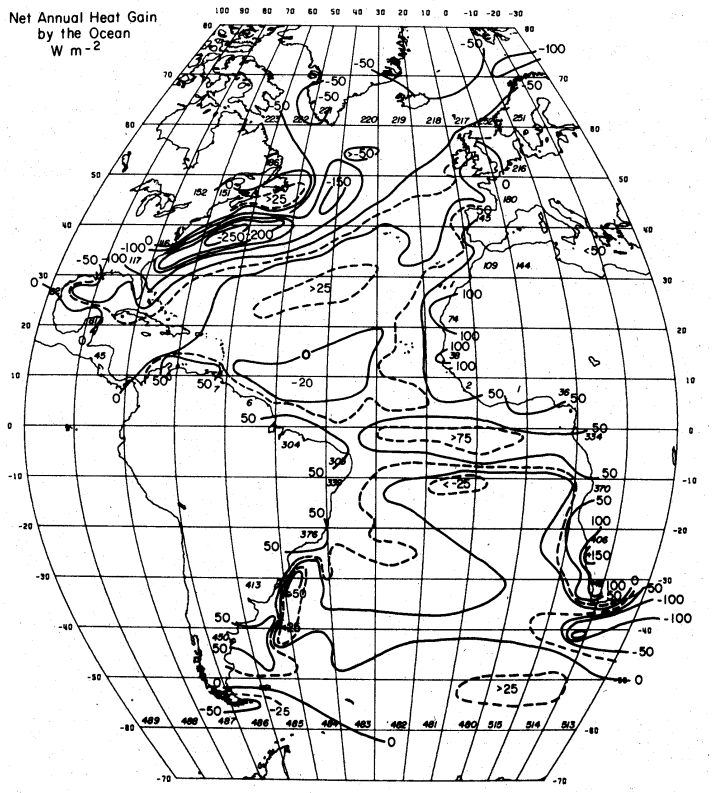

Figure 1.3: *Annual net average heat gain by the Atlantic ocean, in W* m^{-2} *(Bunker 1980). Note the dominant heat loss (negative contours) north of the line connecting Central America with Europe, and the prevailing heat gain (positive contours) in the (sub)tropics.*

As a result of a worldwide collaborative effort of observationalists, modellers and theoreticians, our knowledge of the global thermohaline circulation has increased enormously over the past decades. The global thermohaline circulation in fact consists of two main overturning cells that are characterised by the brand of deep water that is involved (Fig. 1.4, Schmitz 1995). The deepest of these cells involves Antarctic Bottom Water (AABW), a class of deep water formed in the ice-covered seas surrounding the Antarctic continent. Characterised by a very low temperature and a relatively low salinity, it fills the deepest kilometers of all ocean basins (Fig. 1.5). Here it is warmed slightly by downward diffusion of heat, and it returns to the Southern Ocean at only slightly shallower levels. The AABW overturning cell has only limited interaction with the atmosphere, and the resulting heat and salt transports that are brought about by the system are very small. Although modelling studies (Stocker et

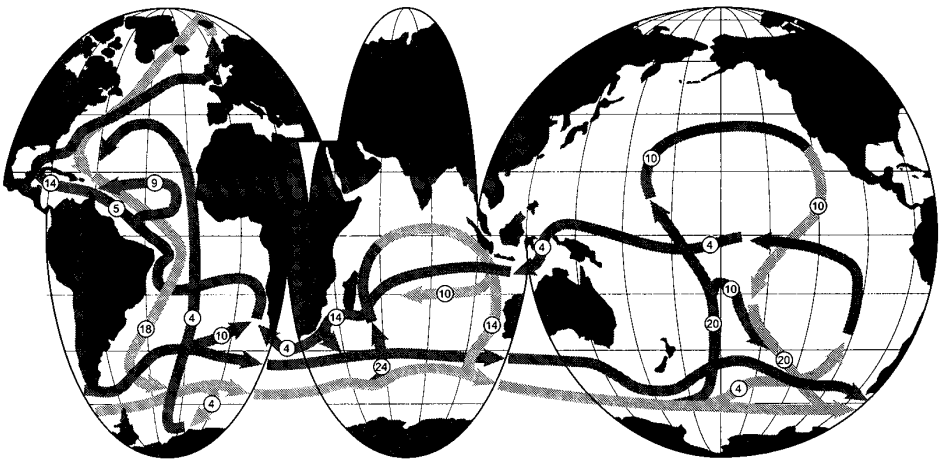

Figure 1.4: *Three-layer breakdown of the main transports and routes of the global thermohaline circulation, based on a compilation of available observations (after Schmitz 1995). Deep transports are gray, shallow and bottom water transports are black.*

al. 1992b) have shown that the strength of the AABW overturning cell influences the production rate of NADW, its importance for global climate is probably rather small.

The importance of the overturning cell involving NADW is beyond doubt. Intense cooling of the surface waters in the northern North Atlantic (primarily the Nordic Seas and the Labrador Sea) destabilises the density stratification, resulting in open-ocean deep convection (Marshall and Schott 1999). This convection mixes the cooled and relatively salty Atlantic surface waters downward, forming the water mass NADW (Fig. 1.5). Driven by the large-scale pressure gradients, this water mass flows southward at depths between roughly 2 and 4 km. Once it has reached the Southern Ocean it becomes part of the Antarctic Circumpolar Current (ACC), through which it is distributed among all ocean basins. There, its characteristics have been clearly identified (Reid and Lynn 1971).

Upwelling must bring this deep water back in the upper thermocline layer. The classical notion about the thermohaline circulation is that this upwelling takes place more or less homogeneously distributed over the World Ocean (e.g., Stommel and Arons 1960). However, recent tracer studies (Toggweiler and Samuels 1993a) and modelling studies (Toggweiler and Samuels 1993b; Shriver and Hurlburt 1997; Döös and Coward 1997) support the view that a large part of the upwelling takes place in the ACC, forced by strong Ekman divergence[1].

[1]This has led Toggweiler and Samuels (1993b, 1995, 1998) to challenge the classical view that the Atlantic overturning circulation is driven by air–sea buoyancy fluxes. They point at the truly circumpolar nature of the Southern Ocean at the Drake Passage latitudes, where no meridional barriers are present to sustain a net meridional geostrophic flow. The northward Ekman transport

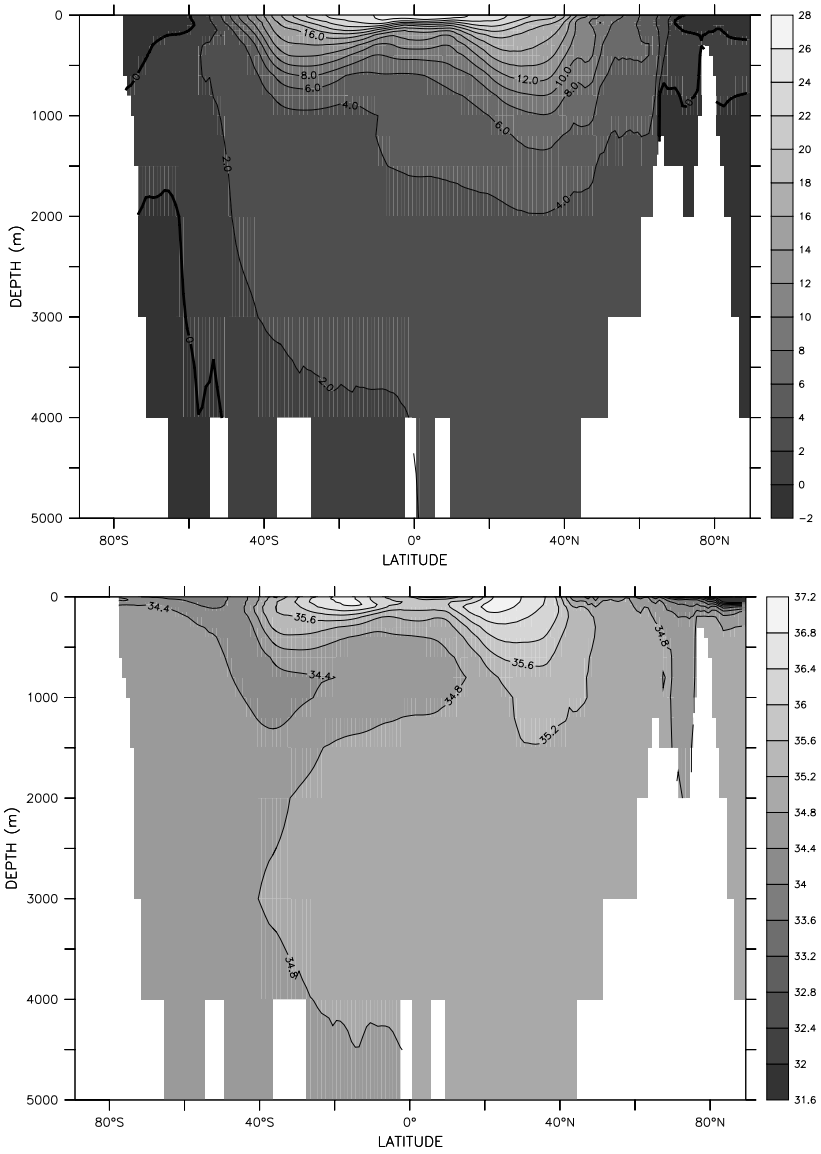

Figure 1.5: *Zonally averaged temperature (upper panel) and salinity (lower panel) in the Atlantic, as derived from the Levitus (1982) climatology.*

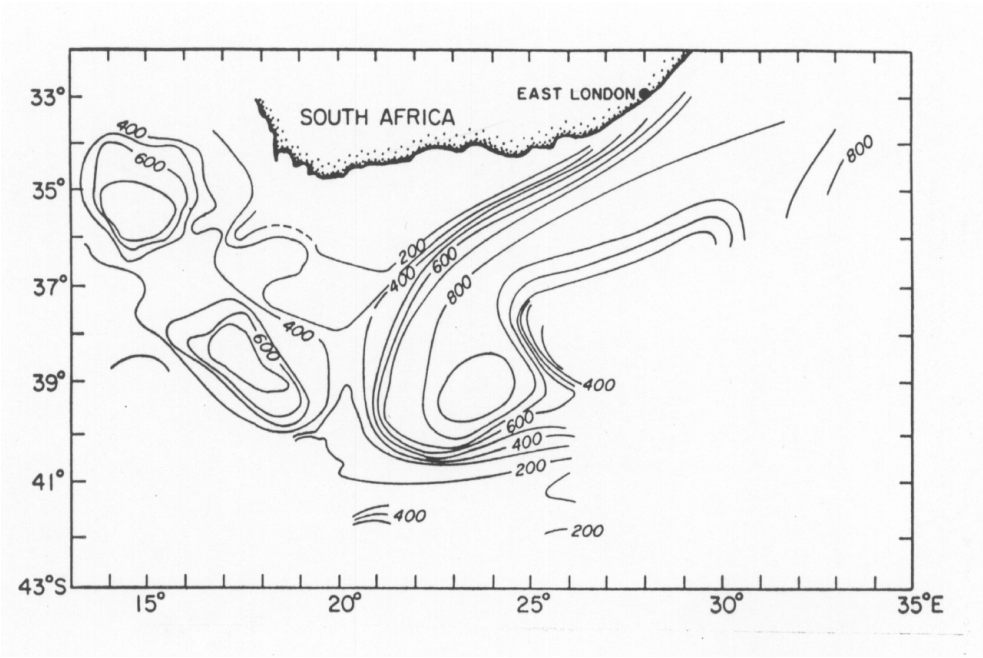

Figure 1.6: *Depth of the 10° C isotherm in the Agulhas Retroflection Area as observed during the spring of 1983 (adapted from Gordon et al. 1987). Clearly visible is the retroflection of the Agulhas Current, and two rings drifting off into the South Atlantic.*

1.3 NADW renewal paths

A component of the global thermohaline circulation that has recently become subject for debate, is the way in which the export of NADW from the Atlantic is compensated. Gordon (1985, 1986) suggested that the NADW upwells into the thermoclines of the Pacific and the Indian Oceans, and re-enters the Atlantic via so-called Agulhas Leakage. He termed this pathway the 'warm water route'. By this process, Indian Ocean water from tropical and subtropical origin leaks into the Atlantic (Figs. 1.6 and 1.7). It is related to the fact that the southern terminus of Africa is more northerly than the latitudes where the zero wind-stress curl vanishes. This has large consequences for the dynamics of the Agulhas Current, the western boundary current of the South Indian Ocean subtropical gyre. Without inertia, the Agulhas would flow

at these latitudes can only be compensated by return transports deeper than the Drake Passage sill. Supported by model results, they argue that only in the northern North Atlantic the stratification is weak enough to form the deep water that feeds this transport. However, Stommel (1957) points at the fact that the Drake Passage latitudes are to a large extent blocked by the island arc made up of the South Shetland-South Orkney-South Sandwich islands. It is probable that these features are not resolved by the numerical models used by Toggweiler and Samuels.

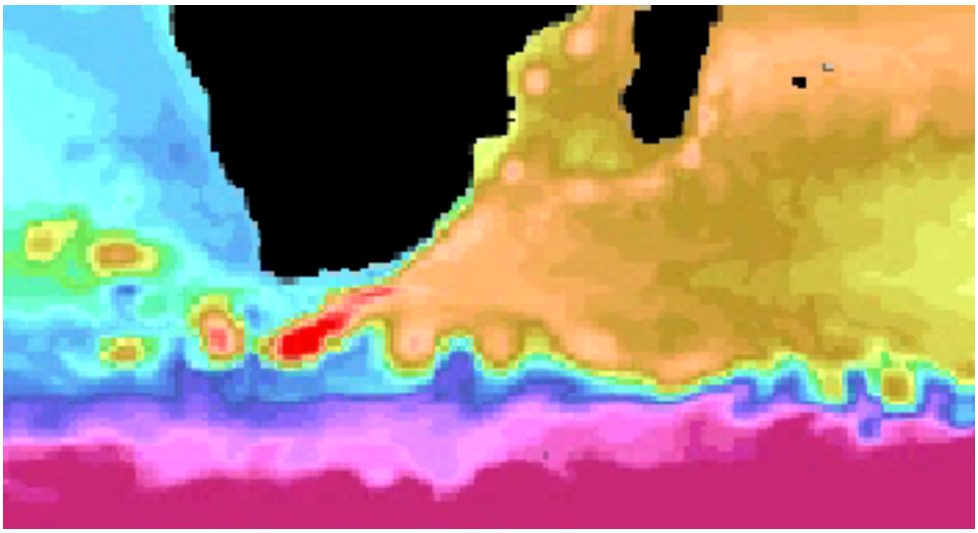

Figure 1.7: *The ring-shedding process, as simulated by the high resolution model OCCAM (Webb et al. 1998). Shown is a snapshot of sea surface height. Clearly visible are the anticyclonic Agulhas rings drifting into the South Atlantic.*

almost entirely into the South Atlantic (De Ruijter 1982). But due to its large inertia, the Agulhas separates from the continent, and proceeds far enough southward to reach the eastward South Indian Ocean Current (De Ruijter and Boudra 1985; Dijkstra and De Ruijter 2000). Due to the conservation of potential vorticity, the current makes a tight anticyclonic turn and meanders back into the Indian Ocean. Instability of the current system in this so-called Retroflection area causes a regular short-cut of the current. The occluded loops, known as Agulhas Rings, are subsequently separated from the main current, and drift off into the South Atlantic (see Lutjeharms (1996) and De Ruijter et al. (1999) for reviews). Once these rings have entered the South Atlantic, they disperse and mix with the surrounding South Atlantic thermocline and intermediate waters. High-resolution modelling studies (Döös 1995; Thompson et al. 1997) support the view that most of the water that compensates for NADW outflow is derived from Agulhas Leakage.

Rintoul (1991) challenged the idea of predominant NADW renewal via Agulhas Leakage. Based on an inversion of hydrographic data, he argued that most of the water that compensates the NADW outflow must have entered the Atlantic as cold and relatively fresh Subantarctic water via the Drake Passage, the 'cold water route'. This water is thought to subduct along the Antarctic Polar Front (Sverdrup et al. 1942), forming a water mass that is characterised by its low salinity, and is known as Antarctic Intermediate Water (AAIW). Its low salinity tongue is clearly visible on meridional sections through the Atlantic (Fig. 1.5). Although AAIW is present

in the Pacific and Indian as well, it nowhere extends so far north as in the Atlantic, suggesting its participation in the overturning circulation. The dominance of the cold water route is supported by most studies that involve the inversion of hydrographic data (Macdonald 1993; Schlitzer 1993, 1996; Boddem and Schlitzer 1995; De las Heras and Schlitzer 1999).

A study of hydrographic observations in the south-eastern corner of the South Atlantic inspired Gordon et al. (1992) to formulate a hybrid scenario. In this scenario, a large part of the Drake Passage derived Subantarctic water first makes a transit through the Indian Ocean before it re-enters the Atlantic via Agulhas Leakage. Nevertheless, ever since Gordon (1985) estimated a 14 Sv Indian-Atlantic interocean exchange by Agulhas Leakage, this estimate has been adjusted to lower values, so that it cannot provide the total compensation for the estimated 14 to 20 Sv NADW export. A review of literature on this topic lead Schmitz (1995) to estimate that about 4 Sv of Agulhas Leakage participates in the overturning circulation.

1.4 Importance of interocean exchange for the thermohaline circulation

1.4.1 The strength of the thermohaline circulation

Due to the highly contrasting water mass characteristics of these two main NADW compensation routes, with the warm water route importing mainly warm and salty thermocline water into the Atlantic, and the cold water route supplying cold and fresh Subantarctic water, it is clear that the way in which NADW export is compensated is important for the heat and salt balance of the Atlantic. Gordon et al. (1992) were the first to speculate about a possible dynamical impact of Agulhas Leakage on the Atlantic overturning strength. They recognised that the salt import brought about by Agulhas Leakage might play a role in maintaining the high surface salinities of the Atlantic. They speculated whether introduction of Indian Ocean salt might precondition the North Atlantic for deep convection. They went even further by asking: "if the Indian Ocean salt input were shut off, might the NADW thermohaline cell run down?"

The hypothesis of Gordon et al. (1992) has made Agulhas Leakage a major climate issue. Since the amount of Agulhas Leakage depends critically on the position of the latitude of zero wind-stress curl, it is probably rather sensitive to changes in the South Indian wind stress climatology. Using foraminifera assemblages of the South Indian Ocean, Howard and Prell (1992) were able to reconstruct the position of the Subtropical Convergence and other Southern Ocean fronts during the last 500 kyr (Fig. 1.8). They concluded that the Subtropical Convergence in the Indian Ocean was shifted several degrees northward during the major glacial periods. This must have reduced the Agulhas Leakage gap considerably, severely attenuating the flow of Indian Ocean water into the Atlantic. This conclusion is supported by records of calcareous plankton in the Cape Basin (Flores et al. 1999). Paleoclimatological records of the Atlantic also show a sudden reappearance of a species of foraminifera

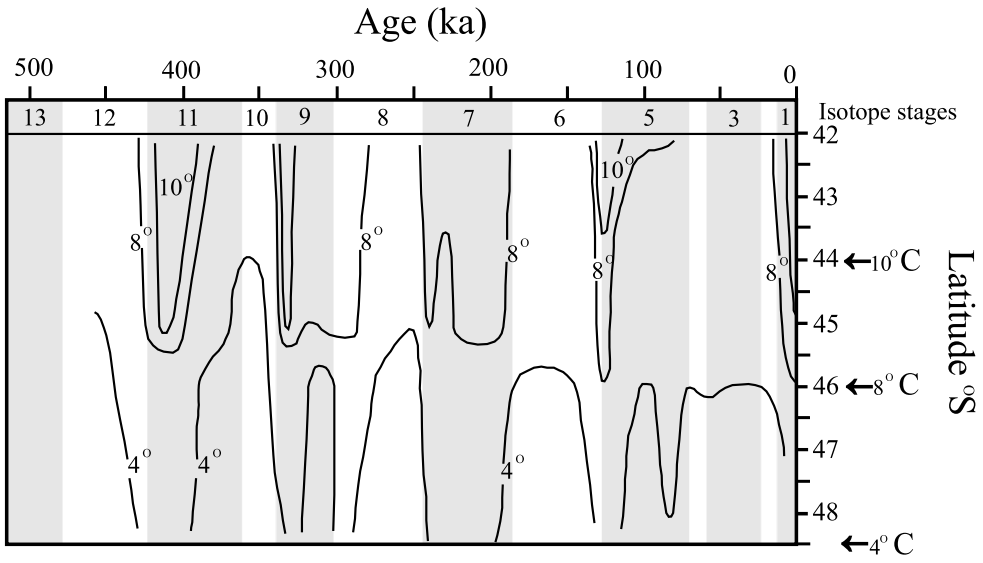

Figure 1.8: *The latitudinal position of the 10° C, the 8° C and the 4° C isotherms in the Indian Ocean during the last 500 kyr, as inferred from foraminifera assemblages (Howard and Prell 1992). These isotherms may be associated with the Subtropical Convergence, the Subantarctic Front and the Antarctic Polar Front, respectively. Shaded intervals indicate interglacial conditions. The arrows on the right indicate the present-day positions of the isotherms. They show that, for instance, the Subtropical Convergence was shifted northward during glacial times. This may have caused a considerable reduction in Agulhas Leakage.*

(*Globorotalia menardii*) at the end of the last glacial. This species had been extinct in the glacial Atlantic, but had survived in the tropical Indian Ocean. Berger and Wefer (1996) suggested that a sudden restart of Agulhas Leakage took place at the end of the last glacial, reseeding the Atlantic with this tropical species (it is not without reason that the Cape of Good Hope is indicated in paleoceanographic literature as 'Cape Valve'). Based on the suggestion of Gordon et al. (1992), Berger and Wefer (1996) speculated that the sudden restart of Agulhas Leakage may have played an active role in restarting the conveyor belt circulation.

At present, Agulhas Leakage seems surprisingly stable, although a continuous monitoring of the Leakage has only been possible since remote sensing techniques came into use (e.g., Lutjeharms and Van Ballegooyen 1988; Gordon and Haxby 1990; Byrne et al. 1995; Feron et al. 1992; Schouten et al. 1999). Nevertheless, an anomalous event of enhanced Agulhas Leakage in the mid-80's was reported by Shannon et al. (1990). They attributed this enhanced leakage to changes in the wind stress field: this caused a poleward shift of the line of zero wind-stress curl and a reduction in

the Agulhas Current transport. It appears to have been followed by a period of anomalously weak Agulhas Leakage. Possibly, a feedback exists between the Indian-Atlantic heat exchange that is induced by Agulhas Leakage and the local wind-stress field, that tends to stabilise the system, but no evidence for this has been found yet (De Ruijter, personal communication).

Cai and Greatbatch (1995) were the first to test the hypothesis of Gordon et al. (1992) in a numerical model. They compared the overturning circulation in two models: in one model Agulhas Leakage was present, while in the other model Agulhas Leakage was shut off by an artificial extension of the African continent. Although shutting off Agulhas Leakage resulted in a cooling and freshening of the Atlantic, they found neither any effect on the density field, nor on the overturning strength. However, the fact that no response in overturning strength was present in their model, despite the obvious changes that took place in the Atlantic thermohaline structure, remains puzzling. Rahmstorf et al. (1996) pointed at the fact that the thermal boundary conditions used by Cai and Greatbatch result in an anomalously weak thermal relaxation. This enabled thermal anomalies to develop almost as freely as saline anomalies, so that their effects on the density field cancelled throughout the whole basin. Furthermore, the approach of comparing two models with and without Agulhas Leakage, did not allow for a systematic study of the sensitivity of the overturning strength to changing Agulhas Leakage.

Since the study of Cai and Greatbatch (1995), no dedicated studies have been performed on the issue of possible impact of Agulhas Leakage on the overturning strength. Therefore, the question how and to what degree Agulhas Leakage has impact on the Atlantic overturning circulation, has not been satisfactorily answered yet.

1.4.2 The stability of the thermohaline circulation

Although the restart of Agulhas Leakage at the end of the last glacial may well have played a role in the recovery of the conveyor belt circulation, it seems improbable that the restart is a linear response to changing forcing or, for instance, a change in Agulhas Leakage. The discovery by Stommel (1961), that thermohaline driven flow in an oceanic context may exhibit multiple equilibrium states under identical forcing, yields a plausible mechanism for explaining some of the abrupt Pleistocene climate changes (e.g., Broecker et al. 1985); in the presence of multiple equilibria, finite-amplitude perturbations may trigger a switch from one equilibrium to another, resulting in a reorganisation of the climate system.

Multiple equilibria are found in a large variety of models (see Rahmstorf et al. (1996) for an overview). For instance, the two-basin model of Marotzke and Willebrand (1991) features an equally large Atlantic and Pacific, interconnected in the south via an ACC. In this model, four stable equilibria are found, characterised by deep water formation taking place either in the North Atlantic and/or in the North Pacific basin, or in the Southern Ocean. However, the net atmospheric freshwater flux from the Atlantic to the Pacific (Baumgartner and Reichel 1975) imposes an asymmetry on the coupled Atlantic/Pacific circulation system that strongly hinders

the equilibria with North Pacific downwelling. This asymmetry is enhanced by the larger latitudinal extent of the Atlantic (e.g., Stocker and Wright 1991ab; Stocker et al. 1992a; Hughes and Weaver 1994).

Simplified models, modelling a single basin with equatorial symmetry (e.g., Bryan 1986; Thual and McWilliams 1992; Cessi and Young 1992; Quon and Ghil 1992, 1995; Vellinga 1996; Dijkstra and Molemaker 1997), feature two equatorially symmetric circulations with downwelling at the poles (thermally driven) or at the equator (saline driven), and two asymmetric circulations with downwelling in the northern or southern hemisphere (thermohaline driven). However, north–south asymmetries arise from a larger continental area in the northern hemisphere and from a slight meridional asymmetry in the atmospheric freshwater flux. Dijkstra and Neelin (1999) showed that these asymmetries induce a strong preference for the northern sinking circulation in the Atlantic. In fact, these asymmetries deform the thermally driven two-cell circulation so that the northern cell expands and penetrates the southern hemisphere, resembling a weakened northern sinking circulation. Since paleoceanographic data suggest that during the last glacial period NADW formation had not ceased but was strongly reduced (e.g., Sarntheim et al. 1994), switches between these equilibria (that coexist in a limited volume in parameter space) may be a more likely mechanism for explaining Pleistocene climate fluctuations than complete reversals of the northern sinking state.

One of the challenges of the present-day physical oceanography is to determine whether the net effect of all asymmetries favours the conveyor belt circulation to such an extent that it is the only equilibrium possible under present-day (or future) forcing. If so, the conveyor belt would be stable with respect to large amplitude disturbances, and only quantitative changes could be expected in response to, for instance, global warming. If, on the other hand, the real ocean could sustain other circulation patterns as well, then the possibility exists that large disturbances could push the circulation to another equilibrium. This could result in a catastrophic reorganisation of the climate system.

The asymmetry that is the subject of this dissertation is the way in which the Atlantic communicates with the other ocean basins. Shaffer and Bendtsen (1994) studied the effect of the Bering Strait throughflow between the North Pacific and the North Atlantic via the Arctic Ocean. They concluded that an increase in the (relatively fresh) transport could destabilise the conveyor belt circulation in favour of a southern sinking state. However, the largest part of the interocean exchange takes place via the Southern Ocean. It is not known how the north-south asymmetry brought about by the interocean fluxes of heat and salt influence the stability of the conveyor belt circulation.

1.5 The problems addressed in this dissertation

As discussed above, the Atlantic interocean exchange plays a central role in several issues related to the operation and stability of the global thermohaline circulation. A key role herein is often ascribed to the Indian-Atlantic exchange brought about

by so-called Agulhas Leakage. However, few of these claims have been substantiated by systematic investigation. Several aspects concerning the importance of interocean exchange deserve detailed investigation. These aspects are closely related to the fundamental dynamics of the thermohaline circulation, and are important for issues concerning past, present, and future climate.

The following questions will therefore be addressed in the series of studies presented in this dissertation:

- How large is the exchange of water, heat and salt between the Atlantic and the rest of the World Ocean?
- How are these fluxes brought about, or in other words, how does the Atlantic communicate with the other ocean basins?
- What is the influence of these interocean fluxes on the operation and strength of the Atlantic overturning circulation, and how is this influence brought about?
- To what degree do these interocean fluxes influence the stability of the Atlantic overturning circulation, and did Agulhas Leakage play a role in shaping glacial/interglacial transitions?

In **Chapter 2** a summary is given of literature concerning observations of interocean exchange, in order to estimate the amount of water, heat and salt that is exchanged between the Atlantic and the rest of the World Ocean. How interocean exchange takes place in a state-of-the art numerical ocean model is studied in **Chapter 3**. An analysis is made of the transports in OCCAM, a high-resolution model developed at the U.K. Southampton Oceanographic Centre. Although the model's climatology deviates in some aspects from what is known of the real ocean, it provides a consistent view of the spatial characteristics of such a model interocean exchange. In **Chapter 4**, a simple two-dimensional model is used to study the effect of interocean fluxes of buoyancy on the strength of the overturning circulation. The interocean fluxes are represented by lateral fluxes of heat and salt, which are prescribed at the southern boundary of the model domain. The same model is used in a different set up in **Chapter 5**, to address the question of the stability of the overturning circulation in response to interocean fluxes. In this study, interocean exchange is represented by internal sources and sinks of heat and salt. The distributions are based on the fluxes that are obtained from the model analysis of Chapter 3. In **Chapter 6** several experiments are presented with a more realistic three-dimensional ocean model, the low-resolution model LSG. Agulhas Leakage is parametrised by applying sources of heat and salt in the South Atlantic Ocean, and equally large sinks in the South Indian Ocean. **Chapter 7** summarises the main results and conclusions, and gives some suggestions for future work on the subject.

Chapter 2

Estimates of Atlantic interocean exchange

In this chapter, an overview is given of what is known about the exchange of water, heat and salt between the Atlantic and the rest of the World Ocean. Published estimates of the exchange taking place in the north (via the Bering Strait) and in the Southern Ocean (via the Weddell Gyre, the Antarctic Circumpolar Current and Agulhas Leakage) are compiled and discussed[1]*.*

2.1 Introduction

Measuring transports in the ocean has been one of the most important tasks for oceanographers for centuries. Several methods have been developed to estimate transports of water, heat and salt, and the exchange between the basins of the World Ocean. The increase in computing power, allowing for inversions of large sets of data (e.g., Schlitzer 1993), and the availability of satellite data (e.g., Gordon and Haxby 1990, Feron 1994) have increased the number of tools even further during the last decades, and has led to even more accurate descriptions of the ocean circulation. Furthermore, the steadily increasing skill of numerical ocean models (e.g., Semtner and Chervin 1992; FRAM Group 1991; Webb et al. 1998) makes them an increasingly valuable tool in studying ocean processes. Although the representation of the forcing and the physical processes in these models still needs improvement, they provide a picture of the processes in the oceans that is both concise and consistent.

The recent controversy regarding the compensation of North Atlantic Deep Water (NADW) export from the Atlantic, either by Drake Passage derived water (Rintoul 1991), or by Indian Ocean water entering the Atlantic by Agulhas Leakage (Gordon 1986), has generated a lot of interest in determining the Atlantic interocean exchange via the Southern Ocean. In particular the process of Agulhas Leakage has received a

[1] Part of this study has been published in a modified form as part of De Ruijter et al. (1999).

great deal of attention, the uniqueness of its dynamical regime and its possible global impact making it a rewarding subject of oceanographic research. This has resulted in a large number of studies employing a broad range of oceanographic methods.

This chapter summarises what is known about the exchange between the Atlantic and the rest of the World Ocean. It starts off with a discussion of the northern connection between the Atlantic and the Pacific, through the Bering Strait. Then, the exchanges in the Southern Ocean will be addressed, including transport estimates of the Antarctic Circumpolar Current and the Weddell Gyre. Finally an overview will be given of estimates of Agulhas Leakage.

2.2 Bering Strait

In the north, the Atlantic is connected to the Arctic Ocean by the Nordic seas, which are formed by the Greenland, Iceland and Norwegian seas (also called GIN sea). This connection takes place across the Greenland–Scotland ridge system connecting Scotland with Iceland and Greenland. This ridge system has a maximum depth of only 850 m in the Faroe-Shetland Channel. The Nordic seas are connected to the Arctic Ocean via the Fram Strait. On the other side, the Arctic Ocean is connected to the Pacific via the Bering Strait. This passage between Alaska and Siberia is only 85 km wide and 50 m deep, but establishes an important connection between the Pacific and the Atlantic.

Volume transports through the Bering Strait are relatively well determined, as the small geographical extent of the passage allows for rather reliable estimates. Based on current meter data, Coachman and Aagaard (1988) obtained an as yet undisputed value of 0.8 ± 0.1 Sv. In the Arctic Ocean, the freshwater transport is augmented by river discharge and net precipitation, and the net flow across 65°N into the North Atlantic is estimated at 0.93 Sv (Wijffels et al. 1992). This volume transport is characterised by strong seasonal and interannual variability that seems to correlate well with variations in the wind forcing (Coachman and Aagaard 1988). It is nevertheless probable that the mean net northward transport is mainly forced by a pressure difference between the North Pacific and the North Atlantic: the strong salinity contrast between the North Atlantic and North Pacific surface waters results in a significant drop in sea-surface height (Shaffer and Bendtsen 1994).

The importance of this relatively small volume transport is that it is related to a net southward flow throughout the whole Atlantic. Although this flow is reduced on its way southward by net evaporation from the Atlantic (Baumgartner and Reichel (1975) estimated a 0.5 Sv net freshwater export from the Atlantic), it is never annihilated (Wijffels et al. 1992). Furthermore, the 0.8 Sv inflow of 32.5 psu water leads to a 26 Gg s^{-1} southward salt transport throughout the whole Atlantic. As no salt can be exchanged with the atmosphere, this transport has to cross every zonal section through the Atlantic, yielding a powerfull constraint on, for instance, inversion studies (e.g., Holfort 1994).

2.3 The Southern Ocean and the ACC

Contrary to the northern connection, where the exchange is reasonably well determined, the exchange at the southern part of the Atlantic is much more complicated and much harder to determine. Here the Atlantic is connected to the Southern Ocean. This circumpolar ocean is transected by several frontal zones, and consists of highly contrasting water masses. In fact, the communication between the Atlantic and the other basins is brought about by three distinct flow regimes. The strongest is the Antarctic Circumpolar Current (ACC), the enormous flow that encircles the continent of Antarctica. It is driven mainly by the westerly wind regime, but the baroclinic flow also contributes considerably to its volume transport (Nowlin and Klinck 1986). To the north of the ACC, Indian Ocean water escapes westward into the Atlantic by the process of Agulhas Leakage. And south of this current, close to the Antarctic continent, a cyclonic wind curl drives the Weddell Gyre, forming one of the source areas of the Antarctic Bottom Water (AABW). In view of the vast expanse of the Southern Ocean, ranging from polar to subtropical climate zones, the various dynamically intricate regions it incorporates, among which the highly variable Agulhas Retroflection Area and the highly barotropic ACC, the low economic importance of this ocean, and its remoteness and unfavourable climate, it is not surprising that hydrographic measurements and reliable transport estimates in the Southern Ocean are scarce.

Most transport estimates are based on observations made in the Drake Passage, where the latitudinal extent of the Southern Ocean is smallest. Lutjeharms (1982) gives an overview of published estimates of Southern Ocean transports up to 1980. Based on historic hydrographic data, he arrives at a transport of 160 Sv through the Drake Passage, roughly consistent with the other estimates. Georgi and Toole (1982) estimated the exchange of volume, heat and freshwater between the Pacific, Atlantic and Indian Oceans through the Southern Ocean. They used hydrographic data from sections connecting Antarctica with South America (Drake Passage), with South Africa and with New Zealand, to calculate the di- and convergence of these transports in the several sectors of the Southern Ocean. They obtained net volume transports of 127, 140 and 125 Sv, respectively. Nowlin and Klinck (1986) summarised volume transport estimates of the ACC in the Drake Passage, and obtained a mean transport of approximately 134 ± 13 Sv. However, the certainty of all these estimates suffers from the absence of an unambiguous level-of-no-motion. Furthermore, variability results in fluctuations on (semi-)annual timescales of no less than 20% (Nowlin and Klinck 1986).

From the heat and salt transports across their Southern Ocean sections, Georgi and Toole (1982) calculated volume-transport-weighted mean properties by dividing the property transport by the volume transport. For salt, for instance, this can be written as:

$$\tilde{S} = \frac{\overline{vS}}{\overline{v}} = \bar{S} + \frac{\overline{v'S}}{\overline{v}}. \tag{2.1}$$

Here, v' is the deviation from the section mean velocity, so that $\overline{v}\tilde{S}$ is the total salt transport, while $\overline{v'S}$ represents the residual component. Based on a lower value of the weighted mean salinity at the African section (34.418 psu) than in the Drake Passage

(34.444 psu), and an ACC transport of 127 Sv, Georgi and Toole (1982) calculated a 0.1 ± 0.6 Sv freshwater gain in the Atlantic sector of the Southern Ocean. This method is based on the assumption that the salt transport through all sections must be equal, and that the weaker salt flux through the African section must be augmented by a 0.1 Sv volume transport increase to reach the Drake Passage value. They concluded that this freshwater gain is inconsistent with the Baumgartner and Reichel (1975) data on the excess evaporation in the Atlantic, but it is seemingly consistent when the Bering Strait inflow is taken into account. However, Wijffels et al. (1992) pointed out that this consistency is only apparent. They argued that the salinity difference between the African and the Drake Passage sections has to be positive to account for the salt transport of 26 Sv psu that is introduced through the Bering Strait as well. Indeed, with the Georgi and Toole (1982) salt flux estimates through the Drake Passage and the African section, this salt flux constraint can only be met by a 0.86 Sv volume flux divergence in the Atlantic, rather than the 0.1 Sv, and this value is not supported by estimates of $E - P$ in the Atlantic.

Georgi and Toole (1982) calculated the total salt flux through the Drake Passage and obtained transports of 4719 ± 12 Sv psu and 4167 ± 9 Sv psu (two independent estimates from different data sets). These values are, of course, very sensitive to the estimated volume transport of the ACC. The residual components of their salt transport estimates ($\overline{v'S}$ in Eq. (2.1)) amount to -20.824 Sv psu and -20.328 Sv psu through the Drake Passage, and -33.60 Sv psu through the African section.

The total heat flux through the Drake Passage estimated by Georgi and Toole (1982) is 1.43 ± 0.19 PW and 1.27 ± 0.15 PW, in good agreement with the 1.3 PW of Rintoul (1991) and the 1.4 ± 0.3 PW of Macdonald and Wunsch (1996). They furthermore estimated a 0.3 ± 0.3 PW heat loss of the ACC in both the Atlantic and the Pacific sectors of the Southern Ocean, and a 0.6 ± 0.5 PW heat gain in the Indian sector of the Southern Ocean. Two inversions of hydrographic data (Rintoul 1991; Macdonald and Wunsch 1996) obtained a comparable 0.2 PW heat flux convergence in the Atlantic sector of the Southern Ocean. It must be noted that the transport estimates of Georgi and Toole (1982) apply to the Southern Ocean as a whole, and thus include transports by the true ACC, by Agulhas Leakage and by the Weddell Gyre. The implied transport of heat from the Indian to the Atlantic Ocean, for instance, may not be due to the eastward transport by the ACC alone, but by westward heat transport in the Agulhas Retroflection area as well.

2.4 The Weddell Gyre

The Weddell Sea is the main source area of AABW (Sverdrup et al. 1942, p. 612). The circulation in this sea is dominated by a cyclonic gyre, situated in the transition zone between the westerly wind regime and the Antarctic eastwind band. Since the westward current has to supply for AABW, this gyre is not completely closed. Schröder and Fahrbach (1999) estimated the volume transports across the Greenwich meridian to be 61 Sv for the eastward flow in the northern rim current and 66 Sv for the westward return flow in the southern part of the gyre. This leaves 5 Sv for

Authors	Flux (Sv)	reference	date
Harris and Van Foreest (1978)	5	1100 db	03 1969
Gordon (1985)	14	1500 db	11/12 1983
Gordon et al. (1987)	10	1500 db	11/12 1983
Bennett (1988)	6.3	T> 8°C	11/12 1983
	2.8	T> 8°C	02/03 1985
Stramma and Peterson (1990)	8	1000 m	11 1983
Gordon et al. (1992)	10	T > 9°C	12 1989/ 01 1990
	15	1500 db	12 1989/ 01 1990
Garzoli and Gordon (1996)	3	1000 db	06 1992/ 11 1993
Garzoli et al. (1996)	4	1000 db	10 1992/ 09 1995

Table 2.1: *Geostrophic estimates of the direct inflow of Indian Ocean water into the Atlantic.*

conversion into AABW, in agreement with observational estimates of 4 Sv of AABW entering the Atlantic (Schmitz 1995, see Fig. 1.4).

The northern boundary of the Weddell Gyre is formed by the Weddell Front, which separates the Circumpolar water masses from those of the Weddell Sea. Schröder and Fahrbach (1999) observed this front at 55.5°S at the Greenwich meridian. They found no evidence of Weddell Gyre water leaving for the ACC, but Circumpolar Deep Water appears to be entrained into the gyre.

2.5 Agulhas Leakage

2.5.1 Geostrophic calculations of direct Agulhas Leakage

Estimating the amount of Indian Ocean Water that enters the Atlantic through Agulhas Leakage is hard, principally due to its highly intermittent character. Nevertheless, several attempts have been made to estimate the amount of interbasin exchange by direct geostrophic calculations alone (Harris and van Foreest 1978; Gordon 1985; Bennett 1988; Stramma and Peterson 1990) or in combination with other tracer distributions (Gordon et al. 1987; Gordon et al. 1992). Interpreting the results, as tabulated in Table 2.1, remains a difficult task, since hydrographic data alone yield only a snapshot of a highly intermittent process. Geostrophic calculations performed by Gordon (1985) yielded, for instance, a 14 Sv transport between the South African coast and the off-shore edge of an Agulhas ring just off-shore Cape Town. Gordon et al. (1987) concluded that at least 4 Sv of this transport must have been derived from the South Atlantic Current. Furthermore, Olson and Evans (1986) pointed out that a large amount of this transport was due to a jet-like feature between the ring and the coast, and it is therefore unlikely that this transport is independent of the ring shedding events.

Estimates of Agulhas Leakage which are based on a mismatch between the transports of the Agulhas Current and the Agulhas Return Current in the Retroflection

Area are 16 Sv (Gordon et al. 1987) and 5 Sv (Stramma and Lutjeharms 1997). Gordon et al. (1987) calculated that their 16 Sv imbalance could be accounted for by westward growth of the Retroflection region with approximately 3.0 cm s^{-1}, or by a loss of water to the Atlantic Ocean with this amount. This protrusion rate is smaller than the 12 cm s^{-1} estimated by Lutjeharms and Van Ballegooyen (1988) from infrared images. These results indicate that, although the ring shedding event is intermittent, interbasin exchange might elapse with a more constant rate by protrusion of the Agulhas Retroflection, the volume surplus being only now and then released in the form of rings or filaments.

The exchange of heat and salt that is brought about by Agulhas Leakage is not easily calculated neither. For a meaningful estimate it must be known how the inflow of Indian Ocean water is compensated. There are two candidate scenario's that imply completely different amounts of heat exchange. Part of the Agulhas inflow may be compensated at the same level by the export of South Atlantic water, by a branch of the South Atlantic Current that flows into the South Indian Ocean. In this case Agulhas Leakage links the wind-driven gyres of the South Indian and South Atlantic Oceans into one large wind-driven system (De Ruijter 1982), that has been called 'super-gyre' (Gordon et al. 1992). As a matter of fact, analyses of tracer distributions (Gordon et al. 1987; Fine et al. 1988; Valentine et al. 1993) have shown the presence of a large fraction of South Atlantic water in the retroflection region and in the Agulhas Return Current. This suggests that a large portion of the Agulhas inflow is compensated by export of South Atlantic water at thermocline and intermediate levels.

Another possible way of compensating the net input of Indian Ocean water is by the export of NADW (Gordon 1985, 1986). In this case, Agulhas Leakage provides the North Atlantic with water for the production of NADW, thus becoming a direct link in the global thermohaline circulation. As the temperature of the Indian Ocean Thermocline Water contrasts strongly with the temperature of the NADW, and only slightly with that of the South Atlantic thermocline, the heat transports of the two scenario's differ an order of magnitude. Indeed, Gordon (1985) estimated a heat input between 0.023 and 0.47 PW for his presumed 14 Sv Agulhas input, dependent on whether it is compensated by export of South Atlantic Thermocline Waters, or by export of NADW.

To my knowledge, there are no estimates of the salt transport brought about by Agulhas Leakage which are based on direct geostrophic calculations.

2.5.2 Interocean exchange by ring translations

Other estimates of interbasin exchange are based on the translation of Agulhas rings. When the volume of Indian Ocean water that is trapped inside a ring is known, as well as its anomalous heat and salt contents (with respect to the water that is displaced), then the volume, heat and salt fluxes can be deduced from the number of rings that is shed per year.

The large range of volume fluxes per ring (Table 2.2) is due to different assumptions made in the calculations, due to differences between individual rings, and due to

Authors	flux (Sv)	reference	date
Olson and Evans (1986)	0.48-0.61	T> 10°C	11/12 1983
Duncombe Rae et al. (1989)	1.2	total	04/05 1989
Gordon and Haxby (1990)	1.0 - 1.5	T> 10°C	05 1987
	2.0 - 3.0	total	05 1987
M and W-J (1991)[a]	0.4 - 1.1	total	02/03 1983
Van Ballegooyen et al. (1994)	1.05	T> 10°C	02/03 1987
	1.25	T> 8°C	02/03 1987
Byrne et al. (1995)	0.8 - 1.7	1000 db	10 cruises in 1980's
Clement and Gordon (1995)	0.45 - 0.90	1500 db	05 1993
Duncombe Rae et al. (1996)	0.65	total	06 1992, 05/10 1993
Lutjeharms and Cooper (1996)[b]	0.10	total	11 1983, 12 1992
Goñi et al. (1997)	1.0	T> 10°C	09 1992/12 1995

[a] McCartney and Woodgate-Jones (1991)
[b] Filaments

Table 2.2: *Estimates of volume transports induced by the translation of a single ring.*

rings being measured at different distances from the Retroflection area, so in different stages of decay. Gordon and Haxby (1990), for instance, based their upper estimates of the volume fluxes on the outer diameter of the rim of the Agulhas ring. Olson and Evans (1986), however, pointed out that the ring of maximum velocity should be taken instead, as here the density gradients are largest, indicating contrasting water mass characteristics. Also the depth of the rings is chosen quite arbitrarily by different authors. McCartney and Woodgate-Jones (1991) showed that the depth to which Indian Ocean water is trapped is not necessarily the depth at which the ring signature is still present in the depression of isotherms. Following arguments by Flierl (1981), they argued that water can only be trapped above the depth at which the maximum rim velocity exceeds the translation speed.

The natural variations in the size of rings are evident from, for instance, the study by Goñi et al. (1997). They studied 17 Agulhas rings that varied in their volume transport between 0.03 Sv and 2.3 Sv. Table 2.2 shows that the average volume transport brought about by an Agulhas ring is on the order of 1 Sv.

Estimates of heat (F_Q) and salt (F_S) fluxes due to ring translations, as well as the available potential energy (APE) and kinetic energy (KE) contents of some rings, are tabulated in Table 2.3. The estimates presented here are based on the temperature and salinity contrasts between the enclosed water and its immediate surroundings. This supposes that the inflow of Indian Ocean water into the Atlantic is compensated by an equally large return flow of South Atlantic water into the Indian Ocean (i.e. the super-gyre scenario).

Clearly, the heat and salt flux estimates, as well as the APE en KE values, differ by orders of magnitude. Again, this large range may reflect the natural deviations in these ring properties. Duncombe Rae et al. (1996) found the heat flux values of 4

Authors	F_Q (TW)	F_S (Gg/s)	APE (PJ)	KE (PJ)
Olson and Evans (1986)			30.5-51.4	6.2-8.7
Duncombe Rae et al. (1989)	25	0.63		
Duncombe Rae et al. (1992)			38.8	2.3
Van Ballegooyen et al. (1994)	7.5	0.42		
Byrne et al. (1995)			18	4.5
Clement and Gordon (1995)			7.0	7.0
Gründlingh (1995)	6.3–15.8			
Duncombe Rae et al. (1996)	1.74	0.11	11.3	2.01
Lutjeharms and Cooper (1996)[a]	1.1	0.015-0.046		
Garzoli et al. (1996)	1.0-1.6	0.07-0.10	2.8-3.8	
Goñi et al. (1997)			24	

[a]Filaments

Table 2.3: *Estimates of Agulhas ring properties. Heat (F_Q) and salt (F_S) fluxes, as well as the available potential energy (APE) contents of a ring, are calculated with respect to the direct surroundings of the rings.*

Agulhas rings ranging between 0.60 and 1.81 TW, and the salt flux values between 0.04 and 0.12 Gg s^{-1}. They furthermore reported APE values between 7.45 and 23.04 PJ, whereas Goñi et al. (1997) reported values between 1 and 71 PJ for 17 rings.

We may thus conclude that the heat and salt fluxes brought about by an Agulhas ring are in the order of 1-10 TW and 0.1-0.5 Gg s^{-1}, with respect to the surrounding South Atlantic Thermocline Water.

Accurate estimates of the number of rings entering the Atlantic were not made until satellite data became available. Two techniques are commonly in use. Infrared thermal images portray the surface temperatures of the ocean water, revealing different water masses and flow patterns in regions where thermal contrasts are present. The strong thermal contrasts in the region of the Agulhas Current and its Retroflection makes this area suitable for infrared studies, although these studies suffer from the high degree of cloudiness in this area.

Infrared thermal images were used by Lutjeharms and Van Ballegooyen (1988) to study the process of ring shedding in detail. They interpreted abrupt regressions of the Retroflection as ring shedding events, occurring between 6 and 12 times per year in a period between 1978 and 1983 (Table 2.4). The large number of events with respect to the other estimates may indicate a large ring-shedding activity during that period. However, as not all of these events are shown to generate well-developed rings drifting into the Atlantic, this estimate is probably too high.

Lutjeharms and Cooper (1996) used infrared images to study interbasin fluxes brought about by the intrusion of Agulhas filaments into the Atlantic Ocean. These features also contain Indian Ocean water, but are less coherent than rings. Due to their small depth, the volume transport brought about by these features is small, and also their thermal signature is rapidly lost to the atmosphere. Even so, they may

Authors	# (yr^{-1})	device	date
L and Van B (1988)[a]	6-12 (9)	infrared	1978 - 1983
Gordon and Haxby (1990)	5	altimeter	11 1986 - 11 1987
Feron et al. (1992)	4-8 (6)	altimeter	11 1986 - 09 1989
Van Ballegooyen et al. (1994)	6	altimeter	12 1986 - 12 1988
Byrne et al. (1995)	6	altimeter	11 1986 - 08 1989
Gründlingh (1995)	5	altimeter	10 1992 - 11 1993
Duncombe Rae et al. (1996)	4-6	echo sounder	06 1992 - 10 1993
Lutjeharms and Cooper (1996)[b]	6.5	infrared	1987 - 1991
Goñi et al. (1997)	4-7 (6)	altimeter	09 1992 - 12 1995
Schouten et al. (1999)	4-6 (5)	altimeter	11 1992 - 12 1996

[a]Lutjeharms and Van Ballegooyen (1988)
[b]Filaments

Table 2.4: *Estimates of the number of ring shedding events per year. The numbers in brackets denote the average number.*

contribute considerably to interbasin exchange of salt.

Variability in the sea-surface height can be detected by altimeter devices. These devices use radar to measure the distance between the sea surface and the satellite; changes in dynamical structures can be detected when the signals of several passages are compared. This method is not hindered by cloudiness, and is especially usefull in estimating the number of rings that are shed in the Retroflection region. Results found in literature are listed in Table 2.4. An independent estimate of rings crossing the Benguela Current using 16 months of echo-sounder data (Duncombe Rae et al. 1996) is included for completeness.

It is important to realise that ring shedding is a highly irregular process, and that long periods in which no rings are shed may be followed by periods in which a rapid succession of ring shedding events takes place (Goñi et al. 1997). But with an estimated number of 5 or 6 Agulhas rings per year, we can estimate the exchange between the Indian and Atlantic Ocean by the shedding of Agulhas rings to be of the order of 5-6 Sv for volume, 5-60 TW for heat and 0.5-3.0 Gs s^{-1} for salt (if compared with its surroundings). An additional estimate of the exchange by the drift of Agulhas Current filaments into the Atlantic can be deduced from the average of 6.5 of these features per year. With the values from Tables 2.2 and 2.3, we arrive at 0.65 Sv, 7.15 TW and 0.1-0.3 Gg s^{-1}.

2.5.3 Estimates of Agulhas Leakage: inversion studies

Several attempts have been made to infer the impact of Agulhas inflow by inverting hydrographic data. These studies aim to model the mean state of the ocean circulation by combining hydrographic data, physical principles and *a priori* contraints. The data sets used by these studies are often diverse and non-synoptic, and are not

Authors	SW	IW	DW	BW	F_Q (PW)	date
Fu (1981)	15	10	-24	-2	0.85	07/08 1925
	9	6	-20	1	0.88	04/06 1959
Rintoul (1991)	8	5	-17	4	0.25	04/06 1959
Macdonald (1993)	6.1	7.9	-21.6	7.5	0.3	02 1988/02 1989
Schlitzer (1993)	2.2	10.0	-15.8	3.1	-0.05	historical
B and S (1995)[a]	-1.9	9.8	-8.9	1.1	0.04	historical
Schlitzer (1996)	2.0	11.9	-18.7	4.2	0.3	historical
DLH and S (1999)[b]	-4.9	15.3	-13.6	3.0	-0.25	historical

[a]Boddem and Schlitzer (1995)
[b]De Las Heras and Schlitzer (1999)

Table 2.5: *Results from inversion studies, giving the transports in Sv for different water masses across (approximately) 30° S (positive values denote northward transport), and the corresponding heat flux. The water masses are Surface Water (SW), Antarctic Intermediate Water (IW), North Atlantic Deep Water (DW) and Antarctic Bottom Water (BW).*

able to account for, e.g., the intermittent character of the Agulhas Leakage process. Furthermore, any intra- or interannual variability of the system is lost in obtaining a single best-estimate of the climatology. In fact there are two inversion methods in use: most studies use the inverse method of Wunsch (1978) to estimate property balances within an area enclosed by sections of hydrographic data (Fu 1981; Rintoul 1991; Macdonald 1993). Assuming that the flow is in thermal wind balance, reference level velocities are calculated that satify the conservation of water mass properties within isopycnal layers best. In this method it is assumed that the sections are representative for the mean state of the ocean. The method used by Schlitzer (1993, 1996), Boddem and Schlitzer (1995) and De Las Heras and Schlitzer (1999) uses large historical hydrographic data sets to obtain a more statistically consistent solution. Here mass conservation is perfectly satisfied, and a geostrophic flow field and tracer distributions are obtained which approximate the measurements best.

An overview of results of inversion studies is presented in Table 2.5. In this table, volume transports across 30°S in the Atlantic are listed for four different layers, as well as the resulting heat flux. In general, the four layers refer to density classes that are separated by isopycnals. The choice of these isopycnals is more or less arbitrary, and the exact definition of the layers differs between different studies. In practice, the layers are designated by the principal water masses that constitute them, namely AABW, NADW, Antarctic Intermediate Water (AAIW), and Surface (Thermocline) Water.

The most straightforward interpretation of these transports in terms of their origin is to ascribe the flux in the thermocline layer to Agulhas Leakage, and the flow in the intermediate layers to Drake Passage import. This interpretation requires the least water mass transformations, since direct inflow of Thermocline Water is only possible

in the thermocline connection around southern Africa, whereas AAIW seems to be directly formed by subduction of Subantarctic Water masses along the Subtropical Convergence (Sverdrup et al. 1942). However, care should be taken, since it is possible that Subantarctic Water is strongly modified by heat gain in the Atlantic sector of the Southern Ocean, and enters the South Atlantic thermocline (Rintoul 1991). Indeed, Park and Gamberoni (1997) reported the observation of intrusions of Subantarctic Water that crossed the Subtropical Convergence in the Indian Ocean, whereas Lutjeharms and Van Ballegooyen (1988) observed filaments of Subantarctic Water filling the wake of Agulhas rings in the Agulhas Retroflection area. Furthermore, hydrographic observations suggest (Gordon et al. 1992) that considerable exchange takes place between the Indian and Atlantic Oceans at intermediate depths. Agulhas rings are also known to introduce AAIW into the South Atlantic (e.g., McCartney and Woodgate-Jones 1991). Gordon et al. (1992) even ascribed an important role to this Agulhas exchange of AAIW, since they proposed that Subantarctic Water derived from the Drake Passage recirculates in the Indian Ocean before entering the Atlantic by Agulhas Leakage. This scenario is a sort of hybrid between the warm and cold water route scenarios for NADW renewal.

Another complication to the straightforward interpretation of the transports is the fraction of NADW that upwells in the Atlantic sector of the Southern Ocean, and that is driven back into the Atlantic before it has the chance to escape with the ACC. It enhances the overturning transports in the intermediate or thermocline layers without having entered the Atlantic through the Drake Passage or by Agulhas Leakage. Recent studies point to the possible importance of the ACC as main upwelling site for NADW (Toggweiler and Samuels 1993b; Döös and Coward 1997; the study of Drijfhout et al. (1996a) supported the classic idea of more uniformly distributed upwelling), but most of this upwelling seems to occur gradually while circling several times around Antarctica before reaching the surface (Döös 1995).

A final complication concerning the inference of the amount of Agulhas Leakage from these inversion studies is the fact that the usual break-up into density layers does not account for Agulhas Leakage water that recirculates in the Subtropical Gyre of the South Atlantic, and leaves again on approximately the same density level. In fact, only the component of Agulhas Leakage that takes part in the Atlantic overturning circulation is captured by these estimates.

In view of all these considerations, the net transports within the thermocline and intermediate layers, as calulated by inverting hydrographic data (Table 2.5), may at least be considered as upper boundaries on the total amount of Agulhas Leakage that takes part in the overturning circulation: if no supply from the Drake Passage would be present, and if no direct upwelling of NADW would take place in the Southern Ocean, than all of the calculated transports in the thermocline and intermediate layers must have entered the Atlantic through Agulhas Leakage. But the straightforward interpretation discussed above may be closer to the truth, since it is probable that the cold water route does supply water for NADW renewal. In that light, none of the inversion studies favours a large contribution of Agulhas inflow to the Atlantic overturning circulation.

Fu (1981) ascribed his large northward heat transport across 30°S to heat input

Authors	AL	SW	IW	DW	BW	F_Q (PW)	res.
Semtner and Chervin (1992)[a]	30	12	4.7	-18	1.3	0.60	0.5°
Matano and Philander (1993)	8	6.8	1.6	-10.9	2.5	0.19	1.0°
Cai and Greatbatch (1995)	13	4.7	5.6	-10.6	0.3	0.18	3°
Thompson et al. (1997)	30	12.7	6.8	-20.9	1.4	0.51	0.25°
Marchesiello et al. (1998)		5.3	9	-16	1.7	0.29	1.38°
Zhang et al. (1998)	4	8.4	6.8	-16	0		4°

[a]calculations presented by Barnier et al. (1996).

Table 2.6: *Results from modelling studies, giving heat flux across the 30° S latitude, and the transports in Sv for the same layers as in Table 2.5. The column denoted AL gives the actual amount of water that is exchanged by Agulhas Leakage in these models. The last column gives a rough indication of the model resolution.*

through the ACC, possibly unaware of heat input through Agulhas Leakage. Rintoul (1991), using the same data set at his 30°S boundary, pointed out that Fu's extreme heat flux value is possibly generated by overestimation of Ekman transport and underestimation of Bottom Water transport. Rintoul's results needed a 5 Sv conversion of Subantarctic Drake Passage Water into Lower Thermocline Water to support an 8 Sv northward thermocline transport across 30°S. His 0°E section furthermore showed only a 2 Sv net import of Upper Thermocline Water and a 5 Sv export of Lower Thermocline Water, making a large contribution of Agulhas inflow to NADW compensation unlikely. However, since his AJAX-cruise did not cross a ring, his study possibly underestimated the Indian Ocean contribution. The studies (co-)authored by Schlitzer all displayed a large dominancy of Intermediate above Thermocline Water in compensating NADW export.

Several authors *forced* a heat flux across 30°S onto their solution to verify whether such a flux could be consistent with the data. Imposing a 0.3 PW northward heat flux (De Las Heras and Schlitzer 1999) yielded a circulation pattern that is consistent with observations, and resulted in an increased Agulhas Leakage of 3.1 Sv. But northward heat fluxes of 0.69 and 0.88 PW (Rintoul 1991), 0.8 PW (Macdonald 1993), 0.66 PW (Boddem and Schlitzer 1995) and 0.6 PW (De Las Heras and Schlitzer 1999) yielded unrealistic circulation patterns or too high South Atlantic temperatures, and are inconsistent with observations. Rintoul (1991) also forced a 13 Sv warm Agulhas input into the Atlantic, yielding unrealistic circulation patterns as well, suggesting that such a large amount of Agulhas input is inconsistent with his data set.

2.5.4 Estimates of Agulhas Leakage: model studies

With the steadily growing capabilities of numerical ocean models, the process of Agulhas Leakage is simulated with increasing degree of accuracy. In this section the exchange simulated by state-of-the-art models is discussed in comparison with observations.

Numerical models have the advantage that the dynamical fields are known at any place and time. This enables the calculation of net transports that are brought about by intermittent processes (like Agulhas Leakage), so that detailed and consistent descriptions of the interocean exchange can be obtained. In contrast, observational estimates based on hydrographic data often use only a single snap-shot, and thus lack enough time-resolution to calculate reliable estimates of the total exchange. Furthermore, models calculate the absolute flow field, including the barotropic component. Observational estimates of the absolute flow field generally suffer from large uncertainties, since the barotropic component of the flow is not easily determined.

Barnier et al. (1996) distinguished between global ocean models (e.g., Semtner and Chervin 1992; Zhang et al. 1998; Webb et al. 1998), and basin-scale models (e.g., FRAM Group 1991; Matano and Philander 1993; Marchesiello et al. 1998; Biastoch 1998; Biastoch and Krauss 1999). The latter model a sub-domain of the World Ocean, using open boundaries to represent the interaction with the other basins. Further distinction can be made in eddy-resolving (or permitting) models, whose resolution is high enough to simulate processes like Agulhas ring shedding, and low-resolution models, which often fail to produce Agulhas Leakage. Results of several modelling efforts are presented in Table 2.6; the layer breakdown is similar as in Table 2.5.

The Fine Resolution Antarctic Model (FRAM) models the circulation in the Southern Ocean south of 20°S, and its Indian-Atlantic interocean exchange has been intensively studied. Analysis of the diagnostic phase of FRAM showed a number of 2.3 Agulhas rings shed per year, generating a 0.2 PW heat flux and 10 Sv volume flux (the FRAM Group 1991) into the South Atlantic. Lutjeharms and Webb (1995) studied the ring shedding process in more detail and concluded that the model produces rings which are too large, too warm and too salty relative to observed rings. The number of rings is too low, and the shedding takes place too regularly. Thompson et al. (1997) analysed the prognostic phase of FRAM and concluded that Agulhas Leakage contributes 0.51 PW to the 0.65 PW northward heat flux across 34°S in the Atlantic. They calculated a net Agulhas inflow of 30 Sv. Döös (1995) studied Lagrangian trajectories of this model, and arrived at an Agulhas Leakage of 23 Sv (his ventilated and unventilated direct transports from the Indian to the Atlantic). Obviously, the exchange simulated by the model is much larger than observational estimates (Table 2.1). Comparison of the layer breakdown of the meridional transports in FRAM (Table 2.6) with that of inversion studies (Table 2.5) confirms that the model overestimates the contribution of Thermocline Waters to the Atlantic overturning circulation.

De Ruijter et al. (1999) concluded that a realistic representation of the Agulhas system is possible as far as the mean circulation is concerned, but that the mesoscale variability is still poorly represented by numerical models. High-resolution models seem to suffer from anomalously strong Agulhas Leakage (Semtner and Chervin 1992; FRAM Group 1991; Döös 1995; Thompson et al. 1997; Biastoch and Krauss 1999), probably due to unrealistic ring characteristics (Lutjeharms and Webb 1995). This inflow may also be influenced by the relative inability of (cartesian) ocean models to produce reasonable amounts of AAIW (McCann et al. 1994; Thompson et al. 1997), so that a larger supply of Thermocline Water is necessary to compensate for

NADW export. Low-resolution models generally seem to underestimate (Matano and Philander 1993) or lack (Drijfhout et al. 1996a) Agulhas Leakage. The resulting underestimation or absence of Agulhas heat input is often compensated by increased atmospheric heat input into the South Atlantic.

2.6 Conclusion

In this chapter several studies were discussed that deal with the exchange of volume, heat and salt between the Atlantic Ocean, and the rest of the World Ocean. The North Atlantic communicates with the Pacific through the Bering Strait. The transport through this passage is relatively well established: a 0.8 ± 0.1 Sv volume flux enters the Arctic through this Strait, as well as a 26 Sv psu salt flux.

The exchange between the South Atlantic and the rest of the World Ocean is less well determined, mainly due to the large geographical extent of the Southern Ocean, and the intermittent and varying nature of the fluxes across the open boundaries of the Atlantic. Some studies have considered zonal transports through the Southern Ocean as a whole, while others concentrated on the ACC only, the Weddell Gyre or the Agulhas Retroflection Area. A mean ACC volume transport through the Drake Passage of 134 ± 13 Sv (Nowlin and Klinck 1986) seems to be consistent with several other estimates. This transport generates a heat flux of about 1.3-1.4 PW. The total salt flux is dominated by advection of the mean salinity, but estimates of the residual salt transport arrive at -20.58 Sv psu. The strength of the Weddell Gyre is in the order of 60 Sv.

Several methods have been applied to estimate the amount of Agulhas Leakage. The wide range in the resulting estimates can be ascribed mainly to the large variability of this exchange. Estimates based on direct geostrophic calculations range between 3 and 14 Sv, depending on the reference level and the data used. Estimates based on the volume of Agulhas rings and their shedding frequency amount to an exchange of about 6 Sv. Estimates of the heat and salt transports brought about by these rings range between 5 and 60 TW, and between 0.5 and 3.0 Gg s^{-1} on a yearly base (if referenced to their surroundings). An additional exchange by the drift of Agulhas Current filaments into the Atlantic is estimated at 0.65 Sv, 7.15 TW and 0.1-0.3 Gg s^{-1}.

It is concluded that the applicability of inversion studies to deduce the amount of Agulhas Leakage is limited. Most inversion studies agree in their conclusion that participation of a large amount of Agulhas Leakage in the overturning circulation is not consistent with the data, but a quantification of the amount of Agulhas Leakage that *is* supported cannot be given. In general these studies are not able to resolve the component of Agulhas Leakage that is recirculated in the South Atlantic and leaves the Atlantic on approximately the same density level.

Finally we have seen that numerical ocean models are in general not able to simulate Agulhas Leakage sufficiently accurate to offer reliable estimates of the exchange. In general, low-resolution models do not simulate Agulhas Leakage, but seem to compensate for this absent warm water input by increased atmospheric heat input.

High-resolution models do simulate Agulhas Leakage, but tend to overestimate the exchange. We must keep in mind, however, that these models are compared with observations which are characterised by large ranges and uncertainties themselves.

Chapter 3

Atlantic interocean exchange in an OGCM

In this chapter, the exchange of water, heat and salt is studied between the Atlantic and the rest of the World Ocean in the OCCAM General Circulation Model. To this end, the fluxes across a zonal trans-Atlantic section at 34° S and two meridional sections at 20° E and 70° W are analysed. The transports and the thermohaline fields are compared with observations. Furthermore, horizontal and vertical distributions of these fluxes are determined to identify the important regions of the interocean fluxes. Some of these profiles are used as forcing functions in following chapters of this thesis. Finally, the implications of these results for the NADW renewal route are discussed.

3.1 Introduction

The Atlantic Ocean communicates freely with the rest of the World Ocean. It exports its North Atlantic Deep Water (NADW) for distribution among the other basins, and shallower water masses are imported as compensation. The exchange of water masses with different temperatures and salinities results in interocean fluxes of heat and salt. These fluxes strongly influence the thermohaline stratification within the basins that are involved in the exchange. In following chapters of this thesis it is shown that this may have consequences for the strength and stability of the overturning circulation in the Atlantic; the interocean fluxes of buoyancy act as sources or sinks of potential energy, that may be used to drive the flow. In this light, it is obvious that the amount of buoyancy that is exchanged is not the only aspect of interocean exchange that impacts on the Atlantic stratification: the spatial distribution of these fluxes plays a role as well. Obviously, a buoyancy flux at depth has a different impact on the stratification and potential energy of the Atlantic than buoyancy exchange at shallower levels.

In the former chapter an overview was given of earlier studies addressing the exchange of water, heat and salt between the Atlantic and the rest of the World Ocean.

This resulted in a summary of what is known about the interocean exchange, mainly based on observations. However, most of these studies focussed on determining the net fluxes through a section, and did not explicitly address the vertical or horizontal distributions with which these fluxes are brought about. One way to fill this gap in knowledge would be to deduce heat and salt flux distributions from hydrographic data. However, transport estimates based on observations are often highly uncertain. A main source of uncertainty is caused by the difficulty in estimating the barotropic component of the flow, or equivalently in choosing an unambiguous level of no (or known) motion. Transports through narrow straits, like the Bering Strait and, to a lesser extent, the Drake Passage, are relatively well determined from measurements, and are gratefully added to the short list of reliable constraints on the global ocean circulation (e.g., Wijffels et al. 1992; Holfort 1994). But estimating transports across wider sections (like meridional section in the Southern Ocean, for instance) remains a difficult task. And the fact that net transports are often just residual currents in strong and energetic circulation systems, increases their uncertainties even further.

Another aspect that increases the uncertainty of observation-based transport estimates is the fact that hydrographic measurements are often sparse both in time and space. This is especially problematic for determining time-mean transports of current systems that display a high degree of variability, whether on interannual, seasonal or smaller time scales. Furthermore, inversion studies, combining several hydrographic sections into a single and consistent 'best estimate' of the transports, often use non-synoptic sections (e.g., Rintoul 1991) that may be judged incompatible with respect to seasonal or interannual variability. The recent hydrographic dataset from the World Ocean Circulation Experiment (WOCE) comes close to synopticity on interannual time scales (e.g., Holfort 1994), and the increasing use of moored instruments (e.g., Garzoli et al. 1996) allows for better estimates of the time-variability of transports. Better estimates of the time-mean transports throughout the World Ocean may be expected in the near future.

In this chapter, an alternative approach is used: the interocean exchange is studied in a state-of-the-art Ocean General Circulation Model (OGCM). The steadily increasing resolution and the continuing improvements in the physical parameterisations make the newest generation of OGCMs increasingly usefull as tool in studying ocean circulation. Output of numerical ocean models has the advantage that all dynamical fields are known everywhere and at any time, enabling a concise and consistent description of the model's circulation and transports. Furthermore, the barotropic component of the flow is solved as an integral part of the system of equations, and is therefore completely determined.

However, it must be kept in mind that the simulated ocean circulation is a far from perfect representation of the real ocean circulation. One problem often encountered in high-resolution modelling efforts is that the enormous number of degrees of freedom severely contrains the integration period, allowing for model runs of several decades at best. Clearly, with the adjustment time of baroclinic Rossby waves being already in the order of decades, and with the thermohaline fields adjusting on millennial time scales, this is insufficient for the dynamical fields to equilibrate. Another problem that may give rise to unrealistic features in the simulated ocean circulation is

the relatively poor representation of the surface forcing. Using monthly averaged climatologies in annually repeated cycles goes without the variability that characterises the air-sea interaction in the real ocean. And despite the increasing spatial resolution of these models, physical processes remain that cannot be resolved and need to be parametrised. But despite all these, and more, deficiencies and imperfections of numerical models, analysis of their circulation may increase our knowledge of the processes involved in interocean exchange in the real ocean. They provide a view of the exchange that is both concise and consistent, and give an impression of the spatial characteristics of this exchange that is hard to obtain from observational data.

In this chapter the exchange is analysed between the Atlantic and the other oceans in a high-resolution OGCM. To this end, output from the OCCAM model has kindly been made available by the OCCAM group. Two meridional sections at 70°W and 20°E in the Southern Ocean, and one zonal trans-Atlantic section at 34°S, border the Atlantic sector of the Southern Ocean. The 20°E section is subdivided into the three main dynamical regimes at this longitude, namely the Agulhas Retroflection area, the Antarctic Circumpolar Current (ACC) and the Weddell Gyre. The transports and thermohaline fields at the meridional sections are analysed and compared with observations, in particular with two corresponding sections from the Hydrographic Atlas of the Southern Ocean (Olbers et al. 1992). The net fluxes are also compared with a published analysis of the OCCAM-predecessor FRAM (Fine Resolution Antarctic Model, Thompson et al. 1997). The output of this model has been extensively studied (FRAM Group 1991; Saunders and Thompson 1993; Döös 1995; Lutjeharms and Webb 1995), and the results of these studies may help in analysing the fluxes in OCCAM. Subsequently the fluxes across the meridional sections are integrated vertically to identify the horizontal distribution of the heat and salt fluxes. Horizontal integrations show the vertical distributions of these fluxes. In this way, a concise picture of the spatial distribution of the heat and salt fluxes emerges. Finally the results are discussed in the light of the importance of Agulhas Leakage for NADW compensation in the model, leading to error estimates for the heat and salt input brought about by Agulhas Leakage.

3.2 The sections

3.2.1 The OCCAM General Circulation Model

The Ocean Circulation and Climate Advanced Modelling (OCCAM) project is a high-resolution modelling effort at the Southampton Oceanographic Centre, aimed at the development of global ocean models which are suitable for climate studies. The OCCAM model is a modified version of the Bryan-Cox-Semtner code (Webb et al. 1998). It has a resolution of 0.25° in both longitude and latitude, and consists of 36 levels in the vertical. It applies a free-surface formulation, so that the exchange of freshwater with the atmosphere is represented by a freshwater flux, rather than by an implied salt flux. This guarantees salinity to be conserved globally. Details of the model are described in Webb et al. (1998), and more information about the model and products can be found at www.soc.soton.ac.uk/JRD/OCCAM.

In the first main run, the OCCAM model has been integrated for 14 years. During the first 4 years, the model was in a robust diagnostic mode, and the fields of potential temperature and salinity were strongly relaxed to the climatologies of Levitus (1982), Levitus and Boyer (1994) and Levitus et al. (1994). After this diagnostic phase of the spin-up, the model was run in prognostic mode for four more years. The last 6 years of the run have been released for analysis. A 6-year average of the dynamical fields has been constructed to serve as a climatology of the model.

It is obvious that we cannot expect the dynamical fields to have reached an equilibrium in the integration period of only 14 years. The time-scale of adjustment by baroclinic Rossby modes is already in the order of decades (Gill 1982), and the thermohaline fields adjust on time-scales in the order of millenia. Saunders et al. (1999) analysed the model drift in OCCAM, and reported a rise in global temperature of 0.02°C per year. The global temperature at the end of the 14-year run is consequently 0.2°C higher than in the climatologies of Levitus (1982) and Levitus and Boyer (1994), that were used for the model spin-up. Clearly, the short integration period prevents the thermohaline fields from drifting away too far from these observation-based climatologies. In fact, Saunders et al. (1999) reported a sharpening of the thermohaline structures in the model, rectifying the unrealistic smoothness of the climatologies that resulted from the averaging procedures.

Analysis of the meridional transports in the Pacific showed that the model displays considerable storage of heat in this basin, consistent with the general temperature rise. The storage of freshwater in the Pacific turned out to be very small, but the meridional salt transport in the Pacific showed variations in the order of 2 Sv psu, about 10% of the 21.5 Sv psu net transport through the Bering Strait.

3.2.2 The thermohaline fields

Two meridional sections of the U.K. OCCAM model are analysed, one at 70°W (through the Drake Passage) and one at 20°E (between South Africa and Antarctica, crossing the Agulhas region). Additionally, a zonal trans-Atlantic section at 34°S is analysed. Figures 3.1 and 3.2 show the distributions of temperature T (upper panels) and salinity S (lower panels) at the 70°W and 20°E sections, respectively. The large scale thermal and saline structures at these sections can be compared with corresponding sections in the Hydrographic Atlas of the Southern Ocean (plates 65 (20°E) and 74 (75°W) from Olbers et al. (1992). This atlas is also accessible via www.awi-bremerhaven.de/Atlas/SO). The comparison of some key-features are described here.

At 70°W, there is good agreement about, for instance, the depth of the 2°C isotherm just south of the South American continent (2000 m). The latitude where this isotherm surfaces is well reproduced (60°S), although its maximum southward extension is slightly overestimated by the model (66°S vs. 64.5°S in the Atlas). The depth of the 34.2 psu isohaline does not exceed the 500 m in the model, whereas it reaches as deep as 800 m in the Atlas. The salinity of the almost isohaline water at depth (between 34.7 and 34.75 psu) is well reproduced by the model. However, the doming structure of the deeper isohalines in the model is not present in the Atlas.

At 20°E, there is good agreement about the 2000 m depth of the 0°C isotherm

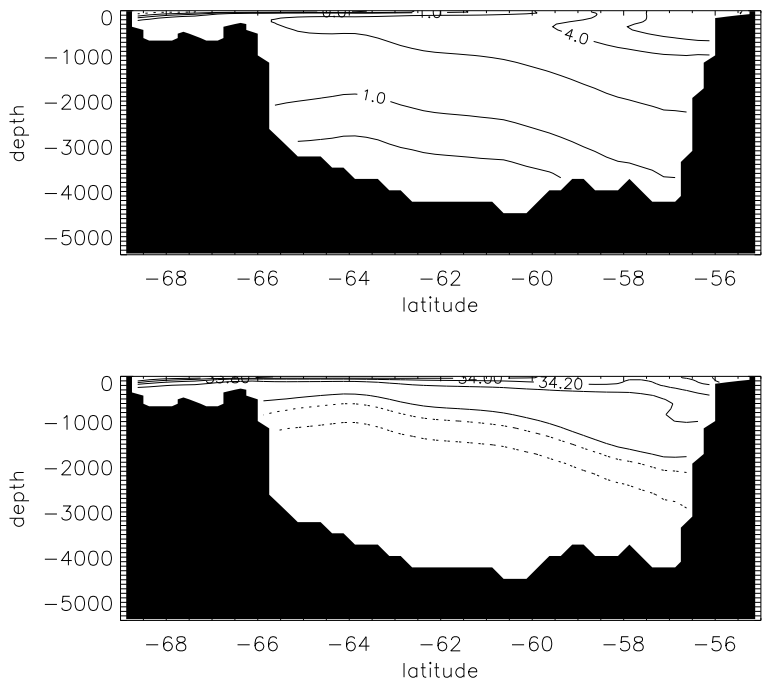

Figure 3.1: *Temperature T (upper panel) and salinity S (lower panel) at the 70° W section through the Drake Passage. Contours of T are (-0.5, 0, 0.5, 1, 2, 4, 6, 9, 12, 15)° C, negative contour is dashed. Contour interval of S is 0.2 psu (solid contours), dashed contours are (34.65, 34.7, 34.75) psu.*

in the area between 70°S and 55°S (i.e., the Weddell Gyre). However, the deeper isotherms shown in the Atlas exhibit a bowl-like structure in this area, whereas they are doming in the model. This must have consequences for the simulation of the baroclinic structure of the Weddell Gyre. There is also good agreement about the position of the 2°C isotherm, situated at 3000 m depth just south of Africa, and surfacing close to 50°S. The model agrees with the Hydrographic Atlas about the salinity of the almost isohaline waters south of 55°S (between 34.65 and 34.70 psu). Furthermore, they agree in the position and salinity of the high-salinity (>34.8 psu) core between 2000 and 3500 m depth south of South Africa. This high salinity is indicative of NADW, and the presence of this water mass in the Agulhas Retroflection Area is in agreement with observations (Gordon et al. 1987). At approximately 44°S, the 34.4 psu isohaline hints at the presence of a low-salinity tongue extending northward, indicating the presence of Antarctic Intermediate Water (AAIW). The model underestimates the northward extension (44°S) and depth (± 850 m) of this isohaline (42°S and 1000 m in the Hydrographic Atlas). This indicates that the subduction of AAIW along the Antarctic Polar Front (Sverdrup et al. 1942) is underestimated in this model, as is often the case in numerical models (e.g., McCann et al. 1994).

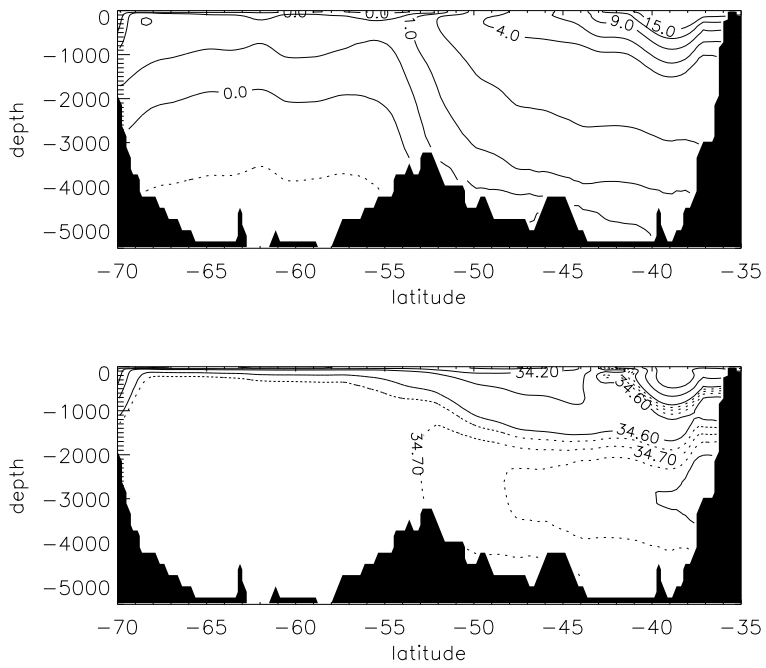

Figure 3.2: *Temperature T (upper panel) and salinity S (lower panel) at the 20° E section between Antarctica and South Africa. Contouring as in Fig. 3.1.*

3.2.3 The flow fields

Figure 3.3 (upper panel) shows that the flow through the Drake Passage is predominantly eastward. At deeper levels, and close to the South American continent, a countercurrent is visible. The total mean volume flux across this 70°W section amounts to 153.57 Sv. This transport of the ACC is somewhat higher than the 134 ± 13 Sv estimate of Nowlin and Klinck (1986), based on a large number of independent observational estimates. The Agulhas Current (AC) is centered around 38°S (Figs. 3.3 (lower panel) and 3.4, (upper panel)). It transports about 100 Sv (Fig. 3.4, lower panel), in close agreement with the 95 Sv estimate of Gordon et al. (1987). The return current at 40°S probably consists of the model equivalents of the Agulhas Return Current (ARC), and that part of the South Atlantic Current that enters the Indian Ocean (SAC). The boundary between the westward AC and the eastward SAC+ARC system is approximately at $\theta_{ac} = 39.00°$S, whereas the southern boundary of the SAC+ARC system (θ_{sac}) is at 41.25°S. Also visible in Fig. 3.4 (upper panel) is the Weddell Gyre. The westward part of this gyre, adjacent to the Antarctic coast, transports nearly 50 Sv. This is of the right order of magnitude as the Schröder and Fahrbach (1999) estimate of 66 Sv across the Greenwich meridian.

Despite the fact that the volume transports of some of the key features are reasonably well simulated, there are some curious features that have not been observed

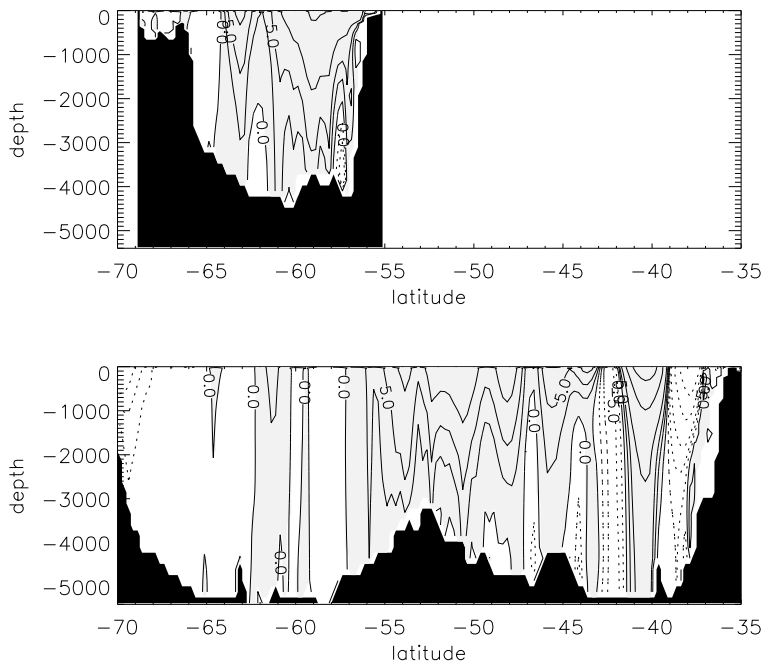

Figure 3.3: *Zonal velocity u at the 70° W section through the Drake Passage (upper panel), and at the 20° E section between Antarctica and South Africa (lower panel). Contours are 0 and ± (2.5, 5, 10, 25, 50, 100) cm/s, negative contours are dashed, shaded areas indicate positive u.*

in the real ocean. South of the SAC+ARC system, for instance, the eastward flow is bounded by a curious and particularly strong current that transports about 25 Sv westward. Inspection of animated time-series of SST and SSH in the Retroflection Area (http://www.soc.soton.ac.uk/JRD/OCCAM/agulhas.html) suggests that the retroflected and meandering Agulhas Return Current generates quite persistent cyclonic eddies just south of the Subtropical Convergence (STC). Cyclonic eddies are observed at the STC South of Africa (Lutjeharms and Valentine 1988), but most of these are found in the vicinity of the Agulhas Plateau, roughly at 27°E. Persistent cyclones immediately south of the Agulhas Retroflection have, to my knowledge, not been observed in the real ocean. They are probably spurious features of the model.

The zonal velocity fields at 20°E and 70°W display a pronounced banded structure (Fig. 3.3), that is even more clear in the vertically integrated transports (Fig. 3.4, upper panel). The fact that this structure appears in a 6-year averaged flow field suggests that the pattern of a succession of jets is quite persistent. Although the Southern Ocean is renowned for its large number of fronts and frontal zones (Nowlin and Klinck 1986), there is no observational evidence that the number of accompanying jets is so large as in this model. The banded structure may be an artefact of averaging mesoscale eddy-activity that is known to take place at the fronts. Alternatively, it

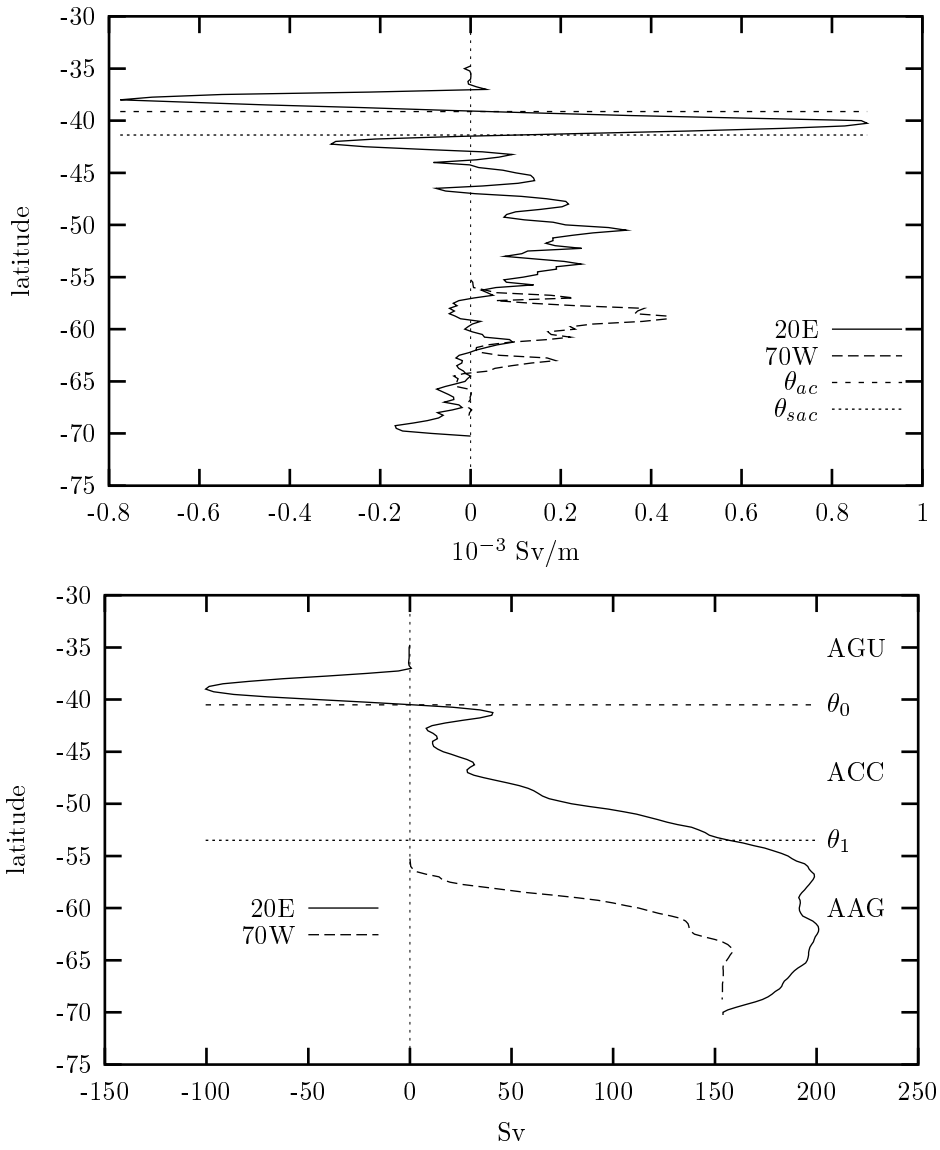

Figure 3.4: *Upper panel: Vertically integrated volume transports across 70° W (Drake Passage, dashed line) and across 20° E (solid line). The latitudes θ_{ac} and θ_{sac} are the southern boundaries of respectively the Agulhas Current and the SAC+ARC system (i.e. zero crossings of the transport). Lower panel: Cumulative zonal transports, integrated southward from the northern boundary. The latitudes θ_0 and θ_1 denote the boundaries between the AGU, ACC and AAG subsections.*

may be caused by jets shifting between two or more preferred positions, possibly related to topographic features. A jet that is in one position part of the year, and in another during the rest of the year, appears in a 6-year average as two distinct jets. However, no indication of the existence of multiple equilibria has been found in the literature. Inspection of the time-dependent flow field could resolve this issue, but this is left for future study.

It is clear that the model representation of the ocean circulation shows some inconsistencies with respect to observations. Although these observations are often highly uncertain themselves, care must be taken when interpreting the model results in terms of the exchange in the real ocean. Nevertheless, I believe that the large-scale characteristics of the thermohaline structure, as well as the dominant current systems, are sufficiently well reproduced to justify continuing the analysis of the interocean exchange in this model.

3.2.4 The subsections

From the cumulative transport curve (Fig. 3.4, lower panel) three subsections of the 20°E section can be defined. The first subsection (denoted AGU) is bounded by the African continent and the latitude θ_0 (40.50°, if rounded to the nearest grid point). At this latitude the cumulative transport crosses zero, so that there is (almost) no net transport (1.66 Sv) through this subsection. This section comprises the Agulhas Current and a part of the SAC+ARC system. The second subsection (denoted ACC) is bounded by θ_0 and θ_1, and contains most of the ACC. The latitude $\theta_1 = 53.50°$S is defined so that the cumulative transport of 155.34 Sv through this section (almost) matches the 153.57 Sv transport through the Drake Passage. The region between θ_1 and Antarctica (denoted AAG) consists of an Antarctic gyre, which can be interpreted as the Weddell Gyre. By construction, the net transport through this section is almost zero (-2.93 Sv) as well.

Thompson et al. (1997), in their analysis of the FRAM model, defined an Agulhas section in a similar way as has been done here. They did not consider separate ACC and Weddell Gyre sections. In places where our results are compared with theirs, the transports of the Weddell Gyre are added to those of the ACC. In these cases, the 20°E section is subdivided into two subsections, the AGU section north of θ_0, and the ACC+AAG section south of this latitude.

3.3 Net fluxes of volume, heat and salt

3.3.1 Calculating the fluxes

The net fluxes of heat and salt across a section are calculated according to:

$$F_Q = \int \rho c_p u (T - T_0) dA \tag{3.1a}$$

$$F_S = \int u (S - S_0) dA. \tag{3.1b}$$

T_0 and S_0 are reference values of temperature and salinity. For the salt flux, multiplying $u(S - S_0)$ with the in-situ density is not consistent with the Boussinesq approximation that has been applied in the model, as $\rho_0 S$ is treated as a conserved quantity, rather than ρS. Often the density is not taken into account at all, and the salt flux is expressed in units of Sv psu (10^6 m^{3}g kg^{-1}s^{-1}). This approach has been adopted here. With ρ and ρ_0 being of the order of 10^3 kg m^{-3}, 1 Sv psu is roughly equivalent to about 1 Gg s^{-1}.

It is assumed that advection is the dominant transport mechanism, and only advective fluxes are considered here. In FRAM, diffusion contributed 20% at best to the total meridional heat transport in the Southern Ocean (Thompson et al. 1997). The diffusive contribution to zonal heat and salt transports must be much smaller, since both the small-scale thermal and haline gradients associated with fronts, as well as the large-scale gradients generated by atmospheric forcing, have a dominant meridional component. The uncertainties introduced by neglecting the diffusive contributions may thus be considered small. Furthermore, as the fluxes are calculated from the climatological fields of temperature, salinity and velocity, the resulting fluxes do not include transient components due to intermittent processes like ring shedding. Especially in the highly variable Agulhas region, this might lead to un underestimation of the actual fluxes of heat and salt. However, analysis of the heat exchange in FRAM (Thompson et al. 1997) has shown that even in the highly variable Agulhas Retroflection region the contribution of this transient term to the heat flux is small.

When heat and salt fluxes are calculated over a section that features a net volume transport, there is some ambiguity in choosing appropriate reference values for temperature and salinity (T_0 and S_0 in Eq. (3.1)). The physical concept of heat transfer is based on temperature differences, and the heat transported by an unbalanced mass flux is consequently undefined. A net mass flux does sustain a flux of internal energy, but this is based on the absolute temperature (in Kelvin). Nevertheless, choosing $T_0 = 0$ may be the most usefull choice, and interprets the heat flux as a temperature flux.

Choosing $S_0 = 0$ unambiguously yields the total salt flux across a particular section. However, when flux profiles are studied, this choice may not be appropriate. Splitting the salinity field into a characteristic value S_0 and a deviation S' yields a salt flux $vS = vS_0 + vS'$ that is obviously dominated by its first component, since S_0 is characteristically in the order of 35 psu, whereas S' is only about 2 psu. Intuitively it may be clear that advection of salt *anomalies* has more dynamical significance than advection of a mean salinity S_0. However, it is not clear what average should be taken to allow for a meaningfull interpretation of the residual fluxes. In the following chapters it is shown how fluxes of heat and salt entering the Atlantic are closely linked to the potential energy balance of this ocean. Exchanging water with the same (potential) temperature and salinity as the Atlantic mean values does neither modify the averaged temperature and salinity, nor the basin-averaged potential energy of the basin. Therefore, the temperature and salinity must be referred to the Atlantic mean values to allow the fluxes to be interpreted in terms of potential energy sources or sinks.

Heat and salt fluxes across the sections 70°W and 20°E have been calculated

section	Volume	Heat flux (PW)			Salt flux (Sv psu)	
	(Sv)	$T_0 = 0$	FRAM	$T_0 = T_m$	$S_0 = 0$	$S_0 = S_m$
70°W	153.57	1.93	1.97	-0.52	5298.05	-67.76
20°E	154.03	1.15	1.19	-1.31	5310.19	-71.66
AGU	1.66	-1.12	-0.51	-1.15	47.17	-10.85
ACC	155.30	2.27		-0.20	5361.40	-64.75
AAG	-2.93	0.00		0.05	-98.38	3.95
ACC+AAG	152.37	2.27	1.70	-0.15	5263.02	-60.80
34°S	-0.49	0.59	0.65		-19.14	
20°E-70°W	0.46	-0.78	-0.78	-0.79	12.14	-3.90
20°E-70°W+34°S	-0.03	-0.19	-0.13		-7.00	

Table 3.1: *Transport values through the different sections. The 20° E section is split into an Agulhas section (AGU), a section that includes the Antarctic Circumpolar Current (ACC), and a section comprising the Weddell Gyre (AAG). Heat and salt fluxes are calculated with respect to zero reference value ($T_0 = S_0 = 0$) and to Atlantic mean values ($T_0 = T_m; S_0 = S_m$). FRAM values (calculated with $T_0 = S_0 = 0$) are from Thompson et al. (1997).*

with respect to zero reference values ($T_0 = 0$ and $S_0 = 0$), and with respect to the Atlantic mean values of potential temperature ($T_0 = T_m$) and salinity ($S_0 = S_m$, Table 3.1, Fig. 3.5). However, the Atlantic mean values of temperature and salinity in OCCAM were not available at this time. The values of T_m and S_m that are used here ($T_m = 3.86$°C and $S_m = 34.94$ psu) have been derived from the Levitus (1982) climatology. This alternative may be considered as the most appropriate, since the model has been initialised with this same climatology (and its Levitus and Boyer (1994) and Levitus et al. (1994) follow-ups). Saunders et al. (1999) report an increase in global mean temperature of only 0.2°C in the subsequent 10 years of integration. Although the temperature change in individual basins may be larger, we assume that the Levitus (1982) values of T_m and S_m are close enough to the OCCAM Atlantic mean values to justify their use in the flux calculations presented here.

3.3.2 Volume fluxes

As the circulation in the model has not reached an equilibrium, the oceanic volume fluxes are probably not in balance. However, Saunders et al. (1999) have shown that the volume storage in the Pacific is small, so we may assume here that the volume storage in the Atlantic is negligible as well. We can express the Atlantic volume balance as follows:

$$V_b - (\overline{u}^{20E} - \overline{u}^{70W}) = V_a, \tag{3.2}$$

where $\overline{u}$ denotes integration of the zonal velocity field over the section indicated, V_b is the Bering Strait import, and V_a is the freshwater export to the atmosphere. According to Saunders et al. (1999), there is a $V_b = 0.675$ Sv inflow through the Bering Strait, and with a 0.46 Sv volume flux divergence between 20°E and 70°W,

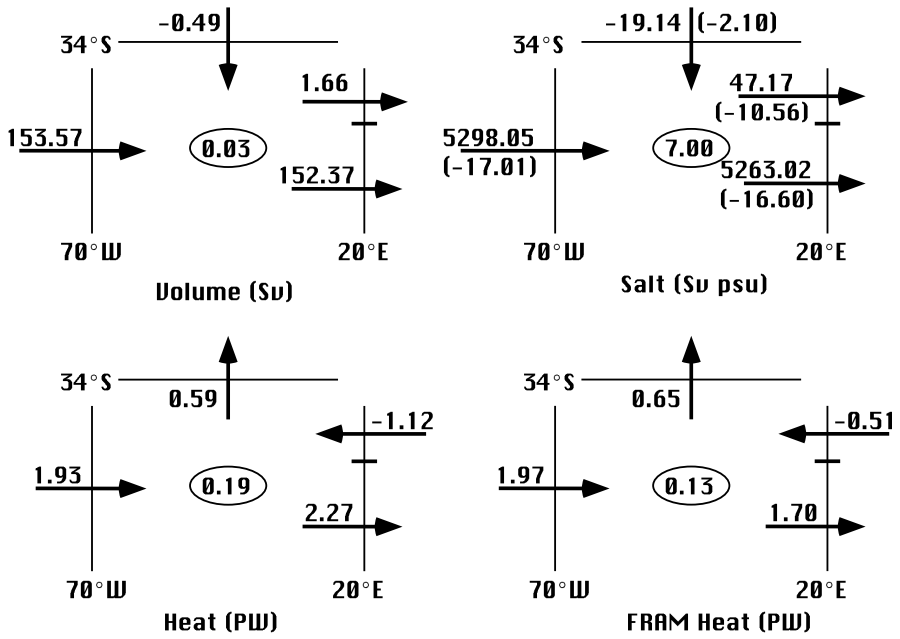

Figure 3.5: *Schematic representation of the volume, heat and salt fluxes in OCCAM across the 70° W, 20° E and 34° S sections, bounding the Atlantic sector of the Southern Ocean. The corresponding heat fluxes in FRAM (Thompson et al. 1997) are included for comparison. The flux convergences, presented in the ovals, reflect the effects of air-sea fluxes, storage, diffusion or eddy transports. The salt transports in parentheses denote residual contributions, i.e.,* $\overline{v'S'} = \overline{vS} - \overline{v}\bar{S}$.

V_a amounts to 0.22 Sv. This value is low compared to the Baumgartner and Reichel (1975) estimate of 0.54 Sv excess evaporation over precipitation in the Atlantic, but agrees in the sign of the flux. This indicates that the Atlantic is correctly simulated as an evaporative basin in OCCAM.

3.3.3 Heat fluxes

The heat fluxes associated with these volume transports are 1.93 PW (with respect to $T_0 = 0.0$) across 70°W and 1.15 PW across 20°E (Table 3.1, Fig. 3.5). The resulting 0.78 PW heat flux convergence in the Atlantic sector of the Southern Ocean is twice as large as the 0.3 ± 0.3 PW estimated by Georgi and Toole (1982) on the basis of hydrographic data. The model also features a 0.59 PW northward heat transport across 34°S in the Atlantic. This amount is relatively high in comparison with South Atlantic heat flux estimates that have been obtained by inversion studies (Table 2.5), but it is in line with other modelling studies (Table 2.6). It causes a 0.19 PW heat flux convergence in the Atlantic sector of the Southern Ocean.

The OCCAM values presented here are in close agreement with the FRAM results of Thompson et al. (1997) (Fig. 3.5). In FRAM, the 0.13 PW heat convergence was augmented by a 0.12 PW atmospheric heat input, resulting in a 0.25 PW storage in the Atlantic sector of the Southern Ocean. But, although in OCCAM the heat transports across 20°E correspond closely to those in FRAM, the subdivision between the AGU and ACC+AAG section is strikingly different. In OCCAM, the Agulhas Retroflection area generates no less than 1.12 PW heat import into the Atlantic, twice as much as the 0.51 PW heat input in FRAM. An explanation for this discrepancy may be found in the fact that the sensitivity of the AGU heat transport to the exact position of the bounding latitude θ_0 is very large, due to very strong meridional gradients in the cumulative heat transport curve (their Fig. 2). Shifting θ_0 one gridpoint to the south reduces the cumulative heat transport to only 0.63 PW (with respect to $T_0 = 0$, Table 3.3).

Furthermore, the 1.12 PW heat input in the Agulhas section also contrasts strongly with the 0.023–0.47 PW observational heat flux estimates of Gordon (1985), that were based on a 14 Sv inflow being compensated either by South Atlantic surface waters or by NADW. This indicates that OCCAM probably overestimates the amount of Agulhas Leakage, as well as its associated heat flux. According to Chapter 2, unrealistically strong Agulhas Leakage is a feature common to several high-resolution OGCMs. Thompson et al. (1997), Semtner and Chervin (1992) and Biastoch and Krauss (1999) all report an Agulhas Leakage of about 30 Sv in their high-resolution models. The reason for this large exchange is not clear, but it may be that some aspects in the retroflection dynamics are not well represented (De Ruijter et al. 1999). Lutjeharms and Webb (1995), for instance, pointed at the excessive size of the Agulhas rings that are shed in the Retroflection Area of FRAM, and their large heat content. Dijkstra and De Ruijter (2000) showed that the modelled separation, inertial overshoot and retroflection of the Agulhas Current are extremely sensitive to the eddy viscosity and horizontal resolution of the model. The OGCMs are probably still too viscous.

3.3.4 Salt fluxes

When addressing the salt balance of the model Atlantic, we have to take storage into account. We can write the salt balance as:

$$V_{Atl}\frac{d\bar{S}}{dt} = V_b S_b - (\overline{uS}^{20E} - \overline{uS}^{70W}), \tag{3.3}$$

where V_{Atl} denotes the volume of the Atlantic basin, and $\bar{S}$ the averaged salinity. With the Bering Strait salinity S_b being 31.9 psu, we have a 21.53 Sv psu Bering Strait salt transport (Saunders et al. 1999). This value is somewhat smaller than the 26.0 Sv psu estimate of Coachman and Aagaard (1988), due to lower Bering Strait salinities and transport in the model. With only a 12.14 Sv psu salt transport difference between 70°W and 20°E, this indicates a storage of 9.39 Sv psu in the whole Atlantic. The 19.14 Sv psu southward salt flux across 34°S indicates that most of this storage (7.0 Sv psu) takes place in the Atlantic south of 34°S.

section	T (°C)	S (psu)
70°W	1.72	34.61
20°E	1.32	34.67
AGU	4.59	34.78
ACC	2.03	34.65
AAG	-0.05	34.65
ACC+AAG	0.85	34.65
34°S	4.20	34.78
Atlantic	3.86	34.94

Table 3.2: *Averaged T and S at the different (sub)sections. The Atlantic averages are calculated from the Levitus (1982) data set.*

By splitting the zonal velocity fields at the meridional sections into an average component with integral $\overline{u}$, and a deviation u' with zero integral, we can rewrite the salt transport difference between 70°W and 20°E as follows:

$$\begin{aligned}\overline{uS}^{20E} - \overline{uS}^{70W} &= \overline{u}^{20E}\bar{S}_{20E} + \overline{u'S}^{20E} - \overline{u}^{70W}\bar{S}_{70W} - \overline{u'S}^{70W} \\ &= (\overline{u}^{20E} - \overline{u}^{70W})\frac{1}{2}(\bar{S}_{20E} + \bar{S}_{70W}) \\ &+ \frac{1}{2}(\overline{u}^{20E} + \overline{u}^{70W})(\bar{S}_{20E} - \bar{S}_{70W}) \\ &+ \overline{u'S}^{20E} - \overline{u'S}^{70W},\end{aligned} \tag{3.4}$$

where $\bar{S}$ denote section-averaged salinities, rather than integrals. Average values of T and S at the several sections are tabulated in Table 3.2. Equation (3.4) states that the salt transport divergence (12.14 Sv psu) in the Atlantic sector of the Southern Ocean can be partly explained by the 0.46 Sv augmentation of the volume transport (15.93 Sv psu), and partly by saltening of the Southern Ocean in the eastward direction (9.23 Sv psu). This saltening is mainly due to the presence of the relatively salty NADW at the 20°E section, and for a smaller part to the presence of subtropical water in the Agulhas Retroflection area (Table 3.2). The deviatory parts $\overline{u'S}$ converge 13.02 Sv psu.

The salt transports $\overline{v(S-S_0)}$ calculated with $S_0 = 0$ (Table 3.1) are dominated by advection of the mean salinity by the mean transport, i.e., the component $\overline{v}\bar{S}$. The residual transports across each (sub)section (Fig. 3.5) are calculated by subtracting this component from the total salt flux. The residual transports across 70°W (-17.01 Sv psu) and 20°E (-30.03 Sv psu, not shown) correspond surprisingly well with those implied by the Georgi and Toole (1982) results (-20.6 and -33.0 Sv psu). We furthermore see that in the Agulhas area 10.56 Sv psu of salt is imported as a consequence of the inflowing water being saltier than the exported water.

3.4 Vertically integrated fluxes

In this section, the zonal transports of heat and salt are vertically integrated. This yields an impression of the geographical distributions of these fluxes at the 70°W and 20°E sections. Temperature and salinity are referred to the Atlantic mean values T_m and S_m, calculated from Levitus (1982).

3.4.1 Heat fluxes

Figure 3.6 (upper panel) clearly shows the large heat transports brought about by the Agulhas Current and the SAC+ARC system. These fluxes are not only due to the large volume transports of these currents (Fig. 3.4), but their temperature deviates strongly from the Atlantic mean value as well (cf. Fig. 3.2, upper panel). In contrast, the amplitudes of the heat transports outside the Agulhas region are considerably smaller. Due to eastward advection of water with temperatures lower than the Atlantic mean values, the heat transports in the ACC are effectively westward.

The maximum westward heat transport is brought about by the Agulhas Current and amounts to about 3.2 PW (Fig. 3.6, lower panel). At the latitude θ_0, which formally separates the AGU from the ACC section, this transport is reduced to 1.15 PW (Table 3.1), since a part of the eastward heat transport of the SAC+ARC system counteracts the Agulhas Current heat input. Only at latitude 47°S has the net heat input through the 20°E section reached its minimum. Further south the small-amplitude ACC heat transports rapidly integrate up again to a value of -1.35 PW at θ_1, indicating an effective 0.20 PW heat input by the 20°E ACC. South of this latitude, the Weddell Gyre mainly recirculates its heat, so that it exports only 0.05 PW from the Atlantic. The ACC effectively exports 0.52 PW of heat to the Pacific across 70°W. So when the ACC proper is concerned, it effectively exports heat and cools the Atlantic at a rate of 0.32 PW. But when the Southern Ocean is considered as a whole, then heat is converged at a rate of 0.78 PW, since the strong and very localised heat input through the Agulhas section grossly exceeds the ACC heat flux divergence.

3.4.2 Salt fluxes

The salt fluxes brought about by the Agulhas Current and the Return Current (Fig. 3.7, upper panel) are by far not as dominant as their heat fluxes. The salt transport brought about by the Agulhas Current (north of θ_{ac}) appears only as a minor peak, since here the salinities are closest to the Atlantic mean values, rendering the effective salt transport relatively small. It is the *eastward* flow between θ_{ac} and θ_{sac} that generates a strong *westward* salt transport, due to the relatively low salinities of the waters in the SAC+ARC. The amplitudes of the ACC salt transports are considerable, and are of the same order of magnitude as those in the Agulhas region. Close to the Antarctic coast, a strong salt export can be discerned by the coastal (westward) component of the Weddell Gyre.

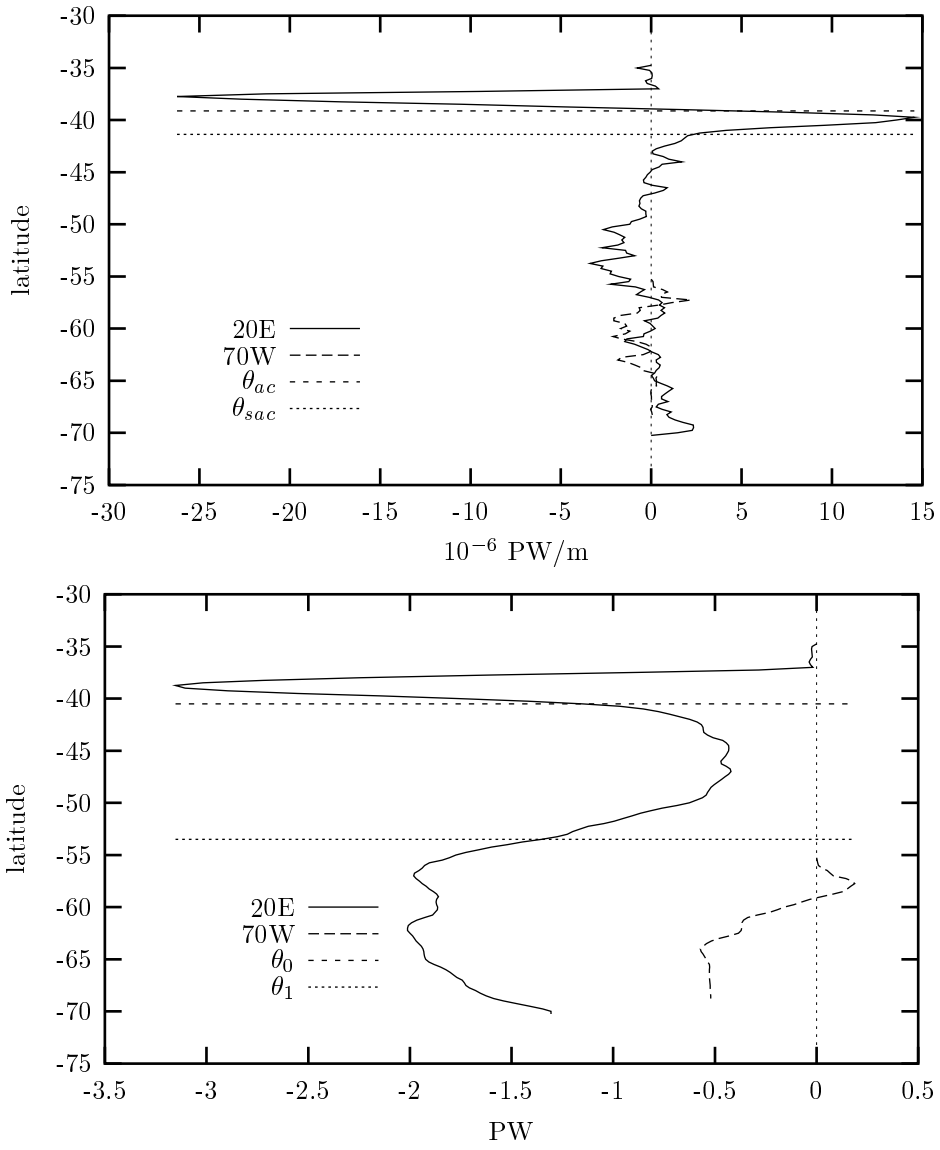

Figure 3.6: *(Upper panel) Vertically integrated heat transports across 20° E (solid line) and 70° W (dashed line), and their cumulative integrals from the northern boundaries of these sections (lower panel). Temperature is referred to the Atlantic mean value T_m from Levitus (1982). Also indicated are the latitudes θ_{ac}, θ_0, θ_{sac} and θ_1, denoting respectively the southern boundaries of the Agulhas Current, the AGU section, the SAC+ARC system and the ACC section (cf. Fig. 3.4).*

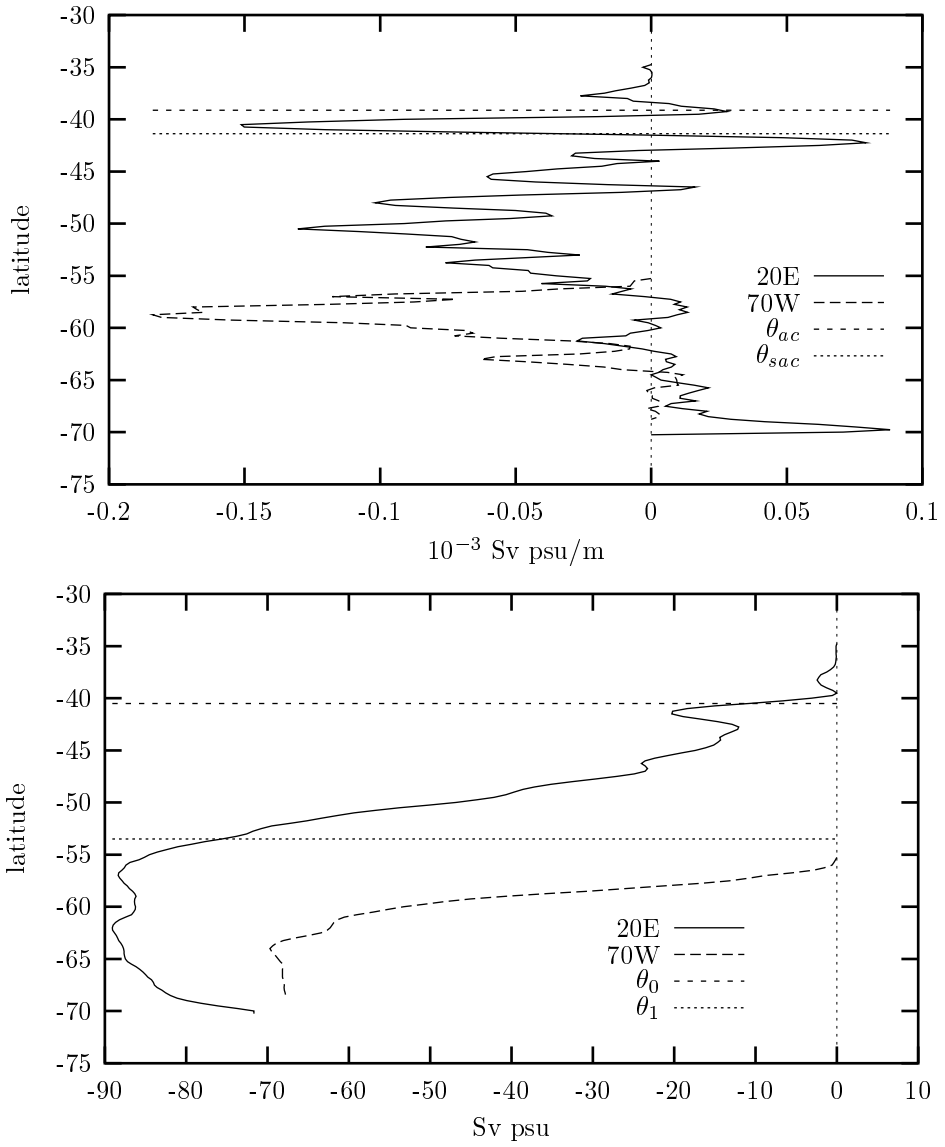

Figure 3.7: *As figure 3.6 but for salt. Salinity is referred to Atlantic mean value* S_m.

The cumulative salt transport (Fig. 3.7, lower panel) confirms the relatively low-profile salt transports in the Agulhas region. Due to the SAC+ARC salt export there is still a -10.85 Sv psu salt input in the Atlantic through the AGU section. The ACC, on the other hand, effectively imports 64.75 Sv psu across 20°E, only to be exported again by the 67.76 Sv psu transport across 70°W. So when the ACC alone is considered, then it acts effectively as a salt sink to the Atlantic. And it is due to the effective salt input in the Agulhas region that the Southern Ocean as a whole imports salt.

3.5 Horizontally integrated fluxes

In the former sections we presented the net fluxes of volume, heat and salt through the several sections bounding the Atlantic sector of the Southern Ocean. We also calculated the geographical distribution of these fluxes in a vertically integrated sense. In this section, the fluxes are integrated horizontally to obtain vertical profiles of the fluxes at the different (sub)sections. These profiles show how fluxes of volume, heat and salt are distributed in the vertical.

3.5.1 Volume fluxes

Figure 3.8 (upper panel) gives an indication of the volume balance of the Atlantic sector of the Southern Ocean, as bounded by the 34°S, 20°E and 70°W sections. It shows the zonally integrated volume transport across the zonal 34°S section, and the difference between the meridionally integrated volume transports across the 20°E and 70°W sections. The sum of these profiles gives the total divergence at each depth of the volume transport.

The transport across 34°S is characterised by a 17.7 Sv northward transport in the upper 1400 m, and a 19.4 Sv southward flow at the depths of NADW. In the deepest kilometer there is a 1 Sv inflow of Antarctic Bottom Water (AABW). This profile indicates that the model simulates a realistic overturning circulation in the Atlantic Ocean; large amounts of deep water are exported from the Atlantic to the Southern Ocean, while the compensating return transports take place at the bottom water level, and at the intermediate and thermocline levels.

The divergence of the net volume transports between 20°E and 70°W does not reflect this pattern at all: only a small 3.6 Sv volume convergence is present at shallow levels, and it is confined to the upper 800 m. Furthermore, there is only an 8 Sv net volume divergence at levels between 800 and 4000 m. The fact that these transports do not match the transports across 34°S indicates that a lot is happening in the Atlantic sector of the Southern Ocean in OCCAM. All in all, there is a 16 Sv net divergence of the volume transports above 1600 m, and an equally large net convergence below this depth, indicating that strong upwelling takes place. It must be noted that this upwelling is not necessarily diapycnal, but occurs mainly along density levels.

In Fig. 3.8 (lower panel) the meridionally integrated volume transports across the AGU and AAG sections at 20°E are plotted, as well as the divergence of the volume

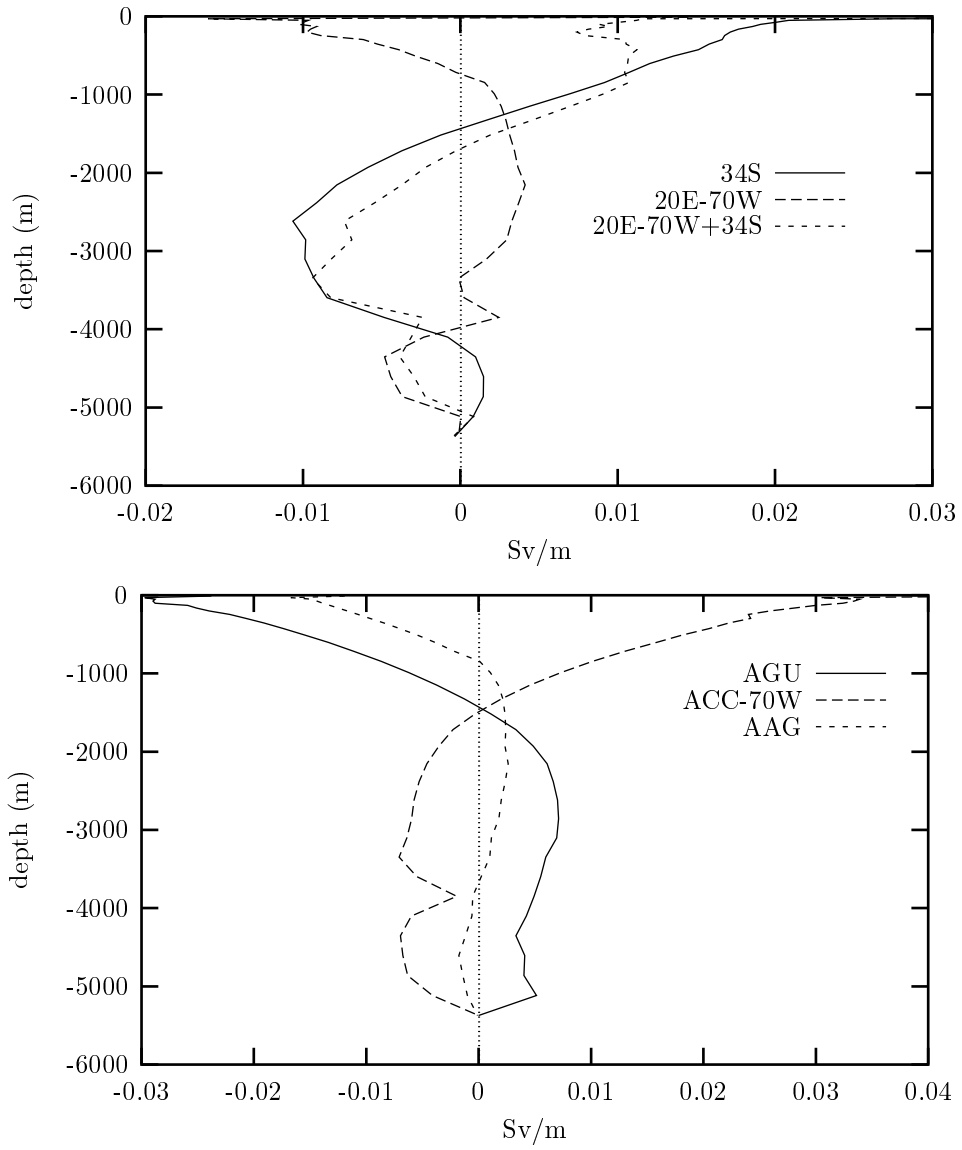

Figure 3.8: *Upper panel: The volume balance of the Atlantic sector of the Southern Ocean, with the volume transport across 34° S (34S), the volume transport divergence between the 20° E and 70° W sections (20E-70W), and the total volume transport divergence (20E-70W+34S). Lower panel: Meridionally integrated volume transports across the subsections AGU and AAG, and the difference between the ACC subsection and the 70° W transport.*

flux in the ACC. The plot shows that in the upper 1400 m of the Agulhas region (AGU) a large amount (17.7 Sv) of water is imported into the Atlantic, whereas deep water is exported below this depth. One is tempted to conclude from comparison with the transports across 34°S (Fig. 3.8, upper panel) that both the export of NADW as well as the compensating return transports take place in the Agulhas Retroflection area. This conclusion cannot be drawn based on integrated transport profiles alone, as is shown below.

The meridionally integrated volume transport of the ACC, both at 70°W and through the ACC section at 20°E, is eastward at almost any depth (not shown). The transport amplitudes are at maximum at the surface, and decrease exponentially to zero at a depth of about 4 km. Only at the 20°E ACC section there is a slight westward transport of bottom water deeper than 3800 m. The difference between the curves (long-dashed line in Fig. 3.8, lower panel) shows a clear 21 Sv divergence of water shallower than 1400 m, and a convergence below this depth. The resemblance in both amplitude and shape between this curve and the (mirrored) curve of the transport through the AGU section is striking: the sum of these two curves never exceeds the 0.005 Sv/m (except for the surface layer, where Ekman transports prevail). This shows that care should be taken when interpreting these curves in terms of the Atlantic overturning circulation: besides the possibility suggested before that the AGU section alone provides the link between the Atlantic and the Pacific/Indian components of the thermohaline circulation, an alternative explanation of the sections is equally valid on the basis of these profiles, namely that almost all shallow water that is input in the AGU section is exported by the divergent volume flux of the ACC, whereas the volume flux convergence at the deeper levels in the ACC is compensated by the export through the AGU section. In that case, a curious deep circulation would be present, and strong upwelling in the Atlantic sector of the Southern Ocean has to account for the flux profile across 34°S. Later on in this chapter it is shown that the water mass characteristics of the deep water in the Retroflection area indicates the presence of NADW; it is argued that most of the NADW export is confined to the Retroflection area.

The Weddell Gyre section (AAG) imports water at shallow levels (above 800 m), albeit with a much smaller amplitude (6.2 Sv) than the AGU section. There is eastward transports at deeper levels and a slight westward transport of bottom water below 3800 m. This is surprising, since the Weddell Gyre is thought to form bottom water, so that an export would be expected. However, the profile integrates transports over more than 15 degrees and incorporates different flow regimes. It is therefore probable that both the eastward flow of deep water and the westward flow of bottom water through the AAG section are part of the same dynamical regimes as the flow through the ACC section.

3.5.2 Heat fluxes

Figure 3.9 (upper panel) clearly shows that in the Atlantic sector of the Southern Ocean the heat fluxes converge at almost all levels. The heat flux difference between the 20°E and 70°W sections below 3000 m is small, but increases rapidly towards

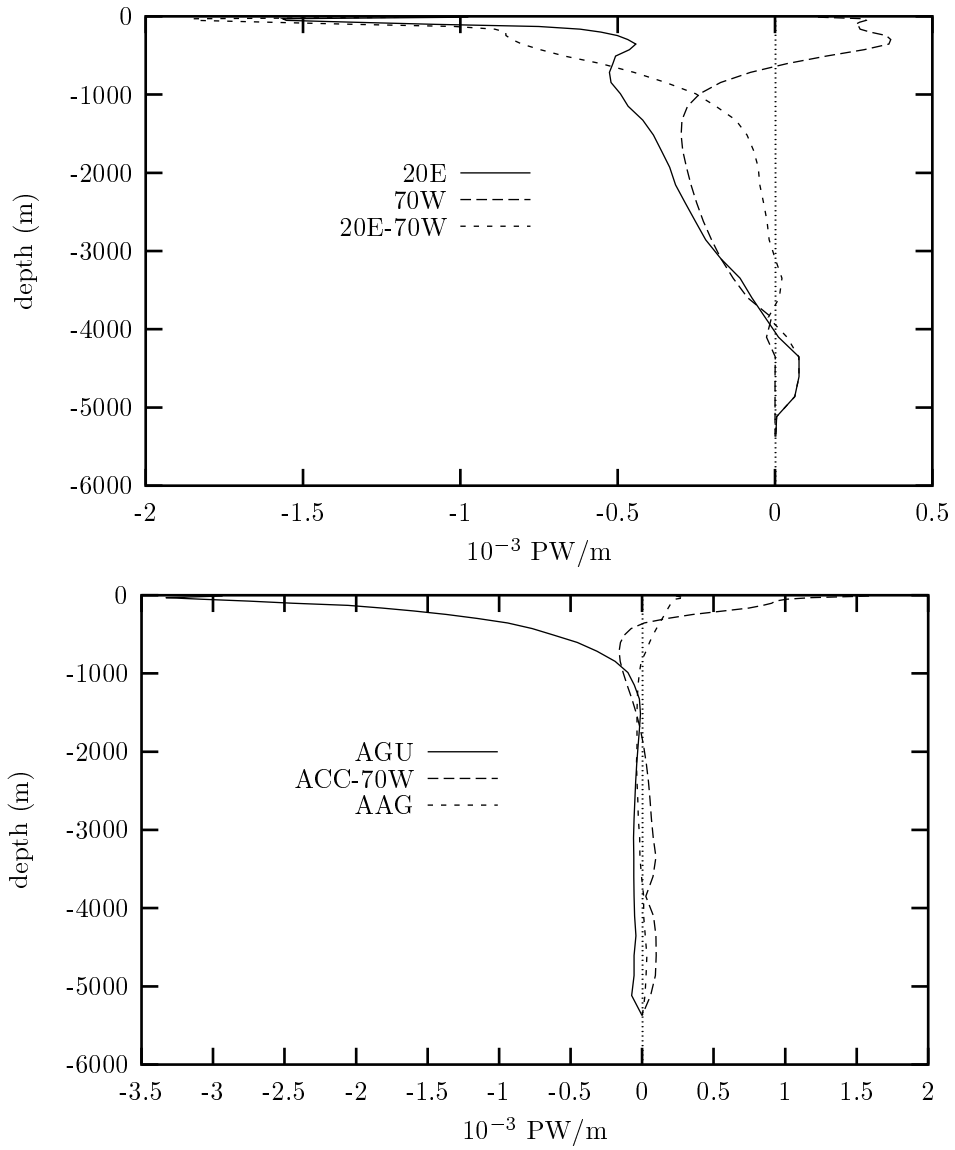

Figure 3.9: *Upper panel: Meridionally integrated heat transports through the 20° E and 70° W sections of the Southern Ocean. Their difference indicates the divergence of the heat flux in the Atlantic sector of this ocean. Lower panel: Meridionally integrated heat transports across the subsections AGU and AAG, and the difference between the heat fluxes through the ACC subsection and 70° W, indicating the heat flux divergence of the ACC.*

the surface. The heat transport across 70°W is characterised by an eastward heat transport above about 700 m. Below this depth the temperature is lower than the Atlantic mean values, so that the dominant eastward volume transport results in a westward heat flux. The structure of the heat flux across the total 20°E section is more complicated, but the contribution of the ACC section (not shown) exhibits a similar structure as the profile of 70°W. The difference between these sections (Fig. 3.9, lower panel) shows a heat flux divergence in the upper 400 m, and a convergence between 400 and 1800 m. Besides by atmospheric warming of the upper layers, this structure may be explained by the volume flux divergence in the upper 1400 m of the ACC (Fig. 3.8): it causes a heat flux divergence in the upper 400 m where $T > T_m$, and a heat flux convergence below this depth where $T < T_m$. The volume flux convergence below 1400 m is responsible for the heat flux divergence at depth: the contribution of the temperature rise at these depths, caused by the inflow of relatively warm NADW, is very small. All in all, the ACC acts as a heat sink for the Atlantic in the upper layer 400 m, and as a heat source in the intermediate layers. At deeper levels, the heat flux divergence is very small.

The eastward heat flux through the Agulhas section clearly dominates the 20°E heat transport in the upper kilometer, but the contribution below this depth is very small. The Weddell Gyre (AAG) exports a small amount of heat across 20°E in the upper layer, but the amplitude of the heat flux is negligibly small in comparison with the fluxes in the Agulhas and ACC regions.

3.5.3 Salt fluxes

The westward salt fluxes through the 20°E and 70°W sections (Fig. 3.10, upper panel) are generated by the eastward volume transport of water that is fresher than the average in the Atlantic. The difference between these profiles is relatively small: there is zero salt flux divergence below 1000 m, and a slight convergence in the upper kilometer, peaking at 75 m and 425 m depth. The Southern Ocean thus acts effectively as a source of salt for the Atlantic ocean.

The salt flux profile across the AGU subsection of 20°E (Fig. 3.10, lower panel) shows a relatively strong salt input in the upper kilometer. At about 1000 m depth there is a slight eastward salt flux, that must be caused by input of the relatively fresh AAIW, that is present at this depth (Fig. 3.2). Below this depth, a more or less constant westward salt flux of about -0.001 Sv psu/m is present. This is due to the export of NADW that is slightly fresher than the Atlantic mean salinity. The sign of this flux is robust with respect to S_m, but a 0.1 psu increase (decrease) in S_m doubles (halves) its amplitude. The AAG section shows an eastward salt flux in the upper kilometer. The amplitude of this Weddell Gyre salt flux is 50% of the Agulhas salt flux and thus surprisingly large. It contributes significantly to the total salt transport across 20°E. The salt flux divergence below 1200 m in the ACC is related to the volume flux convergence at these depths, since $S < S_m$. Again, the sign of this flux is robust with respect to a $\pm$ 0.1 psu change in S_m, but the amplitude varies with $\pm$ 50%. The 0.05 psu increase in salinity at these depths, due to entrainment of salty NADW, plays only a minor role in this divergence. Above the depth of 1200 m,

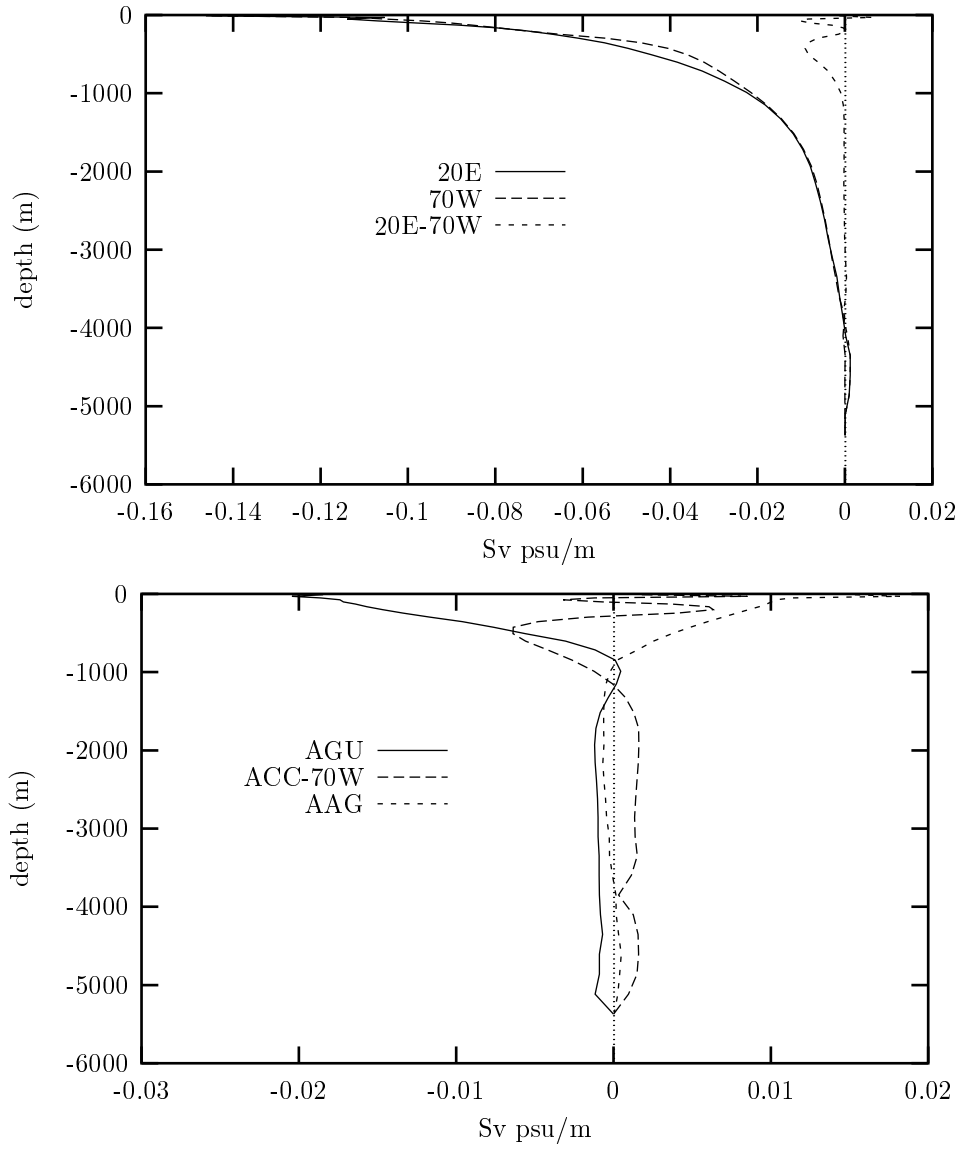

Figure 3.10: *As Fig. 3.9, but for salt.*

regions of convergence and divergence alternate rapidly, with a convergence between 150 and 1200 m, a divergence between 120 and 150 m, a convergence between 40 and 120 m, and finally a divergence in the upper two model layers. Due to this behaviour, the net salt flux divergence amounts to only 3 Sv psu, being exceeded in strength by both the AAG section (3.95 Sv psu) and the AGU section (-10.85 Sv psu).

3.6 Discussion

In the former sections we studied the volume, heat and salt fluxes across the several sections and subsections that separate the Atlantic sector of the Southern Ocean from the rest of the World Ocean. We have seen that the Agulhas area plays a large role in both the heat and salt exchange between the Indian and Atlantic Oceans. The heat and salt input into the Atlantic amounted to 1.15 PW and 10.85 Sv psu (with respect to Atlantic mean temperature and salinity) through the Agulhas section.

Observational estimates of the Agulhas Leakage heat and salt fluxes are based on the amount of water that is exchanged, and on its thermal and saline anomalies, determined with respect to the water that is replaced. The definition of the latitude θ_0, based on a minimal volume transport through the AGU section, suggests that the part of the Agulhas Current that leaks into the Atlantic (and thus passes the AGU section) also returns through this same section. The thermal and saline difference between the ingoing and outgoing water would reflect the net heat and salt input by Agulhas Leakage into the Atlantic. However, we cannot determine the amount of Agulhas Current water that leakes into the Atlantic from the 20°E section alone. There is even no way to tell whether the Agulhas Current does not retroflect completely, leaving no water for Agulhas Leakage at all! In that hypothetical case, the strong export of NADW through the AGU section that is clearly visible in Fig. 3.8 must have been derived from the Drake Passage water alone, rather than from Agulhas Current water. The heat transport through the AGU section would have been deceptively ascribed to Agulhas Leakage.

In this section, the analyses of the former sections are extended by studying the exchange through the Agulhas section at 20°E in more detail. We consider the θ_0-latitude to be the boundary between Agulhas Current and Drake Passage derived water at shallow levels. It is shown that this boundary has to shift to the north when more than 12 Sv of Agulhas Leakage water takes part in NADW compensation, so that less Agulhas water recirculates in the upper layers, while it has to shift southward when less water takes part. This yields error estimates on the heat and salt fluxes brought about by Agulhas Leakage. But before we can obtain some information on the return paths for NADW renewal, we have to make plausible that most of the NADW leaves the Atlantic in the Agulhas region.

3.6.1 NADW route

Figure 3.2 shows a pronounced core of relatively high salinity water just south of South Africa in the 20°E section of the OCCAM model. It is likely that this core

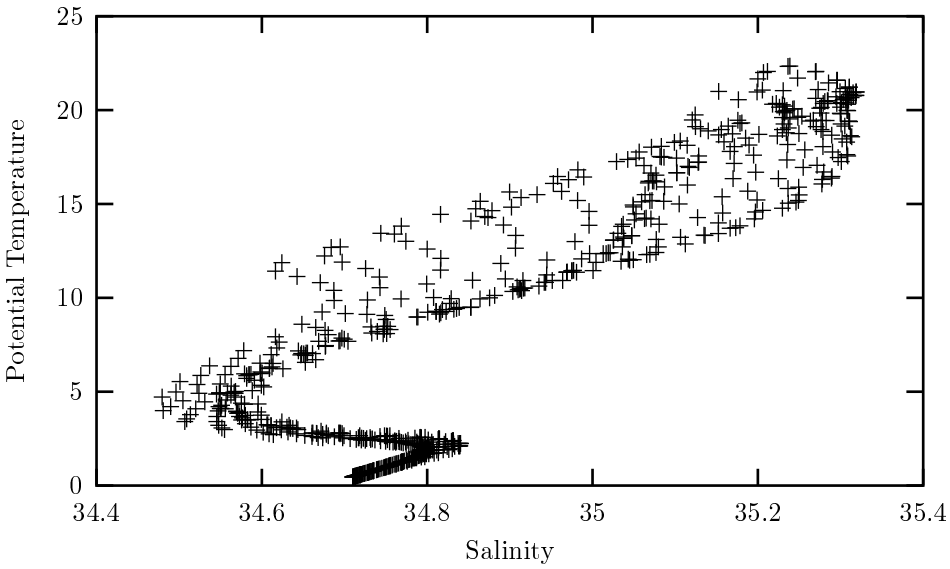

Figure 3.11: *Relations between potential temperature and salinity in the SAC+ARC current system.*

indicates the presence of NADW, the deep Atlantic water mass that is characterised by a relatively high salinity. In the T-S-diagram of the SAC+ARC current system in the model (Fig. 3.11) this high-salinity core of NADW stands out at about 2°C. This diagram also shows the core of low-salinity AAIW around 4.5°C, and the AABW at the lowest potential temperatures. Hydrographic data support the presence of large volumes of NADW in the Agulhas region (Gordon et al. 1987; Valentine et al. 1993). The low salinity water masses at the same depths further south in Fig. 3.2 can be classified as Circumpolar Deep Water (CDW), although the southward extension of the high-salinity tongue indicates some contamination with NADW. This suggests that the largest part of the NADW outflow takes place in the Agulhas region, although a small part might be mixed further southward into the CDW. The meridionally averaged volume transport of the Agulhas section (Fig. 3.8) indeed shows a large amount (17.7 Sv) of deep water being exported in the Agulhas region, whereas deep water seems to converge in the ACC.

To gain more insight in the volume transports of NADW in the SAC+ARC system, we calculated the cumulative volume transport U (Fig. 3.12), by integrating the zonal velocity southward from the African continent (θ_{sa}), and upward from the bottom ($z = -H$):

$$U(\theta, z) = \int_{\theta}^{\theta_{sa}} \int_{-H}^{z} u(\theta', z')\, dz' d\theta'. \tag{3.5}$$

When we interpret water below 4000 m (colder than 1°C) as AABW, we see that only a small amount (-3 Sv) of AABW is carried westward beneath the Agulhas Current

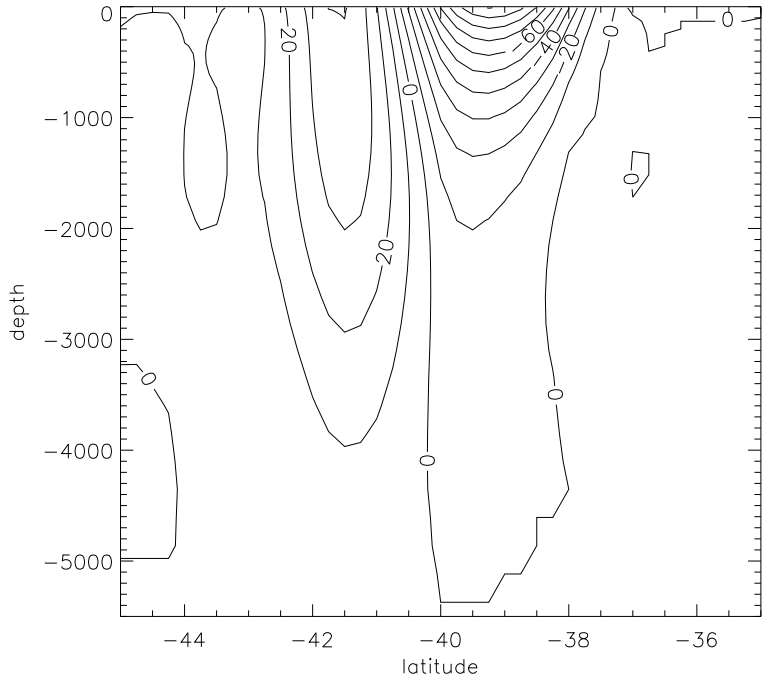

Figure 3.12: *Contour plot of the cumulative volume transport U in the same region, integrated upward from the bottom and southward from the African continent (Eq. (3.5)). The maximum Agulhas transport of -100 Sv is visible at* $\theta_{ac} = -39.00$*, as well as the 0 Sv* $\theta_0 = -40.50$*-latitude and the 41 Sv net transport of the combined AC and SAC+ARC current system (*$\theta = -41.25$*).*

(AC), while the cumulative transport beneath the SAC+ARC current system reaches the value of 10 Sv at this depth, suggesting a net eastward AABW transport of 13 Sv beneath the SAC+ARC. The upper boundary of the deep water mass (NADW) is hard to define: from the T-S-diagram (Fig. 3.11) the thermal boundary between intermediate and deep water must be between 3 and 4°C, which is somewhere between 2000 and 1500 m in the contour plot of Fig. 3.2. When NADW is defined as water between 4000 m and 2000 m (1500 m), the Agulhas Current carries 7 Sv (14 Sv) of NADW westward, while the SAC+ARC carries about 27 Sv (38 Sv) eastward: the net export of deep water is thus 20 Sv (24 Sv). This amount agrees well with the 20 Sv NADW export across 34°S. Clearly, no other deep water mass than NADW is needed to explain the deep transports in this current system, and we may assume that most of the NADW is exported from the Atlantic in the Agulhas Retroflection area.

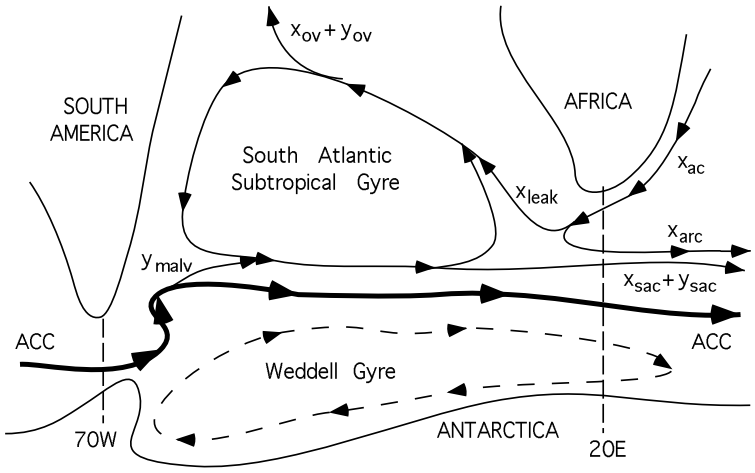

Figure 3.13: *Schematic drawing showing the possible sources of NADW renewal. The Agulhas Current, the Agulhas Return Current and the South Atlantic Current are denoted by x_{ac}, x_{arc} and $x_{sac} + y_{sac}$, respectively. The amounts of Drake Passage or Agulhas derived water that enter the Subtropical Gyre are denoted by y_{malv} and x_{leak}, whereas y_{ov} and x_{ov} denote the amounts that ultimately participate in the overturning circulation.*

3.6.2 Possible return paths

Figure 3.13 shows schematically the possible pathways that can be followed by Agulhas Leakage water (volume transports denoted by x) and Drake Passage inflow (denoted y). Starting with the Agulhas water, the Agulhas Current crosses the 20°E section (x_{ac}), retroflects, and the largest part of the Current crosses the section again as the Agulhas Return Current (x_{arc}). A relatively small part, however, flows into the Atlantic through Agulhas Leakage (x_{leak}). This water can be divided in a component which participates in the overturning circulation (x_{ov}) and one which recirculates in the wind-driven gyre of the South Atlantic (x_{sac}). This part is modified by mixing with South Atlantic water masses and by air-sea interactions, and finally leaves the Atlantic with changed properties as part of the South Atlantic Current system ($\widetilde{x_{sac}}$). The same is true for the overturning component, which returns modified as NADW ($\overline{x_{ov}}$). Most of the Drake Passage input crosses the Atlantic sector of the Southern Ocean in the ACC. A part of this transport flows northward in the Falkland/Malvinas Current, interacts with the Brazil Current in the Brazil-Malvinas Confluence Region, and flows eastward as part of the South Atlantic Current (SAC). A small part (y_{malv}) of this Malvinas transport becomes entrained in the South Atlantic subtropical gyre. One component (y_{ov}) finally leaves the Atlantic as NADW ($\overline{y_{ov}}$), while another part (y_{sac}) leaves the Atlantic after having been modified in the subtropical gyre of the South Atlantic by mixing with South Atlantic water masses and by air-sea interactions ($\widetilde{y_{sac}}$).

In the following, we assume that no South Atlantic Subtropical (gyre) Water is mixed further south than the South Atlantic Current, although Subantarctic Water may be entrained in the Subtropical Gyre (i.e., the fate of y_{ov} and y_{sac}). As it is probable that there is strong two-way mixing across the STC in the Brazil-Malvinas Confluence region, this is a weak, though useful, assumption. We furthermore assume that no NADW is mixed further south than the STC, and that all NADW leaves the Atlantic in, or close to, the Agulhas region. Finally, in the scheme below it is assumed that Drake Passage derived water is confined to the southern part of the SAC+ARC, while Agulhas derived water is confined to the northern part. This does not take into account that cross-frontal mixing is strong in the South Atlantic Current, and that Drake Passage derived water might recirculate in the Subtropical Gyre first, before joining the SAC on its northern side.

3.6.3 Estimating the return transports and associated heat and salt fluxes.

From Fig. 3.4 we see that a part of the SAC+ARC system lies south of the zero-transport latitude θ_0. The maximum westward transport carried by the Agulhas Current is 100.4 Sv, while the transport carried by the eastward jet equals 141.2 Sv, having gained 40.8 Sv in the retroflection by merging with the South Atlantic Current. This suggests a 41 Sv contribution of Drake Passage-derived water masses, as no other water sources could contribute such large amounts of water in that area.

It is clear that using the zero-transport latitude θ_0 to separate the AGU and ACC sections might be quite artificial for estimating the transports of Agulhas and Drake Passage derived water masses, as this latitude is in the center of a very strong jet in which at least 41 Sv must have been derived from the Drake Passage; besides the 10 Sv contribution of AABW, it is not known whether the remaining 30 Sv contributes to the deep water or to the shallow water component of the current system. Figure 3.14 shows schematically different possibilities of the transports across AC and SAC+ARC systems. Latitude θ_{sac} denotes the southern boundary of the SAC+ARC (at 41.25°S), θ_{ac} the southern boundary of the Agulhas Current (39.00°S), and θ_{sa} the South African continent. The Agulhas Current and Return Current are not indicated, except for the components that take part in Agulhas Leakage.

From Fig. 3.12 we can estimate the transports between the main land of South Africa and θ_0: at this latitude, the 17 Sv transport line is found at 2000 m, and the 5 Sv isoline at 4000 m. This indicates that 12 Sv of NADW leaves via the AGU section, whereas the remaining 8 Sv leaves via the ACC section. Ideally, 12 Sv of the 20 Sv NADW is derived from Agulhas Leakage, whereas 8 Sv is derived from the Drake Passage. In that case the upper panel of Fig. 3.14 applies, and the θ_0-line really indicates the boundary between Agulhas and Drake Passage derived water masses. Also the heat and salt fluxes calculated on the AGU and ACC sections refer to these sources properly.

When we assume that all 20 Sv of NADW export is compensated by Agulhas Leakage, then 8 Sv of this deep water exits within the ACC section. In that case, 8 Sv of Drake Passage water leaves the Atlantic across 20°E within the AGU section

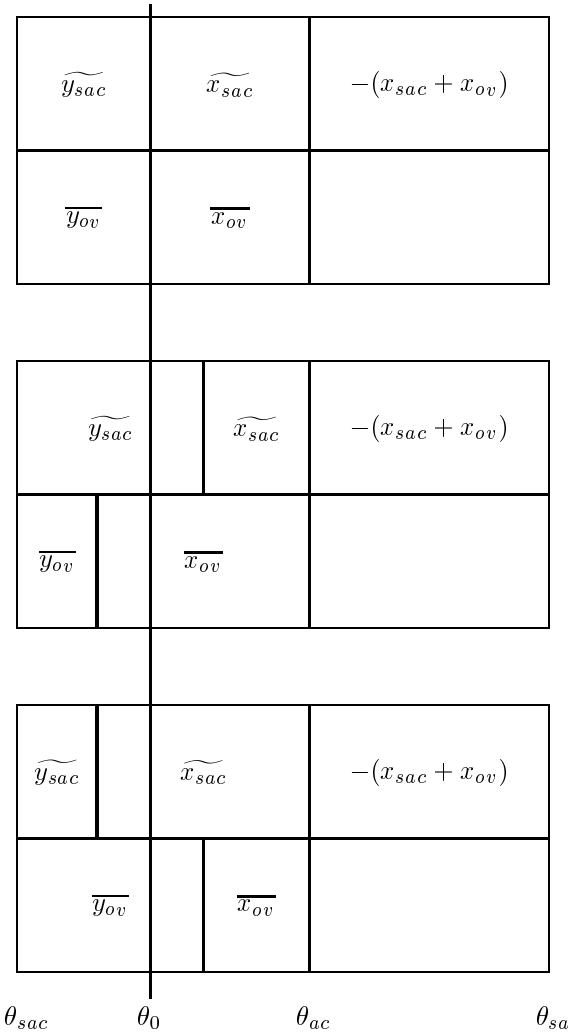

Figure 3.14: *Schematic drawing showing three possible situations of transports across the 20° E section. θ_{sa} indicates the latitude of the African continent, θ_{ac} the southern boundary of the Agulhas Current, and θ_{sac} the southern boundary of the combined South Atlantic and Agulhas Return Current system (i.e., the southern boundary of the subtropical 'super gyre'). At θ_0 the cumulative volume transport crosses zero. x_{sac} and y_{sac} denote the parts of the South Atlantic Current derived from Agulhas water and Drake Passage water, respectively, while x_{ov} and y_{ov} denote the components of NADW compensation which are derived from these sources. The overlines and tildes indicate whether the particular component has obtained NADW or South Atlantic Thermocline characteristics.*

latitude	transport	heat flux (PW)		salt flux (Sv psu)
	(Sv)	$T_0 = 0$	$T_0 = T_m$	$S_0 = S_m$
θ_{ac}	-100.4	-4.70	-3.11	-1.27
$\theta_0 + 0.25$	-21.5	-1.76	-1.42	-6.63
θ_0	1.7	-1.12	-1.15	-10.85
$\theta_0 - 0.25$	21.0	-0.63	-0.97	-15.05
θ_{sac}	40.8	-0.12	-0.78	-20.20

Table 3.3: *Transport values of volume, heat and salt through the AGU section as function of their possible separating latitude. The θ_0-values gives the standard solution, while the -21.5 Sv and +21.0 Sv denote reasonable bounds between which this latitude might be.*

at shallow levels, since the net zero transport north of $\theta = \theta_0$ must be maintained. This situation is sketched by the middle panel of Fig. 3.14 (albeit with $y_{ov} = 0$). It indicates that the θ_0-line is taken too much to the south to divide correctly between Agulhas and Drake Passage derived shallow waters. When, on the other hand, all 20 Sv NADW export is compensated by Drake Passage derived water alone, then the lower panel of Fig. 3.14 applies (with $x_{ov} = 0$). Now, the θ_0-line is taken too much to the north. In that case 12 Sv of the shallow transports derived from Agulhas Current water recirculates outside the AGU section.

The appropriate boundary between Agulhas Current and Drake Passage derived shallow water must therefore lie between the +12 Sv transport latitude and the -8 Sv transport latitude in Fig. 3.4 (lower panel), according to the above analysis. Due to the strong currents, the gradients of the cumulative transport are large, so these transport boundaries fall within one gridspacing (0.25°) from θ_0.

Figures 3.6 and 3.7 (lower panels) indicate that also heat and salt fluxes are quite sensitive to shifting the θ_0-line. Shifting θ_0 northwards one gridspacing (-21.5 Sv, Table 3.3), correcting for the presence of Drake Passage water in the AGU-section, increases the -1.15 PW (-1.12 PW with respect to $T_0 = 0$) Agulhas heat flux to -1.42 PW (-1.76 PW), but decreases the Agulhas salt input to -6.63 Sv psu. Shifting this latitude southward one gridspacing (+21.0 Sv), thus allowing for more Agulhas water in the SAC+ARC, decreases the Agulhas heat flux to -0.97 PW (-0.63 PW), but increases the Agulhas salt input to -15.05 Sv psu. The analysis based on Fig. 3.14 thus yields error-estimates on the heat and salt fluxes brought about by Agulhas derived water. We might therefore estimate the Agulhas heat input at 1.15 ± 0.25 PW and the salt input at 10.9 ± 4.2 Sv psu in this model, dependent on the amount of Agulhas Leakage water that participates in the Atlantic overturning circulation.

In the case that a considerable part of NADW is mixed southward, and leaves the Atlantic south of the SAC+ARC system, the situation is unchanged when this deep water is derived from the Drake Passage water. When it is derived from Agulhas Leakage water, however, the θ_0 latitude is again too much to the south. The most extreme position of θ_0 that can (theoretically) be reached is θ_{ac}: this would mean that all Agulhas Current water leaks into the Atlantic, is converted into NADW, and

leaves the Atlantic in the ACC section. In this case the Agulhas heat input would also have reached the extreme value of 3.11 PW, while the salt flux would have been close to zero.

3.7 Conclusions

In this chapter output from the OCCAM high-resolution general circulation model was analysed, to study the exchange of volume, heat and salt between the Atlantic and the other oceans in this model. Model output has the advantage that the dynamical fields are known at any time and any place, so that the transports in the model can be accurately determined. Furthermore, the barotropic component of the flow field is solved as an integral part of the system of equations. However, the integration time of high-resolution models is in general insufficient to reach an (at least statistical) steady state, and the resulting model drift is an uncomfortable aspect of the model analysis. Nevertheless, comparison of the model output with observations indicated that the model reproduces the large-scale features of the thermohaline fields fairly well: the short integration period prevented the thermohaline fields from drifting away too far from the observation-based climatologies that were used for the spin-up. Also the main current structures were reproduced, although their transports differed in some cases from observational estimates. Several features were identified that lack observational justification. The most important is the overestimation of Agulhas Leakage, and the excessively large heat exchange between the South Indian and South Atlantic Oceans in the Agulhas Retroflection area. The flux profiles presented in this study may thus at best be considered as impressions of what these fluxes could look like in the real ocean. But since, to my knowledge, no observational study addressed the problem of the spatial distribution of the interocean fluxes, this impression may be considered as the best available.

The fluxes across two meridional sections in the Southern Ocean were calculated, namely the Drake Passage section at 70°W and the African-Antarctic section at 20°E. Additionally, a zonal trans-Atlantic section at 34°S was analysed. The fluxes gave an interesting view of the way the Atlantic communicates with the other basins in this model. Most surprisingly, the 20 Sv outflow of NADW (and inflow of shallower water masses) across 34°S is not reflected by the volume flux divergence between 20°E and 70°W. Massive upwelling in the Atlantic sector of the Southern Ocean transfers 16 Sv from deep to shallower levels.

The heat flux across 20°E is dominated by westward heat transport in the Agulhas region. The ACC acts as a sink of heat for the Atlantic, but this is mainly due to atmospheric heating that is related to strong upwelling. The slight temperature rise at depth, caused by entrainment of warm NADW, generates a negligible contribution to the Atlantic heat loss. The contribution of the Weddell Gyre on the heat balance of the Atlantic sector of the Southern Ocean is very small. The vertical heat flux profiles (Fig. 3.9) show that the heat exchange is fully confined to the upper 1000 m. Below this depth, the heat fluxes, and their con- or divergences, are very small.

The salt fluxes brought about by the current systems in the Agulhas region gen-

erate a net salt input into the Atlantic. However, the salt fluxes in the Agulhas area are not as dominant as the heat fluxes through this subsection. The salt flux by the ACC diverges when it traverses the Atlantic; the ACC thus acts as a salt sink. This is caused mainly by the volume flux divergence in the ACC, that is related to the Bering Strait inflow. Entrainment of NADW into the ACC only adds a minor contribution to this divergence. The Weddell Gyre displays an eastward salt transport in the upper 1000 m that is in amplitude about 50% of the salt transport brought about by the Agulhas region. As is the case with the heat exchange, the largest part of the salt exchange is brought about in the upper 1000 m. Although the transports at deeper levels generate salt fluxes, their amplitudes are small, and cancel when added.

Although the transport profiles of the Agulhas section suggest that Agulhas Leakage contributes 12 Sv to the compensation of 20 Sv NADW export, the exact amount cannot be determined, and naturally ranges between 0 and 20 Sv. This uncertainty yields error bounds on the heat and salt exchange that is brought about by Agulhas Leakage in this model. These fluxes are estimated at 1.15 ± 0.25 PW and 10.9 ∓ 4.2 Sv psu (with respect to Atlantic mean values of Levitus (1982)). Crucial to this analysis is the assumption that almost all of the NADW that leaves the Atlantic is exported via the Agulhas region. The presence of a high-salinity core just south of Africa, as well as the strong outflow at deep levels through the Agulhas section (Fig. 3.8), suggest that this assumption may be largely valid.

Chapter 4

Sensitivity of the overturning circulation to lateral fluxes of buoyancy

In this chapter, the thermohaline exchange between the Atlantic and the Southern Ocean is analysed by calculating fluxes across the 30° S section in the Atlantic. The data set used is based on WOCE hydrographic data.

Furthermore, the sensitivity of the overturning circulation to interbasin fluxes of heat and salt is explored. To this end, a 2D Boussinesq model is used that represents the Atlantic between 60° N and 30° S. This model is forced by mixed boundary conditions at the surface, and by fluxes of heat and salt at its southern boundary, at 30° S. It is studied how these lateral buoyancy fluxes influence the overturning strength, and what characteristics are important. Furthermore, the relative importance of surface and lateral buoyancy fluxes is studied[1]*.*

4.1 Introduction

The operation and the stability of the ocean global thermohaline circulation are currently receiving a great deal of attention. The interest has arisen through the realisation that the ocean circulation is an extremely important component in the climate system, and may have played an important role in dramatic climatic events during the last ice-age (e.g., Broecker et al. 1985; Keigwin et al. 1991). Concern with global warming due to anthropogenic influences has increased public and scientific interest in the stability of the oceanic component of the climate system.

An appealing account of how this so-called conveyor belt circulation operates was given by Broecker (1991). He portrayed the overturning circulation as a self-sustained

[1] This study has been published as Weijer et al. (1999).

circulation loop, which is driven by atmospheric freshwater transport from the Atlantic drainage basin to the Pacific. This export of freshwater is brought about by relatively high surface water temperatures, causing evaporation to exceed precipitation in the Atlantic Ocean (e.g., Wijffels et al. 1992). These high temperatures are established by anomalous northward heat transport in the southern part of the Atlantic Ocean, which is a manifestation of the large impact of the conveyor belt circulation. The high Atlantic surface salinities allow the surface water masses to be converted into a dense deep water mass when they are cooled at high latitudes. According to this view the excess salt, which remains when net freshwater is distilled from the Atlantic surface waters, is removed by the lower limb of the conveyor belt and exported with the North Atlantic Deep Water (NADW). A two-dimensional modelling study (Zaucker et al. 1994) indeed displayed a positive relation between the atmospheric freshwater loss from the Atlantic and the overturning strength.

The upper level water masses, which enter the Atlantic to compensate for this outflow of NADW, are derived from basically two sources. They contribute water with highly contrasting water mass characteristics (Schmitz 1995): probably the largest part of the NADW compensation is derived from relatively fresh and cold intermediate waters, which enter the Atlantic as part of the Antarctic Circumpolar Circulation (ACC) through the Drake Passage (Broecker 1991; Rintoul 1991). The remaining part is derived from warm and salty thermocline or central water masses (Gordon 1985, 1986), which enter the Atlantic around the Cape of Good Hope by the process of Agulhas Leakage (Lutjeharms 1996; De Ruijter et al. 1999). However, previous budget calculations (Stommel 1980; Piola and Gordon 1986) failed to reconcile reasonable volume transports of NADW and thermocline and intermediate water return transports with net evaporation from the Atlantic basin.

In a recent paper, Rahmstorf (1996) disputed the view of Broecker (1991). On the basis of a series of global model experiments, he suggested that the average salinity of the water exported from the Atlantic (NADW) is *lower* than that of the water masses that replace it. This indicates that the overturning circulation *gains* freshwater on its way through the Atlantic, by an amount which is called the "active" freshwater flux by Rahmstorf. This active freshwater flux is determined by the saline characteristics of the exported NADW and the returning upper level water masses. It is clear that the overturning circulation does not supply the freshwater for the excess Atlantic evaporation as proposed by Broecker (1991), as it exports freshwater itself. Rahmstorf (1996) argued that only the wind-driven circulation of the South Atlantic subtropical gyre might import enough freshwater to reconcile the evaporative freshwater loss *and* the net freshwater gain of the overturning circulation. The zonal salinity contrast at 30°S in the South Atlantic Ocean does indeed exceed 1.5 psu (Levitus 1982), the highest salinities coinciding with the southward flowing Brazil Current and the lowest with the northward flowing Benguela Current. The large contribution of the gyre-induced salt transport might resolve the inconsistencies encountered in the earlier budget calculations since the overturning circulation is now released from the constraint of having to balance the atmospheric freshwater loss.

Not only are the NADW return transports important for the net interbasin fluxes of heat and freshwater, they might also affect the circulation strength in a more direct

way. Gordon et al. (1992) suggested that the input of salty and warm thermocline water by the process of Agulhas Leakage preconditions the Atlantic for forming deep water. Besides excess evaporation, this process could be an additional reason for the high surface salinities in the North Atlantic. This idea is especially interesting in view of the highly intermittent character of Agulhas Leakage, and the fact that it exists due to coupling of the wind-driven subtropical gyres of the South Indian and Atlantic Oceans (De Ruijter 1982; Lutjeharms 1996; De Ruijter et al. 1999). The input of warm and salty water from the Pacific and Indian Oceans into the Atlantic therefore depends critically on characteristics of the Indian Ocean wind stress fields, and this exchange might be very sensitive to climatological shifts of latitudes of zero wind stress curl. Paleoceanographic data indicate large shifts in the latitudinal positions of the major fronts in the Indian Ocean (Howard and Prell 1992), and suggest that the present-day position of the Subtropical Convergence, which might be thought of as the southern edge of the wind-driven subtropical gyres, is several degrees south of the average position over the last 500 kyr.

Cai and Greatbatch (1995) considered the suggestion of Gordon et al. (1992) by comparing the overturning strength with and without Agulhas Leakage in a low-resolution ocean model. In their model, the overturning strength did not change in response to shutting off the Agulhas Leakage. They blamed this lack of response on the hardly changed density field, as thermal and saline changes almost cancelled each other out. Rahmstorf et al. (1996) suggested that this might have been due to an inappropriately weak thermal coupling to the atmosphere, allowing thermal anomalies to affect the density throughout the basin, instead of in the South Atlantic only. Nevertheless it remains unclear why the overturning does *not* change in response to shutting off Agulhas Leakage, despite considerable changes in several other thermohaline properties of the solution of Cai and Greatbatch (1995).

In this chapter we examine how the strength and the operation of the Atlantic overturning circulation are influenced by interbasin fluxes of heat and salt. We demonstrate that not only the *net* flux of buoyancy across 30°S in the Atlantic is relevant, but the *vertical distribution* of the lateral buoyancy exchange as well. This distribution is a result of the highly distinct thermal and saline characteristics of the exported NADW and the brands of imported shallow level water. We show that the vertical structure of the lateral buoyancy flux can have a larger impact on the overturning strength than its influence on surface salinities and deep convection alone: it directly modifies the balance of potential energy of the Atlantic Ocean and hence the overturning strength. Modification of this vertical distribution, by changing the thermal or saline characteristics of the water masses (e.g., by changing the amount of Agulhas inflow), or by changing the vertical structure of the overturning (e.g., by changing the ratio of thermocline to intermediate water in the compensation), might therefore induce changes in the overturning strength.

The aim of this chapter is to clarify the relative role played by lateral and surface buoyancy fluxes in the operation of the large-scale Atlantic overturning circulation in a simple model context. It is essential to determine the importance of both lateral and surface forcing in order to understand and predict the ocean's response to climatic changes. Given the observed variability of Agulhas leakage and its sensitivity

to characteristics of the wind stress fields in the Indian Ocean, this question is highly relevant for climate studies. It is also important for judging the skill of low and high resolution ocean models, which do not incorporate Agulhas Leakage (Drijfhout et al. 1996a) or fail to reproduce the formation of intermediate water correctly (McCann et al. 1994). It is furthermore relevant for judging the applicability of two-dimensional models of the overturning circulation, which lack the zonal dimension and the associated transport mechanism of the wind-driven circulation (e.g., Zaucker et al. 1994).

In section 4.2 of this chapter, zonally averaged profiles are presented of heat and salt fluxes across 30°S in the Atlantic. These estimates are based on an inversion of several hydrographic data sets from the South Atlantic, that include some recent sections from the World Ocean Circulation Experiment (WOCE). In section 4.3, we describe the simple 2D model of the Atlantic Ocean employed for this study. This model is forced by realistic surface and lateral fluxes, the latter being parametrised as diffusive fluxes. In section 4.4 the impact of these fluxes on the overturning strength is studied. The relevance and implications of these results are discussed in section 4.5, and the main conclusions are summarised in section 4.6.

4.2 Fluxes of heat and salt across 30°S

In this section we present zonally averaged profiles of advective fluxes of heat and salt across 30°S in the Atlantic Ocean. These fluxes represent the thermal and saline coupling between the Atlantic and Southern Oceans, as they account for the interocean exchange of heat and salt via the ocean. They are calculated using the 'best estimate' solution of an inversion discussed by Holfort (1994). He combined hydrographic data from several South Atlantic WOCE sections and some earlier cruises to obtain a best estimate of the balances of mass, salt and heat in the South Atlantic. In the following we will use the meridional mass flux $v_m = \rho v$ (in kg m^{-2}s^{-1}) rather than the meridional velocity v itself.

Denoting the longitude by ϕ and depth by z, we split the meridional mass flux $v_m(\phi, z)$, potential temperature $T(\phi, z)$ and salinity $S(\phi, z)$ at this section into a zonal mean and its deviation, i.e.,

$$\begin{aligned} T(\phi, z) &= \overline{T}(z) + T'(\phi, z) \\ S(\phi, z) &= \overline{S}(z) + S'(\phi, z) \\ v_m(\phi, z) &= \overline{v_m}(z) + v_m'(\phi, z), \end{aligned} \tag{4.1}$$

where

$$(\overline{T}(z), \overline{S}(z), \overline{v_m}(z)) \equiv \frac{1}{L(z)} (\overline{T(\phi, z)}, \overline{S(\phi, z)}, \overline{v_m(\phi, z)}) \tag{4.2}$$

and

$$(\overline{T'(\phi, z)}, \overline{S'(\phi, z)}, \overline{v_m'(\phi, z)}) = 0. \tag{4.3}$$

$L(z)$ is the width of the basin at depth z, and the overbars denote zonal integration (note that $\overline{T}$, $\overline{S}$ and $\overline{v_m}$ are zonal *means*). To calculate heat and salt transports we introduce a reference temperature T_0 and a reference salinity S_0; the appropriate

choices for T_0 and S_0 will be discussed later. The zonally averaged lateral fluxes of heat and salt are given by:

$$F_Q(z) = \frac{1}{L(0)} c_p \overline{v_m (T - T_0)} = \frac{L(z)}{L(0)} c_p \overline{v_m} (\overline{T} - T_0) + \frac{1}{L(0)} c_p \overline{v_m' T'} \qquad (4.4a)$$

$$F_S(z) = \frac{1}{L(0)} \overline{v_m (S - S_0)} = \frac{L(z)}{L(0)} \overline{v_m} (\overline{S} - S_0) + \frac{1}{L(0)} \overline{v_m' S'}. \qquad (4.4b)$$

Applying the factor $L(0)$ in the averaging procedure yields a depth-dependent weight factor $L(z)/L(0)$, which is the relative width of the basin at each depth. This places the fluxes in the deeper and narrower parts of the basin in the right proportions with respect to their shallower counterparts. The first terms on the right-hand sides of Eqs. (4.4) denote heat and salt fluxes brought about by the overturning circulation, the net meridional transport at each depth advecting the zonally averaged temperature and salinity deviation. The second terms denote the contributions of the (largely horizontal) gyre circulation, and arise when velocity anomalies correlate with deviations of the thermal or saline anomalies within a layer.

It is not clear *a priori* what values of T_0 and S_0 should be taken, since every reference state yields an equally valid description of the fluxes. In Appendix 4.A it is shown that, in the context of our model, the appropriate choice for T_0 and S_0 is the averaged value of temperature and salinity in the basin. Only then is the potential energy input of these fluxes into the Atlantic correctly captured in a 2D model. Using the Levitus (1982) data set, we averaged the temperature and salinity for the Atlantic Ocean, starting at 30°S, and going north to the Labrador Sea and the North Atlantic overflow ridges (including the Mediterranean), resulting in mean values $T_0 = 4.83$°C and $S_0 = 35.07$ psu. An indication of the sensitivity of these values to the exact position of the northern boundary was obtained by changing this position between 60°N and 70°N, displaying variations in temperature of 0.04 K and of 0.003 psu in salinity per 10° in latitude. These variations do not significantly change the flux profiles. The heat capacity c_p is taken to be 4000 J kg^{-1}K^{-1} (Table 4.1).

The profiles of the total fluxes of heat and salt (solid lines), the overturning components (long-dashed lines) and the residual components (short-dashed lines) are plotted in Figs. 4.1. The characteristics of the major water masses can be recognised in the overturning components of both heat and salt fluxes. The signal of Antarctic Bottom Water (AABW) is visible below the zero-crossings of the profiles at about 3450 m depth. It is characterised by the export of heat and salt, due to northward transport of water which is fresher and colder than the average Atlantic waters. The influence of NADW is visible between the zero-crossings at about 1150 and 3450 meters. Due to its relatively low salinity and temperature, the southward flow of this water mass implies *northward* fluxes of heat and salt. In the overturning salt flux, the low-salinity Antarctic Intermediate Water (AAIW) is visible between 500 and 1150 m. Here the salt flux is southward due to the net northward transport of this relatively fresh water mass. The overturning fluxes in the thermocline layer are characterised by strong northward transports of heat and salt.

The residual components of the heat and salt fluxes are very small below the upper kilometer: zonal variations in the thermohaline structure are small at these depths,

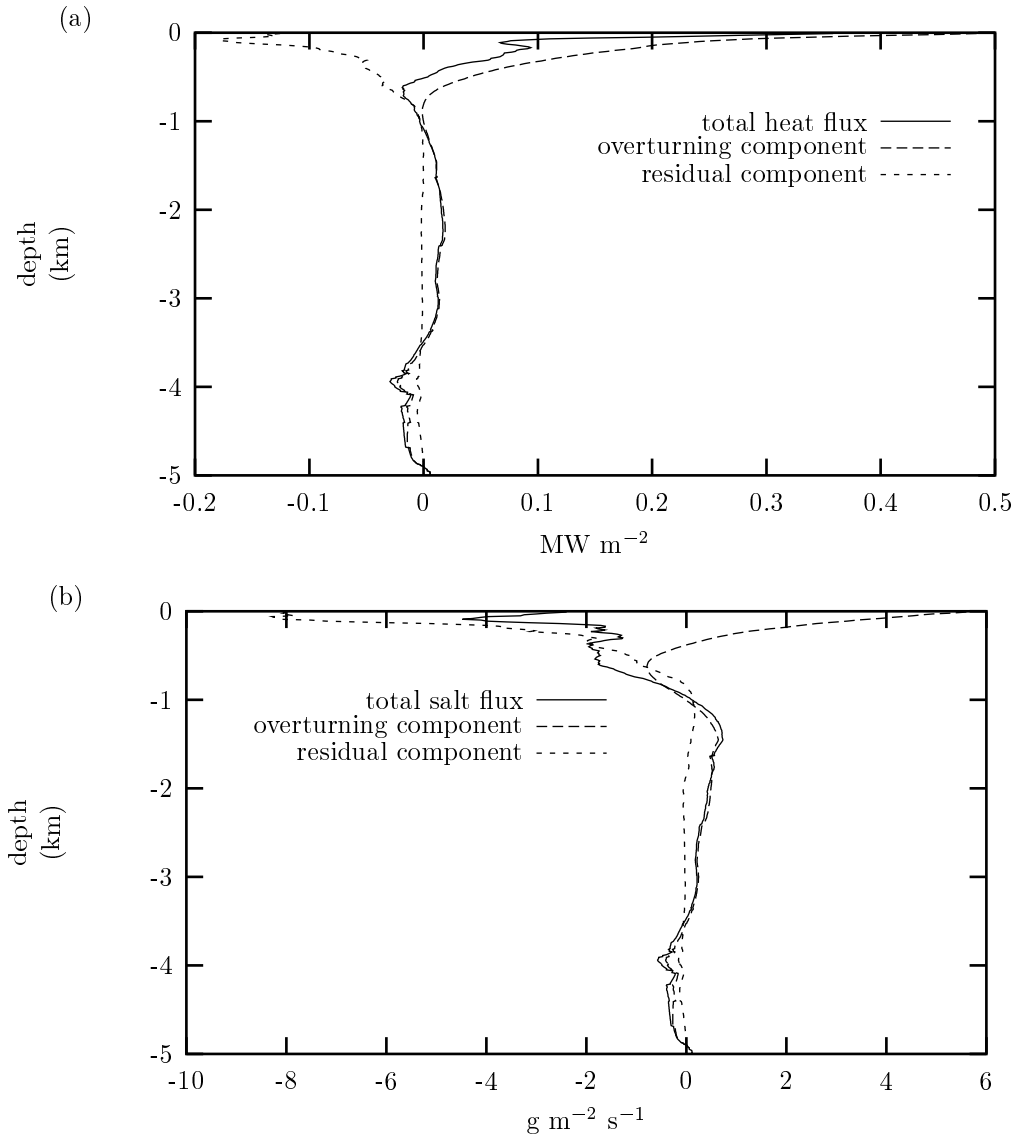

Figure 4.1: *Profiles of meridional advective fluxes of (a) heat (in MW m^{-2}) and of (b) salt (in g m^{-2} s^{-1}) across 30° S in the Atlantic. Solid lines denote the total fluxes, while long-dashed and short-dashed lines denote the overturning and residual components, respectively. Notice the large southward contributions of the gyre-induced residual fluxes in the upper 1000 m, and the northward heat and salt fluxes at NADW level. Data used are from an inversion of WOCE data performed by Dr. J. Holfort (IfM Kiel, Germany).*

Parameter	Symbol	Value
Characteristic length scale	L	$1 \cdot 10^7$ m
Characteristic depth scale	H	$5 \cdot 10^3$ m
Depth of NADW overturning cell	H_N	2828 m
Thermal expansivity	α	$1.9 \cdot 10^{-4}$ K^{-1}
Saline expansivity	β	$7.6 \cdot 10^{-4}$ psu^{-1}
Characteristic temperature range	ΔT	25°C
Characteristic salinity range	ΔS	2 psu
Reference potential temperature	T_0	4.83°C
Reference salinity	S_0	35.07 psu
Reference density	ρ_0	$1 \cdot 10^3$ kg m^{-3}
Gravitational acceleration	g	10 m s^{-2}
Horizontal diffusivity	κ_h	$1 \cdot 10^3$ m^{2}s^{-1}
Vertical diffusivity	κ_v	$1 \cdot 10^{-4}$ m^{2}s^{-1}
Horizontal viscosity	ν_h	$2.25 \cdot 10^3$ m^{2}s^{-1}
Vertical viscosity	ν_v	$2.25 \cdot 10^{-4}$ m^{2}s^{-1}
Heat capacity	c_p	$4 \cdot 10^3$ J kg^{-1}K^{-1}
Aspect ratio	a	$5 \cdot 10^{-4}$
Thermal Rayleigh number	Ra	$1 \cdot 10^4$
Prandtl number	Pr	2.25
Lewis number	Le	1
Buoyancy ratio	λ	0.32
Amplitude of surface salt flux	σ_s	0 – 10
Amplitude of lateral salt flux	σ_l	0 – 16
Amplitude of lateral heat flux	τ_l	0 – 70

Table 4.1: *Symbols and characteristic values of dimensional and non-dimensional parameters used in this study.*

and the horizontal circulation is weak. Here, the total fluxes are controlled by the overturning components alone. Above these depths the residual fluxes of heat and salt become increasingly important. Here the circulation is dominated by the wind-driven circulation of the subtropical gyre, and the zonal differences in temperature and salinity can be as much as 6°C and 1.5 psu between the eastern and western South Atlantic surface waters. Fig. 4.1a shows that in the upper 1000 m the northward heat flux is strongly counteracted by the residual component. In an integrated sense, the residual heat flux accounts for a 0.37 PW reduction in the 0.63 PW overturning heat flux, resulting in a total heat flux of 0.26 PW. The residual salt flux, on the other hand, completely overrules the overturning component in the upper kilometer, and becomes the dominant factor in the total salt flux (Fig. 4.1b). It converts the 7.0 Gg/s *northward* salt transport of the overturning circulation into a -6.2 Gg/s *southward* transport. (Note that the original solution of Holfort also accounts for fluxes brought about by (southward) Ekman flow, and that taking T_0 and S_0 close to

the 30°S section-mean values of temperature and salinity supresses the heat and salt flux contribution of advection by the $\mathcal{O}$(-0.3 Sv) net Atlantic volume flux.)

The sign of the salt flux at NADW levels depends of course on the choice of the reference salinity S_0. However, the sign of the integral of the overturning profile does not. Its positive sign confirms the ideas of Rahmstorf (1996), namely that at 30°S the exported NADW is on average fresher than the water masses that replace it. Therefore, the overturning circulation effectively *exports* freshwater from the Atlantic, and is unable to supply freshwater to compensate for the excess evaporation (Broecker 1991). The analysis of the heat and salt fluxes across 30°S in the Atlantic clearly shows the importance of the wind-driven circulation for both the heat and salt budgets of the Atlantic Ocean.

4.3 The model

4.3.1 Domain and configuration

The model used in this study is adapted from the two-dimensional model used by Dijkstra and Molemaker (1997). The stationary and rotationless Boussinesq equations are solved in a streamfunction-vorticity formulation, in a small aspect ratio configuration. Two different domain configurations are studied: the first one considers a model with equatorially symmetric surface buoyancy forcing. This model, which is denoted as 'global', has been studied by several authors in as many parameter settings (Cessi and Young 1992; Thual and McWilliams 1992; Quon and Ghil 1992, 1995; Dijkstra and Molemaker 1997). The second configuration, called 'Atlantic', applies more specifically to the Atlantic ocean, which we consider bounded by the 30°S parallel. In both cases the model coordinate y ($\in [0,1]$) can be mapped onto the latitude θ:

$$\theta_q(y) = \theta_q^S(1-y) + \theta^N y \qquad\qquad q = G, A \tag{4.5}$$

where θ^N is 60, and θ_q^S is -60 for the global (G) configuration and -30 for the Atlantic (A) configuration.

In addition to surface forcing, the Atlantic configuration of the model can also be forced by *lateral* fluxes of heat and salt, prescribed at the 30°S boundary. In reality, such lateral fluxes are a result of water mass exchange with anomalous salt and heat content, and are therefore of an advective nature. However, in order to avoid open boundary conditions at the southern boundary of our model, we prescribe them as diffusive fluxes, in combination with a no-flow condition. We realise that, by prescribing these fluxes, no feedback from changing Atlantic overturning to these fluxes is allowed. Furthermore the constraint that all deep water must upwell north of 30°S is an unrealistic feature of the model, as most of the NADW produced is exported from the Atlantic (Schmitz 1995).

4.3.2 Equations and scaling

Scale parameters and dimensionless quantities introduced in this section are tabulated in Table 4.1, as well as their characteristic values. Dimensional variables are indicated with a *.

A linear equation of state is used, relating buoyancy B^* to temperature T^* and salinity S^* via $B^* = \rho_0[\alpha(T^* - T_0) - \beta(S^* - S_0)]$. Here α and β are the coefficients of thermal and saline expansion, and T_0 and S_0 are reference values of temperature and salinity. The temperature and salinity deviations are scaled with characteristic scales of thermal and saline variations in the Atlantic Ocean ΔT and ΔS. Scaling buoyancy B^* with $\rho_0\alpha\Delta T$ yields $B = T - \lambda S$. As in Dijkstra and Molemaker (1997), we rescale salinity with the buoyancy ratio $\lambda = \beta\Delta S/\alpha\Delta T$ by introducing $\tilde{S} = \lambda S$. The tilde is dropped in the following.

The meridional and depth coordinates are scaled as $(y^*, z^*) = (Ly, H(z-1))$, where H is the mean depth of the basin, and L the meridional extent. Coefficients of viscosity and thermal diffusivity are denoted by ν and κ, respectively, with subscripts h and v indicating the horizontal and vertical components. Time t^*, streamfunction ψ^* and vorticity Ω^* are scaled with H^2/κ_v, $\kappa_v L/H$ and $\kappa_v L/H^3$. Applying this scaling, we obtain the following equations:

$$\Omega = -a^2\psi_{yy} - \psi_{zz} \tag{4.6a}$$

$$Pr^{-1}\left[\frac{\partial\Omega}{\partial t} - J(\psi,\Omega)\right] = Ra(T-S)_y + a^2\frac{\nu_h}{\nu_v}\Omega_{yy} + \Omega_{zz} \tag{4.6b}$$

$$\left[\frac{\partial T}{\partial t} - J(\psi,T)\right] = a^2\frac{\kappa_h}{\kappa_v}T_{yy} + T_{zz} \tag{4.6c}$$

$$Le\left[\frac{\partial S}{\partial t} - J(\psi,S)\right] = a^2\frac{\kappa_h}{\kappa_v}S_{yy} + S_{zz} \tag{4.6d}$$

where $J(a,b)$ denotes the Jacobian operator $a_y b_z - a_z b_y$. The Prandtl number $Pr = \nu_v/\kappa_v$ is taken to be 2.25, in line with the Dijkstra and Molemaker (1997) and Quon and Ghil (1992) values, whereas the aspect ratio $a = H/L$ is taken to be $5 \cdot 10^{-4}$. The Lewis number, Le, which is the ratio between eddy diffusivities of salinity and temperature, is taken to be unity, since turbulent mixing of salt and temperature is assumed to take place at the same rate.

Estimates of the Rayleigh number $Ra = \alpha g\Delta T H^5/\nu_v\kappa_v L^2$ based on realistic parameter values (Table 4.1) are of the order $\mathcal{O}(10^{10} - 10^{11})$. However, applying a Rayleigh number of this order of magnitude would result in an unrealistically strong overturning circulation as rotational effects are not included in our model. The presence of rotation tends to stabilise a convective system, as pressure forces are not balanced by viscous friction, as in our model, but by the Coriolis force. This effectively reduces the Rayleigh number by a factor Ta^{-1}, where Ta is some kind of Taylor number, being proportional to the square of the Coriolis parameter (e.g., Chandrasekhar 1961; Van der Schrier and Maas 1998, their Eq. (17g)). In this study Ra is given the low value of 10^4, to enable the performance of calculations on grids with a manageable resolution. Furthermore, it has been shown (Dijkstra and Molemaker

1997) that the qualitative behavior of the system is not very sensitive to Ra, once its value is large enough.

As argued by Quon and Ghil (1995), small aspect ratio geophysical fluid systems can only be advective when the ratio of vertical and horizontal diffusivities (and viscosities) is also very small. Estimates of these parameters in the real ocean are of the order of 10^{-4} and 10^{3} m^{2}s^{-1} for κ_v and κ_h respectively. This yields a ratio κ_v/κ_h of the order $\mathcal{O}(10^{-7})$, which is of the same order of magnitude as a^2. So by taking the ratios κ_v/κ_h and ν_v/ν_h equal to a^2, we place our model in the advective regime. From Eqs. (4.6) it is clear that the dimensionless vertical and horizontal diffusive transports are now of the same order of magnitude.

4.3.3 Boundary conditions

Let Γ denote the boundary of the domain and $\mathbf{n}$ its outward normal, and let subscripts s, r, b and l refer to the surface, right (northern), bottom and left (southern) sides of the domain. We prescribe all walls to be free slip:

$$\psi = \Omega = 0 \qquad \text{for } \mathbf{x} \in \Gamma. \tag{4.7a}$$

The boundary conditions for temperature are:

$$\begin{aligned} T &= T_s(y) && \text{for } \mathbf{x} \in \Gamma_s \\ \nabla T \cdot \mathbf{n} &= \begin{cases} \tau_l F_l^T(z) & \text{for } \mathbf{x} \in \Gamma_l \\ 0 & \text{for } \mathbf{x} \in \Gamma_r, \Gamma_b \end{cases} \end{aligned} \tag{4.7b}$$

and for salinity:

$$\nabla S \cdot \mathbf{n} = \begin{cases} -\sigma_s F_s^S(y) & \text{for } \mathbf{x} \in \Gamma_s \\ \sigma_l F_l^S(z) & \text{for } \mathbf{x} \in \Gamma_l \\ 0 & \text{for } \mathbf{x} \in \Gamma_r, \Gamma_b \end{cases}, \tag{4.7c}$$

where the amplitudes τ_l, σ_l and σ_s are parameters of the system. The $\mathcal{O}(1)$ functions $F_l^T(z)$, $F_l^S(z)$ and $F_s^S(y)$ are derived in the following sections.

The zonally averaged profile of Atlantic ocean surface temperatures (Levitus 1982) can be modeled reasonably well by a cosine function of the form:

$$T_s(y) = \cos\left(\frac{\pi}{60}\theta(y)\right) \tag{4.8}$$

where the mapping $\theta(y)$ is given by Eq. (4.5). This profile of prescribed temperature T_s is plotted in Fig. 4.2 (solid line).

Three estimates of the surface freshwater flux over the Atlantic ocean, which is equal to the difference between precipitation, run-off and evaporation (denoted $P-E$ for convenience), are shown in Fig. 4.3. Zaucker et al. (1994) derived the profiles from ECMWF data (long-dashed line) and from the Oort (1983) climatology (short-dashed line) assuming that the volumes of freshwater apply to a 60° wide ocean basin, in order to obtain units of m^{3}m^{-2}s^{-1}. The solid line was obtained from the

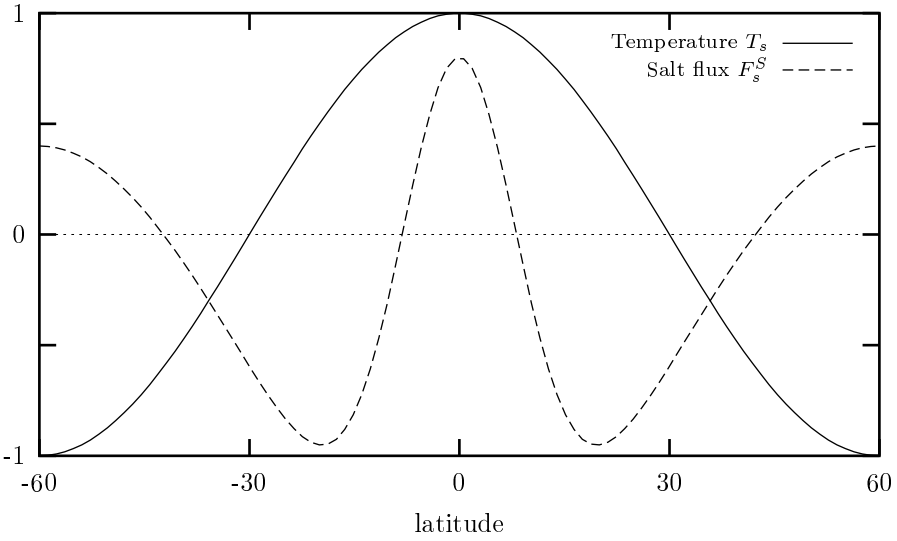

Figure 4.2: *Profiles of prescribed surface temperature T_s and surface salt flux F_s^S as a function of latitude.*

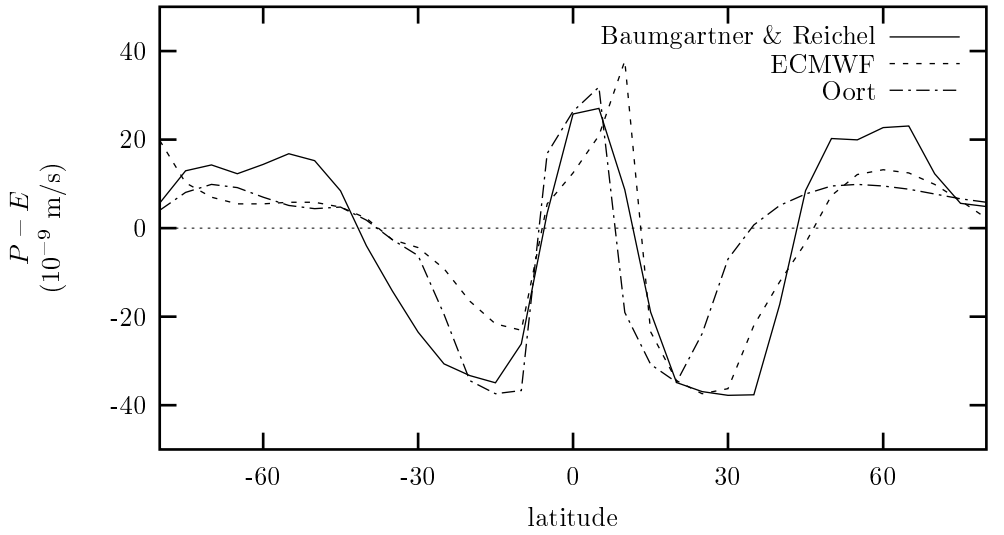

Figure 4.3: *Profiles of $P - E$ (in $10^{-9} m\ s^{-1}$) for the three different datasets as indicated in the figure.*

Baumgartner and Reichel (1975) dataset, by making the same assumption. Although the three profiles differ in detail, they agree on the particular form of the $P - E$ profiles in the Atlantic basin: they all show excess precipitation at high latitudes, excess evaporation at midlatitudes, and a high precipitative maximum over equatorial regions, at latitudes of the Intertropical Convergence Zone (ITCZ). In many 2D studies of the global thermohaline circulation, this precipitative maximum has not been taken into account, although it constitutes a considerable input of freshwater and may have a considerable impact on the stability and structure of possible overturning states.

We averaged the three profiles and symmetrised the result with respect to the equator. A simple analytical function was fitted through this profile $\widehat{F}_s^S(\theta)$ between 60°S and 60°N, yielding an $\mathcal{O}(1)$ profile $F_s^S(y)$ and an amplitude $A = 33.1 \cdot 10^{-9}$ m/s:

$$F_s^S(y) = \widehat{F}_s^S\left(\theta(y)\right)/A = -\cos\left(\frac{\pi}{60}\theta(y)\right) + 2.4\,\exp\left[-\left(\frac{\theta(y)}{12}\right)^2\right] - 0.6 \qquad (4.9)$$

where the mapping $\theta(y)$ is again given by Eq. (4.5). The function $F_s^S(y)$ is plotted in Fig. 4.2 (dashed line). The freshwater flux is equivalent to a (virtual) diffusive salt flux with:

$$\frac{\partial S}{\partial z} = -\frac{\lambda H S_s}{\kappa_v \Delta S}\widehat{F}_s^S(\theta) = -\frac{\lambda H S_s A}{\kappa_v \Delta S}F_s^S(y) = -\sigma_s F_s^S(y). \qquad (4.10)$$

Here S_s is a characteristic salinity for the ocean surface, taken to be 36.0 psu. Using the parameter values from Table 4.1, we obtain a dimensionless amplitude $\sigma_s = 9.5$ for the surface salt flux.

The Atlantic thermohaline circulation does not consist of the NADW overturning cell alone. It is a complex combination of two overturning cells, with deep water also forming in the Antarctic region. The part of this AABW that flows into the Atlantic Ocean is converted into a brand of deep water called Lower NADW (LNADW). It is exported from the Atlantic again just above the level at which it entered (Schmitz 1995). Stocker et al. (1992b) have shown that these overturning cells interact, and that the strength of the NADW cell is influenced by the strength of the AABW circulation. In our study we are principally interested in the interplay between surface processes and interbasin fluxes, and their effect on the deep water formation in the northern part of the Atlantic Ocean. With that objective we designed the Atlantic model configuration ($q = A$ in Eq. (4.5)). This configuration excludes the formation area of AABW, and it is therefore unable to model the dynamics of the bottom water circulation and its interaction with the NADW cell. To make the lateral forcing in our model consistent with this exclusion, we eliminate the influence of AABW by truncating our heat and salt flux profiles (Fig. 4.1) at the depth below which only AABW and LNADW are assumed to be present. This depth was found by integrating the meridional mass transport across 30°S downward. It reversed sign at depth $H_N = 2828$ m, and we assume that all NADW export above this depth is compensated by the import of shallower water masses.

The total heat and salt flux profiles $\widehat{F}_l^T(z^*)$ and $\widehat{F}_l^S(z^*)$ of Figs. 4.1 are approximated by functions of the form $B\left[\exp(z^*/a) - b\cos(2\pi z^*/c)\right]$, yielding the dimen-

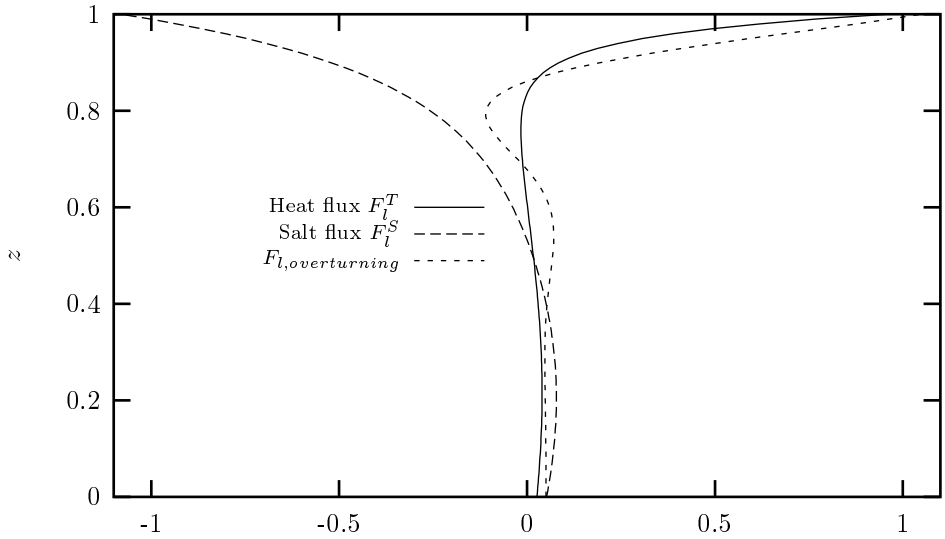

Figure 4.4: *Profiles of prescribed lateral heat (F_l^T) and salt (F_l^S) fluxes. The overturning salt flux profile $F_{l,overturning}$ is used in the discussion.*

sionless flux profiles $F_l^T(z)$ and $F_l^S(z)$ (Fig. 4.4):

$$\widehat{F}_l^T\left(z^*(z)\right)/B^T \approx \exp\left[21(z-1)\right] - 0.04\cos\left[4(z-1)\right] = F_l^T(z) \tag{4.11a}$$

and

$$\widehat{F}_l^S\left(z^*(z)\right)/B^S \approx -\exp\left[8(z-1)\right] - 0.08\cos\left[4(z-1)\right] = F_l^S(z), \tag{4.11b}$$

where $z^* = H_N(z-1)$ and $H_N = 2828$ m are used. The amplitudes B^T and B^S are 0.30 $\mathrm{MWm^{-2}}$ and 4.13 $\mathrm{gm^{-2}s^{-1}}$. The advective heat flux is equivalent to a prescribed diffusive flux with:

$$\frac{\partial T}{\partial y} = -\frac{L}{\kappa_h \Delta T \rho_0 c_p}\widehat{F}_l^T(z^*) = -\frac{H^2 B^T}{\kappa_v L \Delta T \rho_0 c_p}F_l^T(z) = -\tau_l F_l^T(z). \tag{4.12}$$

Assuming a ΔT of 25°C, the parameter τ_l takes the value 75.0. Accordingly, the advective salt flux is equivalent to a prescribed diffusive flux when:

$$\frac{\partial S}{\partial y} = -\frac{\lambda L}{\kappa_h \Delta S \rho_0}\widehat{F}_l^S(z^*) = -\frac{\lambda H^2 B^S}{\kappa_v L \Delta S \rho_0}F_l^S(z) = -\sigma_l F_l^S(z). \tag{4.13}$$

Using the parameter values of Table 4.1, we obtain a dimensionless amplitude σ_l of 16.5. Note that the amplitude of the lateral heat flux is almost 5 times as large as the lateral salt flux, and 7.5 times as large as the surface salt flux.

In this study we focus on steady state solutions, so the balances of heat and salt must be closed. Since in our model the salt flux is prescribed at all boundaries, and taken zero at the bottom and the northern boundary, we have to take care that the net surface salt flux equals the net lateral salt flux. It is therefore convenient to split the surface salt flux $F_s^S(y)$ and the lateral salt flux $F_l^S(z)$ into the net components I_s^S and I_l^S, and the shapes $\widetilde{F}_s^S(y)$ and $\widetilde{F}_l^S(z)$ which have zero integral. In most cases we use $\sigma_s \widetilde{F}_s^S(y) + \sigma_l I_l^S$ as surface salt flux rather than $F_s^S(y)$, to assure that the net lateral salt flux is balanced by a net surface salt flux of equal magnitude. With $I_l^S < 0$, this extra surface salt input corresponds to net evaporation from the basin.

The stationary form of Eqs. (4.6) and the boundary conditions of Eqs. (4.7) are discretised on a non-equidistant grid: vertically the grid refines upward, while horizontally the grid refines in both directions. Most computations were performed on a grid with 121 gridpoints in the meridional direction, and 61 in the vertical direction. A steady-state solver is used to obtain stationary solutions. Branches of these steady states are followed through parameter space using a branch-following technique as described in Dijkstra et al. (1995).

4.3.4 Integral characteristics

In this study we want to examine and understand the response of the overturning strength to changes in the thermohaline forcing. We analyse the behavior of the solutions by investigating integral balances of the system. This approach has the advantage that non-linear advective terms are eliminated, and that only volume-integrated and boundary properties are relevant.

Denoting volume-integration by brackets $< . >$, the volume-integrated potential energy U is defined as $U = - < zB > = - < z(T - S) >$, where $B = T - S$ is the buoyancy (note that the buoyancy ratio λ has been absorbed in S). Multiplying the advection-diffusion equation of buoyancy by z and integrating over the model domain, we obtain:

$$\frac{dU}{dt} = \Delta B_v + \oint z\mathbf{F} \cdot \mathbf{n}\, d\Gamma - < wB >, \tag{4.14}$$

where $\mathbf{F}$ $(= \mathbf{F}^T - \mathbf{F}^S)$ denotes the boundary fluxes of buoyancy. ΔB_v $(= \Delta T_v - \Delta S_v)$ in Eq. (4.14) is defined as:

$$\Delta B_v \equiv \int_0^1 B|_{z=0}^{z=1}\, dy \tag{4.15}$$

and represents the (internal) source of potential energy due to (downward) turbulent mixing of buoyancy. In the ocean this mixing is supported by external mechanical energy sources like internal wave breaking, tidal dissipation and wind stirring (Huang 1998). The second (external) source (or sink) of potential energy in Eq. (4.14) is brought about by boundary fluxes of potential energy like air-sea buoyancy fluxes or advective exchange with other oceans. The buoyancy production $< wB >$ $(=< wT > - < wS >)$ indicates potential energy loss due to vertical advection of buoyancy and effectuates the conversion of potential energy into kinetic energy.

The balance of kinetic energy is obtained by multiplying the vorticity equation by ψ and integrating over the domain:

$$Pr^{-1}\frac{dE}{dt} = Ra < wB > -D. \tag{4.16}$$

The volume-integrated kinetic energy E and dissipation D (note that $D \geq 0$) are given by:

$$E = \frac{1}{2} < \psi_z^2 + a^2\psi_y^2 > \tag{4.17a}$$

$$D = - < \psi\nabla^2\Omega > = < \psi_{zz}^2 + (1+a^2)\psi_{yz}^2 + a^2\psi_{yy}^2 > . \tag{4.17b}$$

In a steady state the time derivatives in Eqs. (4.14) and (4.16) are zero, so the right hand sides of the equations must vanish. Consequently, the buoyancy production $< wB >$ simply relates the (internal and external) sources (and sinks) of potential energy to the dissipation of kinetic energy:

$$< wB > = \Delta B_v + \oint z\mathbf{F}\cdot\mathbf{n}\, d\Gamma \tag{4.18a}$$

$$Ra < wB > = D. \tag{4.18b}$$

In our study we combine a buoyancy flux $F_s(y)$ at the surface with a flux $F_l(z)$ at the southern boundary of our domain. These fluxes can be split into a net component I_s and I_l, which are equal in a steady state, and shape functions $\widetilde{F}_s(y)$ and $\widetilde{F}_l(z)$ which have zero integral. For this configuration the boundary integral in Eq. (4.18a) is evaluated in Appendix 4.B, and equals:

$$\oint z\mathbf{F}\cdot\mathbf{n}\, d\Gamma = \frac{1}{2}I_s - K_v, \tag{4.19}$$

where K_v $(= K_v^T - K_v^S)$ is defined as:

$$K_v \equiv \int_0^1 z\widetilde{F}_l(z)\, dz \tag{4.20}$$

and contains information on the shape of the lateral buoyancy flux. Note that the boundary integral in Eq. (4.19) contains no information on the shape of the surface buoyancy flux $\widetilde{F}_s$.

Analogous to the potential energy, the buoyancy torque P is defined as $P = - < yB > = - < y(T-S) >$, and a balance similar to Eq. (4.14) is obtained:

$$\frac{dP}{dt} = \Delta B_h + \oint y\mathbf{F}\cdot\mathbf{n}\, d\Gamma - < vB > . \tag{4.21}$$

The meridional buoyancy difference ΔB_h $(= \Delta T_h - \Delta S_h)$ is defined analogous to ΔB_v:

$$\Delta B_h \equiv \int_0^1 B|_{y=0}^{y=1}\, dz. \tag{4.22}$$

Equation (4.21) shows that the buoyancy torque can change due to meridional diffusion of buoyancy, boundary fluxes of buoyancy torque and meridional advection of buoyancy. Volume-integration of the vorticity equation yields the relation:

$$Pr^{-1}\frac{d<\Omega>}{dt} = Ra\Delta B_h + <\nabla^2\Omega>, \tag{4.23}$$

stating that basin-integrated vorticity can be generated by a meridional buoyancy difference ΔB_h and dissipated by viscous friction. In steady state, there is a balance between production and dissipation of buoyancy torque, and of vorticity, via ΔB_h:

$$\Delta B_h = <vB> - \oint y\mathbf{F}\cdot\mathbf{n}\, d\Gamma \tag{4.24a}$$

$$Ra\Delta B_h = -<\nabla^2\Omega>. \tag{4.24b}$$

The boundary integral in Eq. (4.24a) can be analysed in a similar way as the integral in Eq. (4.18a). With the same considerations concerning the background potential energy, as outlined in Appendix 4.B, applied to the background buoyancy torque, this results in:

$$\oint y\mathbf{F}\cdot\mathbf{n}\, d\Gamma = K_h + \frac{1}{2}I_l \tag{4.25}$$

where K_h $(= K_h^T - K_h^S)$ is defined as:

$$K_h \equiv \int_0^1 y\widetilde{F}_s(y)\, dy. \tag{4.26}$$

The boundary integral in Eq. (4.25) contains information on the shape of the surface buoyancy flux only, but not on the shape of the lateral flux.

In this section two balances were obtained relating large-scale properties of the thermohaline distributions to the velocity field. The steady state kinetic energy balance Eq. (4.18b) relates the dissipation D (Eq. (4.17b)) to the buoyancy production $<wB>$, and via the potential energy equation Eq. (4.18a) to boundary values and fluxes of T and S. In the limit of small aspect ratio ($a \to 0$), Eq. (4.17b) yields a relatively simple relation between D and ψ_{max}, as only two terms in D remain, $<\psi_{zz}^2>$ and $<\psi_{yz}^2>$, or equivalently $<v_z^2>$ and $<v_y^2>$. When considering a solution with one circulation cell, both derivatives are roughly proportional to ψ_{max}, as can be shown by a simple estimate of these derivatives (Dijkstra and Molemaker 1997). This yields a relation between D, and thereby $<wB>$, and ψ_{max} which is approximately quadratic.

The vorticity balance (4.24b) relates the meridional buoyancy difference to the vorticity dissipation. This dissipation is linearly related to Ω, which in turn is linear in ψ. This suggests that the relation between ΔB_h (or equivalently the meridional large-scale pressure difference) and ψ_{max} might be linear, as well.

4.4 Results

4.4.1 Symmetric vs. non-symmetric basin: Comparison of two NPP states

Since we study the Atlantic overturning circulation in a domain which is closed at 30°S ($q = A$ in Eq. (4.5)), it is important to investigate whether the overturning circulation in such an asymmetric domain is representative for a similar circulation in a domain extending all the way south to, say, 60°S ($q = G$ in Eq. (4.5)). In this section we show that both models are able to produce a circulation pattern which resembles the zonally averaged overturning circulation in the Atlantic: this circulation is characterised by strong downwelling in the northern part of the basin, and weak upwelling in the rest of the basin. In accordance with the nomenclature of Thual and McWilliams (1992), these northern downwelling pole-to-pole states are denoted by NPP.

In order to obtain an Atlantic domain NPP (ANPP) state, an NPP solution was calculated on the global domain (GNPP) first (defined by the mapping $q = G$ in Eq. (4.5)). At $y = 0.25$ (30°S) the advective and diffusive fluxes of heat and salt were diagnosed, and they were prescribed as diffusive fluxes at $y = 0$ (30°S) of the Atlantic domain (defined by the mapping $q = A$ in Eq. (4.5)):

$$F_l^T(z) = v(T - T_0) - T_y \tag{4.27a}$$

$$F_l^S(z) = v(S - S_0) - S_y. \tag{4.27b}$$

In Appendix 4.A it is shown that reference values T_0 and S_0 should be taken equal to the average values of T and S in the $y \geq 0.25$-part of the global domain, in order to make the potential energy input of the fluxes equal in both models. The advective part of the fluxes in Eqs. (4.27) turned out to be about 6 to 9 times smaller than the diffusive parts, so the thermal and saline gradients at 30°S do not differ much between the models.

The streamline patterns of the GNPP state north of 30°S (Fig. 4.5a) and the ANPP state (Fig. 4.5b) show strong resemblance between the two main NPP circulation cells, which have their cores at the same latitudes and depths. The circulation of the ANPP state is slightly stronger ($\psi_{max} = 7.31$) than that of the GNPP state ($\psi_{max} = 6.01$). The Atlantic state shows a well-developed counter-rotating circulation cell at the southern boundary, a feature which is much weaker and shallower in the global domain. The thermal and saline fields of the two solutions show strong resemblance as well (not shown). The ANPP state appears to be slightly warmer and saltier at the southern boundary, due to downward heat and salt advection by the stronger secondary cell.

Due to the procedure of diagnosing and prescribing the fluxes at 30°S, the ANPP state experiences the same thermohaline coupling with the (virtual) region south of 30°S as the GNPP state north of $y = 0.25$. The two models differ primarily in the momentum balances, as in the Atlantic model no exchange of vorticity and kinetic energy with the Southern Ocean is possible. In order to estimate the consequence of this neglect, we calculated the balance of production and dissipation of kinetic

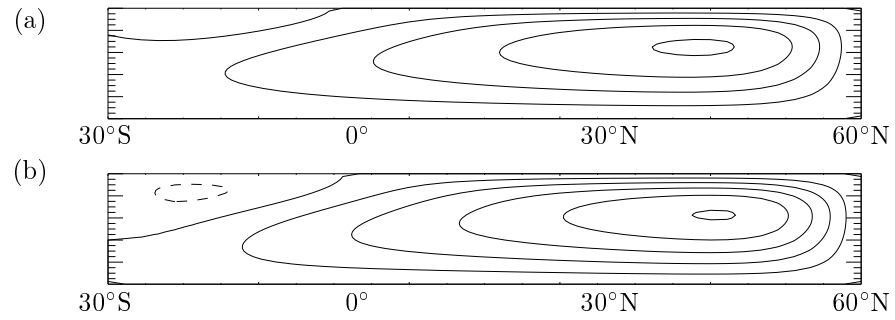

Figure 4.5: *Streamfunction profiles of NPP states at* $\sigma_s = 16.0$ *in the (a) global domain north of 30° S, and (b) its Atlantic domain counterpart. At the southern boundary of the latter state fluxes of heat and salt are prescribed which are diagnosed at* $y = 0.25$ *in the global state. Streamfunction is scaled with the maximum of the Atlantic state in both panels. Solid contours denote clockwise circulation (negative* ψ*), and have an increment of* 0.2.

energy in the two subdomains of the GNPP state ($y < 0.25$ and $y > 0.25$). It turns out that only 1.4% of the kinetic energy that is generated in the northern part is transported to the southern part. This means that the energy balance of the northern subdomain is as good as closed, and that the southern part plays a negligible role in the generation and dissipation of kinetic energy of the large-scale overturning circulation. Later we show that the balance between production ($Ra < wB >$) and dissipation (D) of kinetic energy (Eq. (4.18b)) yields an univocal relation between the overturning strength ψ_{max} and the large-scale characteristics of the thermohaline fields that determine $< wB >$ (Eq. (4.18a)). This suggests that the relation between ψ_{max} and $< wB >$ in this northern subdomain of the GNPP state may be quite similar to this same relation in the ANPP state. It therefore seems reasonable to assume that the response of the Atlantic state to changing the lateral heat and salt fluxes will be at least qualitatively similar to the response that the global state would display, were we able to force the same heat and salt fluxes at its interior $y = 0.25$ position. In the following analyses we assume that the representation of the GNPP state by its cut-off Atlantic counterpart is justified, and we will focus our attention on the NPP states of the model in the Atlantic configuration.

4.4.2 Realistic lateral fluxes

First we investigate the impact of the thermal component of interbasin exchange on the overturning circulation by applying a lateral heat flux $F_l^T(z)$ (Eq. (4.11a), solid line in Fig. 4.4), which accounts for heat input at a shallow level. Starting from the Atlantic NPP state with $\sigma_s = 10$ ($\sigma_l = 0$), we increase the heat flux amplitude τ_l from 0 to a value of 70, which is a realistic value according to the scaling in Eq. (4.12).

The strength of the overturning cell, given by the maximum value of the stream-

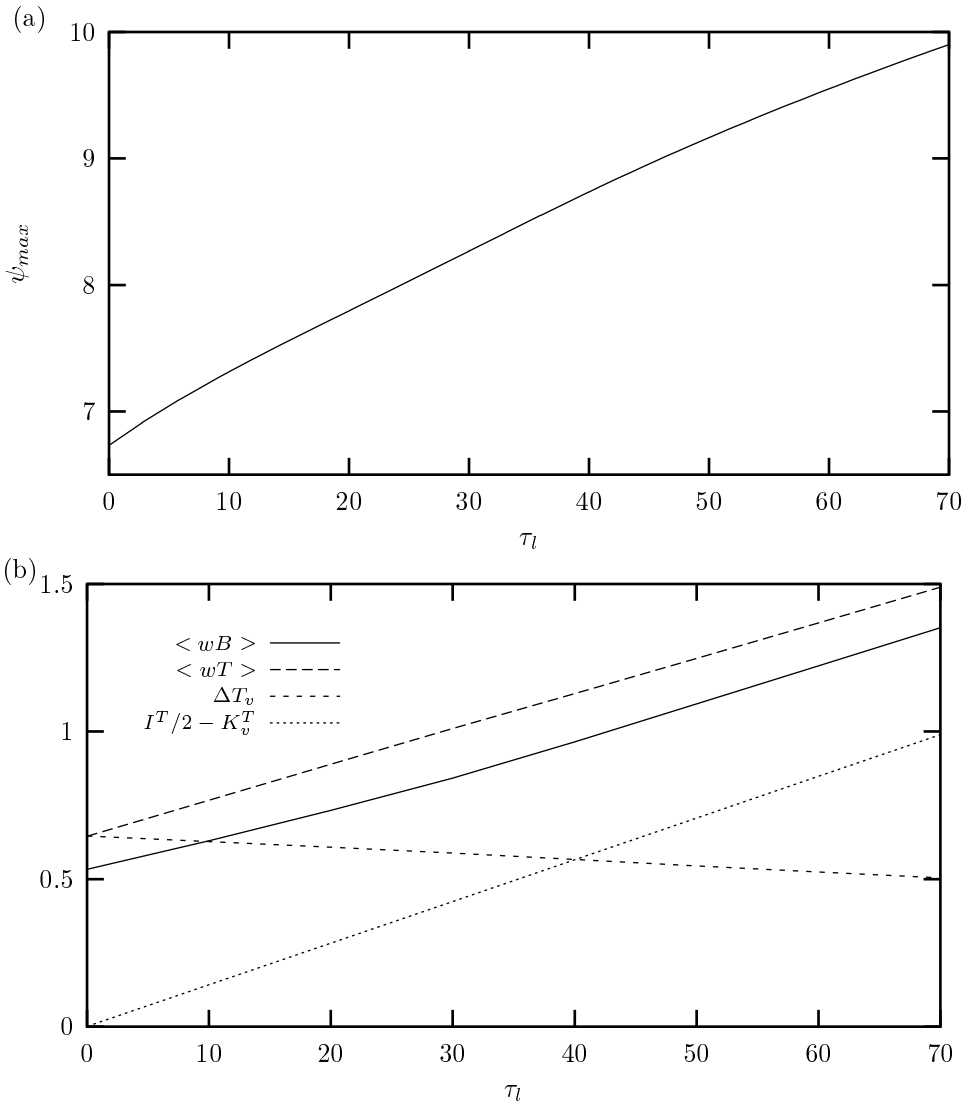

Figure 4.6: *Relations between lateral heat flux amplitude τ_l and (a) overturning strength ψ_{max}, and (b) buoyancy production $< wB >$ and its thermal component $< wT >$. In steady state, $< wT >$ equals the sum of the vertical temperature difference ΔT_v and the boundary flux contribution $I^T/2 - K_v^T$. The lateral heat flux F_l^T is plotted in Fig. 4.4 (solid line) and given by Eq. (4.11a). The value $\tau_l = 70$ is representative for observed fluxes across 30°S (Eq. (4.12)).*

function ψ_{max}, increases significantly as the amplitude τ_l of the lateral heat flux is increased (Fig. 4.6a). The governing terms in the energy balance of Eq. (4.18a) (Fig. 4.6b) show that this increase in ψ_{max} corresponds to a strong increase in buoyancy production $< wB >$, reflecting the balance between production and dissipation of kinetic energy (Eq. (4.18b)). This increase in $< wB >$ is almost completely accounted for by its thermal component $< wT >$, as its saline component $- < wS >$ is not affected by the strong increase in overturning strength. This is surprising, as a change in the balance between vertical advection ($< wS >$) and diffusion (ΔS_v) of salt was certainly expected in response to a strong increase in basin-wide upwelling.

Figure 4.6b furthermore shows the dominant role played by the boundary integral $\oint z\mathbf{F}^T \cdot \mathbf{n}\ d\Gamma$, which, according to Eq. (4.19), can be split into a contribution from the net flux $I^T/2$, and a shape contribution $-K_v^T$. It turns out that an increase in net surface cooling tends to strengthen the circulation: buoyancy removal at the surface is a source of potential energy and its contribution to the buoyancy production is positive ($I^T/2 = 0.027\ \tau_l$). The particular shape of the lateral heat flux counteracts this tendency: its contribution to the buoyancy production is negative ($-K_v^T = -0.014\ \tau_l$), as heat input at a shallow level stabilises the stratification and extracts potential energy from the system. However, this weakening effect is too small to balance the strengthening influence of net surface cooling: the sum of both contributions is positive ($0.013\ \tau_l$) and is responsible for the increase in overturning strength with increasing τ_l.

Despite the tendency of the lateral heat flux to stabilise the stratification, the vertical thermal difference ΔT_v can be seen to decrease slightly. This reflects an increase in bottom temperature, because surface temperatures are fixed. This warming of the deeper part of the basin is related to the increase in circulation strength, causing increased northward advection of warm subsurface waters and consequently downwelling of warmer waters.

To explore how the saline component of ocean interbasin exchange modifies the overturning circulation, we now add a lateral salt flux to the lateral heat flux of the former section ($\tau_l = 70$). The profile of this salt flux F_l^S (Eq. (4.11b), long-dashed line Fig. 4.4) accounts for lateral salt export from the upper layer. The amplitude σ_l is increased from zero to 16, which is a realistic value according to the scaling of Eq. (4.13). As mentioned before, the $\sigma_l I_l^S$ net salt export brought about by the lateral salt flux is compensated by salt import through the surface of the same magnitude to maintain a flux balance. This extra surface salt input corresponds to net evaporation from the basin.

The overturning strength increases slightly when σ_l is increased (Fig. 4.7a, solid line). The most relevant terms in the buoyancy production (Fig. 4.7b) show that this increase is related to a decrease in the positive (weakening) value of $< wS >$ (note that $B \propto -S$). Again the contribution of the boundary fluxes dominate the balance. The net surface salt input removes buoyancy from the surface and increases the buoyancy production by an amount of $I^S/2 = -0.055\ \sigma_l$. The specific shape of the lateral salt flux exports salt at a shallow level and stabilises the stratification, thus reducing the buoyancy production by an amount of $-K_v^S = 0.063\ \sigma_l$. Contrary to the lateral heat flux, this weakening effect of the lateral salt flux turns out to be

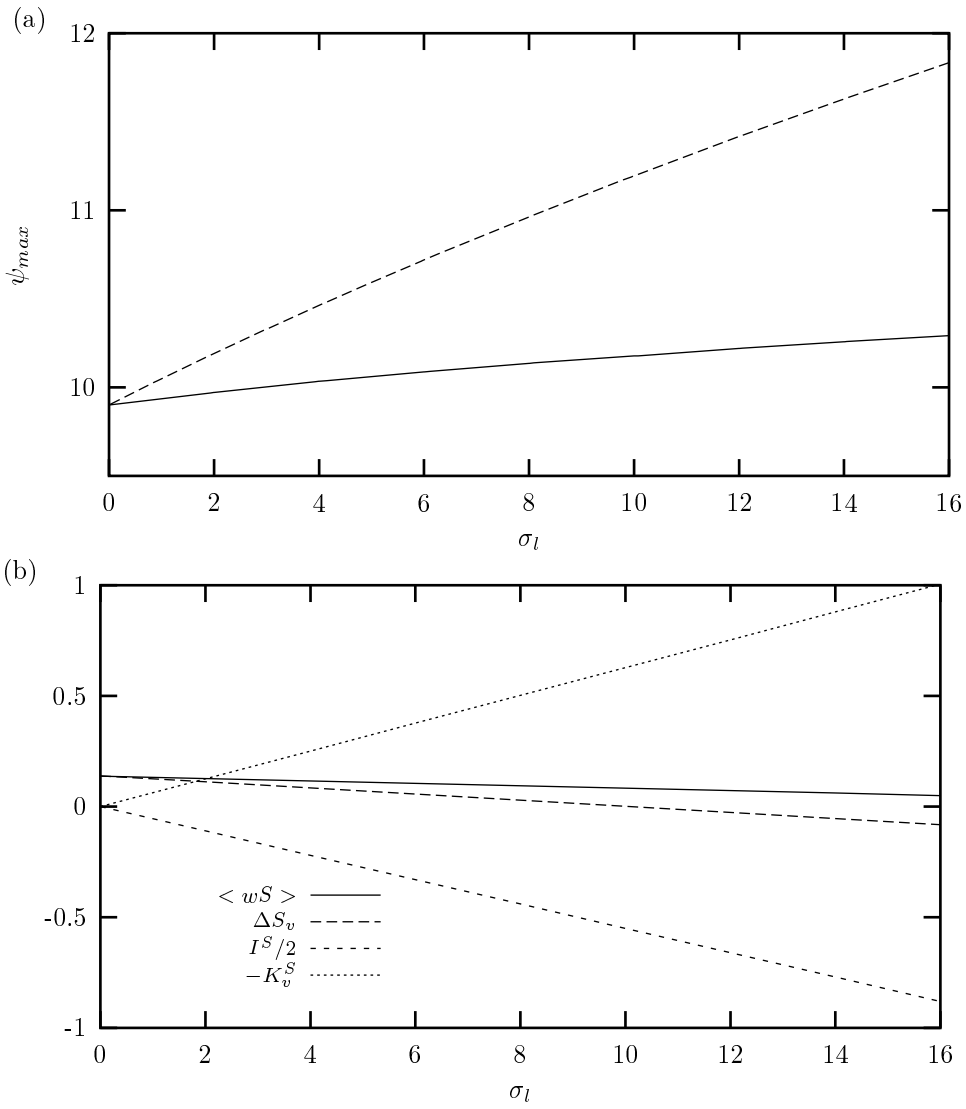

Figure 4.7: *(a) Relation between the lateral salt flux amplitude σ_l and overturning strength ψ_{max}, for a lateral salt flux with vertical profile F_l^S (solid line) and for a vertically uniform lateral salt flux (dashed line). (b), (c) Relation between the lateral salt flux amplitude σ_l and the saline component $< wS >$ of the buoyancy production for the vertical profile case (b) and for the vertically uniform case (c). In steady state, $< wS >$ equals the sum of the vertical salinity difference ΔS_v and the boundary flux contributions $I^S/2 - K_v^S$. The flux profile F_l^S is plotted in Fig. 4.4 (long-dashed line) and given by Eq. (4.11b). The value $\sigma_l = 16$ is representative for observed fluxes across 30° S (Eq. (4.13)). Note that $< wB > \propto - < wS >$, so a positive value of $< wS >$ tends to brake the flow.*

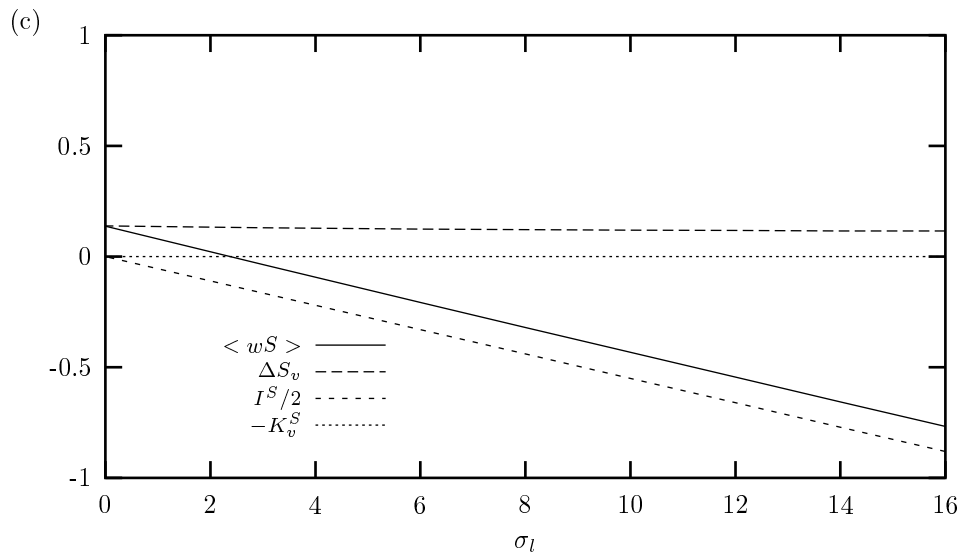

Figure 4.7: *Continued.*

large enough to balance, and even exceed the strengthening effect of net surface salt input.

The stabilizing influence of the shape of the lateral salt flux is also reflected by the decrease and sign reversal of the vertical salinity difference ΔS_v in Fig. 4.7b. As ΔS_v reflects the basin-integrated diffusive vertical salt flux, this sign reversal implies that the originally downward diffusive salt flux is reversed, and that salt is now diffused *upward*. This source of potential energy is *indirectly* caused by the shape of the lateral salt flux, and counteracts the weakening *direct* contribution of this shape ($-K_v^S$). The *total* effect of the lateral salt flux is eventually weaker than that caused by the net surface salt input ($I^S/2$), resulting in the slight increase in $< wB >$.

The suggestion that ΔS_v is modified by the particular shape of the lateral salt flux, rather than by a net surface salt flux, is verified in a subsequent case: we increased the amplitude of a *vertically uniform* lateral salt flux $\sigma_l I_l^S$ ($I_l^S < 0$) from zero to 16. The absence of the vertical profile (Fig. 4.7a, dashed line) makes the overturning strength much more sensitive to changes in the salt flux strength σ_l: the relevant terms in the energy balance (Fig. 4.7c) show that the strengthening influence of net surface salt input is no longer counteracted by the shape contribution $-K_v^S$, as this term is zero in this case. The stratification ΔS_v remains unchanged; we can conclude that the vertical profile of the lateral salt flux was largely responsible for changing the stratification in the previous experiment, rather than the net surface salt flux.

4.4.3 Thermohaline forcing and overturning strength

In this section we examine which changes in the external forcing (the boundary fluxes of buoyancy) tend to affect the overturning strength most. To that end, we compare the sensitivity of the circulation strength to changes in the surface and lateral buoyancy fluxes, and analyse this sensitivity in terms of the two integral balances Eqs. (4.18) and (4.24), as introduced in section 4.3.4.

In this section we keep the net flux of salt through the surface and the lateral boundary fixed at $16\, I_l^S$ as we independently increase the amplitudes σ_s ($\sigma_l = 0$) and σ_l ($\sigma_s = 0$) of the shapes of the surface and lateral salt fluxes $\widetilde{F}_s^S(y)$ and $\widetilde{F}_l^S(z)$. The circulation strength ψ_{max} turns out to be very sensitive to the amplitude σ_l of the lateral salt flux, whereas the sensitivity to the amplitude σ_s of the surface salt flux is very small (Fig. 4.8a). The relevant terms in the buoyancy production confirm that the shape of the lateral flux impacts directly on the balance of potential energy through the term $-K_v^S$ (Fig. 4.8b). The shape of the surface flux, on the other hand, only changes this balance indirectly, by modifying the saline stratification ΔS_v (Fig. 4.8c).

The relevant terms in the saline component of ΔB_h (Eq. (4.24a)) show that the change in amplitude σ_l of the lateral salt flux has almost no effect on the balance of the buoyancy torque (Fig. 4.9a). The change in the amplitude σ_s of the surface salt flux, however, does influence this balance significantly through the term K_h^S (Fig. 4.9b). This change, reflecting an increase in the meridional transport of freshwater by the atmosphere, is counteracted by an increase in the meridional advection $< vS >$, rather than by an increase in ΔS_h. Increasing the amplitude of the surface salt flux does therefore not result in a significant increase in the vorticity production (Eq. (4.24b)) or circulation strength.

Equations (4.18a) and (4.24a) show that in a steady state changes in the distribution of the boundary fluxes (as reflected by K_v or K_h) must be balanced by changes in advective or diffusive transports. Since our model is in the advective regime, as is the real ocean, changes in K_v or K_h appear to be balanced by advection (through $< wB >$ and $< vB >$) rather than by diffusion (ΔB_v or ΔB_h)(Figs. 4.8 and 4.9). This means that changes in the boundary fluxes that impact on the potential energy (e.g., via $I/2$ or K_v) directly influence the conversion of potential to kinetic energy (accomplished by $< wB >$), and thereby the flow strength. These changes appear to be really *forced* upon the flow. This does not hold for changes in the boundary fluxes that impact on the buoyancy torque (e.g., via K_h). Since these changes are again responded to by advection $< vB >$, rather than by diffusion ΔB_h, they do not directly influence the production of vorticity (accomplished by ΔB_h). In our model the source of vorticity ΔB_h is *determined* by the flow, rather than that it *forces* the flow. We conclude that, in our model and in the specific parameter regime studied, the overturning circulation is much more sensitive to variations in the shape and amplitude of the lateral buoyancy fluxes than to similar variations in the surface fluxes. This is due to the fact that the shapes of the lateral fluxes have a much stronger (direct) impact on the potential energy of the system than those of the surface fluxes, which modify the potential energy only in an indirect way.

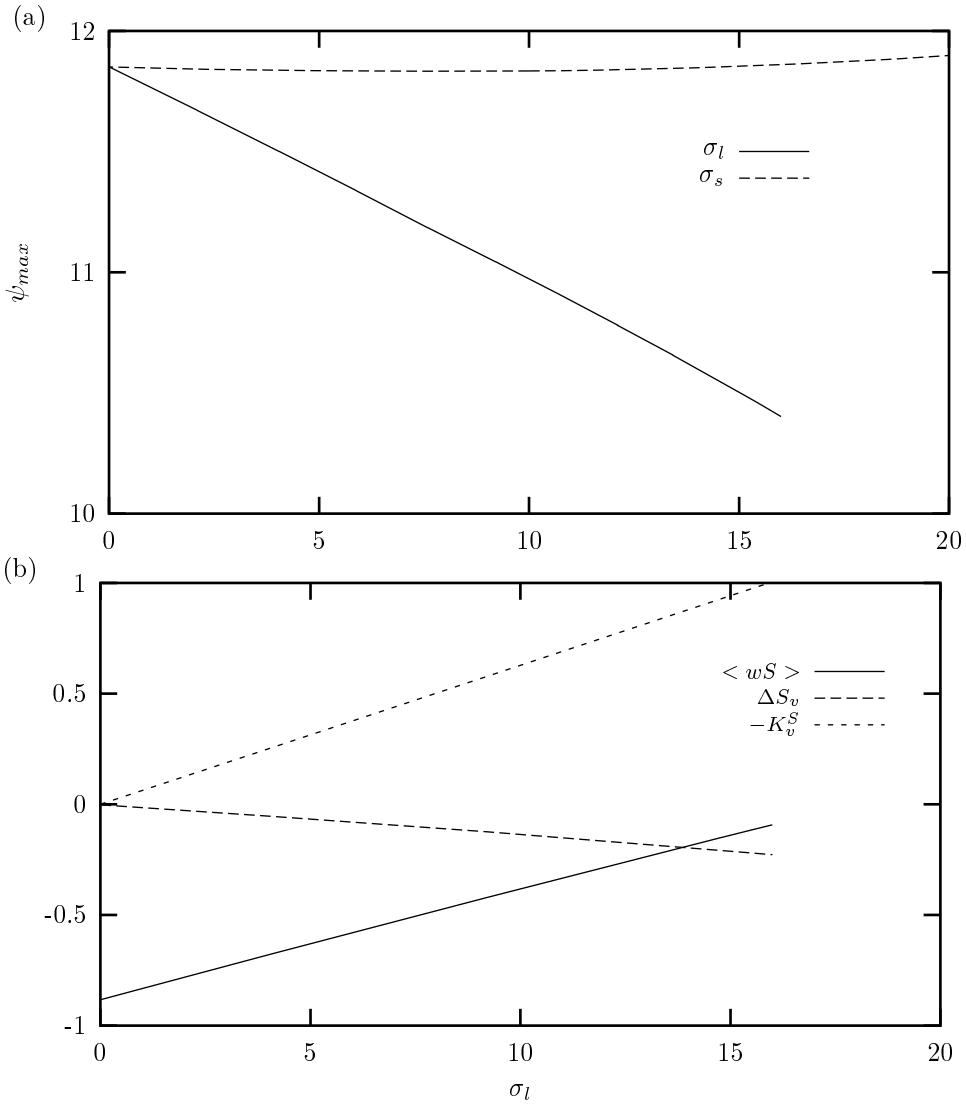

Figure 4.8: *(a) Overturning strength ψ_{max} as a function of lateral salt flux amplitude σ_l (solid line) and surface salt flux amplitude σ_s (dashed line). The net flux was kept fixed, and only the amplitudes of the profiles were changed. In (b) and (c) the relevant terms in the buoyancy production are plotted for both cases, showing that the shape of the lateral flux contributes directly to the energy balance through $-K_v^S$, while the shape of the surface salt flux only influences the energy balance in an indirect way through ΔS_v.*

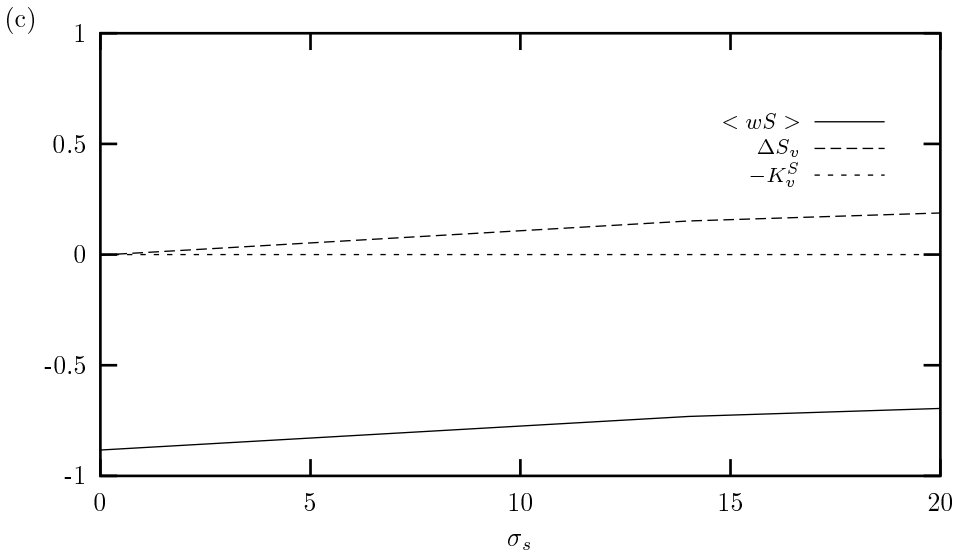

Figure 4.8: *Continued.*

4.5 Discussion

4.5.1 Scaling relations

According to the discussion in section 4.3.4, we expect the relation between ψ_{max} and the buoyancy production $< wB >$ to be approximately quadratic, whereas the relation between ψ_{max} and the meridional buoyancy difference ΔB_h is expected to be approximately linear. In Fig. 4.10, the meridional buoyancy difference ΔB_h and the buoyancy production $< wB >$ are plotted as a function of ψ_{max} for all experiments performed. Linear and quadratic fits to these results are included to indicate that the presumed relations hold quite well in this model.

These two scaling relations displayed by this model correspond to the first order balances between density gradients and the angular momentum in the meridional plane, which are found in the rotationless limit of a low order projection of the Navier-Stokes equations by Van der Schrier and Maas (1998). Their model gives a physical justification to the frequently used box models (e.g., Stommel 1961), which *impose* a linear relation between overturning strength and meridional density gradient. However, once rotation is included, this relation is complicated. Scaling relations based on thermal wind balance yield a 1/3 power-law relation (e.g., Bryan 1987) between overturning strength and meridional density scale. Nevertheless, low-resolution OGCM's (e.g., Rahmstorf 1996) appear to follow the linear relation rather than the power-law dependence, when, according to Rahmstorf, most of the NADW upwelling takes place outside the Atlantic.

The quadratic relation between the overturning strength ψ_{max} and the buoyancy production $< wB >$ (Fig. 4.10) shows that a quadratic relation exists between ψ_{max}

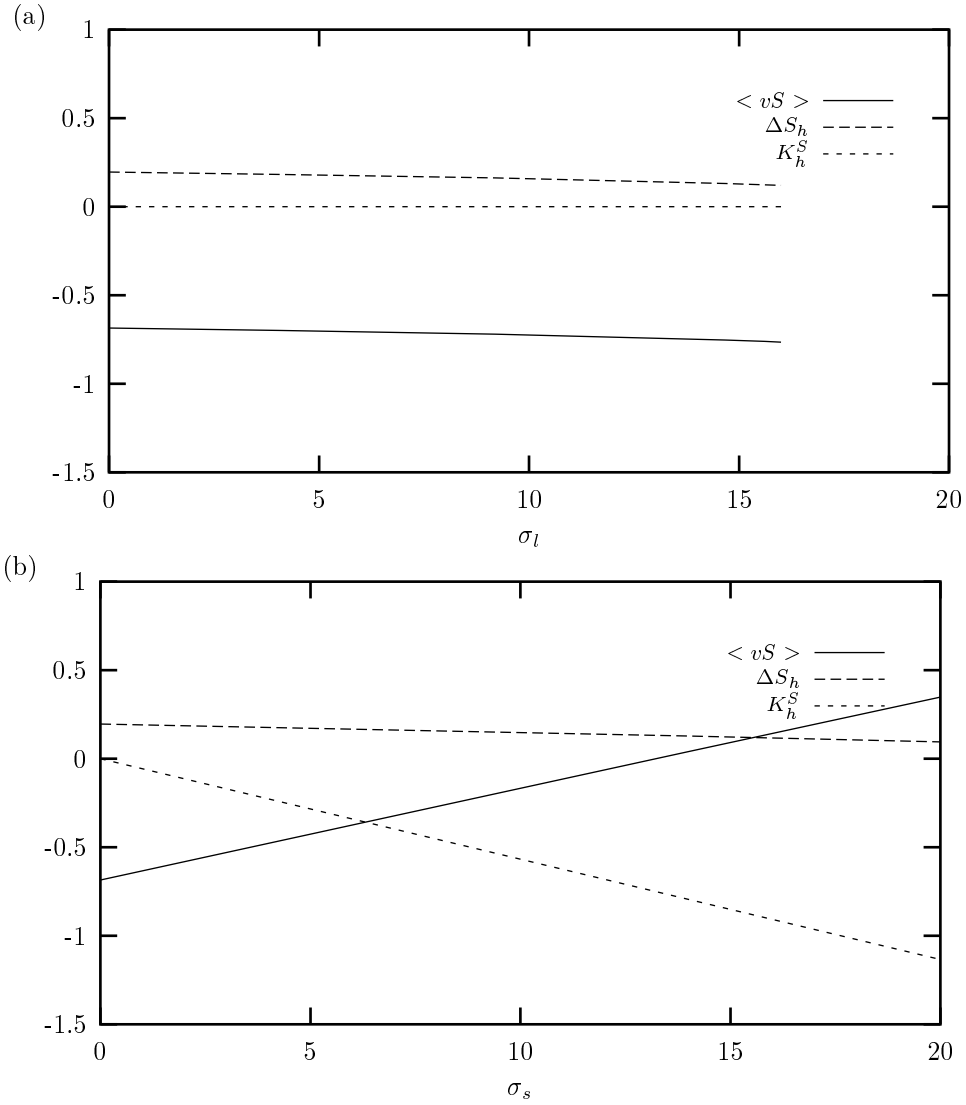

Figure 4.9: *The relevant terms in the balance of the buoyancy torque (Eq. (4.24a)) for the same cases as in Fig. 4.8. The increase in the lateral flux (a) has almost no impact on this balance, whereas the increase in the surface flux (b) causes the change in* K_h^S. *This change is balanced by the advection term* $< vS >$ *rather than by the meridional salinity difference* ΔS_h.

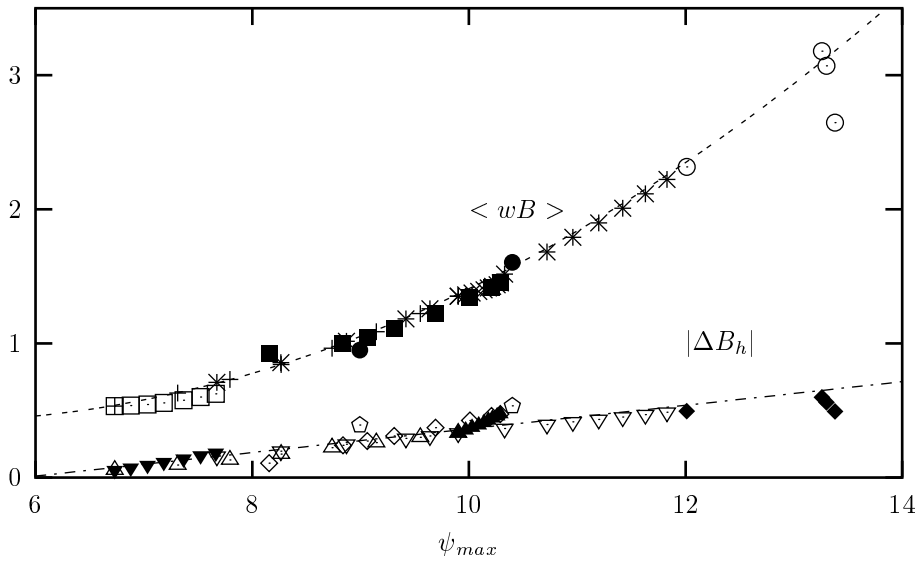

Figure 4.10: $< wB >$ *and* ΔB_h *set out against* ψ_{max} *for all experiments performed. Curves are best-fit quadratic* ($< wB >$) *and linear* (ΔB_h) *functions.*

and a net surface buoyancy flux I_s, since I_s contributes directly to $< wB >$ (Eqs. (4.18) and (4.19)). This suggests that the strength of the Atlantic overturning circulation is directly related to the net freshwater export from the Atlantic basin. This is in agreement with the findings of Zaucker et al. (1994) and Rahmstorf (1996), who found a similar relation in different model contexts. In our model this relation is based on the fact that a net surface buoyancy flux is a source of potential energy, and that it supplies energy to drive the overturning circulation. We do not know whether the agreement between our model and the models of Zaucker et al. (1994) and Rahmstorf (1996) is based on equivalent physics.

4.5.2 Thermohaline component of the lateral salt flux

In section 4.2 it was shown that there is a large difference between the total lateral salt flux at 30°S and its overturning component, both in shape and in net transport (Fig. 4.1b). As our 2D model lacks the residual transport by the wind-driven gyres, one could argue about which flux to use as appropriate lateral forcing for this model. So far, we have chosen to use the total salt flux, which is the true thermohaline flux, as it is consistent with net evaporation from the Atlantic basin. However, this choice forces the overturning circulation (or unrealistically strong meridional diffusion) to account for net evaporation, whereas in reality this is accounted for by the wind-driven gyre circulation. The large southward salt flux across 30°S, for instance, is represented in our model by a diffusive flux at the southern boundary. This requires

a meridional gradient in salinity which freshens the surface layers, although in reality Atlantic thermocline salinities are extremely high. On the other hand, prescribing the overturning component of the salt flux gives a wrong sign to the net flux. It might, however, give more credit to the thermohaline structure in the Atlantic: the large influx of thermocline water saltens the surface layer, while a fresh subsurface layer might be generated by the salt export at intermediate depths (long-dashed line in Fig. 4.1b).

To study the consequence of prescribing the overturning component of the salt flux, instead of the total flux, we performed a transformation between the total salt flux, as given by Eq. (4.11b) and here denoted $F_{l,total}$, and a representation of the overturning component, $F_{l,overturning}$, as follows:

$$F_l(z) = (1-\mu)F_{l,total}(z) + \mu F_{l,overturning}(z). \tag{4.28}$$

The main characteristics of the overturning salt flux (strong salt input in the upper layer, an export maximum at subsurface levels, and net salt import) are well modelled by a flux of the following form (short-dashed line in Fig. 4.4):

$$F_{l,overturning}(z) = \cos\left[12.4(z-1)\right] * \exp\left[8.0(z-1)\right] + 0.05, \tag{4.29}$$

which was obtained by fitting the function to the upper 2828 m of the overturning salt flux (Fig. 4.1b). The transformation is performed at $\sigma_s = 10$, $\tau_l = 70$, and $\sigma_l = 16$.

The terms governing the buoyancy production show a significant change as μ is changed from 0 ($F_l^S = F_{l,total}$) to 1 ($F_l^S = F_{l,overturning}$) (Fig. 4.11): the weakening effect of salinity ($< wS > > 0$) increases with μ, resulting in a decrease in overturning strength from about 10 to 8. It turns out that the net surface flux and the shape of the lateral profile interchange their roles in the energy balance during the transformation: the net surface salt source changes into a salt sink, losing its positive contribution to the buoyancy production ($-I^S/2 > 0$), and ending up weakening the flow ($-I^S/2 < 0$). Accordingly, as the shape changes from a shallow salt sink to a shallow salt source, its originally weakening influence ($K_v^S < 0$) is reversed and becomes a strengthening contribution ($K_v^S > 0$). The difference between the total salt flux profile and its overturning component is confined to the upper 20% of the domain. This leaves the vertical displacement of salt from its source to its sink relatively small: the buoyancy generated by advecting salt from the surface to the shallow lateral salt sink ($\mu = 0$, total lateral salt flux) is small, as is the buoyancy that is lost by uplifting salt from its lateral source to the surface ($\mu = 1$, overturning component). In fact, it is this change in direction that causes the increase in $I^S/2 - K_v^S$. Figure 4.11 also shows a rather strong increase in the saline stratification. This clearly shows the ability of the overturning salt flux to increase the salinities of the surface waters.

We have seen that the two-dimensionality of our model, and consequently the lack of the essentially horizontal gyre transport, makes a consistent representation of the salt transports and forcing very difficult. The transformation experiment has illustrated the differences between two possible flux profiles: although prescribing the total salt flux is the most consistent choice with respect to the sign of the net salt flux, the overturning component is more consistent with Rahmstorf's (1996) concept

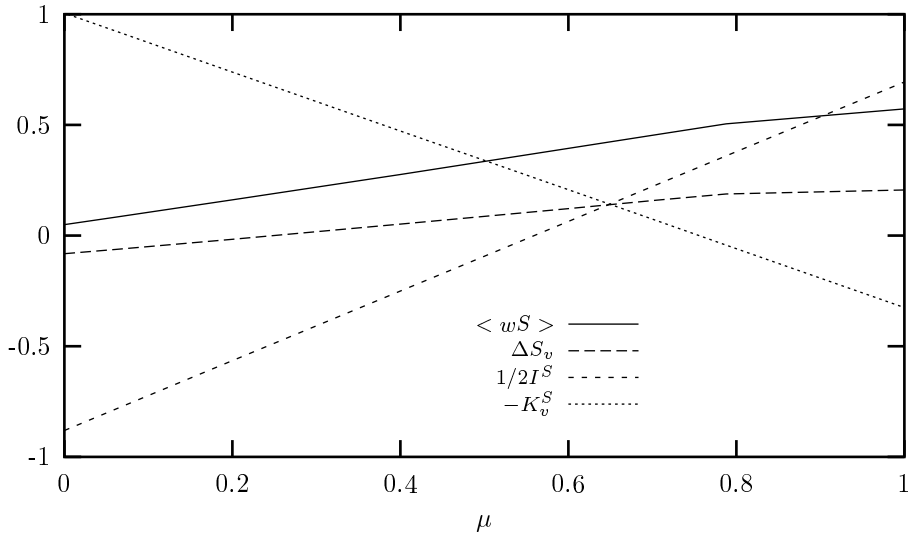

Figure 4.11: *Saline component of the buoyancy production* $< wS >$ *and its components as a function of the parameter* μ. $\mu = 0$ *denotes the model with the total salt flux prescribed, whereas at* $\mu = 1$ *the zonally averaged overturning component is prescribed (see Fig. 4.4). Note that an increase in* $< wS >$ *corresponds to an increase in the weakening effect of salinity on the circulation strength (a decrease in* $< wB >$*).*

of active freshwater forcing. However, we do not know the surface profile of this active freshwater forcing, and just adding a constant freshwater input to the observed profiles of $E - P$, as was done in this study, is also quite arbitrary. These results indicate that care should be taken when using 2-D models, as they fail to resolve residual fluxes of heat and salt properly.

4.5.3 The model

Although the model is not appropriate to quantify the processes studied, we believe that is has shown basic principles governing the operation of the overturning circulation which may be independent of details of the model: when the basin-integrated energy balances of the real ocean or of a realistic ocean model are calculated, then these integral balances are governed by very much the same processes as described in this chapter. The only relevant mechanism of potential energy removal which is not represented in this model is mesoscale convection. Bryan (1987) and Huang (1998) analysed the energy cycles of a single-hemispheric GCM with rectangular geometry, driven by thermohaline forcing, and with (Bryan) and without (Huang) wind forcing. In both studies mesoscale convection turned out to be the largest sink of potential energy, and only a small fraction (generally some 10%) of the energy input by vertical mixing (equivalent to ΔB_v in our model) was directly converted into kinetic energy

of the large-scale overturning circulation.

In general, the potential energy U of a density driven fluid in motion contains a background component U_r, and a component known as available potential energy U_a, which is the amount of energy that would be released if the flow were halted and the density field settled in its least energetic distribution, with energy content U_r (Huang 1998). Contrary to the potential energy U, for instance, the available potential energy U_a *can* be modified by the meridional distribution of surface buoyancy fluxes, albeit at the expense of U_r. For a transient system, the time-evolution of the available potential energy U_a might give a better description of the behaviour of the system, since the reference energy U_r can be considered as merely 'dead weight', and is not available to drive the flow. To that end it is comparable to the basin-averaged potential energy U_0, as introduced in Appendix 4.B. In this study, however, we only considered steady state solutions. For these states the sources and sinks of U and of U_a are ultimately the same, since the reference energy U_r (as well as U and U_a) is constant. As we furthermore focussed on energy *conversions*, the exact values of the energies U, U_a and U_r are not relevant. Although the U_a contents of a solution is the amount of potential energy that *could be* converted into kinetic energy, we studied the amount of energy that *is* converted into kinetic energy.

The presence of the boundary at 30°S results of course in a rather poor representation of the overturning circulation, since in reality most of the NADW leaves the Atlantic to spread out over the entire World Ocean, instead of being upwelled north of 30°S. Due to this NADW export and the corresponding return transports, the Atlantic exchanges momentum with the Southern Ocean, leaving the balances of kinetic energy and vorticity in the Atlantic Ocean not closed. The magnitude of this exchange in the real ocean and its importance for the overall balances is not known. Therefore, we cannot assess how the neglect of this exchange modifies the sensitivity of the circulation strength to changes in the thermohaline forcing. In section 4.4.1 we have shown that there is a strong similarity between the Atlantic NPP state and the global domain NPP state, which is similar to the NPP states found in equivalent models of the thermohaline overturning circulation (e.g., Quon and Ghil 1992, 1995; Dijkstra and Molemaker 1997). However, since most of the upwelling in the global domain takes place north of 30°S as well (Fig. 4.5a), this state is not representative for multi-basin thermohaline circulation. Although in our model the exchange of kinetic energy with the southern part of the Atlantic is neglected, the exchange of potential energy is captured correctly by our approach of prescribing the lateral fluxes of heat and salt. The *nature* of buoyancy fluxes, whether advective or diffusive, is not relevant for the basin-integrated balance of potential energy in the Atlantic (Eq. (4.18a)).

In our model, the overturning circulation exhibits a strong sensitivity to a net surface buoyancy flux, for instance due to net surface cooling or net evaporation. In reality, however, the thermohaline overturning circulation is a global circulation pattern, with upwelling in the ACC, and in the Pacific and Indian Oceans. The heat or freshwater that is extracted from the Atlantic must be compensated by heat and freshwater input in the other basins. This buoyancy input on the upwelling branch of the overturning circulation would undo the potential energy gain of the Atlantic. The fact that the quadratic relation between the overturning strength and net Atlantic

evaporation is found in models which do include the Pacific (cf. section 4.5.1) might give rise to the speculation that the energy gain of the Atlantic is not completely undone in the rest of the World Ocean. Indeed there is evidence that a part of the NADW upwelling is accomplished in the wind-driven upwelling regimes of the ACC, rather than by slow uniformly distributed and buoyancy-driven upwelling (Toggweiler and Samuels 1993b; Shriver and Hurlburt 1997; Döös and Coward 1997). This implies that the wind-driven upwelling might supply at least a part of the energy needed for driving the Atlantic overturning circulation.

As advective fluxes are directly linked to the circulation, it is probable that feedback effects exist between the overturning strength and the lateral fluxes that could not be captured by our model. It is not clear how the advective heat and salt fluxes would respond to a change in the overturning circulation: such a change not only modifies the flow field, but the distributions of heat and salt, as well. It is therefore not possible to anticipate whether these feedbacks increase or decrease the sensitivity of the flow strength to changes in the lateral fluxes.

There are numerous feedbacks between the ocean and the atmosphere that can seriously affect the sensitivity and stability of the ocean's overturning circulation (Rahmstorf et al. 1996), and it is therefore important to take these into account in climate sensitivity studies. In this study we have forced the circulation at the surface with mixed boundary conditions for temperature and salinity, which are among the simplest representations of ocean/atmosphere interaction possible. Although this choice might not be realistic, it is certainly illustrative for the fact that the equilibration time scale of a sea-surface temperature anomaly is much smaller (here taken to be zero) than that of a sea-surface salinity anomaly (here taken to be infinity).

It was shown that in this model the overturning circulation is relatively insensitive to changes in the meridional distribution of the surface buoyancy flux, as this distribution does not impact on the potential energy balance. Unless the *net* surface buoyancy flux is modified, the influence of more realistic surface boundary conditions on the energy balance is probably confined to changes in the vertical buoyancy difference ΔB_v. However, the fact that in our model ΔT_v was partially constrained by the fixed surface temperatures, whereas ΔS_v was unconstrained, did not result in large differences in the response to changing thermal and saline forcing. Therefore we do not expect a large change in the role of ΔB_v when more active boundary conditions are applied. It is therefore improbable that incorporation of more active air-sea interaction drastically changes the sensitivity of the circulation to changing forcing. However, for the time-dependent response of the system the choice of boundary conditions may be essential.

4.5.4 Implications for the impact of Agulhas Leakage

What can we say about the importance of Agulhas Leakage for the conveyor belt circulation? Does the Indian-Atlantic interbasin exchange of heat and salt through Agulhas Leakage significantly influence the overturning strength, as was speculated earlier (Gordon 1986, Gordon et al. 1992)? What will happen if Agulhas leakage is shut off, and the South Atlantic surface salinities drop by about 0.5 psu?

A decrease in South Atlantic surface salinities will probably not influence the *net* flux of salt across 30°S dramatically. Retrieving a certain amount of freshwater ($E-P$) from slightly fresher surface water will reduce the virtual salt flux, and consequently the surface buoyancy removal. On the other hand, reduction of the section-averaged salinity at 30°S reduces the salt flux brought about by the net mass transport across that section (Bering Strait transport minus the amount of $E-P$). This reduction has to be compensated by salt fluxes induced by the overturning or the gyre circulations. These changes, however, will influence the net flux of salt by less than 1.5 % and, as they work in the opposite direction, might cancel each other out.

The influence of reduced Agulhas Leakage on the *shape* of the salt flux profile may be more important, as a 0.5 psu drop in a 2.0 psu salinity *anomaly* is significant. According to Eq. (4.4), it is the overturning component of the salt flux that is directly related to the mean surface salinity anomaly (referred to the Atlantic mean salinity S_0) of the South Atlantic, and internal processes will determine whether the circulation responds to a decreased salt flux by changing the residual component of the salt flux (involving the zonal salinity structure of the South Atlantic thermocline), or by changing the overturning component (involving the salt stratification of the whole Atlantic, or the overturning circulation itself). A change in the latter will influence the circulation strength most, as it involves vertical advective fluxes of buoyancy by the meridional overturning circulation.

Freshening of Atlantic surface waters might reduce the convective activity in the formation region of NADW, as suggested by Gordon et al. (1992), and so reduce the production of deep water. On the other hand, the resulting reduction of the salinity stratification will enhance the downward diffusion of buoyancy, which turned out to be a (relatively small) source of potential energy in our model.

What about heat input by Agulhas Leakage? If Agulhas Leakage can be held partly responsible for the large northward heat flux in the South Atlantic (Thompson et al. 1997), it is also responsible for large atmospheric heat loss in the Atlantic. When the influence of this northward heat flux on evaporation is considered (Gordon 1986), then Agulhas heat input might be responsible not only for net surface cooling, but also for net surface saltening. As in our model surface buoyancy loss turned out to be the largest source of potential energy, shutting off Agulhas Leakage might have a double impact on the energy balance of the Atlantic, and result in a reduction in the overturning strength. An interesting possibility is therefore that not the Agulhas salt input but the Agulhas heat input influences the overturning strength most.

Can we now explain the results obtained by Cai and Greatbatch (1995)? In their model, shutting off Agulhas Leakage didn't influence the outflow rate of deep water. They argued that the thermal and saline changes canceled each other out, leaving the density field almost unaffected. Nevertheless, several aspects of the thermohaline circulation seemed to have changed as a response to shutting off Agulhas Leakage, and some of these changes might have had some influence on the balance of potential energy in the model ocean: the net northward heat flux across 30°S seemed to have been reduced (their Fig. 12), and consequently the surface buoyancy loss and the associated potential energy gain; there appeared to have been a warming and saltening of the surface waters in the northern North Atlantic, possibly due to reduction of the

deep convection in this region, which would have caused a reduction in the associated sink of potential energy; although the thermal and saline changes might have canceled, the shift of 0.7 Sv from thermocline to intermediate water masses might have changed the shape contribution of the lateral buoyancy flux. It is therefore not clear whether in the model of Cai and Greatbatch (1995) none of these changes in the potential energy balance was large enough to influence the overturning strength, or if several effects canceled, leaving the NADW outflow unchanged.

The results of this study have shown that the overturning strength is very sensitive to details of the interbasin fluxes of heat and salt. This means that an impact of Agulhas Leakage on the overturning circulation is probable. At the same time, it emphasises the possible importance of South Indian Ocean wind regimes for the thermohaline circulation, as this seems to be controlling the amount of Agulhas Leakage. Influence of southern hemisphere winds on Atlantic overturning strength was suggested previously by Toggweiler and Samuels (1993a), although they proposed a different mechanism: they argued that the deep southward transport below Drake Passage sill depth, required to compensate for unbalanced northward Ekman transport in the Drake Passage latitude band, can have been derived only from North Atlantic downwelling. In their numerical experiments the Atlantic overturning strength was governed by this Ekman inflow, rather than by thermohaline forcing. Rahmstorf and England (1997), however, showed that the use of mixed boundary conditions by Toggweiler and Samuels (1993a) suppressed the role of the thermohaline component of the overturning circulation. Using more realistic boundary conditions, they showed that the contribution of Drake Passage Ekman flows is only a fraction of the total amount of NADW formed.

4.6 Summary and Conclusions

In the first part of this chapter we analysed the thermohaline exchange between the Atlantic Ocean north of 30°S and the Southern Ocean. We used an inversion of hydrographic data, including recent WOCE data, to calculate the meridional heat and salt fluxes across the Atlantic 30°S section. A large difference between the total lateral salt flux and its overturning component turned out to be the most striking feature of the zonally averaged profiles. As the former yielded a net southward salt flux, consistent with net Atlantic evaporation, the latter was characterised by a northward net flux, indicating that on average the exported NADW is fresher than the compensating return flows. This confirms the idea of Rahmstorf (1996) that salt transports due to the horizontal, wind-driven, gyre circulation are an essential component of the Atlantic salt budget.

We studied the influence of these lateral fluxes on the strength and operation of the overturning circulation by prescribing them at the southern boundary of a simple two-dimensional model of the Atlantic Ocean. The sensitivity of the flow strength to changes in this lateral forcing was examined and analysed in terms of integral balances of the system. The main advantage of this approach is that the results are rather independent of the details of the momentum balance, indicating that the conclusions

drawn in this study may be relevant for the real ocean.

The analyses have shown that especially the *net* components of the heat and salt fluxes have a large positive impact on the overturning strength in our model. Both net surface cooling (corresponding to a northward heat flux at 30°S in the Atlantic) and saltening (due to excess evaporation in the Atlantic) are sources of potential energy of the system and tend to strengthen the flow. The *shapes* of the lateral flux profiles turn out to have a dual influence on the potential energy of the system. As their particular shapes tend to stabilise the stratification, they extract potential energy from the system directly, and tend to weaken the flow. This effect is slightly counteracted by an increase in the downward diffusion of buoyancy, which is a source of potential energy. The results of this study also indicate that, in the parameter regime considered, the circulation strength is more sensitive to changes in the shape of the lateral buoyancy flux, than to changes in the meridional distribution of the surface buoyancy flux, as the latter does not explicitly change the potential energy input of the system.

We conclude, on the basis of this study, that not only the amount of heat or salt that is imported into the Alantic is relevant for the operation of the overturning circulation, but that also the vertical distribution of this exchange is relevant. A climatological shift in the importance of intermediate or thermocline water for compensating NADW export, or a change in the thermohaline characteristics of these water masses, might therefore influence the Atlantic overturning strength considerably.

This study shows the importance of interocean fluxes of heat and freshwater, caused by the atmosphere *and* the ocean, for the operation of the global-scale ocean circulation. This emphasises the need for truly global models for studies of climate dynamics and climate change, and for correct representations of the interbasin fluxes in these models. The model results and the analysis of the hydrographic data also emphasise one of the major shortcomings of 2D models which fail to account for residual wind-driven fluxes of heat and salt. Care should be taken when using these models for sensitivity studies of the thermohaline circulation, as Rahmstorf (1996) has shown that the sign of the net active freshwater flux is crucial for the stability of overturning states.

4.A Appropriate values for T_0 and S_0

In this appendix we will show that the appropriate choices for the reference values T_0 and S_0 in Eqs. (4.4) and Eqs. (4.27) are the average values of temperature and salinity of the basin under consideration, in this case the Atlantic Ocean north of 30°S. Only then will the potential energy input of these fluxes into the Atlantic be correctly represented in our model.

We consider the evolution-equation for basin-integrated potential energy Eq. (4.14), the basin under consideration being the Atlantic north of 30°S. No *a priori* model constraints have been used in deriving this equation: the unspecified boundary buoyancy flux $\mathbf{F}$ contains the realistic advective flux at the 30°S section or its diffusive model equivalent, and so the equation applies both to the Atlantic Ocean and to our model. When we split the vertical velocity w into the basin-averaged part $w_0 =< w >$ and a deviation w', we can write the buoyancy production as:

$$< wB >= w_0 < B > + < w'B > . \tag{4.A1}$$

As the real ocean is not closed at 30°S, and mass exchange takes place with the Southern Ocean, the net vertical transport w_0 will not vanish. This means that in reality we have, besides the residual term $< w'B >$, a change in potential energy due to net vertical flow advecting the average buoyancy $< B >$. In our model w_0 *is* zero, as the model domain is closed. In order to make the buoyancy production in our model comparable to that in the real ocean, the term $w_0 < B >$ must vanish. The definition of $B^* = \rho_0 [\alpha(T^* - T_0) - \beta(S^* - S_0)] = \rho_0 \alpha \Delta T(T - \lambda S) = B_0 B$ now shows that the correct choice for T_0 and S_0 is to take the basin-averaged values: only then do the diffusive fluxes in our 2D model represent the potential energy input of the real advective fluxes in a comparable way.

4.B Potential energy and the reference depth

The explicit appearance of the vertical coordinate z in the definition of potential energy, as well as in the boundary integral $\oint z\mathbf{F} \cdot \mathbf{n}\ d\Gamma$ of Eq. (4.18), might give rise to some ambiguity about the invariance of the potential energy formulation with respect to the particular choice of the reference level. Obviously a potential energy $U'(\Delta z) = - < (z - \Delta z)B >$, which is defined with respect to a reference level Δz above the bottom, is $\Delta z < B >$ larger than U, while the boundary integral $\oint (z - \Delta z)\mathbf{F} \cdot \mathbf{n}\ d\Gamma$ is an amount $\Delta z \oint \mathbf{F} \cdot \mathbf{n}\ d\Gamma$ smaller. As the behaviour of our system must be independent on the choice of reference level, the time-evolutions of U and $U'(\Delta z)$ are linked via:

$$\frac{d}{dt} < B >= - \oint \mathbf{F} \cdot \mathbf{n}\ d\Gamma = -I. \tag{4.B1}$$

where I is the net boundary buoyancy flux (positive outward). In steady state conditions, both $d < B > /dt$ and I must evidently be zero. We can split the potential energy U into a basin-averaged part $U_0 = - < z >< B >= - < B > /2$ and a

deviation $\widetilde{U} = - < z(B - < B >) >= U + < B > /2$. The time-evolution of U_0 equals:

$$\frac{dU_0}{dt} = -\frac{1}{2}\frac{d}{dt} < B >= \frac{1}{2}I \tag{4.B2}$$

and indicates that $I/2$ of the contribution of the boundary fluxes is used for increasing the background state U_0. A change in this background potential energy, however, is not relevant from a dynamical point of view. One way to remove these changes is to consider the time-evolution of $\widetilde{U}$, rather than of U:

$$\frac{d\widetilde{U}}{dt} = \frac{dU}{dt} - \frac{dU_0}{dt} = (...) + \oint z\mathbf{F}\cdot\mathbf{n}\, d\Gamma - \frac{1}{2}I \tag{4.B3}$$

We note that $\widetilde{U}$ is equal to the potential energy referenced to midlevel, i.e. $U'(1/2) = - < (z - 1/2)B >= U + < B > /2 = \widetilde{U}$. With this reference, the background potential energy, say $U_0'(\Delta z)$, equals zero.

In this study we use a surface buoyancy flux $F_s(y)$ at the top of the domain and a lateral buoyancy flux $F_l(z)$ at the southern boundary, so the boundary integral in Eq. (4.18a) contains two non-zero contributions:

$$\oint z\mathbf{F}\cdot\mathbf{n}\, d\Gamma = \int_0^1 F_s(y)|_{z=1}\, dy - \int_0^1 zF_l(z)|_{y=0}\, dz. \tag{4.B4}$$

When we separate the fluxes F_s and F_l into net components I_s and I_l, which must be equal in a steady state, and shape functions $\widetilde{F}_s(y)$ and $\widetilde{F}_l(z)$ which have zero integral, the surface component of the boundary integral equals:

$$\int_0^1 F_s(y)\, dy = I_s, \tag{4.B5}$$

whereas the component of the lateral boundary yields an integral denoted by K_v:

$$\int_0^1 zF_l(z)\, dz = \frac{1}{2}I_l + \int_0^1 z\widetilde{F}_l(z)\, dz = \frac{1}{2}I_l + K_v. \tag{4.B6}$$

The resulting expression for the boundary integral now becomes:

$$\oint z\mathbf{F}\cdot\mathbf{n}\, d\Gamma - \frac{1}{2}I = I_s - \frac{1}{2}I_l - K_v - \frac{1}{2}(I_s - I_l) = \frac{1}{2}I_s - K_v. \tag{4.B7}$$

It is interesting to note that the contribution of the boundary integral contains no information on the net lateral buoyancy flux I_l, but only on the *shape* of the lateral buoyancy flux $F_l(z)$. Evidently, a (homogeneously distributed in the vertical) net lateral buoyancy input does not affect the potential energy $\widetilde{U}$, as it only affects the background potential energy U_0. On the other hand, the surface contribution (Eq. (4.B5)) contains information on the *net* buoyancy flux only, but not on the shape of the surface buoyancy flux $F_s(y)$. Obviously this shape, which accounts for meridional redistribution of buoyancy within a basin, does not directly influence the potential energy of the system.

Chapter 5

Remotely induced stability of the thermohaline circulation

In this chapter it is studied how interocean exchange of heat and salt influences the strength and stability of the Atlantic overturning circulation. As in Chapter 4, a 2D Boussinesq model of the Atlantic is used, but here it ranges from 60° S to 60° N. The interocean exchange is represented by source/sink distributions of heat and salt. The distribution of these sources is based on the interocean fluxes in OCCAM, the high-resolution OGCM that was analysed in Chapter 3.

It is studied how the strength and stability of the present-day overturning circulation (and of other possible circulation patterns) is modified by the Southern Ocean buoyancy fluxes, as well as by Bering Strait inflow. In particular the role of Agulhas Leakage is addressed, in light of the 'warm vs. cold water route' controversy, and the possible role played by Agulhas Leakage during, and at the end of the last ice-age.

5.1 Introduction

The Atlantic communicates intensively with the other ocean basins via the Southern Ocean (see Chapter 3). It interacts with the Pacific mainly via the Antarctic Circumpolar Current (ACC). On its traverse through the Atlantic sector of the Southern Ocean, this current is supplied with North Atlantic Deep Water (NADW), and it leaves some of its Subantarctic Water behind. These waters form the source of Antarctic Intermediate Water (AAIW), of which a part is finally converted into NADW (e.g., Rintoul 1991). The Indian Ocean exchanges water with the Atlantic mainly in the form of large rings that are shed from a retroflecting Agulhas Current (e.g., De Ruijter et al. 1999). How much of this Agulhas Leakage water is used for NADW production is not known in detail, but a contribution of 4 Sv (Schmitz 1995) seems plausible.

The highly contrasting water mass properties of the two possible renewal paths, via Drake Passage or via Agulhas Leakage, implies that the ratio of the contribu-

tions is important for the salt and heat balance of the Atlantic. Gordon et al. (1992) suggested that Agulhas Leakage could have dynamical impact on the meridional overturning circulation as well: the salt input salinifies the Atlantic surface waters and preconditions them for the formation of NADW. During glacial times Agulhas Leakage may have been severely reduced, due to a more northerly position of the Subtropical Convergence Zone (STCZ, Howard and Prell 1992; Flores et al. 1999). Compared to the present-day wind field, a northward shift of only a few degrees would be sufficient to effectively shut off the connection between the Subtropical Gyres of the South Indian and South Atlantic Oceans (De Ruijter 1982). The reappearance at the end of the last glacial of a species of foraminifera (*Globorotalia menardii*) that had been extinct in the glacial Atlantic, but not in the Indian Ocean, also points at reduced or absent Agulhas Leakage during glacial periods. This lead Berger and Wefer (1996) to speculate that the restart of Agulhas Leakage at the end of the last glacial period could have played a role in the simultaneous re-establishment of a firm Atlantic overturning circulation.

Paleoclimatic records indicate that both during past glacial and interglacial stages climate instabilities have regularly interrupted the prevailing cold or warm conditions (e.g., Dansgaard et al. 1993). The most alarming events in view of future global warming scenarios are the sudden returns to glacial conditions during the Eem, the last interglacial that was characterised by a somewhat warmer climate than at present (GRIP Members 1993). The discovery by Stommel (1961), that thermohaline driven flow in an oceanic context may exhibit multiple equilibrium states under identical forcing, yields a plausible mechanism for explaining some of the abrupt Pleistocene climate changes (e.g., Broecker et al. 1985): in the presence of multiple equilibria, finite-amplitude perturbations may trigger a switch from one equilibrium to another, resulting in a dramatic reorganisation of the climate system. It raises the question whether under present-day (or future) forcing the so-called conveyor belt circulation is unique, or that a finite amplitude disturbance like, or resulting from, global warming could cause the ocean circulation to switch abruptly to another equilibrium state.

Multiple equilibria have been found in a large variety of models (see Rahmstorf et al. (1996) for an overview). Marotzke and Willebrand (1991), for instance, studied a model of the global ocean with simplified model geometry, featuring equally large Atlantic and Pacific Oceans, connected via a Southern Ocean. They identified four equilibria, characterised by deep water formation taking place either in the North Atlantic and/or in the North Pacific basin, or in the Southern Ocean. However, asymmetries between the Atlantic and Pacific strongly hinder the equilibria with North Pacific downwelling (e.g., Stocker and Wright 1991ab; Stocker et al. 1992a; Hughes and Weaver 1994), leaving the states with downwelling either in the North Atlantic or in the Southern Ocean as only candidates for regime switches.

However, paleoceanographic studies suggest that during the last glacial period NADW formation had not ceased, but was strongly reduced (e.g., Sarntheim et al. 1994). Indeed, several models (e.g., Manabe and Stouffer 1988; Rahmstorf 1994, 1996; Dijkstra and Neelin 1999) feature multiple equilibria that are characterised by a weaker or stronger North Atlantic overturning cell. Rahmstorf (1994) has shown that in his Ocean General Circulation Model (OGCM) different strengths of the At-

lantic overturning circulation were related to different distributions of the convective areas in the northern North Atlantic. Dijkstra and Neelin (1999) identified two equilibria resulting from north-south asymmetries in the basin geometry and in the surface freshwater flux of the Atlantic. They identify the strong overturning state as a conventional pole-to-pole circulation, that is thought to represent the present-day overturning in the Atlantic (e.g., Bryan 1986). The state with weak overturning is related to the thermally driven two-cell solutions featuring equatorial upwelling, found in models that have equatorial symmetry (e.g., Thual and McWilliams 1992; Dijkstra and Molemaker 1997). The asymmetries in the model of Dijkstra and Neelin (1999) cause a southward shift of the upwelling region, and a strengthening of the northern overturning cell.

Shaffer and Bendtsen (1994) studied the effect of the asymmetry brought about by Bering Strait transport on the stability of the conveyor belt circulation in a 3-box model, representing the North Pacific, the North Atlantic, and the rest of the World Ocean. They found that an increased freshwater inflow into the North Atlantic may destabilise the conveyor belt circulation in favour of a southern sinking state. They speculate that the strong climatic variability during the Eem may have been caused by alternation of periods with low Bering Strait transport, allowing for both the northern and southern sinking states, and with high Bering Strait transport, allowing for the southern sinking state only. Although this theory does explain the onset of the cold events, it gives no explanation for the reestablishment of the conveyor belt circulation during periods when both southern and northern sinking states can exist.

The source of north-south asymmetry that is addressed in this study is the fact that the Atlantic exchanges water, heat and salt with the rest of the World Ocean mainly via the Southern Ocean. The way this exchange takes place evidently depends on the way the NADW export from the Atlantic is compensated. In Chapter 4, the impact of interocean fluxes of buoyancy on the strength of the overturning circulation has been investigated. It was concluded that the circulation is very sensitive to the vertical redistribution of buoyancy that was implied by the lateral flux profiles. However, the model domain was asymmetric as it extended from 30°S to 60°N. This did not allow for studying the fate of the different equilibrium solutions that are present in models that do have equatorial symmetry, so no conclusions could be drawn with respect to the stability of the circulation. Furthermore, the exchange between the Atlantic and the Southern Ocean across 30°S was modelled by prescribed fluxes of heat and salt at the southern model boundary. This did not allow for a systematic determination of the impact of each of the two paths of NADW renewal, the cold water route via the ACC and the warm water route via Agulhas Leakage.

The goal of this study is to investigate how Southern Ocean exchange modifies the strength and stability of the northern sinking circulation, and what role is played by the two sources of NADW renewal. In particular we focus on the impact of Agulhas Leakage, to determine whether the presence of the warm (and salty) water path of NADW renewal has dynamical influence on the overturning circulation, as suggested by Gordon et al. (1992). The stability of the overturning circulation is tested under influence of the Southern Ocean sources, and with respect to Bering Strait freshwater input.

The model used is basically identical to the 2D Boussinesq model presented in Chapter 4. However, the domain ranges from 60°S to 60°N so that the basic equatorial symmetry is retained. Furthermore, the interocean fluxes of heat and salt are distinctively represented as source or sink distributions. This allows for estimating the impact of the warm and cold water routes of NADW renewal. In section 2 the model is described, as well as the sources that are used as a parametrisation of the interocean exchange. The amplitudes and distributions of these sources are based on the interocean fluxes in OCCAM, the high-resolution OGCM (Webb et al. 1998) that was studied in Chapter 3. In section 3 the model is forced with only the South Atlantic interocean fluxes, and the sensitivity of the overturning strength is studied for different scenarios of NADW compensation. Furthermore, the stability of this circulation is studied with respect to freshwater input through the Bering Strait. This chapter is concluded by a summary and discussion of the results (section 4).

5.2 Model set-up

5.2.1 The model

The model that is used to study the influence of the heat and salt source/sink distributions has been described in Chapter 4. The main difference is that the present configuration models the overturning circulation in the Atlantic Ocean from 60°S to 60°N. Latitude and depth are non-dimensionalised through $\theta = 60(2y-1)$ and $\tilde{z} = H(z-1)$. The influence of the Agulhas Leakage and the ACC on the heat and salt balance is modelled by heat and salt source distributions $Q^{(T,S)}(y,z)$. The dimensionless advection-diffusion equations for heat and salt now become:

$$vT_y + wT_z = T_{yy} + T_{zz} + Q^T(y,z) \tag{5.1a}$$

$$vS_y + wS_z = S_{yy} + S_{zz} + Q^S(y,z). \tag{5.1b}$$

The model is forced at the surface with a prescribed surface salt flux that is symmetrical with respect to the equator. Its profile is given by Eq. (4.9) and it is plotted in Fig. 4.2. Surface temperature is restored towards a fixed atmospheric temperature profile T^*, given by (Fig. 4.2):

$$T^*(y) = 0.5 + 0.5\cos 3y \tag{5.2}$$

The surface heat flux is thus given by:

$$-F_T = \frac{\partial T}{\partial z} = b_T(T^*(y) - T). \tag{5.3}$$

The relaxation constant b_T is set at 100, a value that is characteristic for OGCMs (Dijkstra and Molemaker 1997).

	τ_{agu}	τ_{acc}	σ_{agu}	σ_{acc}	σ_{bs}	I_s^S
OCCAM	6.27	2.14	0.95	0.64	0.36	1.94
basic	6	2	1	3	0	2

Table 5.1: *The dimensionless source amplitudes, as used in the basic source configuration, and those implied by OCCAM and observational estimates. The net surface salt flux I_s^S is consistent with a 0.5 Sv net surface freshwater export (Baumgartner and Reichel 1975). A Bering Strait salt export $\sigma_{bs} = 0.36$ is consistent with the Coachmann and Aagaard (1988) estimate. Note that the value of σ_{acc} is increased in the basic configuration to close the salt balance.*

5.2.2 The sources

The source distributions are split into an Agulhas component and an ACC component, which can be varied independently via the source amplitudes τ and σ:

$$Q^T(y,z) = \tau_{agu} Q^T_{agu}(y,z) + \tau_{acc} Q^T_{acc}(y,z) \tag{5.4a}$$

$$Q^S(y,z) = \sigma_{agu} Q^S_{agu}(y,z) + \sigma_{acc} Q^S_{acc}(y,z). \tag{5.4b}$$

The dimensionless amplitudes τ and σ and the dimensionsless distribution functions Q^T and Q^S can be related to the real sources of heat and salt that are implied by interocean exchange. However, no sufficiently detailed information about the spatial distribution of these interocean fluxes have been found in the literature. Therefore the climatology of the high-resolution OGCM OCCAM (Webb et al. 1998) is used. In Chapter 3 and in Appendix 5.A the interocean exchange of this model is analysed, revealing that the model is not in balance and that storage of salt takes place in the Atlantic. Furthermore, it was found that the model displays some unrealistic features when compared with observations. Nevertheless, it was concluded that the large-scale transports and thermohaline structures are reasonably well reproduced to justify a carefull use of the OCCAM flux profiles as a basis of the source distributions in this study. In Appendix 5.A it is shown how the interocean fluxes in OCCAM are used to construct distributions of the sources that are applied in this model, and to estimate characteristic values for their amplitudes.

Table 5.1 (first column) shows the dimensionless source amplitudes implied by the OCCAM interocean fluxes, a realistic Bering Strait salt transport (Coachmann and Aagaard 1988), and a 0.5 Sv surface freshwater export (Baumgartner and Reichel 1975). However, the salt sources and sinks do not add up to 0, so that the salt balance:

$$\sigma_{agu} - \sigma_{acc} - \sigma_{bs} + I_s^S = 0 \tag{5.5}$$

does not hold. This is partly due to geometric effects like the irregular width of the Atlantic basin and the convergence of meridians. This impedes a consistent mapping of the fluxes on a meridional strip of constant width. For another part, the non-zero sum of the fluxes is caused by storage of salt in the OCCAM model, and the residual transports that were not included in the calculation (i.e., eddy fluxes and diffusion). The values of σ_{agu} and σ_{acc} were determined from the OCCAM climatology, and are

probably least representative for the real ocean. The choice was made to adjust the strength of the ACC salt source so that it matches the sum of the other sources. When Bering Strait salt export is not included, the ACC salt sink increases from $\sigma_{acc} = 0.64$ to 2.89, while otherwise we have $\sigma_{acc} = 2.53$.

In Appendix 5.A the construction of the source distributions is described. Analytical functions are fitted to the profiles derived in Chapter 3. A spatial view on the resulting source/sink distributions is provided by the wire plots of Fig. 5.1, which show the Agulhas and ACC heat (upper panel) and salt (lower) sources, all with (dimensionless) amplitude 1. The Agulhas heat source profile shows strong heat input in the subsurface layer, whereas the ACC heat sink profile is characterised by heat export from the upper layer. A slight heat input is present at intermediate levels. The Agulhas salt flux profile is characterised by strong salt input at shallow levels and a vertically homogeneous salt input at deep and bottom water levels. At intermediate depths there is a minimum in eastward salt transport. The ACC salt source shows a similar structure, but of opposite sign. It features a shallow salt export, an input of salt at intermediate depths, and a small export at the deeper levels.

The Bering Strait salt flux is modelled by a lateral salt flux through the northern boundary of the domain. The profile is taken to be exponential in the vertical, so that:

$$F_{bs}^S = \sigma_{bs} \frac{c}{1 - e^{-c}} e^{c(z-1)}. \tag{5.6}$$

The parameter c is given the value 17, so that its corresponding depth scale of about 300 m is characteristic of the depth of the shallow overflow ridges in the northern North Atlantic.

5.3 Results

5.3.1 The basic experiment (no Bering Strait)

Figure 5.2 shows the streamfunction, temperature and salinity fields of the solution that is forced with the basic source configuration. This configuration is characterised by an Agulhas heat source of amplitude $\tau_{agu} = 6$, an ACC heat sink of amplitude $\tau_{acc} = 2$, an Agulhas salt source of amplitude $\sigma_{agu} = 1$ and an ACC salt sink of amplitude $\sigma_{acc} = 3$. The amplitude of the surface salt flux profile σ_s is set at 10, and there is a net surface salt input $I_s^S = 2$. Bering Strait salt export has not been included at this point ($\sigma_{bs} = 0$).

The circulation that has developed is characterised by a strong overturning with downwelling in the northern part of the domain. The overturning strength, as measured by the maximum value of the streamfunction ψ_{max}, is 10.5 in dimensionless units. With the dimensional streamfunction ψ^* being related to its scaled counterpart via $\psi^* = \kappa_v L/H\psi$ (see Chapter 4), this corresponds to a dimensional streamfunction of about 0.27 m^2/s per longitudinal meter, or, if applied to a basin of 60° wide, a transport of 18 Sv. This overturning strength agrees well with the 20 Sv estimate of Broecker (1991).

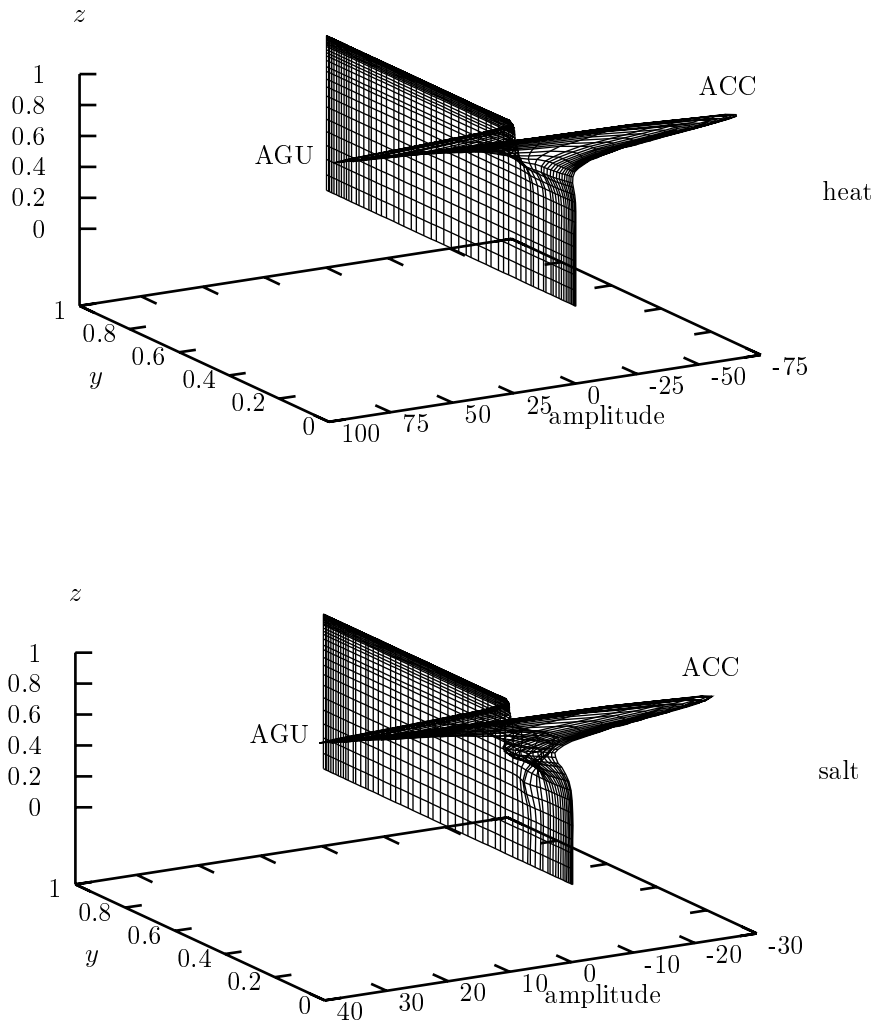

Figure 5.1: *Wire plot representations of the combined Agulhas and ACC heat (upper panel) and salt (lower panel) source/sink distributions, all with (dimensionless) amplitude 1.*

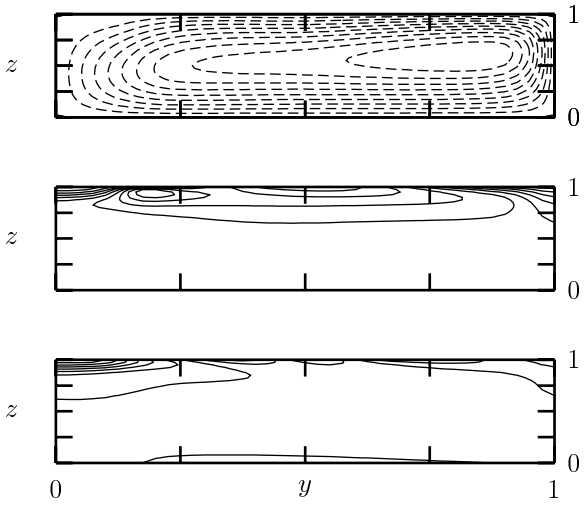

Figure 5.2: *Streamfunction(upper panel), temperature (middle panel) and salinity (lower panel) fields for the basic solution. Variables are scaled with their maxima. Contour spacing is 0.1. Note the strong stratification in the ACC area. Dashed contours in upper panel denote clockwise circulation.*

The temperature field (Fig. 5.2, middle panel) shows a well developed thermocline. The strong Agulhas source is responsible for the subsurface temperature maximum at $y = 0.17$. The salinity field displays a strong minimum at the most southerly latitudes, where the ACC salt sink extracts salt from the Atlantic. From this fresh pool a low-salinity tongue is advected northward to well within the subtropics. This feature resembles the northward penetration of the relatively fresh AAIW into the Atlantic (Fig. 1.5).

Comparison of the model's surface salinities (Fig. 5.3, 'no Bering Strait') with observations ('Levitus') shows that the position and amplitudes of the subtropical maxima and tropical minimum are well reproduced. The low salinities in the ACC region reflect the fact that the amplitude of the ACC salt sink is increased with respect to the OCCAM estimate to close the salt balance. This approach has disproportionally increased the salt export at shallow levels; closure of the salt balance by a vertically homogeneous correction might have resulted in a more realistic sea surface salinity.

The model's North Atlantic salinities are, on the contrary, too high with respect to the observations. Inclusion of a Bering Strait salt flux at the northern boundary of the domain (with a realistic value of the amplitude $\sigma_{bs} = 0.36$) does not result in the necessary freshening of the North Atlantic (Fig. 5.3, 'Bering Strait'). It is probable that the absence of zonal structures in this model is partly responsible for this discrepancy: in this model, southward penetration of the Bering Strait freshwater input is inhibited by the northward flow of the overturning circulation. In the real

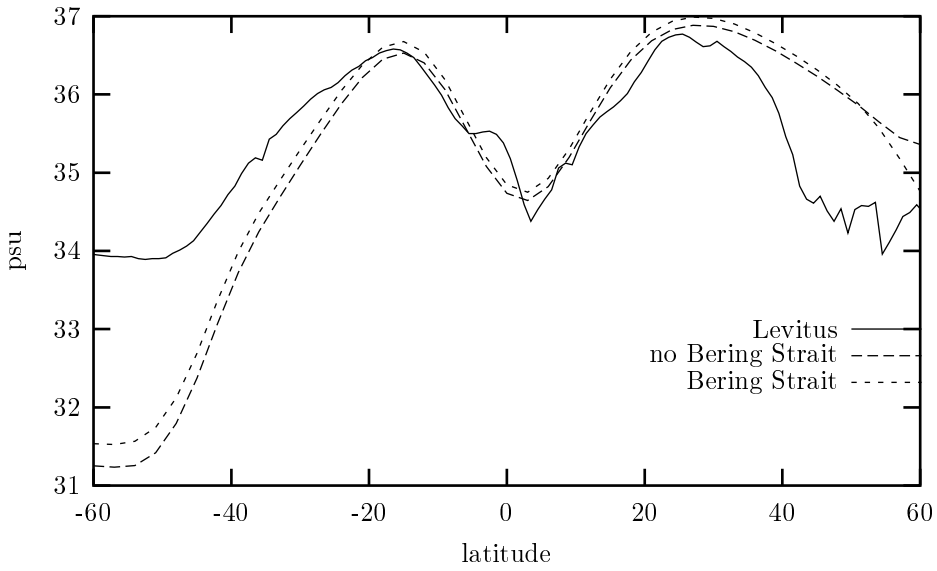

Figure 5.3: *Observed zonally averaged Atlantic sea-surface salinity (Levitus 1982), compared with the surface salinity of the solution with basic source configuration ('no Bering Strait'), and a solution where a realistic ($\sigma_{bs} = 0.36$) Bering Strait salt export is included ('Bering Strait').*

ocean, however, meridional transports of salt and freshwater are accomplished by the wind-driven circulation as well. This would allow the freshwater input from the Arctic Ocean to be advected southward, in spite of the northward transport induced by the overturning circulation.

5.3.2 Impact of Agulhas Leakage

Starting from the basic solution, we decrease both the amplitude of the Agulhas heat and salt sources to study the response of the overturning circulation to the influence of the so-called warm water route. Upon reducing the strength of the Agulhas heat source τ_{agu} from 6 to 0, the surface heat flux adjusts itself in such a way that the heat balance remains closed. The reduction of the Agulhas heat input thus results in a reduced net surface heat loss, and leads to a smaller source of potential and kinetic energy. Consequently, the strength of the overturning circulation drops from 10.5 to 7.5 (i.e., from 18 to 13 Sv dimensionally), reflecting an averaged sensitivity of 0.5 per unit heat source amplitude.

For salinity, however, the surface flux is prescribed and cannot adjust to close the balance. So when reducing the Agulhas salt input σ_{agu} from 1 to 0, a choice must be made where the reduced salt input is compensated. This choice is not obvious. The net surface freshwater flux is determined by the difference between precipitation and

evaporation in the catchment area of the Atlantic, and it is not very likely that it depends markedly on the presence or absence of Agulhas salt input. It is likely that net evaporation is influenced to some extent by the Agulhas heat input in the South Atlantic, but reduction of this heat input, and thus the excess evaporation, leads to a *decrease* in the (virtual) surface salt input.

It is probable that shutting off Agulhas Leakage would result in a reduced salt export in the ACC region. Three possible scenarios are tested to get an idea of the tendency of the response, and of possible sensitivities. These scenarios keep the amplitude σ_{acc} of the basic ACC salt sink profile constant: the reduction in the export is accomplished by addition of an extra salt source to this basic ACC profile. The scenarios differ in the vertical distribution of this additional source, and thus represent different scenarios for NADW renewal.

Cold water scenario A vertically homogeneous salt source is added in the upper 2500 m of the ACC region. This case mimics a dominant role of the so-called 'cold water route' for NADW renewal, since the salt that is imported in the Agulhas region does not leave the Atlantic in the form of NADW, but somehow ends up in the upper layers of the ACC.

Hybrid scenario A vertically homogeneous salt source is added over the whole depth range in the ACC region. The resulting reduction in the net salt export is now homogeneously distributed over the whole depth range. Both interpretations of the cold and warm water scenarios now partly apply.

Warm water scenario The additional salt source is now applied over the deeper half of the domain. In this scenario all Agulhas salt input leaves the Atlantic with the NADW, so that reduction of this input results in reduced deep salt export. Since the participation of Agulhas Leakage water in forming NADW is now considerable, it may represent the so-called 'warm water route' of NADW renewal.

Figure 5.4 clearly shows that Agulhas salt input enhances the Atlantic overturning circulation if at least a part of the Agulhas Leakage water participates in the NADW production (hybrid and warm scenarios). A vertically homogeneous compensation (hybrid) reduces the overturning strength with 0.6, while a deep compensation warm (water scenario) reduces the strength even with 1.3. In the case of a shallow compensation (cold water scenario) the overturning strength is almost unchanged.

In Chapter 4 it was described in detail how in this type of models the vertical transport of buoyancy from its sources to its sinks is accomplished predominantly by vertical advection. The vertical distance between the sources and the sinks of buoyancy thus plays a crucial role in determining the kinetic energy production, and consequently the strength of the overturning circulation. The present analysis confirms this picture: shallow salt input by Agulhas Leakage increases the ocean's potential energy, and salt removal by export of salty NADW enables the circulation to convert this potential energy into kinetic energy. If, on the other hand, the salt is removed at a shallow level, the vertical distance from salt source to sink is much smaller, and less potential energy can be released.

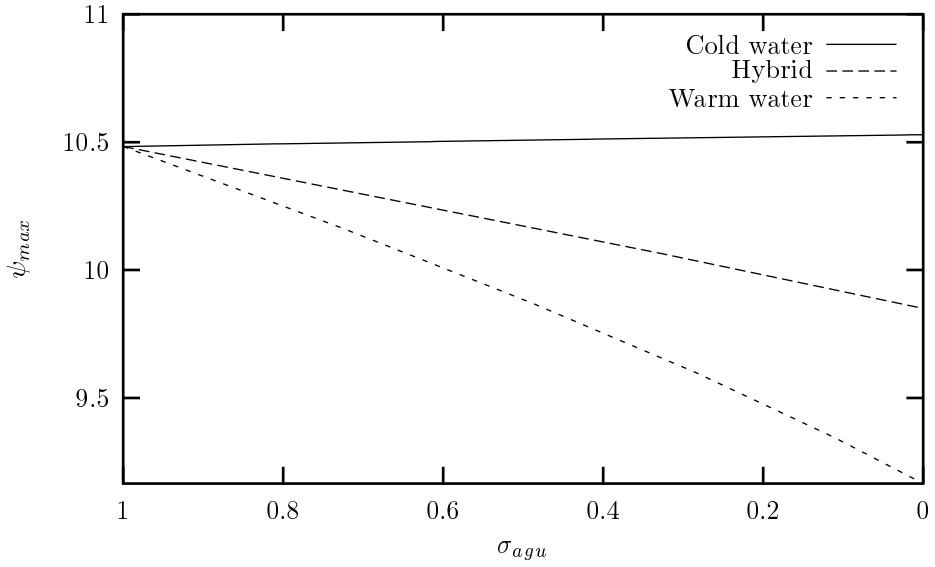

Figure 5.4: *The overturning strength as a function of the Agulhas salt flux strength for the three scenarios mentioned in the text.*

5.3.3 Uniqueness of the basic solution

In this section it is shown that the northern sinking solution that is forced by the basic source configuration is unique in the sense that no other equilibria are found under the same forcing conditions. To this end we study how the bifurcation structure of the symmmetrical model is disturbed when sources and sinks of heat and salt are applied. Figure 5.5 shows the bifurcation diagram of the undisturbed system, that has reflective symmetry with respect to the equator. The streamfunction in the right-hand side of the domain (ψ_{rhs}) is diagnosed to monitor the solution when the amplitude σ_s of the surface salt flux is modified. For low values of σ_s only a thermally driven solution (TH) exists, that is symmetrical and displays downwelling at both poles (Fig. 5.6, upper panel). At the pitchfork bifurcation P_1 this solution loses stability, and two asymmetrical solutions branch off. These solutions are characterised by downwelling at the northern (NPP, Fig. 5.6, middle panel) or southern (SPP) polar region, and they become stable at the limit points L_N and L_S. These solutions recombine with the symmetrical branch at the pitchfork bifurcation P_2. Beyond P_2 only a saline driven circulation (SA, Fig. 5.6, lower panel) exists, with downwelling in the evaporative subtropical regions, and upwelling at the equator and the poles.

When a buoyancy source or sink is applied at the latitudes where the Atlantic interacts with the rest of the World Ocean, say in the Agulhas region, the equatorial symmetry of the original model is broken. Figure 5.7 shows the resulting bifurcation diagrams when the Agulhas heat source distribution is applied with a purely exponen-

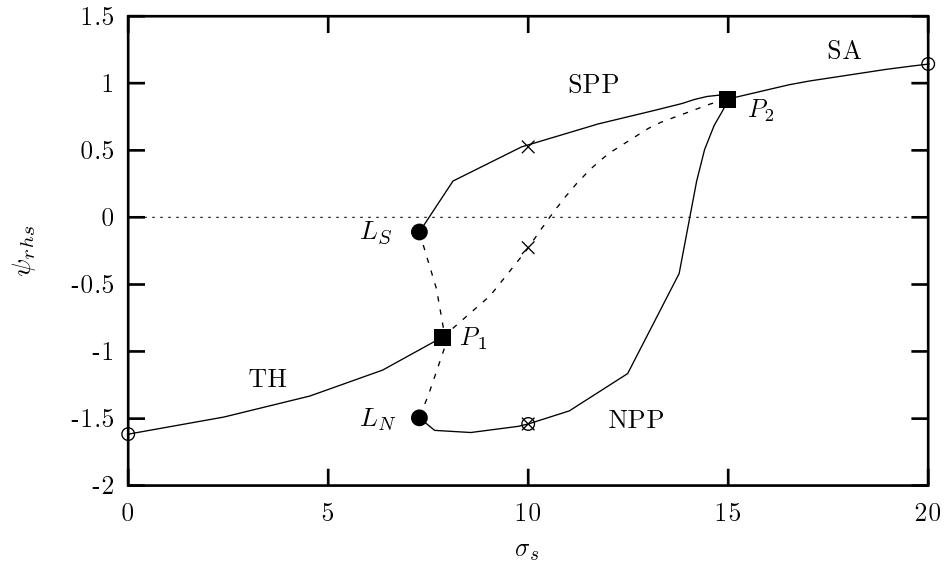

Figure 5.5: *Bifurcation diagram of the symmetric model without internal sources and zero net surface salt flux ($I_s^S = 0$). Control parameter is the surface salt flux amplitude σ_s, and the solutions are monitored with the streamfunction value in the (arbitrarily chosen) point $(y, z) = (0.85, 0.91)$, in the right-hand side of the domain (ψ_{rhs}). Negative values denote clockwise circulation. Stable branches are solid, unstable branches are dashed. Indicated are the thermally driven branch (TH), the saline driven branch (SA), and the northern sinking and southern sinking pole-to-pole circulations (NPP and SPP). The squares denote the pitchfork bifurcations P_1 and P_2, whereas the limit points L_S and L_N are indicated by dots. The open circles indicate the position of the solutions shown in Fig. 5.6, whereas the crosses at $\sigma_s = 10$ correspond to those on the 'no sources' curve of Fig. 5.10.*

tial shape in the vertical (according to Eq. (5.A13) and Table 5.A1, but with $a_4 = 0$), and with a positive ($\tau_{agu} = 0.1$, upper panel) or negative ($\tau_{agu} = -0.1$, lower panel) amplitude. The plots clearly show that the pitchfork bifurcations P_1 and P_2 have changed into the limit points L_1 and L_2. When the positive heat source is applied, the NPP circulation is connected to the TH branch via the limit points L_N and L_1, and a small branch of unstable solutions. For slightly larger source amplitudes, these limit points merge, rendering the transformation of the TH solution into the NPP solution continuous. For large values of σ_s the NPP branch is continuously connected to the saline driven solutions (SA). The SPP solution has become isolated, and it can only exist in the window bounded by limit points L_S and L_2. For larger values of τ_{agu}, this window shrinks drastically, until (at $\tau_{agu} = 0.31$) these limit points merge into a single isolated point in parameter space (Fig. 5.8, upper panel, dashed line). For higher values of τ_{agu}, the region of multiple equilibria has disappeared, and the

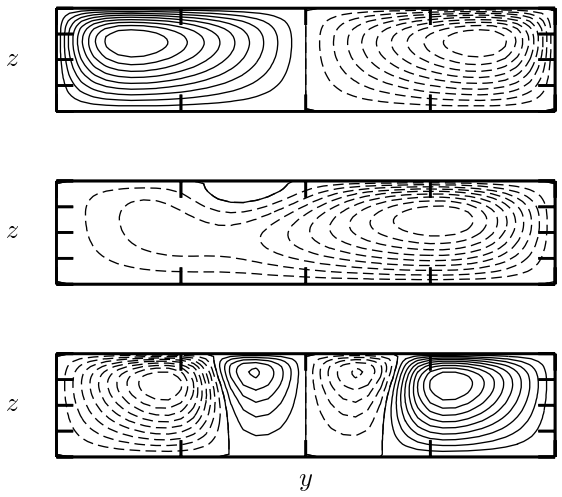

Figure 5.6: *Three solutions of the symmetrical model, corresponding to the open circles in the bifurcation diagram of Fig. 5.5. Streamfunctions are normalised with respect to their maxima. Shown are a thermally driven circulation (TH, $\sigma_s = 0$, upper panel), a pole-to-pole circulation (NPP, $\sigma_s = 10$, middle panel), and a saline driven solution (SA, $\sigma_s = 20$, lower panel). Dashed (solid) contours denote (anti-)clockwise circulation.*

NPP solution is the only circulation that is possible for a realistic value of the surface salt flux ($\sigma_s = 10$).

For a negative heat source ($\tau_{agu} = -0.1$, Fig. 5.7, lower panel), the roles of NPP and SPP are reversed, so that the NPP branch is now isolated. The limit points L_N and L_2 merge at about $\tau_{agu} = -0.23$ (Fig. 5.8, upper panel, solid line), so that the NPP solutions cease to exist below this value.

The break-up of the original bifurcation diagram under the influence of a salt source or sink is comparable to the thermal case. Figure 5.8 (lower panel) shows, however, that the amplitudes beyond which the NPP ($\sigma_{agu} > 0.06$) and the SPP ($\sigma_{agu} < -0.07$) cease to exist are considerably smaller than their thermal equivalents. Evidently, the existence of the pole-to-pole circulation patterns is more sensitive to saline than to thermally induced asymmetries.

The regime diagram of Fig. 5.9 shows the areas in σ_{agu}–τ_{agu}–space where NPP and SPP solutions (co)exist. The basic source configuration features a net heat source of amplitude 4 ($\tau_{agu} - \tau_{acc}$) and a net salt sink of amplitude -2 ($\sigma_{agu} - \sigma_{acc}$). This places its NPP solution far in the upper-left quadrant of Fig. 5.9 (indicated by the upper arrow), well outside the existence area of the SPP solutions. The configuration without Agulhas heat and salt sources features both a net heat and salt export ($-\tau_{acc} = -2$, $-\sigma_{acc} = -3$), and corresponds to a point in the lower-left quadrant of

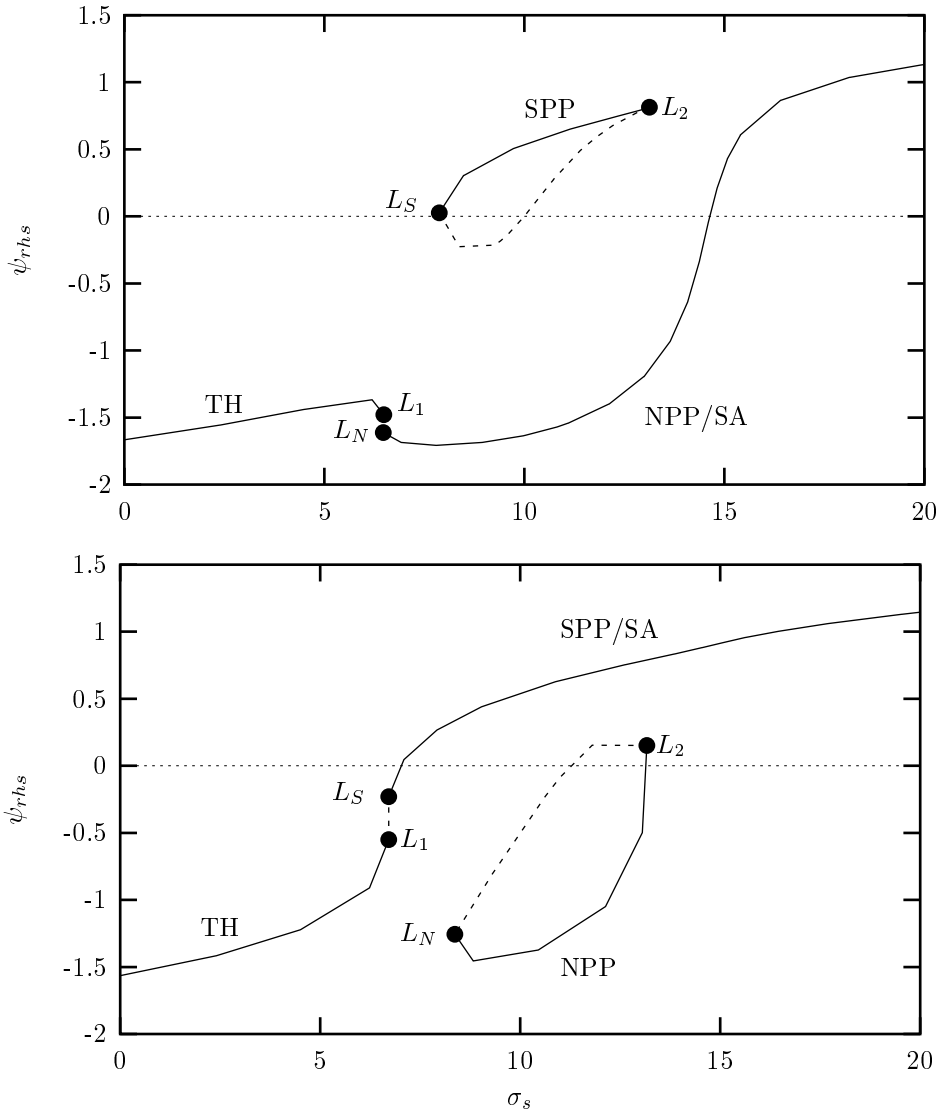

Figure 5.7: *Bifurcation diagrams of the model with a positive ($\tau_{agu} = 0.1$, upper panel) and negative ($\tau_{agu} = -0.1$, lower panel) heat source in the Agulhas region. Due to the loss of the equatorial symmetry, the pitchfork bifurcations P_1 and P_2 are broken up into limit points L_1 and L_2. A positive heat source in the Agulhas region (upper panel) stabilises the northern sinking solution (NPP) and connects this branch continuously to the saline driven solution (SA), and via limit points L_1 and L_N to the branch of thermally driven solutions (TH). A negative heat source hinders the NPP circulation and isolates its branch in parameter space.*

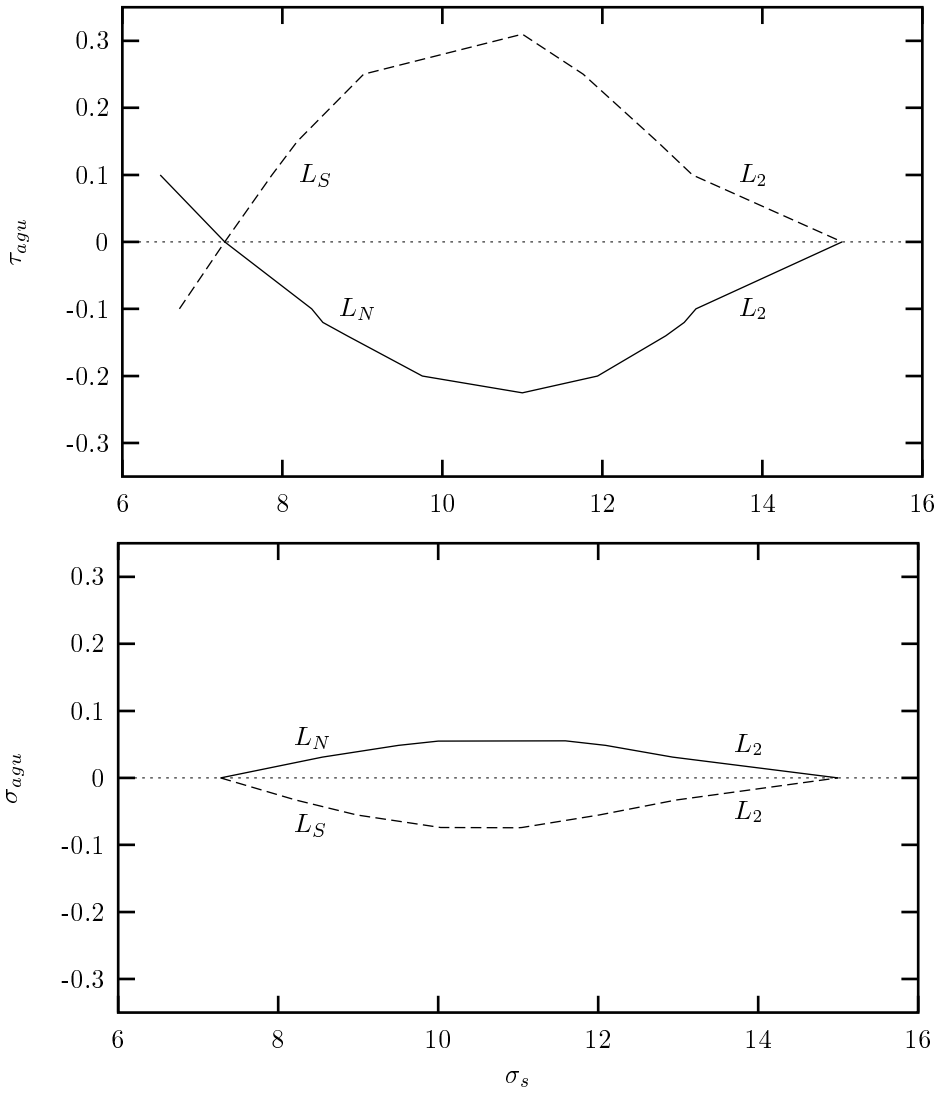

Figure 5.8: *The position of the limit points L_S, L_N and L_2 as a function of τ_{agu} (upper panel) and σ_{agu} (lower panel). The heat and salt source distributions are identical and decay exponentially with depth. A net salt source is compensated by an offset in the surface salt flux. For negative τ_{agu} (or positive σ_{agu}) the NPP solution only exists in the window bounded by L_N and L_2, and is completely absent for values smaller than $\tau_{agu} = -0.23$ (or larger than $\sigma_{agu} = 0.06$). For positive τ_{agu} (or negative σ_{agu}) the NPP solution cannot be clearly distinguished from the SA and TH branches, since NPP transforms continuously into the SA branch, and the limit points L_1 and L_N disappear for increasing source amplitudes.*

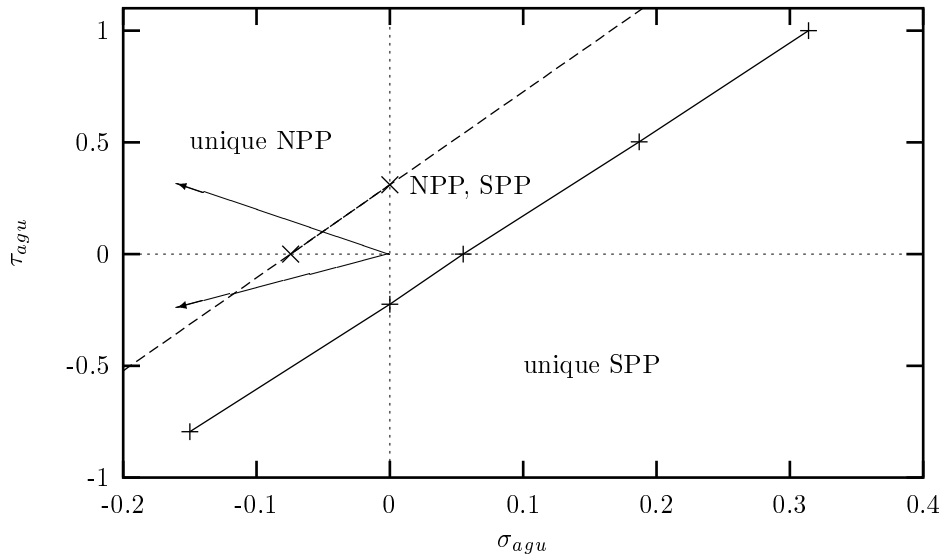

Figure 5.9: *Regime diagram showing the areas in σ_{agu}–τ_{agu}–space where NPP and SPP solutions exist. Heat input and salt export in the Agulhas region ($\tau_{agu} > 0$ and $\sigma_{agu} < 0$) favour the existence of the NPP solutions, whereas heat export and salt input ($\tau_{agu} < 0$ and $\sigma_{agu} > 0$) hinder their existence. The arrows point approximately in the direction (-2,4) of the basic source configuration (upper arrow) and the configuration (-3,-2) without Agulhas Leakage (lower arrow). Both configurations are situated in the 'unique NPP' regime.*

the plot (indicated by the lower arrow). It is situated well above the line separating the NPP and the NPP/SPP areas. This means that the buoyancy fluxes brought about by interocean exchange in the Southern Ocean favour the northern sinking solution considerably. The imposed asymmetries furthermore inhibit the existence of the southern sinking solutions, making regime switches from a northern sinking to a southern sinking circulation unlikely.

5.3.4 Multiple equilibria in the presence of Bering Strait inflow

In the former section we have seen that the exchange of buoyancy between the Atlantic and the rest of the World Ocean via the Southern Ocean strongly favours the northern sinking circulation state. It even dispels the competing southern sinking solution from the area in parameter space that may be considered as representative for the real ocean. However, the Atlantic also exchanges freshwater with the Pacific via the Bering Strait, and it is conceivable that the freshwater input into the North Atlantic hinders the northern sinking circulation. In this section we study how the areas of

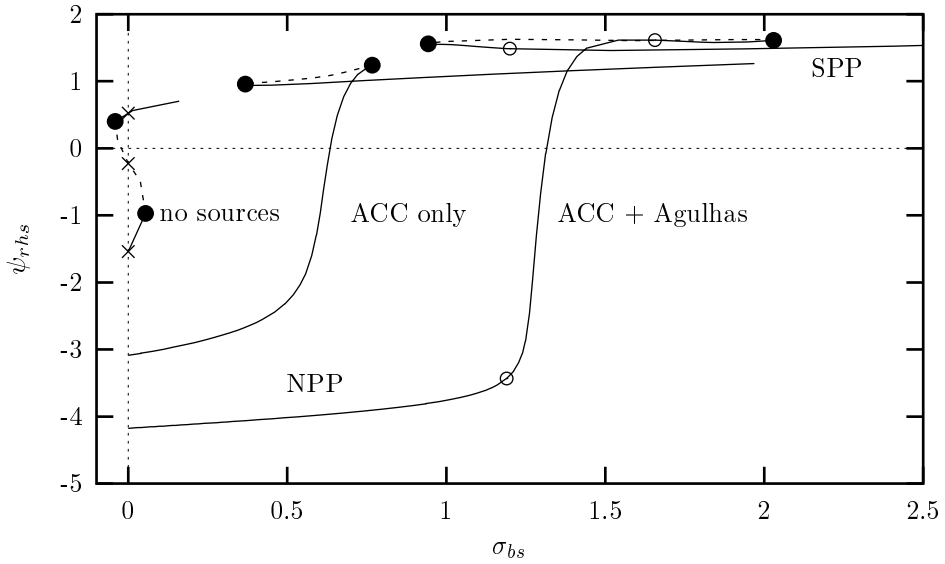

Figure 5.10: *Value of ψ_{rhs} as a function of the amplitude of the Bering Strait salt export σ_{bs}. The curve denoted 'ACC+Agulhas' is constructed with all Southern Ocean sources present, whereas the 'ACC only'–curve is constructed with the ACC distributions only. Increased Bering Strait salt export is compensated by decreased ACC salt export. In the 'no sources' case, no Southern Ocean sources are present, and increased Bering Strait salt export is compensated by decreased surface salt input to retain the basic symmetry of the model. A realistic value of σ_{bs} is 0.36, so shutting off Agulhas Leakage would bring the model close to the regime where the NPP and SPP solutions coexist. The open circles indicate the positions of the solutions shown in Fig. 5.11, whereas the crosses at $\sigma_{bs} = 0$ correspond to those at $\sigma_s = 10$ in Fig. 5.5.*

existence of the NPP and SPP solutions are influenced by Bering Strait freshwater import. The strength of the Bering Strait salt export is controlled by the parameter σ_{bs}. In the experiments, the amplitude of the ACC salt sink is adjusted to satisfy the balance of Eq. (5.5).

Figure 5.10 shows ψ_{rhs} as function of the Bering Strait salt flux σ_{bs} for three different source configurations. The curve denoted 'ACC+Agulhas' is constructed from the basic source configuration that has been described in section 5.3.1. The northern sinking circulation pattern, that is so firmly established in the basic source configuration, is stable with respect to a very large Bering Strait freshwater input (Fig. 5.11, upper panel). Only when the amplitude exceeds the value of 1.2 a counterrotating cell develops, that rapidly expels the main overturning cell towards the south (Fig. 5.11, middle panel). Between the limit points at $\sigma_{bs} = 2.03$ and 0.94, the clockwise rotating cell is eliminated completely, and a southern sinking solution is firmly established (Fig. 5.11, lower panel). This solution is stable for larger values of σ_{bs}.

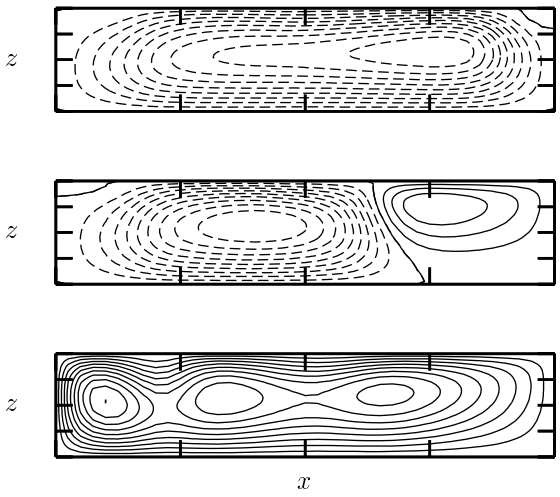

Figure 5.11: *Streamfunctions of the solutions corresponding to the open circles on the curve 'ACC+Agulhas' of Fig. 5.10. Upper panel shows an NPP solution on the lower branch in Fig. 5.10 ($\sigma_{bs} = 1.2$), middle panel shows a solution with the downwelling shifted to the subtropical latitudes ($\sigma_{bs} = 1.65$), and the lower panel is an SPP solution ($\sigma_{bs} = 1.2$).*

Reducing Agulhas Leakage heat and salt sources towards zero (i.e., switching from the 'ACC+Agulhas' branch to 'ACC only') strongly reduces the strength of the overturning circulation, as has been shown in the former section. This reduction has large consequences for the stability of the circulation with respect to Bering Strait freshwater input. The curve denoted 'ACC only' in Fig. 5.10 shows a dramatic shift in the position of the limit points. The limit point with the lowest value of σ_{bs} is shifted towards 0.37, and is now close to the value of 0.36 that may be considered representative for the present-day situation. This suggests that shutting off Agulhas Leakage could drag the overturning circulation close to a regime where southern sinking solutions might exist under the same surface forcing. Finite amplitude disturbances (like freshwater input from a melting Greenland ice sheet) might trigger a dramatic shift.

Figure 5.10 confirms the findings of the former section that the NPP solution is unique when it is forced by the basic source configuration. The curve denoted 'no sources' was created in the absence of the Southern Ocean buoyancy sources, and shows three zero-crossings that correspond to three points on the bifurcation diagram of the model with reflective symmetry (Fig. 5.5, at $\sigma_s = 10$). It thus connects the NPP branch, via the unstable TH/SA solutions, with the SPP branch. Upon introducing the Southern Ocean sources, the curve 'no sources' transforms into the curves 'ACC only' or 'ACC+Agulhas', and the two zero-crossings that are associated with the TH/SA and SPP branches disappear. This leaves NPP as the only possible solution

for $\sigma_{bs} = 0$.

5.4 Summary and discussion

5.4.1 Importance of NADW renewal paths

In this chapter we studied the impact of interocean fluxes of heat and salt on the strength and stability of the thermohaline circulation in the Atlantic Ocean. We forced a 2D model of the Atlantic overturning circulation with source/sink distributions of heat and salt that represented the exchange between the Atlantic and the rest of the World Ocean via the ACC and via Agulhas Leakage. The amplitudes and profiles of these distributions are based on the climatology of the high-resolution ocean model OCCAM, since no sufficiently detailed information about the spatial structure of interocean fluxes was found in the literature. A detailed analysis of the interocean exchange in this model, described in Chapter 3, showed that the model is not in equilibrium, and that it displays some unrealistic features when compared with observations. Nevertheless, it was concluded that the large-scale transports and thermohaline structures are reasonably well reproduced to justify a carefull use of the OCCAM flux profiles as a basis of the source distributions in this study.

It was shown that the Southern Ocean source configuration that reflects to some extent the present-day interocean exchange, strongly promotes the strength and stability of the overturning circulation in this model. It imposes an asymmetry on the Atlantic that strongly favours the northern sinking circulation. In fact, it turned out that only a weak Southern Ocean buoyancy source is enough to inhibit the southern sinking solution from existing, so that in this model the northern sinking solution is unique under present-day forcing conditions. A factor 3 increase in the relatively fresh transport through the Bering Strait would be necessary to bring the model into a regime where multiple equilibria exist.

It turned out that especially the Indian-Atlantic interocean exchange through Agulhas Leakage is an important stimulating factor of the overturning circulation in this model. The presence of Agulhas heat input promotes the overturning circulation in two ways: the increased temperature in the southern part of the basin enhances the meridional density gradient, and the net surface cooling increases the energy supply that drives the flow. The impact of Agulhas salt input on the overturning strength depends on its fate: if Agulhas Leakage water participates in the overturning circulation, so that its salt leaves the Atlantic with NADW, it strongly promotes the overturning circulation due to the potential energy release. If, on the other hand, Agulhas Leakage water does not participate in the overturning circulation, its salt recirculates in the South Atlantic subtropical gyre, and leaves the Atlantic with the South Atlantic Current or the ACC; its influence on the overturning circulation is consequently small. These results impose dynamical significance to the discussion about how NADW export is compensated. They indicate that it is important for the Atlantic overturning circulation whether the source water of NADW has entered the Atlantic through Drake Passage, with cold and fresh subantarctic characteristics, or via Agulhas Leakage, with warm and salty (sub)tropical qualities.

5.4.2 Northern sinking preference

In this chapter it was shown that the Southern Ocean interocean exchange imposes an asymmetry on the Atlantic that strongly favours the northern sinking circulation. However, the source distributions that were used in this model represent fluxes that are consistent with, and to a certain extent generated by, the present-day overturning circulation. And since this circulation is clearly in a northern sinking state, the imposed asymmetry is not independent of the present-day circulation. If an alternative circulation pattern would generate interocean fluxes that are different, and favourable for *that* particular state, then the stability of these states would have been underestimated by the approach used here. The northern sinking state would have been biased by the choice of the sources. That this is the case for temperature is almost beyond doubt: the equatorward heat flux, a feature that is unique to the South Atlantic, is to a large extent generated by the overturning circulation (e.g., Rintoul 1991).

On the other hand, not all processes that generate interocean transports are necessarily connected to the overturning circulation. Agulhas Leakage is probably a predominantly wind-driven feature[1] (De Ruijter et al. 1999). It is probable that the Agulhas heat input influences the South Atlantic stratification and the atmospheric heat flux, independent of whether Agulhas Leakage water participates in the Atlantic overturning circulation. So even if no Agulhas Leakage water would take part in the overturning circulation, it would probably still sustain a net input of heat and salt and thus influence the large scale pressure field and overturning strength. Nevertheless, even if the northern sinking state is biased by the fact that the sources are diagnosed from a model circulation that is in this state, it is clear that the interocean fluxes brought about by this circulation pattern provide a powerfull feedback that stabilises it.

5.4.3 Possible implications for climate switches

Since Agulhas Leakage depends on characteristics of the Indian Ocean wind stress field (De Ruijter et al. 1999), it may be rather sensitive to changes in the wind field climatology. Agulhas Leakage was probably severely reduced during the last glacial, due to a more northerly position of the STCZ (Howard and Prell 1992; Flores et al. 1999). The results of this study show that this may have played an important role in reducing the stability of the overturning circulation in the glacial Atlantic. Reduction or absence of Agulhas Leakage may have made this circulation more susceptible to regime switches and instabilities. Nevertheless, it must be noted that in the model context that has produced Fig. 5.10 no multiple equilibria exist when the Bering Strait is closed ($\sigma_{bs} = 0$). Since this situation prevailed during the last glacial period, other factors must have reduced the stability of the overturning circulation even further to generate the observed climate changes. The results furthermore support the suggestion of Berger and Wefer (1996) that the common start-up of NADW production and the opening of Agulhas Leakage at the end of the last ice-age could be more than

[1] It is possible that interoceanic pressure differences, induced by thermohaline processes, to some extent assist in this exchange.

just a simultaneous response to external forcing: a restart of Agulhas Leakage, due to a southward shift in the position of the STCZ, may have had a stimulating effect on the recovery of the conveyor belt circulation. This exchange may thus provide a powerfull feedback in the climate system.

Reconstructions of glacial deep water circulation not only suggest that the overturning circulation was reduced in strength (rather than absent), but that the source region of NADW was shifted to regions south of Iceland as well (Keigwin et al. 1991; Sarntheim et al. 1994). Manabe and Stouffer (1988) and Rahmstorf (1994) explained the reduction in overturning strength by transitions between equilibria with weaker and stronger overturning circulations, as found in several models (e.g., Manabe and Stouffer 1988; Rahmstorf 1994, 1996; Dijkstra and Neelin 1999). However, none of these transitions seem to produce a southward shift in the downwelling region. Figure 5.10 shows a transition that might explain the glacial North Atlantic climate changes. This transition is related to a southward shift of the main downwelling area from the northern polar region (Fig. 5.11, upper panel) to the subtropics (Fig. 5.11, middle panel), or even further south. Although this transition in the present configuration does not involve limit-points and hysteresis behaviour, the heat transport towards the northern North Atlantic region is reduced abruptly, once the downwelling site has left the North Atlantic sub-polar regions. However, Fig. 5.10 shows that the transition requires an increased freshwater input into the northern North Atlantic, which is not consistent with the situation during the last glacial when the Bering Strait was closed. Nevertheless, this mode may have played a role in generating the brief episodes of cooler climate in Europe at the end of the last glacial period (including the Younger Dryas event). Paleoclimatic records indicate that these events of reduced NADW production coincided with enhanced meltwater discharge (Keigwin et al. 1991).

The result that the Southern Ocean buoyancy exchange stabilises the overturning circulation indicates that it may be more stable than has been suggested by the 3-box model of Shaffer and Bendtsen (1994). In fact, the bifurcation diagram of Fig. 5.10 suggests an alternative and more consistent interpretation of the large climatic variability during the Eem (GRIP Members 1993). In Fig. 5.12, the difference between their mechanism and the interpretation suggested by Fig. 5.10 is schematically illustrated. In the Shaffer and Bendtsen case, a northern sinking pole-to-pole (NPP) circulation would not be the only circulation possible under normal Eemian Bering Strait freshwater input, since a southern sinking state (SPP) could be stable under the same forcing conditions as well. Increasing the inflow would force the circulation to switch to a southern sinking state. Upon returning to normal conditions, the circulation would reenter the regime where both SPP and NPP are stable. However, it would take a large-amplitude perturbation to force the circulation to leave the stable southern sinking circulation, and to restore the northern sinking state (the '?' in Fig. 5.12).

When north-south asymmetries in the ocean are such that the northern sinking state is favoured above the southern sinking circulation, then the northern sinking circulation may be the only one possible under normal Eemian (and present-day) forcing conditions and Bering Strait inflow. An increase in Bering Strait throughflow would drag the northern sinking circulation into the window of multiple equilibria, so

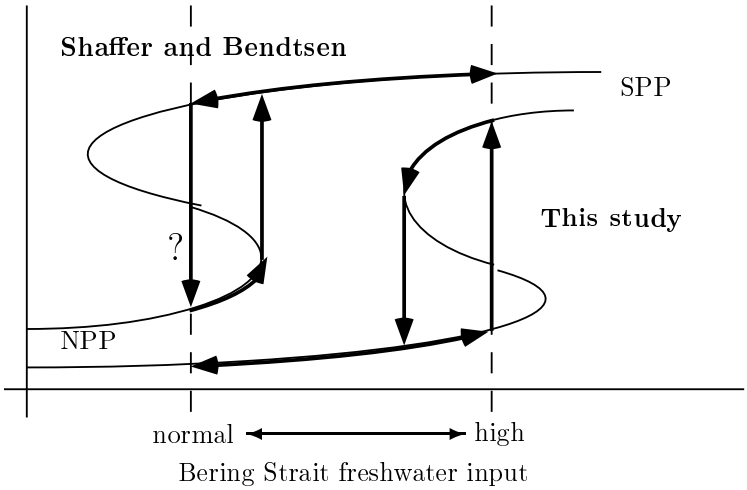

Figure 5.12: *Diagram showing possible transitions during the Eem caused by changing Bering Strait inflow. If the northern sinking (NPP) circulation is not or only weakly preferred above a southern sinking (SPP) state ('Shaffer and Bendtsen'), an increased inflow would force a switch to SPP. Upon returning to normal conditions, a recovery of NPP could only be triggered by a large-amplitude disturbance. In the case of strong NPP preference ('This study'), the increase in Bering Strait inflow brings the circulation in the regime where NPP and SPP coexist, and a switch may easily be triggered by the increased freshwater input into the North Atlantic. Upon returning to normal conditions, the NPP is immediately restored, since it is the only possible circulation under these circumstances.*

that a finite-amplitude perturbation could trigger the switch to the southern sinking state. The increased inflow of freshwater into the North Atlantic would certainly favour such a switch. A return to normal Eemian Bering Strait conditions would force the ocean to leave the region of multiple equilibria. This would result in a recovery of the northern sinking circulation.

5.5 Conclusion

In this chapter we examined the role that is played by interocean fluxes of buoyancy in stabilizing the present-day overturning circulation. It was shown that realistic sources and sinks strongly favour a circulation that resembles the present-day Atlantic overturning circulation, characterised by major downwelling at the northern polar latitudes (NPP circulation). The sources also increase the stability of this circulation: only a small buoyancy input at southerly latitudes is enough to prohibit the existence of a southern sinking circulation (SPP), leaving the NPP circulation as a unique, and thus stable, solution. A factor 3 increase in the Bering Strait freshwater import would be necessary to bring the SPP circulation back into existence.

Especially the Indian–Atlantic transfer of heat and salt, brought about by Agulhas Leakage, turned out to contribute considerably to the strength and stability of the northern sinking circulation. According to this model, shutting off Agulhas Leakage, and consequently the warm water route for NADW compensation, reduces the overturning strength considerably. These results imply that the way in which the NADW renewal takes place has implications for the strength of the Atlantic overturning circulation, giving the discussion about the warm vs. cold water route for NADW compensation dynamical significance. The results furthermore suggest that the absence of Agulhas Leakage may have played a role during the last ice-age, when the thermohaline circulation was weaker and exhibited much stronger variability than at present. The sudden restart of the Atlantic overturning circulation at the beginning of the Holocene may well have been stimulated by the re-opening of the Agulhas gap.

5.A The sources

The salt balance of the Atlantic revisited

In this appendix we relate the heat and salt sources of our model to the fluxes brought about by Agulhas Leakage and the ACC in OCCAM. However, it is not clear how the salt balance of the Atlantic changes when salinity is referred to a non-zero reference salinity S_0. Therefore the salt balance of the Atlantic must be addressed first.

In Chapter 5 the interocean fluxes of heat and salt are represented by source distributions. These sources are based on the interocean fluxes in OCCAM, the high-resolution OGCM that was studied in Chapter 3. In that chapter the salt balance of the Atlantic was analysed with respect to a zero reference salinity $S_0 = 0$. However, the profiles were calculated with $S_0 = S_m$, with S_m being the Atlantic mean salinity. Only then are these profiles suitable for use in these models, since exchanging water with the same salinity (and temperature) as the average Atlantic water does not influence the ocean's potential energy. But it is not *a priori* clear how this non-zero reference salinity modifies the salt balance.

In Chapter 3 we derived the following balances of volume (Eq. (3.2)):

$$V_b - (\overline{u}^{20E} - \overline{u}^{70W}) = V_a \tag{5.A1}$$

and salt (cf. Eq. (3.3)):

$$V_{Atl}\frac{d\bar{S}}{dt} = V_b S_b - (\overline{uS}^{20E} - \overline{uS}^{70W}) + R. \tag{5.A2}$$

The residual R is added here to account for exchange processes that are not captured by the fluxes in the climatology, like eddy transports and diffusion. The salt fluxes that are applied in this chapter are calculated with respect to the Atlantic mean salinity S_m from Levitus (1982). With $S = S_m + S'$, we have:

$$V_{Atl}\frac{d\bar{S}}{dt} = V_b S_b - (\overline{uS'}^{20E} - \overline{uS'}^{70W}) - (\overline{u}^{20E} - \overline{u}^{70W})S_m + R, \tag{5.A3}$$

so that:

$$\overline{uS'}^{20E} - \overline{uS'}^{70W} = V_b(S_b - S_m) + V_a S_m - V_{Atl}\frac{d\bar{S}}{dt} + R. \tag{5.A4}$$

According to Table 3.1, there is a 3.90 Sv psu salt flux convergence between 20°E and 70°W. With $V_b = 0.675$ Sv and $S_b = 31.9$ psu, the Bering Strait accounts for a -2.05 Sv psu salt export (first term in the right hand side of Eq. (5.A4)). With the 7.69 Sv psu contribution of the 0.22 Sv Atlantic volume flux convergence (V_a), the total salt flux convergence adds up to 9.54 Sv psu. Clearly, the salt storage and the unresolved transports in R are important terms in the salt flux balance.

In Chapter 3 the 20°E section was divided into an Agulhas part (AGU), a part that comprises the ACC (ACC), and a subsection that crosses the Weddell Gyre (AAG). It seems improbable, however, that the the Weddell Gyre heat and salt fluxes exert direct influence on the NADW overturning cell. Indirectly it may influence the

NADW production via the AABW overturning cell (Stocker et al. 1992b), but models like the one used here do in general not produce this cell. Therefore we take the ACC and AAG sections together in this study, so that the Southern Ocean communication takes place in the Agulhas regime and the combined ACC and Weddell Gyre regime. Accordingly we can write the salt flux divergence between 20°E and 70°W as the sum of two components:

$$\overline{uS'}^{20E} - \overline{uS'}^{70W} = \overline{uS'}^{20E,AGU} + (\overline{uS'}^{20E,ACC+AAG} - \overline{uS'}^{70W}). \tag{5.A5}$$

The source amplitudes

In our model, we solve for circulation in a meridional plane. In fact, the 2D Boussinesq equations are equivalent to the 3D equations per zonal meter when zonal boundaries, rotation and zonal gradients are absent. So in order to make the OCCAM heat and salt inputs compatible with this meridional slice approach, we have to think of these sources as being distributed over the width of the Atlantic.

The approach used to convert the flux divergences into the dimensionless source amplitudes and distributions is as follows: First we introduce the dimensional sources, $\widetilde{Q}^r_q(\theta,\tilde{z}), r = T,S; q = agu, acc$ (in Wm^{-3}, $\mathrm{gm}^{-3}\mathrm{s}^{-1}$). These sources are written as:

$$\widetilde{Q}^T_q(\theta,\tilde{z}) = \widetilde{\tau}_q Q^T_q(y,z) \tag{5.A6a}$$

$$\widetilde{Q}^S_q(\theta,\tilde{z}) = \widetilde{\sigma}_q Q^S_q(y,z). \tag{5.A6b}$$

The (dimensionless) distribution functions Q^r_q are constructed so that their integral over the meridional/depth plane is 1. The parameters $\widetilde{\tau}$ and $\widetilde{\sigma}$ thus control the net input of heat or salt. They are related to the integrated fluxes of Table 3.1 via:

$$\widetilde{\tau}_{agu} = -\overline{uT'}^{20E,AGU}/HLW_{agu} \tag{5.A7a}$$

$$\widetilde{\sigma}_{agu} = -\overline{uS'}^{20E,AGU}/HLW_{agu} \tag{5.A7b}$$

$$\widetilde{\tau}_{acc} = (\overline{uT'}^{20E,ACC+AAG} - \overline{uT'}^{70W})/HLW_{acc} \tag{5.A7c}$$

$$\widetilde{\sigma}_{acc} = (\overline{uS'}^{20E,ACC+AAG} - \overline{uS'}^{70W})/HLW_{acc}. \tag{5.A7d}$$

Here, W_{agu} and W_{acc} denote the width of the Atlantic at the latitudes where the exchange takes place. The Agulhas exchange takes place at about 40°S, where the Atlantic is approximately 80° wide and $W_{agu} = 6.85 \cdot 10^6$m. Equivalently, the ACC exchange takes place at, say, 50°S, where the width of the Atlantic is close to 90° and $W_{acc} = 6.46 \cdot 10^6$m. $H = 5 \cdot 10^3$m and $L = 1.34 \cdot 10^7$m are taken as characteristic depth and length scales of the basin.

Finally, the dimensional amplitudes are scaled according to:

$$\tau_q = \frac{H^2}{\kappa_v \rho_0 c_p \Delta T}\tilde{\tau}_q \quad ; \quad \sigma_q = \frac{\lambda H^2}{\kappa_v \rho_0 \Delta S}\tilde{\sigma}_q. \tag{5.A8}$$

With characteristic values taken from Table 4.1, this leads to $\tau_{agu} = 6.27$, $\tau_{acc} = 2.14$, $\sigma_{agu} = 0.95$ and $\sigma_{acc} = 0.64$.

A 0.5 Sv net surface freshwater loss from the Atlantic (Baumgartner and Reichel 1975) may be converted into a virtual net input of salt in the dimensionless units of our model as well. A basin of 60° degrees wide, ranging from 60°S to 60°N, has an average width B of $5.54 \cdot 10^6$ m. The net evaporation per square meter thus amounts to $\tilde{I}_s^S = 6.74 \cdot 10^{-9}$ ms^{-1}. According to Eq. (4.10), this amount is equivalent to a dimensionless net surface salt flux I_s^S of 1.94.

In a similar way we can convert the Bering Strait salt export to dimensionless values. In OCCAM this Bering Strait transport amounted to 2.05 Sv psu, and when Coachman and Aagaard (1988) are consulted, this amount is 1.95 Sv psu. With again supposing the Atlantic to be 60° wide and 5 km deep, we have a salt sink at 60°N of $\tilde{\sigma}_b = 0.12$ g m^{-2}s^{-1}. According to Eq. (4.13), this is equivalent to a dimensionless net flux of $\sigma_{bs} = 0.36$.

The source distributions

For the spatial distributions of the Agulhas and ACC sources we also turn to the analyses of the OCCAM fluxes, as performed in Chapter 3. Of course, the detailed distribution of the heat and salt fluxes is too complicated to be of direct use for our simple model. Instead we try to capture the main characteristics of the sources in a simple analytical function. First we separate the distributions in a y-dependent part and a z-dependent part:

$$Q_q^r(y,z) = g_q(y)\, f_q^r(z) \qquad r = T,S; q = agu, acc \tag{5.A9}$$

The meridional distributions $g_{agu}(y)$ and $g_{acc}(y)$ of the Agulhas and ACC sources are modelled by:

$$g_q(\theta(y)) = \frac{1}{I_q} \exp\left[-\left(\frac{\theta - \theta_q}{\sigma_q} \right)^2 \right] \qquad q = agu, acc \tag{5.A10}$$

where θ_q and σ_q denote the center and the meridional width of the sources. These are taken to be $-40°$ and $5°$ for the Agulhas sources ($q = agu$) and $-50°$ and $10°$ for the ACC sources ($q = acc$). The coefficient I_q is the integral of the exponential:

$$I_q = \frac{1}{2}\sqrt{\pi}\sigma_q \left[\mathrm{erf}\left(\frac{60 - \theta_q}{\sigma_q} \right) + \mathrm{erf}\left(\frac{60 + \theta_q}{\sigma_q} \right) \right] \qquad q = agu, acc \tag{5.A11}$$

so that the integral of $g_q(y)$ equals 1.

The vertical profiles of the distributions, $f_q^r(z), (r = T,S; q = agu, acc)$ are based on the fluxes that have been derived in chapter 3. Using a least-squares method, we fitted a simple analytical function $\widetilde{f}_q^r(\tilde{z})$ to the data of the general form:

$$\begin{aligned} \widetilde{f}_q^r(\tilde{z}) &= \tilde{a}_1 \cos(\tilde{a}_2 \tilde{z})\, e^{\tilde{a}_3 \tilde{z}} + \tilde{a}_4 & (5.A12)\\ &= \tilde{a}_1 \left[\cos(a_2(z-1))\, e^{a_3(z-1)} + a_4 \right] \\ &\equiv \tilde{a}_1 I_f f_q^r(z) \qquad r = T,S; q = agu, acc. & (5.A13) \end{aligned}$$

	$\widetilde{f}^T_{agu}$	$\widetilde{f}^T_{acc}$	$\widetilde{f}^S_{agu}$	$\widetilde{f}^S_{acc}$
$\tilde{a}_1$ (10^{-3} PW m^{-1}/10^{-2} Sv psu m^{-1})	-3.42	1.35	-2.33	1.81
$\tilde{a}_2$ (10^{-3} m^{-1})	0.00	3.00	2.05	3.72
$\tilde{a}_3$ (10^{-3} m^{-1})	3.72	2.11	2.28	1.89
$\tilde{a}_4$ (10^{-5} PW m^{-1}/10^{-3} Sv psu m^{-1})	-4.34	3.70	-1.01	0.96
$a_2 = H\tilde{a}_2$	0.0	15.0	10.3	18.6
$a_3 = H\tilde{a}_3$	18.6	10.6	11.4	9.5
$a_4 = \tilde{a}_4/\tilde{a}_1$	0.013	0.028	0.043	0.053

Table 5.A1: *Best-fit parameter values for the heat and salt flux profiles.*

The term $I_f = a_3/(a_2^2+a_3^2)+a_4$ is the integral of the expression between the brackets, making the integral of $f_q^r(z)$ equal to 1. The values that yield the best fit of Eq. (5.A13) to the heat and salt flux profiles are tabulated in Table 5.A1.

The vertical profiles of the Agulhas and ACC heat sources, as obtained from the OCCAM model, and their best-fit approximations ($\widetilde{f}^T_{agu}$ and $\widetilde{f}^T_{acc}$) are shown in Fig. 5.A1. The Agulhas heat source profile shows the strong heat input in the upper 1000 m. The ACC heat sink profile is characterised by heat export from the upper layer, and heat input in the intermediate layer. In chapter 3 we have seen that this export has been caused by volume flux divergence at a depth where the water is cooler than the Atlantic average. These characteristics are well reproduced by the fit.

The vertical profiles of the Agulhas and ACC salt sources, as obtained from the OCCAM model, and their best-fit approximations ($\widetilde{f}^S_{agu}$ and $\widetilde{f}^S_{acc}$) are shown in Fig. 5.A2. The Agulhas salt flux profile shows the shallow salt input very well. Also visible is the minimum in eastward salt transport at the depths of the Intermediate Water, and the constant eastward salt transport at deep and bottom water levels. All these features are well reproduced by the fitted function. The ACC salt flux divergence curve shows a similar structure, but of opposite sign. Here we have a shallow export, an input of salt at intermediate depths, and an export at the deeper levels. Again, these features are well reproduced by the fitted function.

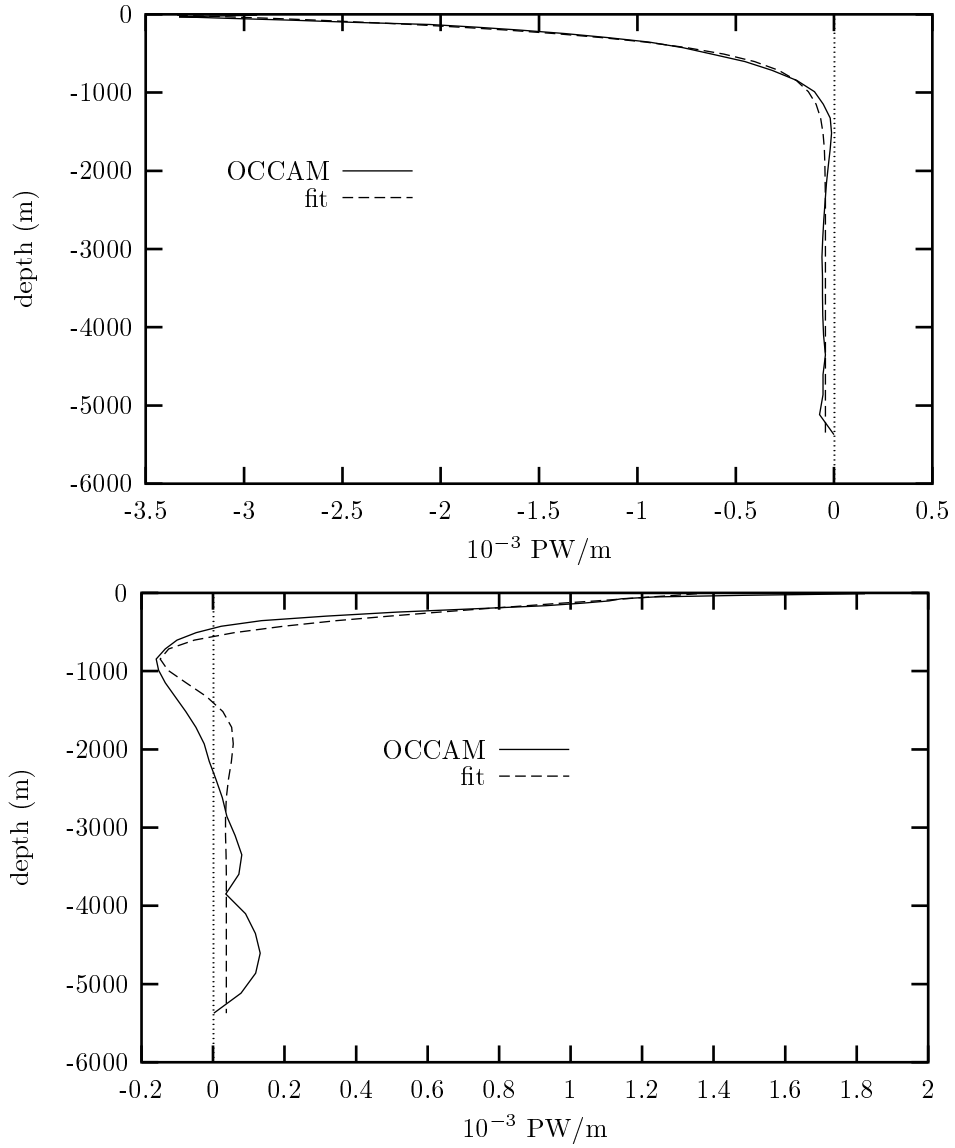

Figure 5.A1: *Vertical profiles of (upper panel) the Agulhas heat flux and (lower panel) the ACC+AAG heat flux from OCCAM, and their best-fit approximations.*

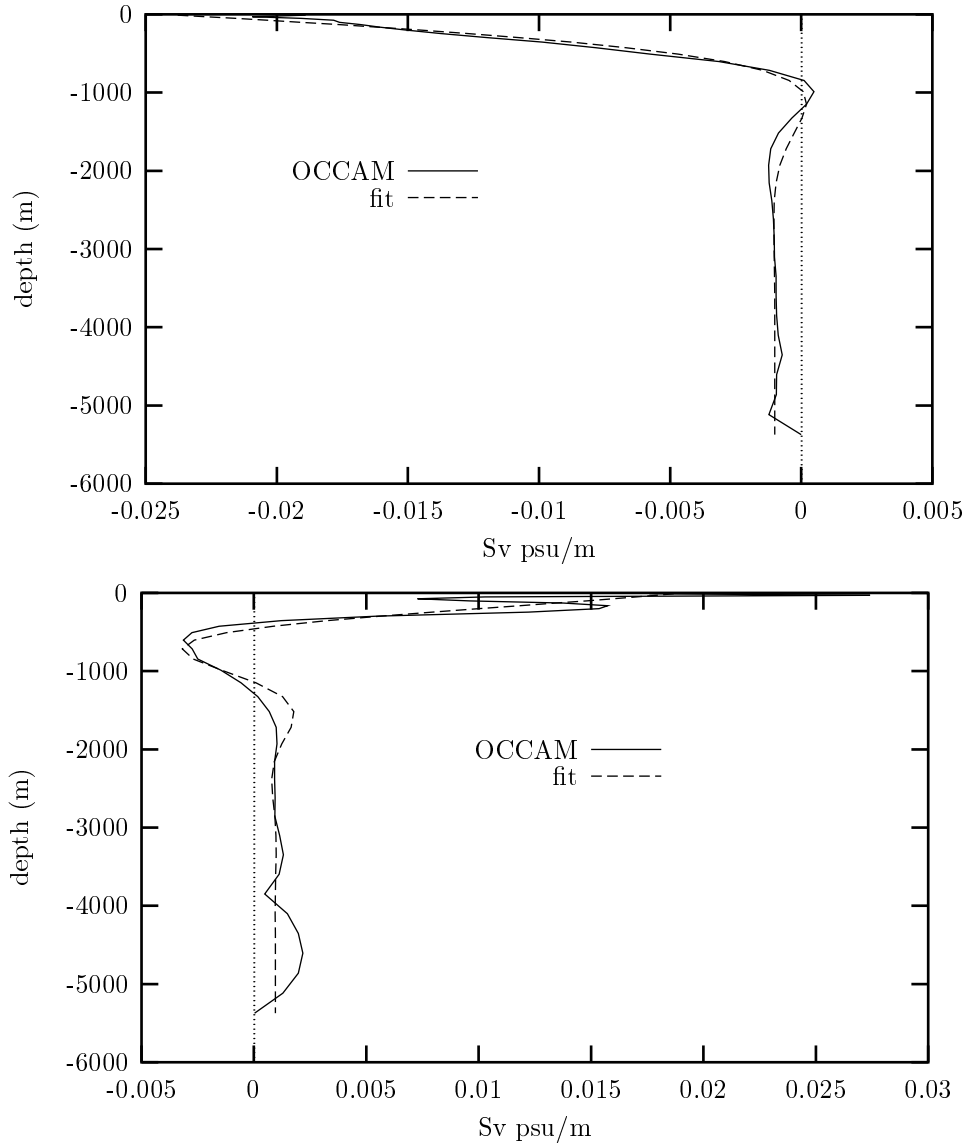

Figure 5.A2: *Vertical profiles of (upper panel) the Agulhas salt flux and (lower panel) the ACC+AAG salt flux from OCCAM, and their best-fit approximations.*

Chapter 6

Response of the overturning circulation to South Atlantic buoyancy sources

In this chapter it is studied how the Atlantic overturning circulation in an Ocean General Circulation Model responds to Agulhas heat and salt input. The Hamburg Large-Scale Geostrophic (LSG) model is used, and Agulhas Leakage is parametrised by sources of heat and salt in the South Atlantic Ocean. First it is studied how the overturning circulation responds in a quasi-steady manner to slow variations in the source amplitudes. In two additional experiments the source amplitudes are changed abruptly, to study the fast adjustment of the overturning circulation. The relevant mechanisms and time-scales of this adjustment process are identified.

6.1 Introduction

The Atlantic surface waters are by far the saltiest in the World Ocean (e.g., Levitus 1982), and contrast strongly with the surface waters in, for instance, the North Pacific. This contrast is thought to be one of the factors responsible for deep water being formed mainly in the North Atlantic, and not in the North Pacific (Warren 1983). The high salinities of the Atlantic thermocline waters are in general ascribed to the excess evaporation and associated freshwater export from the Atlantic basin, that is estimated at about 0.7 Sv north of 35°S (Baumgartner and Reichel 1975). Gordon (1985, 1986) was the first to recognise that so-called Agulhas Leakage might play a role in maintaining the high Atlantic surface salinities as well. The water entering the Atlantic through Agulhas Leakage is saltier than the surrounding South Atlantic waters (Gordon et al. 1987); it is derived mainly from the evaporative subtropical Indian Ocean (Indian Ocean Central Water, Gordon et al. 1992), and it is subjected to strong evaporative activity in the Agulhas Retroflection area (Gordon et al. 1987;

Van Ballegooyen et al. 1994). On the basis of this observation, Gordon et al. (1992) suggested that Agulhas Leakage might be an important link in maintaining the present overturning rates, since it preconditions the northern North Atlantic for forming North Atlantic Deep Water (NADW).

However, the strength of the thermohaline overturning circulation may not be simply determined by the salinity of the Atlantic thermocline waters and the strength of the convective activity in the northern North Atlantic. Classical scaling theory (Welander 1971) combines the thermal wind balance, the continuity equation, and the vertical advection/diffusion balance to derive a relation between characteristic scales of the density field, the velocity field, and the thermocline depth. Applied to a closed basin, this yields a third-power relation between the overturning strength and a characteristic density scale. In global ocean models (Hughes and Weaver 1994; Rahmstorf 1996) the overturning strength was found to be linearly related to large-scale meridional density and pressure gradients. Nevertheless, these views involve salinity and temperature *differences* across the basin, rather than their absolute values. The question of the impact of Agulhas Leakage on the Atlantic overturning circulation therefore relates to the problem how thermal and saline anomalies are dispersed through the ocean, how they interact with the atmosphere, and how they finally modify the large-scale pressure distribution in the Atlantic.

Cai and Greatbatch (1995) addressed the hypothesis of Gordon et al. (1992) by comparing two models of the global ocean circulation; in one model Agulhas Leakage was present, whereas in the other it was inhibited by an eight degrees southward extension of the African continent. The strength of the Atlantic overturning circulation in their model was unaffected by the presence or absence of Agulhas Leakage. They argued that the heat and salt inputs brought about by Agulhas Leakage cancel with respect to density, leaving the density field of the Atlantic largely unchanged. However, Rahmstorf et al. (1996) pointed at the unrealistically weak thermal coupling between the ocean and atmosphere in the model of Cai and Greatbatch (1995), who used a so-called zero heat capacity atmosphere model. This may have severely hindered the development of density anomalies. Furthermore, the approach of Cai and Greatbatch (1995) did not allow for a sensitivity study, and hence the robustness of the response was neither questioned nor tested.

The question has also been addressed in the 2D modelling studies of Chapters 4 and 5. Contrary to the results of Cai and Greatbatch (1995), these studies do show a large sensitivity of the overturning strength to interbasin fluxes of heat and salt. Although these models display a linear relation between the meridional pressure gradient and the overturning strength (consistent with the findings of Hughes and Weaver (1994) and Rahmstorf (1996)), it was shown that the response of the overturning strength is controlled by the energy conversions. The reason for this is that these 2D models are in the advective regime, so that vertical transports of heat and salt, and thus of buoyancy, are mainly accomplished by vertical advection. And it is by vertical advection of buoyancy (the 'buoyancy production') that potential energy is converted into kinetic energy. In a 3D ocean, the situation is much more complex. Most of the kinetic energy is present in the horizontal flow field, and it is not clear how a source of kinetic energy of the horizontal flow (by buoyancy production) influences the strength

of the circulation in the meridional/depth plane. Furthermore, it is likely that low-resolution global circulation models are more diffusive than our 2D models, and it may be expected that diffusion and convective adjustment compete with advection in accomplishing the vertical transports. It is thus not clear what role is played by buoyancy production in the potential energy balance under changing Agulhas heat and salt input.

Clearly, the question to what degree Agulhas Leakage influences the strength of the Atlantic overturning circulation has not been answered unambiguously, yet. In the present study, this question is addressed using the low-resolution Hamburg LSG model. Due to its coarse spatial resolution and high viscosity, the model does not resolve Agulhas Leakage under realistic wind stress forcing (Drijfhout et al. 1996a). Therefore, the Agulhas heat and salt exchanges are parametrised by heat and salt sources in the South Atlantic (and equally large heat and salt sinks in the South West Indian Ocean, from which Agulhas Leakage originates). In this way the thermohaline impact of Agulhas Leakage can be studied systematically, without explicitly affecting the momentum balance. It is studied whether changes in convective activity generate the response (as suggested by Gordon et al. (1992)), or whether it is determined by changes in the large-scale density and pressure distributions (as suggested by the studies of Hughes and Weaver (1994) and Rahmstorf (1996)). Furthermore, the energy conversions in the model are analysed, to find out whether the conclusions from our 2D model studies are supported by more realistic 3D models. Finally the processes are studied that govern the adjustment of the overturning circulation to changes in the Agulhas sources. This might shed light on the mechanisms that generate the response in the overturning circulation, and on their corresponding time scales.

The model is introduced in section 2. The spin-up procedure is described, and the circulation is evaluated that was used as starting point of the experiments. The section concludes with a description of the source/sink parametrisation that is used to model the Agulhas input of heat and salt. In section 3 the results of the main experiment are presented and analysed, concerning an integration over 10 kyr. In section 4 the results of two adjustment experiments are analysed. Section 5 discusses the implications of the results, and evaluates the Agulhas Leakage parametrisation.

6.2 The model

6.2.1 The Hamburg LSG model

The Hamburg Large-Scale Geostrophic (LSG) model has been developed for climate studies, and it was described in detail in Maier-Reimer and Mikolajewicz (1992) and Maier-Reimer et al. (1993). The model design is based on original ideas by Hasselmann (1982). He noted that for dominant patterns of climate variability the spatial scales are generally much larger than the internal Rossby radius of deformation, and that the time scales are much larger than the periods of gravity waves or barotropic Rossby waves. Scaling the equations of motions with these considerations in mind leads to a baroclinic velocity field that is diagnostically determined from the density field, and to a barotropic velocity field that is in balance with sea level variations,

wind stress and bottom torque. The only prognostic equations remaining are the tracer equations.

However, Maier-Reimer et al. (1993) pointed out that a straightforward implementation of this idea did not work because of numerical instability problems. In the present version of the model the fast modes have been filtered out by integrating the complete set of primitive equations with a semi-implicit time-stepping method, and by neglecting non-linear advection of momentum. This allows for a time step of 30 days. The model has a free-surface formulation, with a sea-surface height (ζ) that is prognostically determined, and filtered every time step. The ocean is coupled to a simple thermodynamic sea-ice model.

The model is discretised on an Arakawa E-grid (Arakawa and Lamb 1977). It has an effective horizontal resolution of $3.5^\circ \times 3.5^\circ$, and 11 vertical levels, centered at depths of 25, 75, 150, 250, 450, 700, 1000, 2000, 3000, 4000 and 5000 m.

6.2.2 The equations

For the momentum equations, the standard hydrostatic and Boussinesq approximations are applied. Vertical friction and non-linear advection of momentum are neglected. The equations for the horizontal velocity field $\mathbf{u_h}$ are thus given by:

$$\frac{\partial \mathbf{u_h}}{\partial t} + f\mathbf{k} \times \mathbf{u_h} = -\frac{1}{\rho_0}\nabla_h p + \frac{1}{\rho_0}\tilde{\boldsymbol{\tau}} + A_h \nabla_h^2 \mathbf{u_h}. \tag{6.1}$$

Here A_h is the horizontal eddy viscosity ($4 \cdot 10^5 \mathrm{m}^2\ \mathrm{s}^{-1}$), ρ_0 a reference density (1020 kg m^{-3}), $\mathbf{k}$ is the unit vector in the z-direction, f is the Coriolis parameter, p the pressure, and ∇_h the horizontal gradient operator. The wind stress (Hellerman and Rosenstein 1983) is divided by the depth of the upper layer to yield $\tilde{\boldsymbol{\tau}}$, and is applied as a source of momentum in the upper layer alone. The vertical velocity w is obtained by integrating the continuity equation:

$$\frac{\partial w}{\partial z} = -\nabla_h \cdot \mathbf{u_h}. \tag{6.2}$$

The surface elevation ζ is treated prognostically via:

$$\frac{\partial \zeta}{\partial t} = w + F_{fr} \qquad \text{at } z = 0, \tag{6.3}$$

where F_{fr} is the surface freshwater flux (taken positive in case of freshwater input). The pressure p is related to the density ρ and the sea-surface elevation ζ according to:

$$p = g\rho_0\zeta + g\int_z^0 \rho(z')dz' \tag{6.4}$$

with g the gravitational acceleration (9.81 m s^{-2}).

Prognostic equations for potential temperature θ and salinity S are:

$$\frac{\partial(\theta, S)}{\partial t} + \mathbf{u} \cdot \nabla(\theta, S) = q^{(\theta,S)} - \nabla \cdot \mathbf{F_D}^{(\theta,S)}, \tag{6.5}$$

where $\mathbf{F_D}^{(\theta,S)}$ denotes the diffusive flux of potential temperature and salinity. These equations are solved with implicit time-stepping methods. To render the scheme unconditionally stable, a first-order upwind scheme for the tracer advection is used. Such a scheme is known for its high numerical diffusion. In fact, this diffusion can be made explicit (Maier-Reimer et al. 1993), yielding a diffusive flux as follows:

$$\mathbf{F_D}^{(\theta,S)} = -\mathsf{D} \cdot \nabla(\theta, S). \tag{6.6}$$

The diffusion tensor D has non-zero diagonal elements $|u|\Delta x + D_h, |v|\Delta y + D_h$, and $|w|\Delta z$. The explicit diffusion coefficient D_h ($2 \cdot 10^2$ m^{2}s^{-1}) is added to the horizontal components to avoid mode-splitting effects, which can arise when staggered grids are used.

The source terms $q^{(\theta,S)}$ in Eq. (6.5) consist of three parts:

$$q = q_{boundary} + q_{convection} + q_{source}. \tag{6.7}$$

The first term denotes the air-sea fluxes, which are in fact treated as sources of heat and freshwater in the first layer. However, the salt content of the upper layer is conserved when the freshwater flux is applied, so that $q^S_{boundary} = 0$. The second term describes the vertical redistribution of heat and salt due to the convective adjustment procedure, and the third term denotes the contribution of the explicitly defined sources, as used in the experiments.

The fully non-linear UNESCO (1981) equation of state is used. Furthermore, a convective adjustment scheme is applied that interchanges unstably stratified pairs of layers in one downward sweep. This resolves most, though not all, of the instabilities. Due to the continuing development of the model, the present code has been improved in several details with respect to the version of Maier-Reimer et al. (1993). Among these improvements are the use of Bryden's (1973) polynomial expression to convert the potential temperature θ to the in-situ temperature T (Maier-Reimer et al. (1993) use a linearised equation), details of the ice model, and details of the solution method. Furthermore, a higher value of the viscosity is used in the present model ($4 \cdot 10^5$ m^{2}s^{-1} vs. $5 \cdot 10^4$ m^{2}s^{-1} in Maier-Reimer et al. (1993)).

6.2.3 The source distribution

Heat and salt exchange by Agulhas Leakage takes place by the inflow of Indian Ocean water into the south-east Atlantic, and a compensating return transport leaving the Atlantic. The inflowing Indian Ocean water is characterised by higher temperatures and salinities than the surrounding South Atlantic thermocline waters. Based on this difference in water mass properties, Van Ballegooyen et al. (1994) estimated the heat and salt exchange by an average of 6 Agulhas rings per year at about 0.045 PW and 2.52 Gg/s. This is probably an underestimation: Agulhas Leakage is not only sustained by the shedding of large rings, but also by Agulhas Current water leaking directly into the Atlantic (Gordon et al. 1987), partly in the form of filaments (Lutjeharms and Cooper 1996). Moreover, the exact amount of heat and salt that is exchanged can only be determined when the temperature and salinity is known of the

water that is exported to compensate for the Agulhas water input. If, for instance, a large part of the Agulhas inflow is compensated by outflow of NADW, then the corresponding heat flux may be up to an order of magnitude larger (Gordon 1985).

In this model, Agulhas heat and salt input is parametrised by sources of heat and salt in the South Atlantic Ocean (denoted by $q_{Atlantic}$). To close the heat and salt budgets, equal amounts of heat and salt are extracted from the south-west Indian Ocean, where the leakage originates (q_{Indian}). The strength of the sources are controlled by a dimensionless amplitude σ, that relates the volume integrals of the sources to the original Van Ballegooyen et al. (1994) values:

$$< q_{Atlantic} >= - < q_{Indian} >= \sigma Q_{VanBallegooyen}, \tag{6.8}$$

where the brackets denote volume integration. A value of $\sigma = 1$ thus represents the original Van Ballegooyen et al. (1994) heat and salt exchange of 0.045 PW and 2.52 Gg/s.

The horizontal distribution of the sources in the South Atlantic (Fig. 6.1) reflects to some extent the corridor that is taken by the Agulhas Rings before they cross the Walvis Ridge (Byrne et al. 1995; Schouten et al. 1999). The sources thus represent the release of the anomalous heat and salt contents when Agulhas rings decay. The north-westerly part of the distribution coincides with the extension of the Benguela Current, that advects the released heat and salt further north. The heat and salt removal from the south-west Indian Ocean is distributed over the Agulhas Return Current and the South Indian Current.

The vertical profiles of these sources decay exponentially with depth (Fig. 6.2). An *e*–folding depth scale of 300 m is chosen so that the exchange taking place on intermediate levels is represented as well (Gordon et al. 1992).

6.2.4 The spin-up

To be able to clearly identify the response of the circulation to the applied perturbations, the experiments must be started from a well-equilibrated solution. To this end, the well-known spin-up procedure is used. According to this procedure, the model is forced with restoring surface boundary conditions on temperature and salinity first. When a steady state is reached, the freshwater flux of this state is diagnosed. The restoring condition on salinity is then replaced by prescription of this freshwater flux, and the model is said to be forced by mixed boundary conditions.

The temperature is restored to monthly mean air temperatures derived from the COADS data set (Woodruff et al. 1987). An air-sea coupling coefficient of 40 W m^2K^{-1} is used, equivalent to a time constant of 58 days. In the first phase of the spin-up, sea-surface salinity was restored to the annual mean climatology of Levitus (1982). The time constant was taken to be 38 days.

After 10 kyr of integration, the trend in the basin-averaged temperature and salinity was less than $3 \cdot 10^{-3}$K and $6 \cdot 10^{-5}$ psu per century. At this point, the strength of the Atlantic meridional overturning was about 19.5 Sv, whereas the NADW outflow across 30°S was about 10 Sv. These values are smaller than those of the circulation described by Maier-Reimer et al. (1993), who obtained 23 Sv and 17 Sv for the

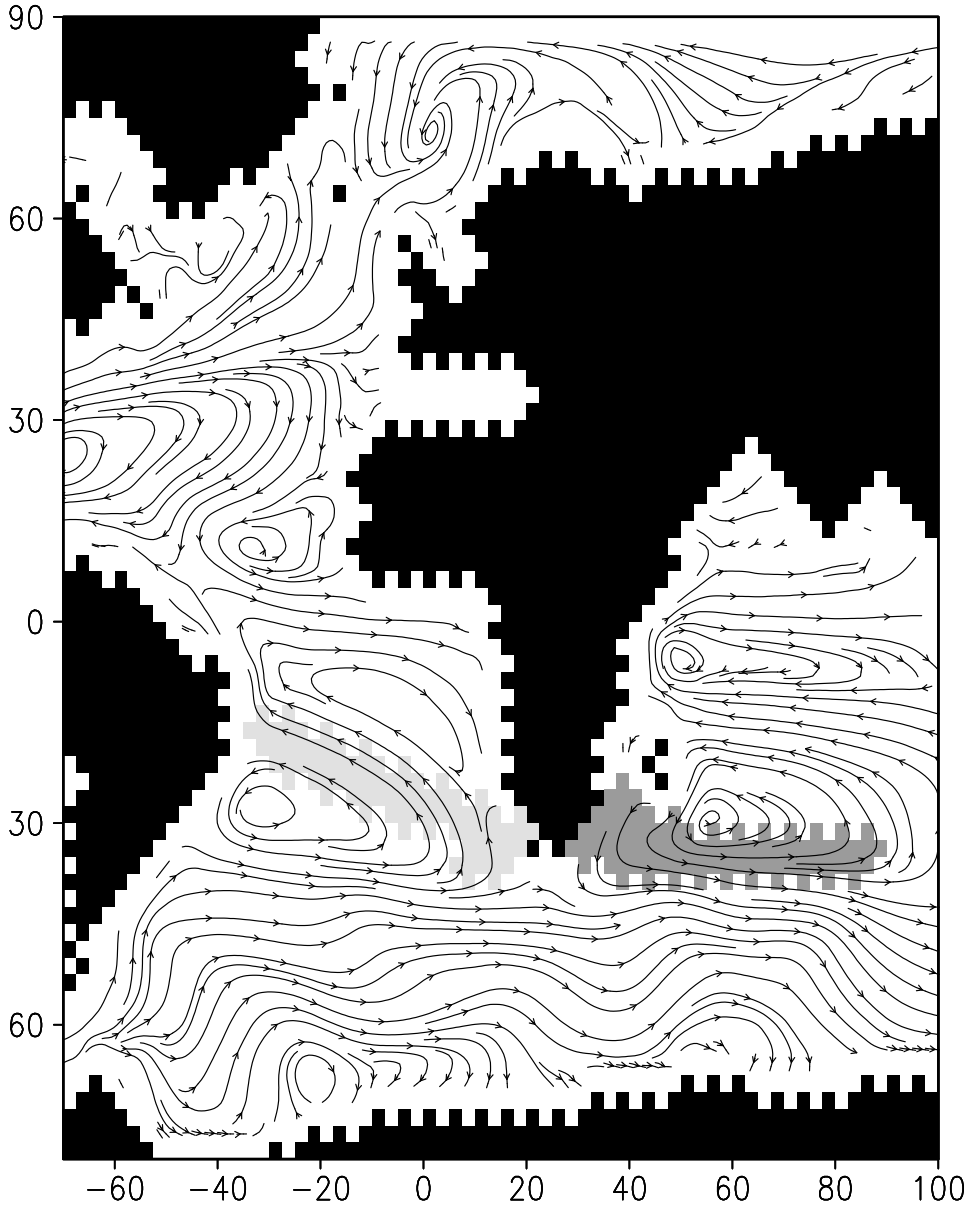

Figure 6.1: *Horizontal distribution of the heat and salt sources in the Atlantic (light grey areas) and sinks in the Indian (dark grey areas) Oceans. Superimposed are streamlines at 150 m depth. The source/sink distributions represent the exchange of heat and salt between the Indian and Atlantic Oceans by Agulhas Leakage.*

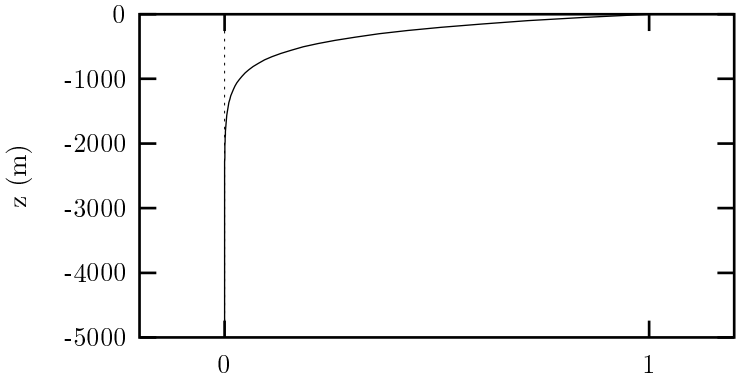

Figure 6.2: *Vertical profile of the heat and salt source distributions.*

overturning and outflow, respectively. This difference is mainly caused by the smaller value of the viscosity used by them ($5 \cdot 10^4$ m^{2}s^{-1}). A run with this same low viscosity yielded a 24.1 Sv overturning and a 14.6 Sv outflow, but the time it took to reach an equilibrium turned out to be much longer. Since our interest is largely qualitative, the higher value of the viscosity is used for the experiments presented here.

From the equilibrated solution with restoring conditions on both temperature and salinity, 10 years of the freshwater flux were diagnosed and averaged into one annual freshwater flux cycle. Figure 6.3 shows the annual-average of this freshwater flux cycle, zonally integrated over the Atlantic. Comparison of this flux profile with the estimate of Baumgartner and Reichel (1975) shows that the basic features of the observations are well reproduced. Nevertheless, the excess precipitation in the equatorial regions is larger in the model, and the subtropical evaporative maxima are underestimated. This difference is also reflected by the total freshwater export from the Atlantic north of 30°S. This export amounts to 0.25 Sv in the model, while Baumgartner and Reichel (1975) estimate an export of no less than 0.7 Sv. It must be noted that, according to Wijffels et al. (1992), the Baumgartner and Reichel (1975) estimate is highly uncertain, and that errors may add up to 0.6 Sv at 35°S when a modest uncertainty of 30% in the $E - P$ fields is assumed.

The model was run for another 1500 years prescribing this freshwater flux in the configuration with mixed boundary conditions. The switch from restoring to mixed boundary conditions resulted in a slight adjustment, with the Atlantic overturning strength dropping from 19.5 Sv to 17.7 Sv.

The meridional overturning streamfunction (Fig. 6.4, upper panel) shows a well developed NADW cell, and a well developed Antarctic Bottom Water (AABW) cell beneath it. The 18 Sv NADW production is close to Broecker's (1991) estimate of 20 Sv, but the 9 Sv outflow is lower than the estimated 14 Sv (Schmitz 1995). This indicates that this model overestimates the NADW upwelling taking place within the Atlantic. If NADW upwelling would be homogeneously distributed over the World

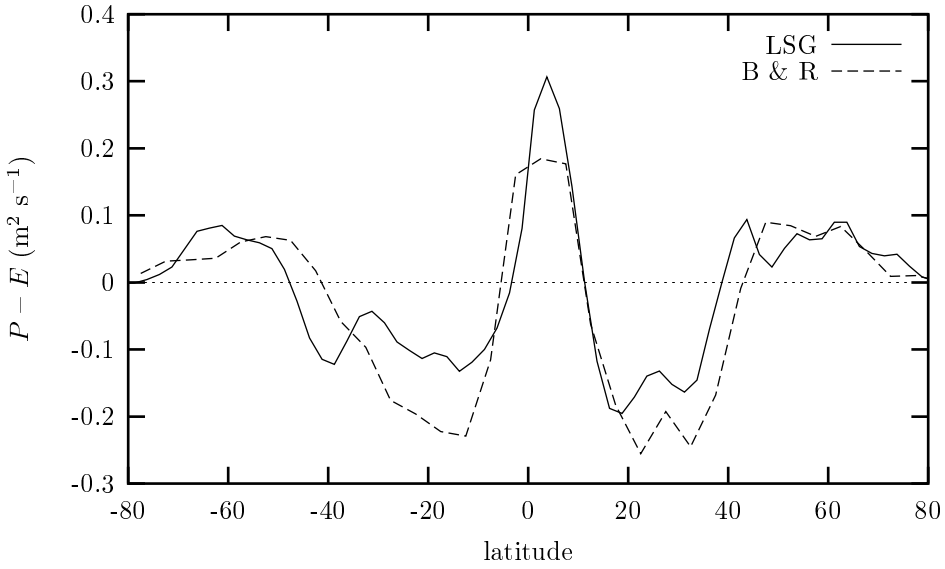

Figure 6.3: *The zonal integral over the Atlantic of the model's surface freshwater flux ($P-E$, in $m^3m^{-1}s^{-1}$, 'LSG'). This freshwater flux is diagnosed from the configuration with restoring boundary conditions, and forces the model in the configuration with mixed boundary conditions. The freshwater flux of Baumgartner and Reichel (1975) is added for comparison ('B & R'). The model overestimates the excess precipitation in the tropics, and underestimates the excess evaporation in the subtropics.*

Ocean (Stommel and Arons 1960), then the fraction of NADW that is upwelled in the Atlantic would be closer to 25% than to 50%. The 8 Sv AABW inflow is higher than observed values (4 Sv, Schmitz 1995).

The thermal structure of a meridional section (30°W) through the Atlantic (Fig. 6.4, middle panel) may be compared with the zonally averaged temperature field of the Levitus (1982) climatology (Fig. 1.5, upper panel). Several features are quite well reproduced by the model. For instance, the 10°C and 4°C isotherms are at approximately the correct depth, and the double-bowl structure of the thermocline in the (sub)tropics is simulated as well. The temperature in the deep ocean is slightly lower than in Fig. 1.5, probably due to the stronger AABW cell in the model. The salinity structure (Fig. 6.4, lower panel) clearly shows the high-salinity tongue of NADW, situated at 3000 m depth (Fig. 1.5, lower panel). However, its salinity of 35 psu is higher than observed (34.8 psu). Furthermore, the low-salinity tongue, characteristic of Antarctic Intermediate Water (AAIW), is almost completely absent.

Despite these quantitative differences, the model simulates the overall characteristics of the Atlantic overturning circulation and the Atlantic thermohaline structures sufficiently well to justify its use in the experiments described below.

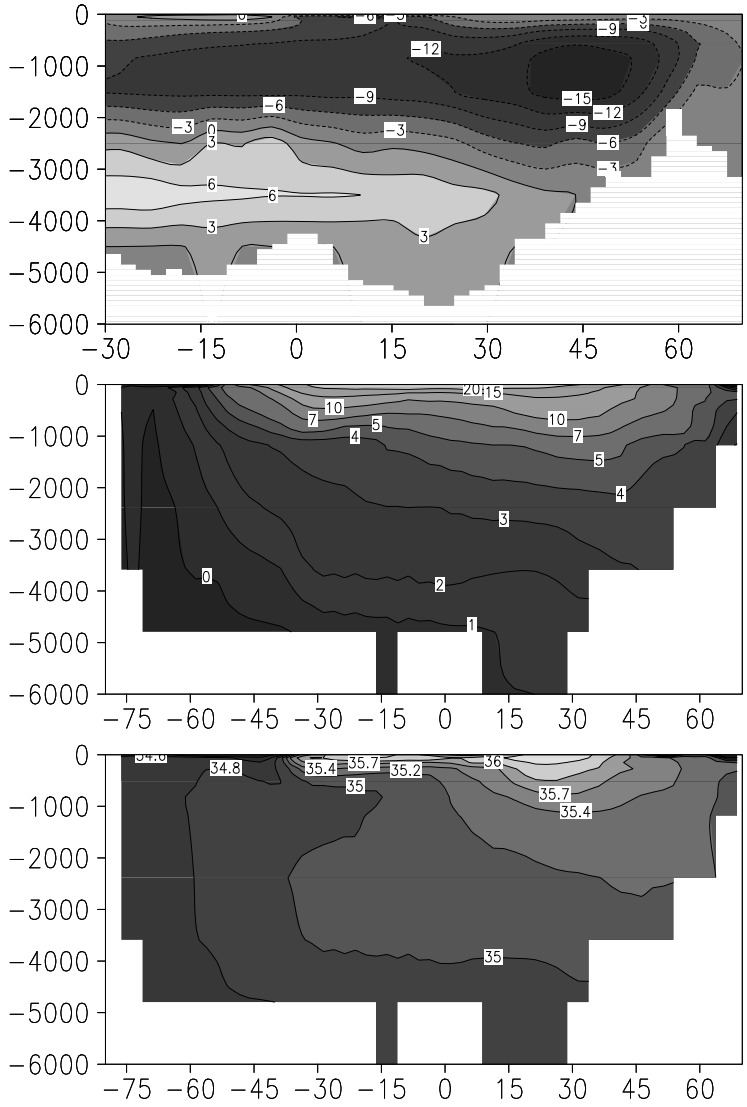

Figure 6.4: *Meridional overturning streamfunction in the Atlantic (upper panel), and profiles of temperature (middle panel) and salinity (lower panel) along 30° W in the Atlantic of the final spin-up solution (mixed boundary conditions). Please note that upper panel ranges from 30° S to 70° N, while the lower two panels range from 80° S to 70° N.*

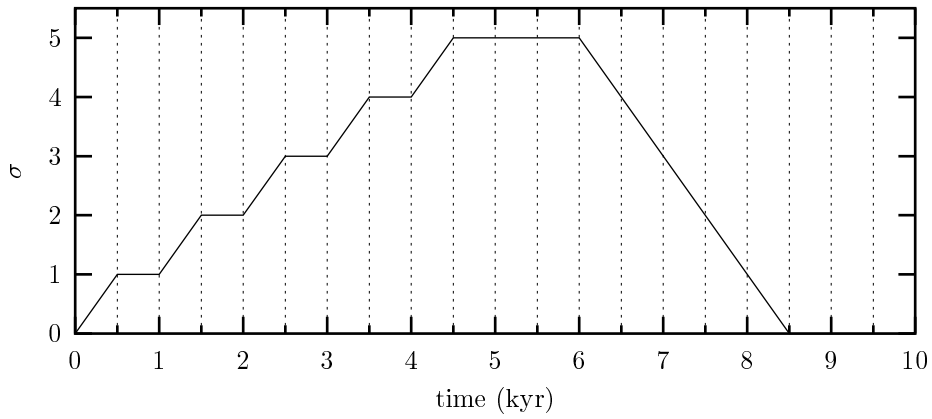

Figure 6.5: *Dimensionless source amplitude σ as function of time as applied in the slow source experiment. A value of 1 accounts for the original Van Ballegooyen et al. (1994) values (0.045 PW for heat and 2.52 Gg/s for salt).*

6.3 Slow source modification

6.3.1 Overturning response

In this experiment, the amplitudes of the heat and salt sources are increased from 0 to 5 times the Van Ballegooyen et al. (1994) value in steps of 500 years (Eq. (6.8); Fig. 6.5). After each dimensionless unit increase, σ is kept constant for another 500 years to allow further equilibration of the solution. When σ has reached the value of 5 at 4.5 kyr, it is kept constant for 1500 years, and it is decreased again in the following 2500 years.

The time scale with which the source amplitude is increased is longer than the adjustment time scale of the flow. This adjustment time is in the order of a decade, when a characteristic propagation speed of baroclinic Rossby waves of 2 cm/s (Gill 1982, p. 510) is taken, and a characteristic length scale in the order of 10^6–10^7m. This allows for a continuous balance in the momentum equations, and a well-equilibrated circulation. However, the time scale for the thermohaline fields to equilibrate is much longer than these 500 years. With the basin-averaged value of $|w|$ being in the order of $5 \cdot 10^{-7}$m s^{-1}, and with Δz being O(1000 m), we have a characteristic vertical diffusivity of $5 \cdot 10^{-4}$m s^{-1}, corresponding to a vertical diffusive time-scale of about 1600 years. So it cannot be expected that the tracer fields are fully balanced. Nevertheless, Fig. 6.6 shows that the adjustment of the flow is very weak during the phases of the experiment in which the source amplitudes are constant: the final equilibration phases of the thermohaline fields do not impose large changes on the flow field after the initial adjustment.

The response of the Atlantic overturning circulation to the changes in source amplitudes is measured by critical values of the zonally integrated overturning stream

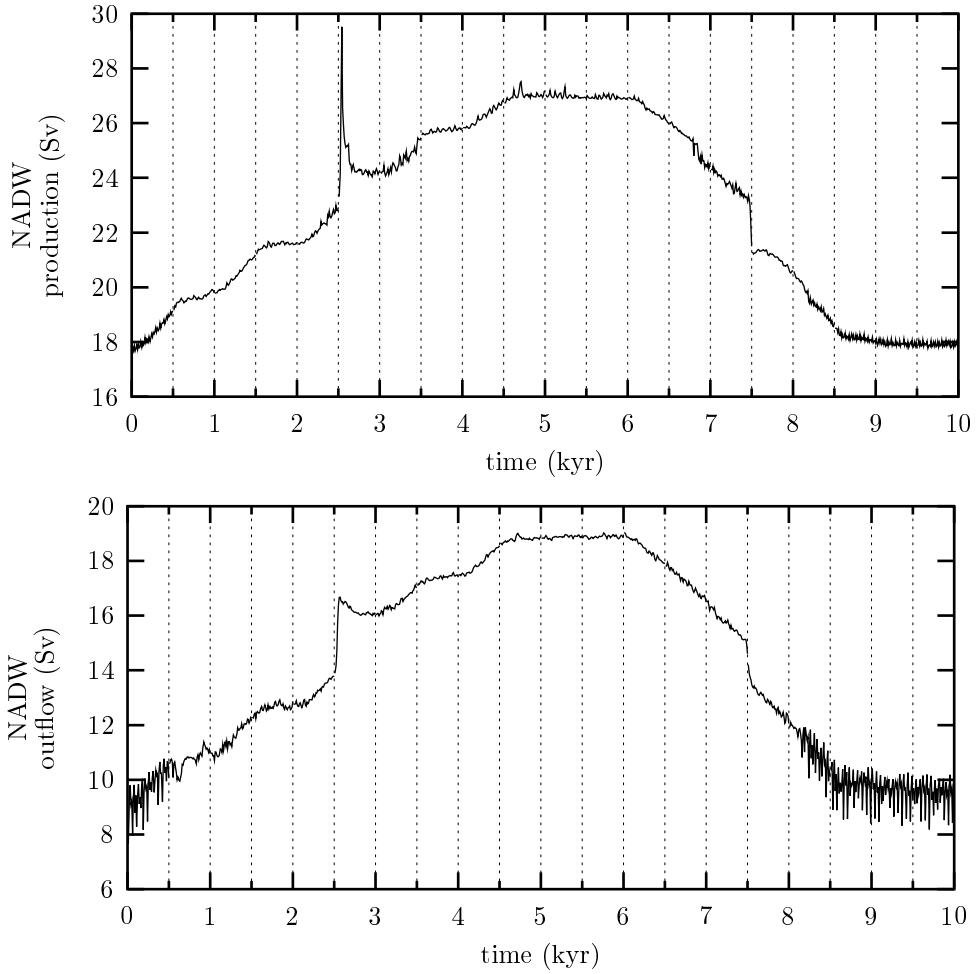

Figure 6.6: *Response of the NADW production (upper panel) and the NADW outflow across 30° S (lower panel) for the slow source experiment. The amplitudes of the Agulhas heat and salt sources are changed according to Fig. 6.5. The NADW production and outflow show a linear response, as well as non-linear jumps at 2.5 and 7.5 kyr. The variability during the first 0.5 kyr and the last 2 kyr reflects an oscillation in the Southern Ocean, particularly influencing the NADW outflow.*

function (integrated upward). The 'NADW production' is defined as the minimum value of this streamfunction in the North Atlantic, and measures the strength of the Atlantic overturning circulation. The 'NADW outflow' is defined as the minimum value of the streamfunction at 30°S, and measures the outflow of that component of NADW that is derived from surface waters, rather than from AABW.

The overturning circulation displays a particularly strong response to changes in the Agulhas heat and salt source amplitudes. Figure 6.6 shows that the relation between the production and outflow of NADW and the source amplitude is mainly linear (Fig. 6.6): except for the events at 2.5 and 7.5 kyr, the stepwise shape of the source amplitude evolution (Fig. 6.5) is reproduced in the response of the overturning circulation. The strength of the AABW overturning cell (not shown) does not display this linear response. The overturning strength also displays a non-linear response: at 2.5 and 7.5 kyr, both the NADW production and outflow show stepwise adjustment. The resulting increase in the strength of the NADW overturning cell between 2.5 and 7.5 kyr results in a 0.5 Sv drop in the 8 Sv AABW transport.

For NADW outflow rates below 12, this exchange is strongly influenced by an oscillation in the Southern Ocean, with a period of about 25 yr. This oscillation is related to phases of reduced and enhanced convective activity in the Southern Ocean, and associated thermal and saline anomalies. In that respect, it resembles the 320 yr oscillation found by Mikolajewicz and Maier-Reimer (1990). Their oscillation was characterized by switches between two states, featuring weak or strong convective activity in the Antarctic region. Pierce et al. (1995) identified this oscillation to be a variation on Welander's (1982) flip-flop oscillation. However, the 25 yr period of the oscillation in this model comes closer to the 20 yr oscillation of Drijfhout et al. (1996b), or the < 10 yr period of the Antarctic Circumpolar Wave (Haarsma and Selten 1998; Weisse et al. 1999; Bonekamp et al. 1999). Detailed analysis of this oscillation is left for further study.

6.3.2 The linear response

Figure 6.7 shows that the NADW production is linearly related to the meridional pressure difference in the upper 1500 m. This suggests that an increase of the source amplitudes stimulates the overturning circulation by enhancing the meridional gradients of the large-scale pressure field. Near the source area, the heat and salt sources generate only a weak positive density anomaly that is confined to the near-surface layers. Here, the development of the thermal anomaly is inhibited by strong surface relaxation, whereas at depth the thermal and saline anomalies compensate with respect to their effect on density. On its way north, the thermal anomaly is more and more attenuated by atmospheric heat loss, and the density anomaly is amplified. The resulting meridional gradient in the anomalous density field strengthens the (positive) meridional gradient in the baroclinic pressure field. This generates an anomalous southward baroclinic transport, for reasons that will be discussed later. This southward transport must be compensated by a northward barotropic flow, for reasons of continuity. Again, this meridional transport seems to be generated by enhancement of the (negative) meridional gradient of the barotropic pressure field. This

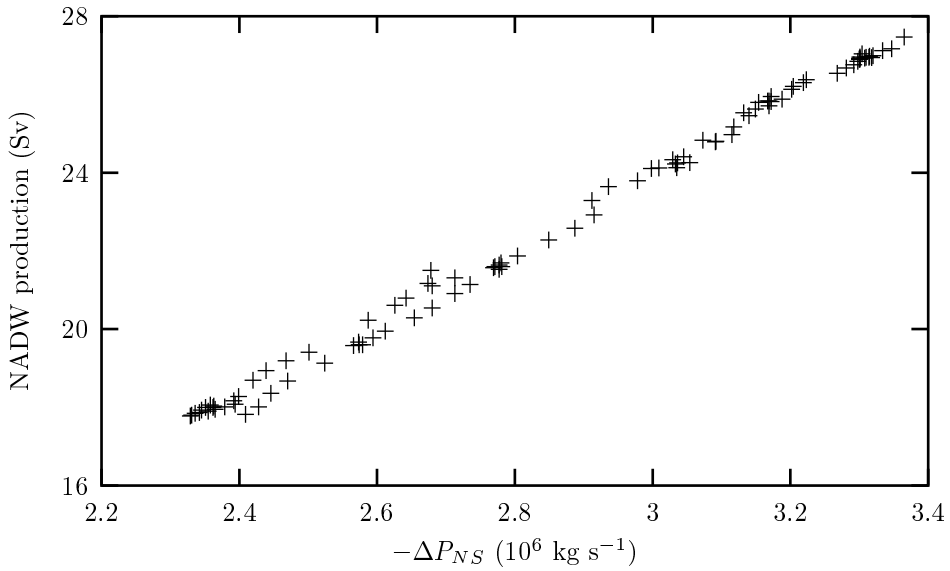

Figure 6.7: *NADW production as function of the meridional pressure difference, measured by* ΔP_{NS}. $\Delta P_{NS} = P_N - P_S = P(53^\circ N) - P(30^\circ S)$, *where* $P(\theta) \equiv \int_{-1500}^{0} \bar{p} dz$, *with* $\bar{p}$ *the zonally averaged pressure at latitude* θ.

reduces the anomalous positive pressure gradient and associated southward transport at depth, and generates a negative pressure gradient and a northward flow at shallower levels (Fig. 6.7).

However, from geostrophic considerations it is clear that a meridional pressure gradient generates zonal, rather than meridional, flow. A geostrophically balanced meridional transport can only be driven by zonal pressure gradients. It is thus not clear how the linear relation between the meridional pressure gradient and the overturning strength in Fig. 6.7 is accomplished. Figure 6.8 shows that the enhanced northward transport across 30°S is not geostrophically balanced in this model: the geostrophic component of the northward transport in the upper 1500 m is more or less constant during the experiment. The increased meridional transport resulting from the enhanced overturning must therefore be frictionally controlled, since no other forces are present to balance the Coriolis force. This conjecture is supported by the fact that the anomalous transports in both the shallow and the deep layers are confined to the western boundary layers (Fig. 6.9). In these boundary layers the velocity gradients are largest, and viscous effects are expected to dominate. A final indication that the enhanced overturning may be frictionally controlled is the fact that vorticity dynamics requires meridional transports in the ocean's interior to be balanced by vortex-stretching effects. The meridional transports of the overturning circulation are thus related to up- and downwelling via $\beta v = f \frac{\partial w}{\partial z}$. However, in our model there is a 1–to–1 relation between the NADW outflow across 30°S and the

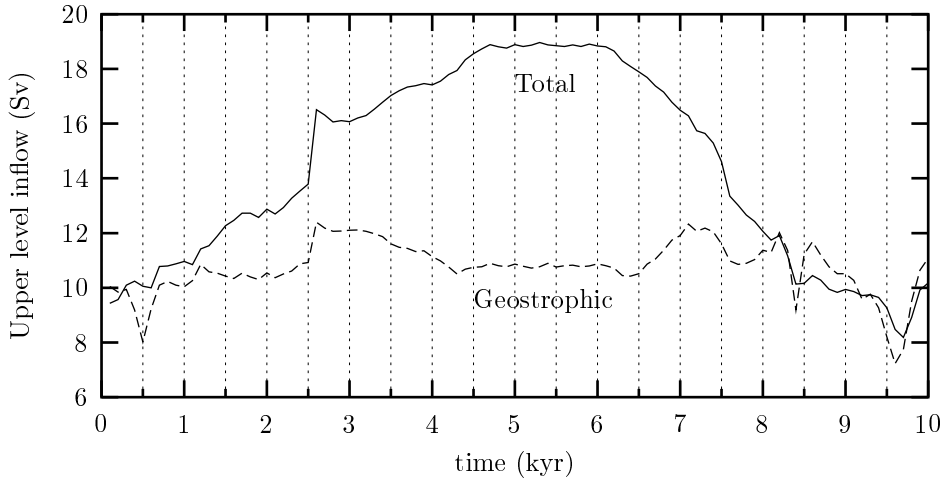

Figure 6.8: *Northward transport across 30° S in the upper 1500 m (solid line) and its geostrophically balanced component (dashed line). Note that sample frequency is 1 per 100 yr.*

NADW production (Fig. 6.10). A change in NADW production is thus accompanied by an equally large change in NADW outflow, and the amount of NADW upwelling within the Atlantic basin (8.5 Sv) remains almost constant. The lack of response of the basin-wide upwelling to changes in the meridional overturning transports shows that the changes in planetary vorticity are not balanced by vortex stretching. Only by friction in the viscous western boundary layers may the meridional transports lose or gain vorticity to balance the planetary vorticity changes.

These three observations suggest that the enhanced overturning circulation, generated by the South Atlantic heat and salt sources, is frictionally controlled, rather than geostrophically balanced. However, conclusive evidence should come from an analysis of the local force balances in the model, but this is left for future study.

6.3.3 Nonlinear response

Analysis of the output fields reveals that the change in overturning strength at 2.5 kyr is accompanied by a sudden increase in convective activity in the northern North Atlantic, and a westward expansion of the convecting area (Fig. 6.11). At 7.5 kyr, the reverse happens, and the convective activity is strongly reduced. The sudden changes in convective activity are also clearly reflected by jumps in the upward convective transports of heat (Fig. 6.12) and salt (not shown).

The abruptness of the response suggests that a shift in convective activity is triggered when a certain threshold is exceeded. This threshold is related to the stratification in the North Atlantic, and causes a marginally stable area to become unstable and vice-versa. The upward shift at 2.5 kyr takes place when the source amplitude σ

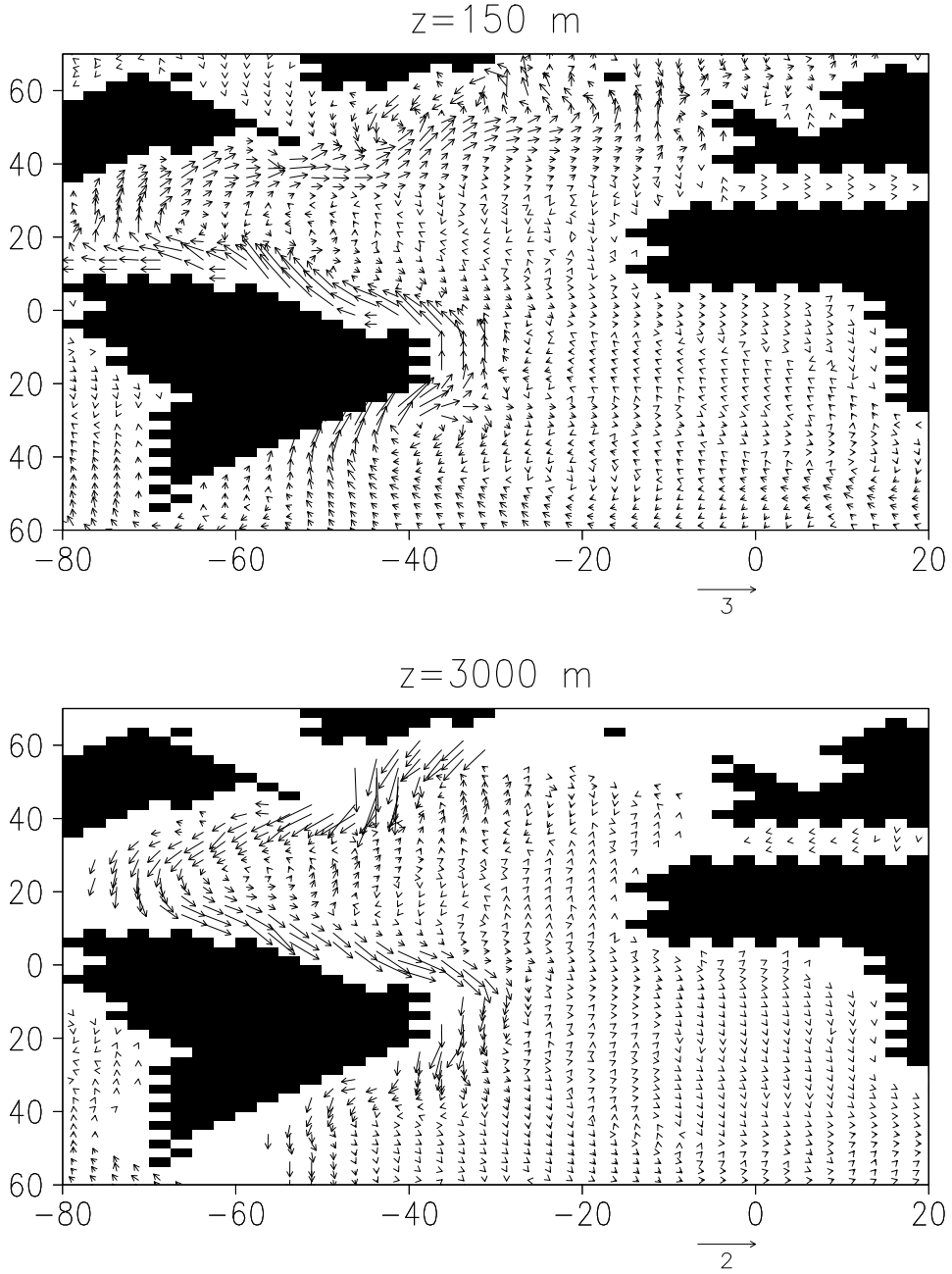

Figure 6.9: *Velocity anomaly (in cm s^{-1}) at 3.5 kyr (with respect to t=0) at 150 m (upper panel) and 3000 m (lower panel).*

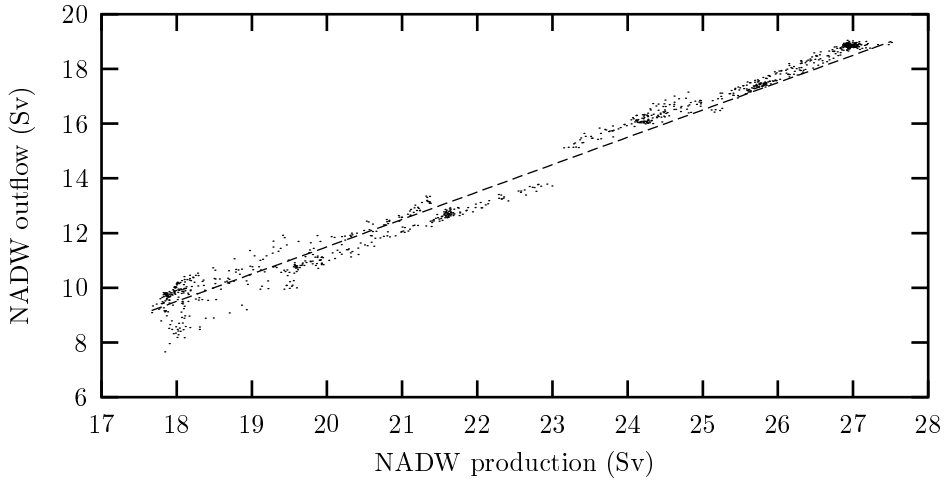

Figure 6.10: *Relation between NADW production and outflow for the slow source experiment. The dotted line represents the curve 'NADW production = NADW outflow + 8.5', indicating that the amount of NADW that is upwelled within the Atlantic is almost constant (8.5 Sv). The rest of the NADW that is produced leaves the Atlantic.*

has reached the value of 3, while the downward shift at 7.5 kyr takes place at $\sigma = 2$ (Fig. 6.12). It is therefore unlikely that the abrupt changes in convective activity are directly related to the strength of the sources in the South Atlantic. The overturning strength is about 23 Sv both at the time of the upward and downward shift. This suggests that the threshold is related to the strength of the overturning circulation, and its associated northward advection of salt from subtropical latitudes. If this advection exceeds a certain strength, it may destabilise areas in the northern North Atlantic that were formerly stably stratified. This points to a scenario where the Agulhas sources influence the North Atlantic convective activity indirectly, via their influence on the overturning strength and the northward advection of salt from subtropical regions. However, determining the exact cause of the convective switches, and their peculiar relation with the overturning strength, would need much more detailed analyses of the relation between overturning strength and the thermohaline stratification. Such an analysis is left for future study.

Several studies have shown (Lenderink and Haarsma 1994; Rahmstorf 1994, 1995) that the procedure of convective adjustment in Ocean General Circulation Models (OGCMs) may give rise to multiple equilibria, i.e., the coexistence under identical forcing conditions of several equilibria that differ only in the intensity and the spatial distribution of the convective activity. Hysteresis effects could cause an experiment to end up in a different equilibrium than it started from. Figure 6.12 shows that this is the case in the present experiment: for $\sigma < 2$, the convective intensity of the equilibria at the start of the experiment is slightly lower than the intensity of the equilibria that are reached at the end, despite the fact that they experience identical forcing.

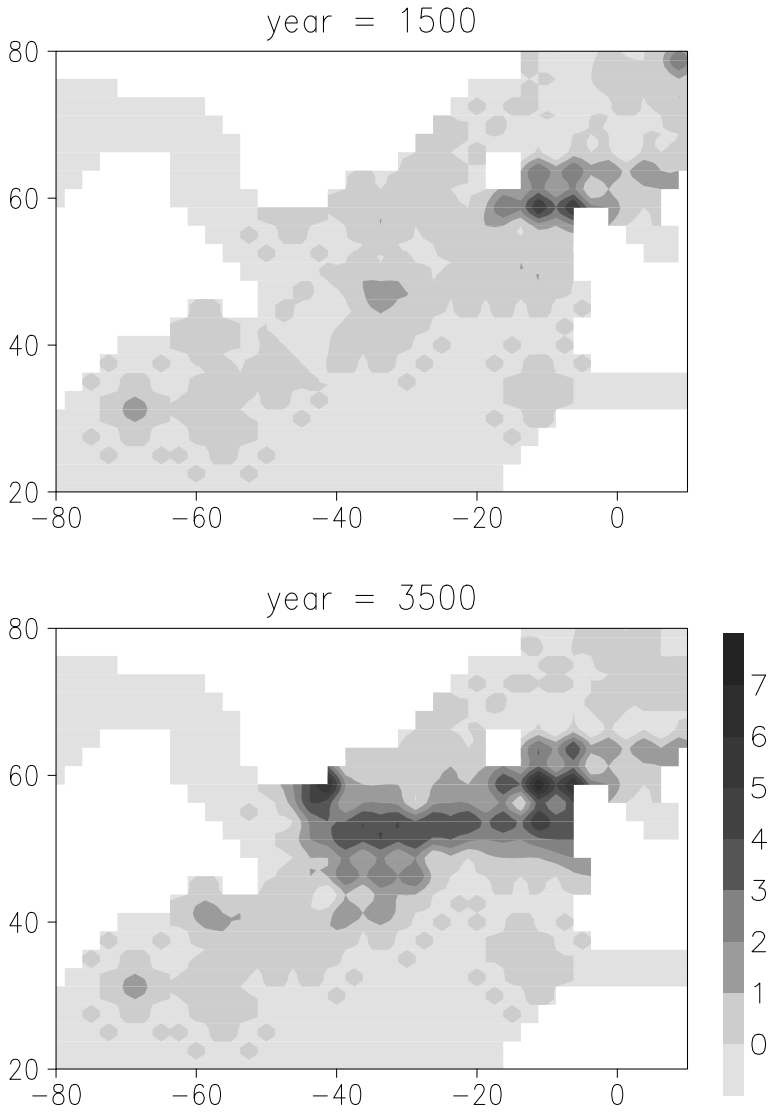

Figure 6.11: *Anomalous number of convective adjustment events between the second and third layer (across 100 m) before (1500 yr, upper panel) and after (3500 yr, lower panel) the impulsive event at year 2500 in Fig. 6.6.*

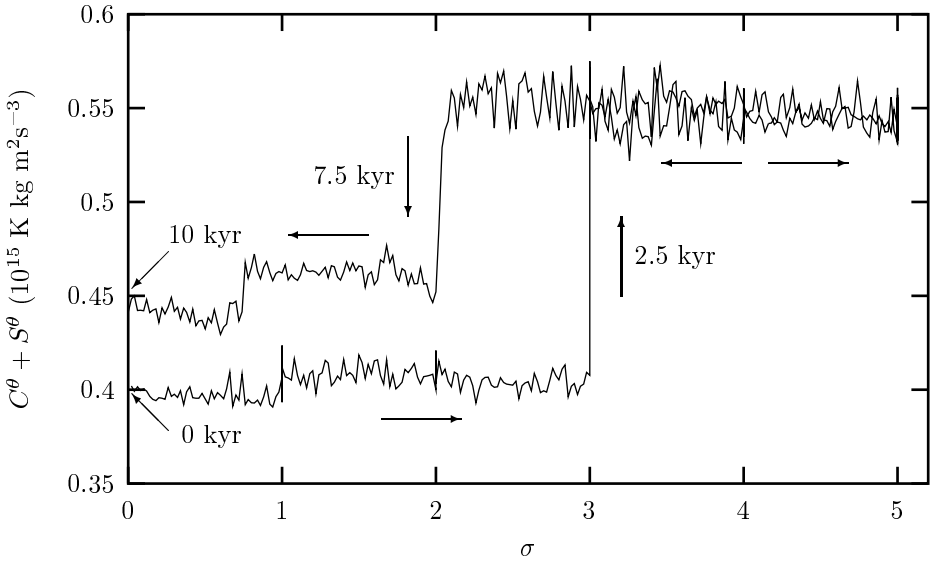

Figure 6.12: *Strength of the convective activity as a function of the source amplitude σ during the slow source experiment. Convective activity is measured by the upward convective heat transport, $C^\theta + S^\theta$ (Eq. (6.12)). In the text it is shown that $C^\theta + S^\theta$ represents the convective intensity better than C^θ alone. The jump to a higher level of convective activity at 2.5 kyr occurs at $\sigma = 3$, whereas the return to a lower level occurs at $\sigma = 2$, giving rise to a hysteresis loop. Note that the solution at 10 kyr displays a higher convective intensity than the solution at 0 kyr, despite the same source amplitude $\sigma = 0$. This indicates the coexistence of at least two equilibria under the same forcing conditions.*

However, the equilibria for $\sigma < 2$ differ only slightly in the spatial distributions of the convective areas, compared to the difference between the equilibria that coexist for $2 < \sigma < 3$ (see Fig. 6.11).

These multiple equilibria are probably an artefact of the convective adjustment procedure (Vellinga 1998), which is an ad-hoc representation of mesoscale convection that cannot be resolved by these models. As every gridpoint is searched for instabilities, and mixed if necessary, the procedure is a grid-scale process, giving rise to horizontal discontinuities in the thermohaline fields. Although it is likely that in the real ocean the distribution of convective areas is more or less stochastically determined as well, its discontinuous representation in ocean models is quite uncomfortable. Therefore, it is likely that this mechanism is not very robust, and that it depends on model details, like the exact formulation of the convective adjustment algorithm and the grid spacing.

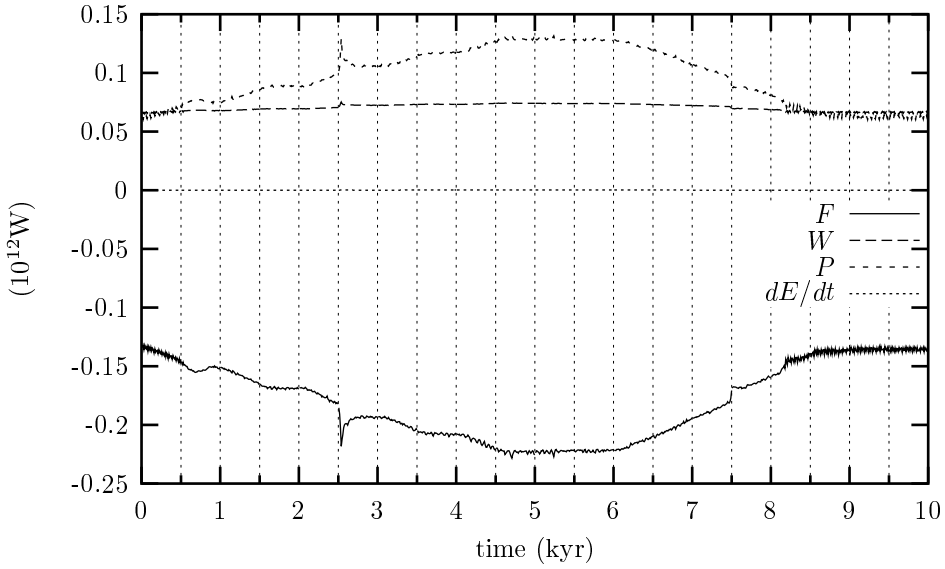

Figure 6.13: *The dominant terms in the kinetic energy equation, being viscous dissipation F, work done by wind stress W, and work done by pressure forces P. Time-rate of change of the kinetic energy dE/dt is several orders of magnitude smaller.*

6.3.4 Energy conversions

The basin-integrated kinetic energy of the horizontal flow E is defined as $< \frac{1}{2}\rho_0 \mathbf{u_h}^2 >$, where the brackets denote volume-integration over the (sub)basin under consideration. In the analyses below, the integrations are performed over the Atlantic and Arctic Oceans, bounded by 30°S and by the Bering Strait. The kinetic energy balance is given by (Holland 1975):

$$\frac{dE}{dt} = - < \mathbf{u_h} \cdot \nabla_h p > + < \mathbf{u_h} \cdot \tilde{\boldsymbol{\tau}} > + \rho_0 A_h < \mathbf{u_h} \cdot \nabla_h^2 \mathbf{u_h} >, \qquad (6.9)$$

featuring the work done by pressure forces (P), the work done by the wind stress (W), and the viscous dissipation (F) as the sources and sinks of kinetic energy.

In the Atlantic, dE/dt is several orders of magnitude smaller than the individual source and sink terms, so that W, P and F are permanently in balance. Figure 6.13 shows that at 0 kyr, the input of kinetic energy is equally divided between W and P. However, at 5 kyr the work done by the pressure forces is almost doubled, while the energy input by the wind stress is unchanged. This indicates that the work done by the pressure forces and the viscous dissipation respond strongly to the changes in the source amplitudes.

In fact, the strength of the overturning circulation appears to be linearly related to the pressure work (Fig. 6.14) and the viscous dissipation. This is contrary to the response in the 2D models, where the overturning strength is quadratically related to

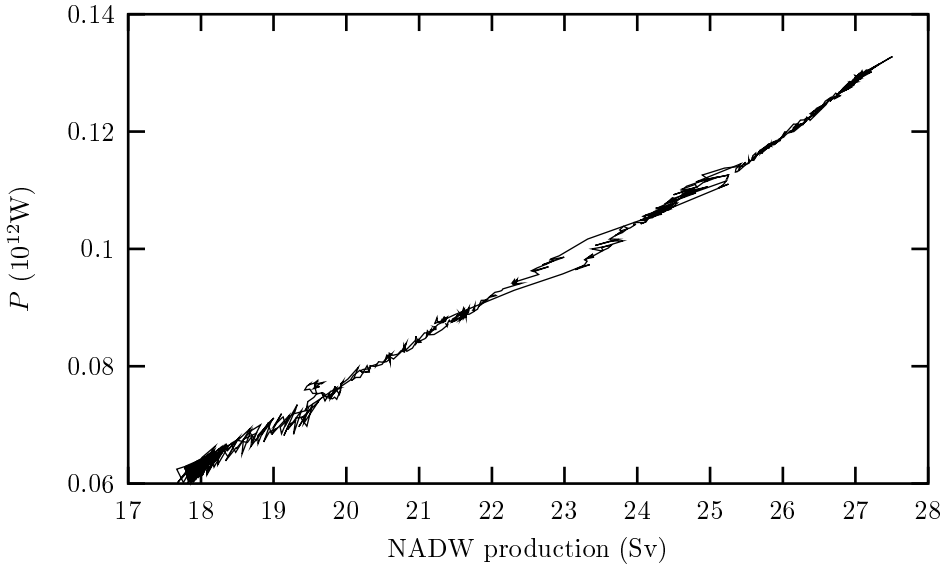

Figure 6.14: *Work done by pressure forces set out against the overturning strength.*

the dissipation and the buoyancy production. It may be that the the curve in Fig. 6.14 represents the flat part of a parabola, so that the relation *seems* linear, but is in fact quadratic. A run that surveys the regime of weak overturning strengths could solve this problem, but this is left for future study.

In Appendix 6.A it is shown that the work done by pressure forces is made up of several contributions:

$$\begin{aligned} - < \mathbf{u_h} \cdot \nabla_h p > = & - \rho_0 g \int \zeta w \; dA_S + \rho_0 g \int \zeta v \; dA_I - g < \rho' w > \\ & - g \int \rho' v z \; dA_I - g \int \rho'_z V z \; dA_I . \end{aligned} \tag{6.10}$$

Here, $\rho'(\mathbf{x})$ is the density anomaly with respect to the background profile $\overline{\rho}(z)$, and $V(x,z) = \int_{-H(x)}^{z} v(x,z')dz'$ is the volume transport between a level z and the bottom. The first two terms on the right-hand side of Eq. (6.10), say P_Z, concern the work done by the changes in the barotropic pressure field. The first component (P_{Z1}) is an integral over the ocean's surface A_S, and depends on the sea surface height and its vertical velocity: when, for instance, a positive sea-surface height anomaly is lowered, potential energy is released and converted into kinetic energy. The second term (P_{Z2}) is the integral over the zonal section at 30°S in the Atlantic (denoted by the area A_I) and measures the work done on the other basins by the barotropic pressure field of the Atlantic. The term $g < \rho' w >$ is the so-called buoyancy work (P_B), and measures the kinetic energy input by buoyancy forces. The last two terms measure the work done on the other basins by the buoyancy forces in the Atlantic. The fourth term

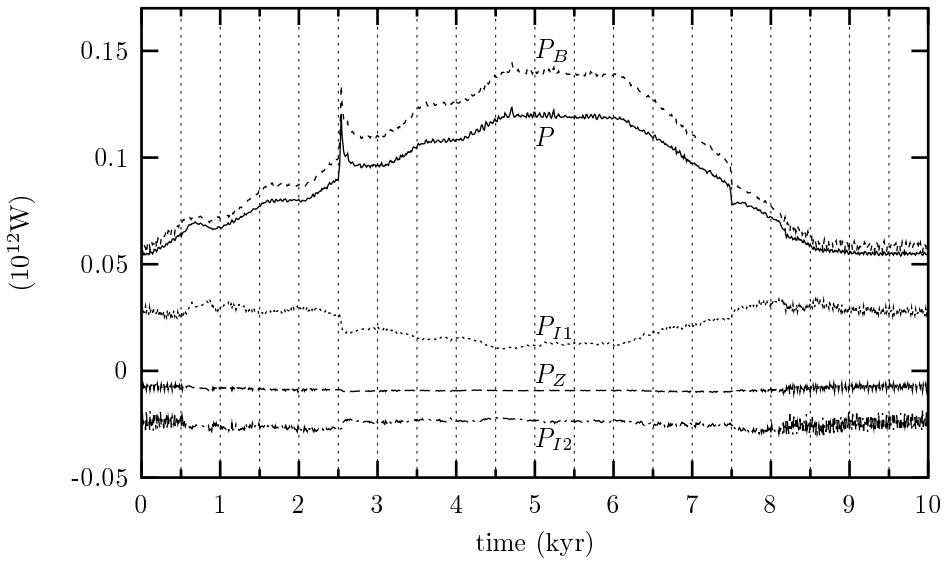

Figure 6.15: *Pressure work P and its contributions by the barotropic pressure field (P_Z), the buoyancy production (P_B), and the work done on the other basins by the buoyancy forces (P_{I1} and P_{I2}). The buoyancy production is the dominant contributor to the pressure work. The terms P_Z and and P_{I2} are almost constant throughout the experiment indicating that the changes in P are mainly caused by P_B and P_{I1}.*

(P_{I1}) is related to the exchange of potential energy, as is shown later, while the fifth term (P_{I2}) is related to the stratification of the (anomalous) density distribution.

Figure 6.15 shows that the buoyancy production P_B is the dominant contributor to the pressure work P. The contributions of the barotropic pressure field P_Z and the exchange terms P_{I1} and P_{I2} are relatively small, and only P_{I1} responds when the Agulhas source amplitudes are changed. This indicates that the kinetic energy required to increase the overturning strength is supplied mainly by the buoyancy forces within the Atlantic Ocean. The work done on or by the other basins is relatively unimportant, as is the work done by the barotropic pressure field.

The buoyancy work converts potential into kinetic energy, and also appears in the potential energy balance. The basin-integrated potential energy can be written as $U = g < \rho z >$. Again, the density field can be split into a background stratification $\overline{\rho}(z)$ and a deviation $\rho'(\mathbf{x})$. Since $\overline{\rho}(z)$ is determined mainly by the compressibility of sea water, and thus depends on the depth of a water parcel rather than on its thermohaline characteristics, it takes no part in the advective-diffusive transports of density. When it is furthermore assumed that the background stratification does not change, the time-rate of change of U can be written as (Holland 1975):

$$\frac{dU}{dt} = \quad g < \rho' w > + g \int \rho' v z \, dA_I + g < F^{\rho}_{D,z} > + g \int F^{\rho}_{D,y} z \, dA_I$$

$$+ g < zq^{\rho} > + g \int \rho \zeta F_{fr} \, dA_S + g \int \rho \zeta w \, dA_S + R. \tag{6.11}$$

Here it is assumed that density satisfies the same advection-diffusion equation (6.5) as potential temperature and salinity. The first term on the right-hand side of Eq. (6.11) is the buoyancy production term, equal to P_B in the kinetic energy balance of Eq. (6.10), but of opposite sign. It thus represents the conversion from potential to kinetic energy by buoyancy forces. The second term is the exchange of potential energy with the other basins via advection of density. This term is equal to the work done by the buoyancy forces within the Atlantic on the rest of the World Ocean, i.e., the term P_{I1} in Eq. (6.10). The third and fourth term denote the potential energy change due to vertical diffusion of heat and salt, or by diffusive exchange with the other oceans. These terms represent the input of external mechanical energy by processes like tidal dissipation, internal wave breaking or wind stress input (Huang 1998). The term $g < zq^{\rho} >$ indicates the sources of potential energy by the boundary conditions, by the convective adjustment procedure, and by the sources that are explicitly prescribed in this study. The sixth and seventh terms cancel in steady state, when $w = -F_{fr}$ in Eq. (6.3). These terms represent the potential energy input by the surface freshwater flux, and the conversion of this potential energy into kinetic energy. This conversion term appeared as P_{Z1} in Eq. (6.10). Terms arising from the non-linearity of the equation of state are not explicitly calculated and are denoted by R.

Thermal and saline contributions to the potential energy can be defined as $U^{\theta} = \rho_0 g < z\theta >$ and $U^S = \rho_0 g < zS >$, and their time-rates of change are analogously:

$$\frac{d}{dt} U^{(\theta,S)} = A^{(\theta,S)} + D^{(\theta,S)} + C^{(\theta,S)} + S^{(\theta,S)} + B^{(\theta,S)} \tag{6.12}$$

where:

$$A^{(\theta,S)} = \rho_0 g < (\theta, S) w > + \rho_0 g \int (\theta, S) \; v \; z \; dA_I \tag{6.13a}$$

$$D^{(\theta,S)} = \rho_0 g < F_{D,z}^{(\theta,S)} > + \rho_0 g \int F_{D,y}^{(\theta,S)} z \, dA_I \tag{6.13b}$$

$$C^{(\theta,S)} = \rho_0 g < z q_{convection}^{(\theta,S)} > \tag{6.13c}$$

$$S^{(\theta,S)} = \rho_0 g < z q_{source}^{(\theta,S)} > \tag{6.13d}$$

$$B^{\theta} = \rho_0 g < z q_{boundary}^{\theta} >, B^S = 0. \tag{6.13e}$$

Figure 6.16 shows the evolution of the dominant sources and sinks of potential energy. It turns out that diffusion D is the largest source of potential energy. This is obviously caused by the thermal contribution (Fig. 6.17), as the downward salt diffusion (Fig. 6.18) counteracts this tendency. It is possible that the significant doming is related to the strong decrease in saline diffusion between 2.5 and 7.5 kyr. The diffusion is strongly counteracted by the advective terms A, and the contribution of convective adjustment C. The direct contribution of the source, S, is very small with respect to the other terms, as the contributions of the heat and salt sources almost cancel with respect to density.

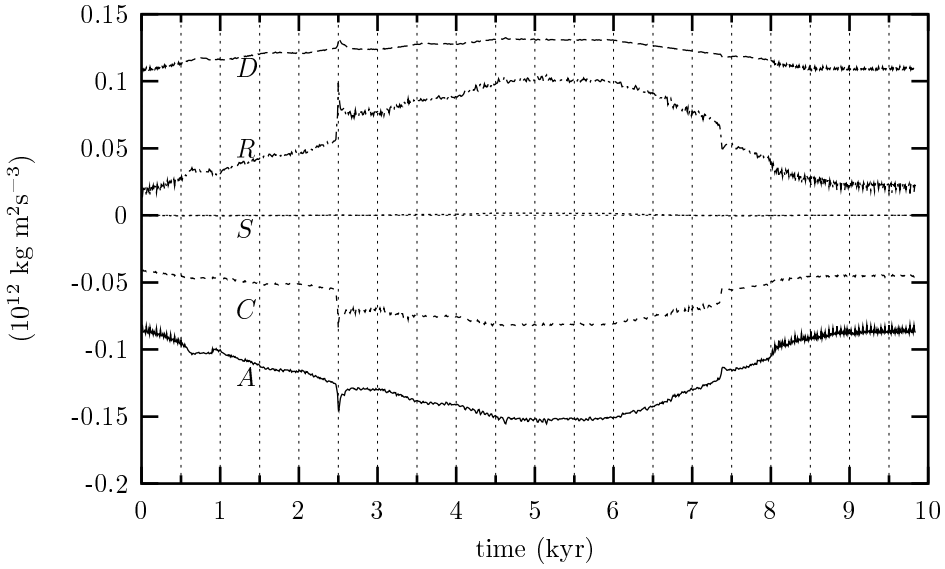

Figure 6.16: *The dominant terms in the potential energy balance of the Atlantic (Eq. (6.11)). Shown are the advective contributions* ($A = g < \rho' w > + g \int \rho' v z \, dA_I$)*, the diffusive contributions* ($D = g < F^{\rho}_{D,z} > + g \int F^{\rho}_{D,y} z \, dA_I$)*, the convective contribution* ($C = g < z q^{\rho}_{convection} >$)*, and the source contribution* ($S = g < z q^{\rho}_{source} >$)*. The term R denotes the residual contributions, and is simply* $-(A + D + C + S)$*, since* $dU/dt \approx 0$.

A striking feature in Fig. 6.16 is the residual term R, resulting from the non-linearity of the equation of state. Its contribution is significant and indicates that the potential energy balance cannot be closed by the obvious advection/diffusion processes alone. Indeed, attempts to close the density budget also failed. Two examples may serve as an illustration of the problems arising from these non-linearities. Due to the non-linear dependency of density on temperature and salinity, the thermal and saline expansivities α and β are not constant. This may result in a net mass flux across a section that has zero net heat and salt fluxes. The surface heat flux, for instance, acts as a continuous sink of mass, since the heat gain takes place mainly in the low latitudes where α is large, whereas the heat loss takes place in high latitudes where α is small. In Appendix 6.B it is shown how the pressure-dependence obscures a transparant analysis of the potential energy balance, as well. It turns out that the convective adjustment procedure is a source of density, despite the fact that it is strictly heat and salt conserving. This net density source is the main contributor to C in Fig. 6.16. Net mass fluxes and sources like these must consequently be accompanied by internal mass sources and sinks, and terms like these are not easily determined.

Although the buoyancy production seems to capture the transfer of potential energy to kinetic energy succesfully in this model, we cannot explain the response of A

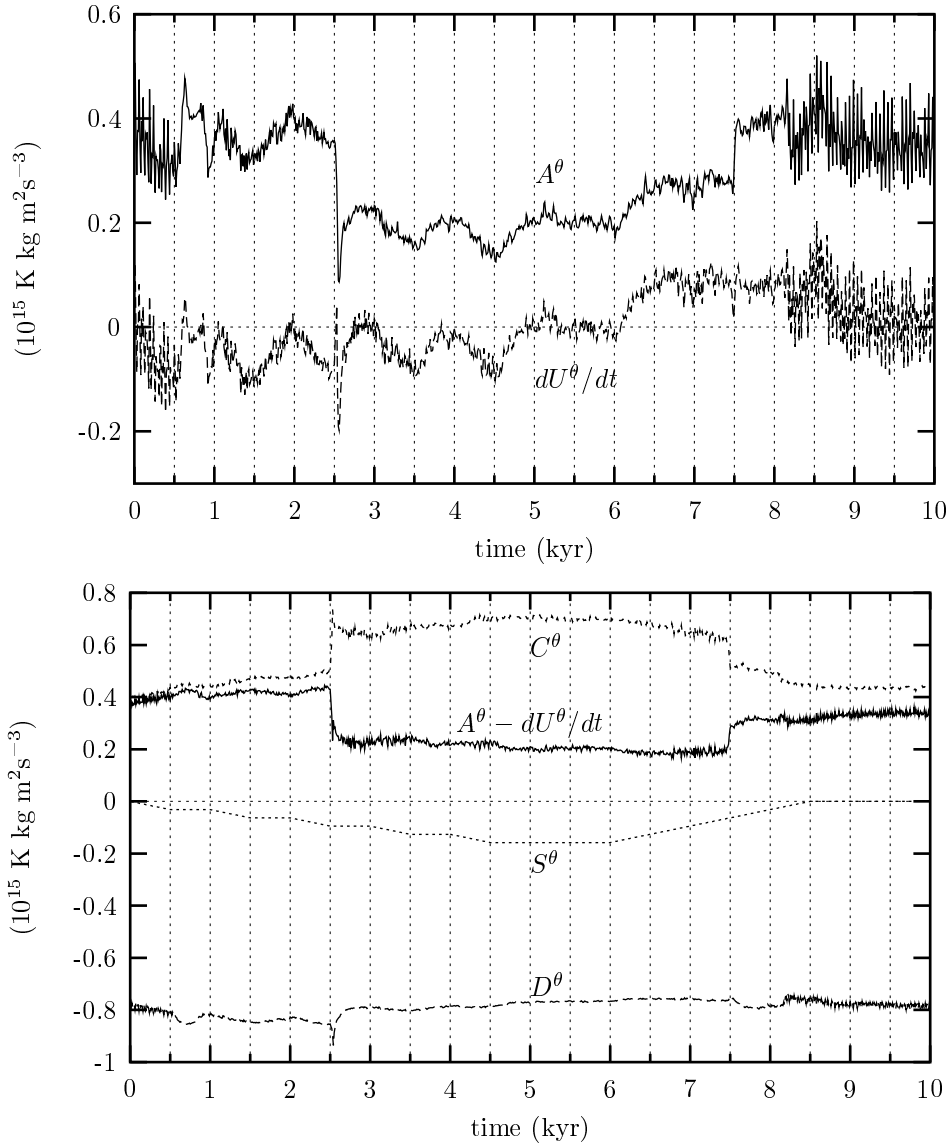

Figure 6.17: *The thermal contribution to the potential energy balance of the Atlantic, according to Eq. (6.12). The upper panel shows that fluctuations in the advective contributions* A^θ $(= \rho_0 g < \theta w > + \rho_0 g \int \theta v z \; dA_I)$ *are largely unbalanced, and are reflected by the fluctuations in the time-derivative* dU^θ/dt*. The lower panel shows the balanced component of the advection* $(A^\theta - dU^\theta/dt)$*, the diffusive contributions* D^θ $(= \rho_0 g < F^\theta_{D,z} > + \rho_0 g \int F^\theta_{D,y} z \; dA_I)$*, the convective contribution* C^θ $(= \rho_0 g < z q^\theta_{convection} >)$ *and the source contribution* S^θ $(= \rho_0 g < z q^\theta_{source} >)$*. The contribution* B^θ *of the surface heat flux is neglegibly small, and is not included.*

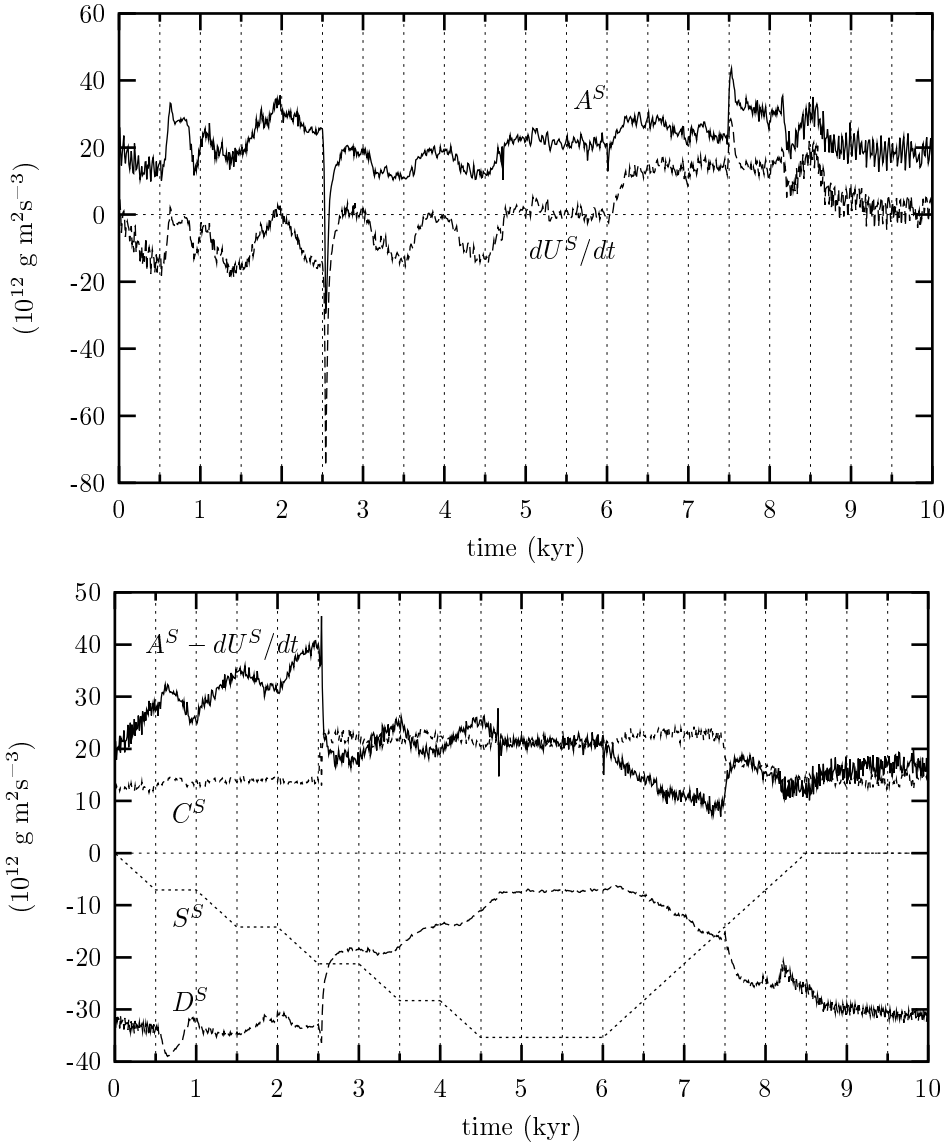

Figure 6.18: *The saline contribution to the potential energy balance of the Atlantic, according to Eq. (6.12). The upper panel shows that fluctuations in the advective contributions ($A^S = \rho_0 g < Sw > -\rho_0 g \int Svz\ dA_I$) are largely unbalanced, and are reflected by the fluctuations in the time-derivative dU^S/dt. The lower panel shows the 'balanced' component of the advection ($A^S - dU^S/dt$), the diffusive contributions ($D^S = \rho_0 g < F^S_{D,z} > + \rho_0 g \int F^S_{D,y} z\ dA_I$), the convective contribution ($C^S = \rho_0 g < zq^S_{convection} >$), and the source contribution ($S^S = \rho_0 g < zq^S_{source} >$).*

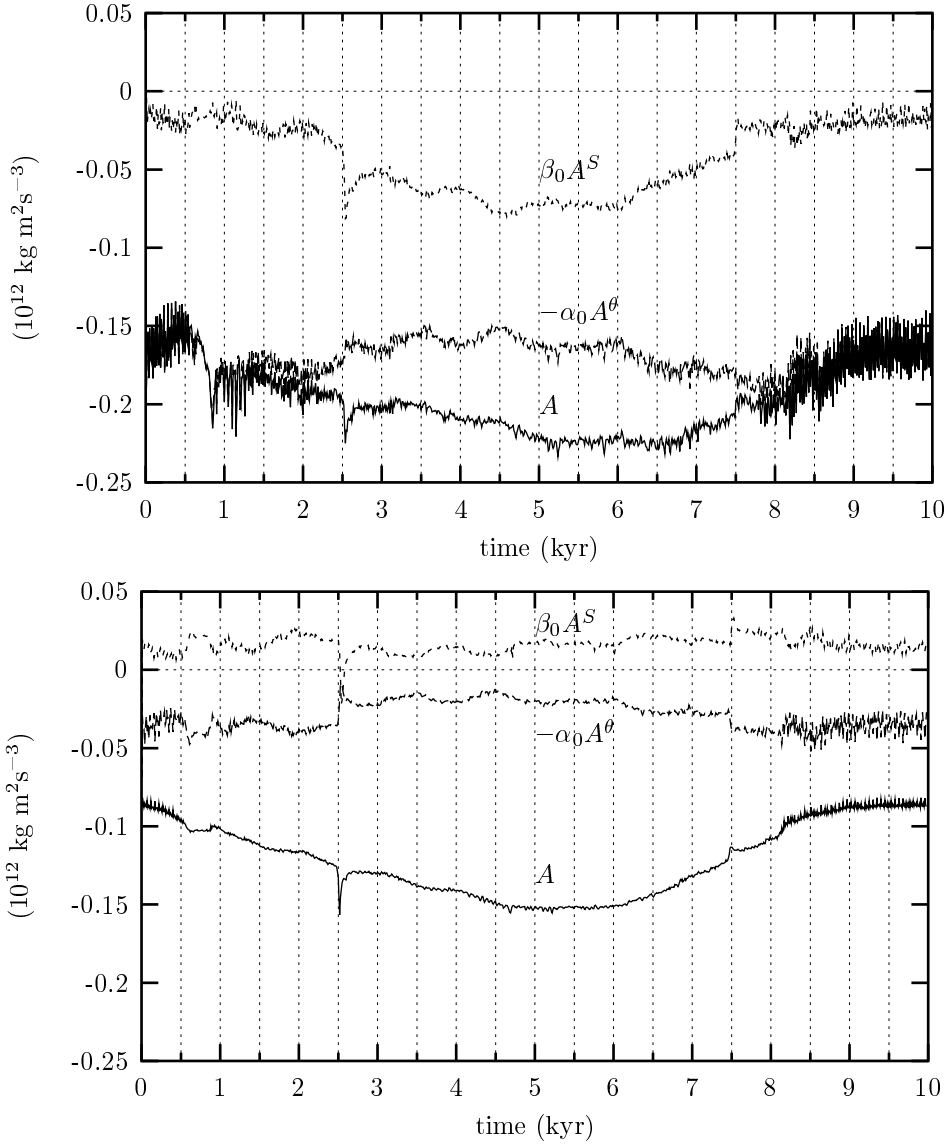

Figure 6.19: *Advective terms for the World Ocean (upper panel) and for the Atlantic (lower panel). The upper panel shows that the buoyancy production ($A = g < \rho' w >$) is closely linked to its thermal ($A^\theta = \rho_0 g < \theta w >$) and saline ($A^S = \rho_0 g < Sw >$) equivalents, via the thermal and saline expansivities (here taken as $\alpha_0 = 1.0 \cdot 10^{-4}$ and $\beta_0 = 7.6 \cdot 10^{-4}$). The lower panel shows that this relation is obscured when the Atlantic is considered only, and interocean fluxes must be taken into account ($A = g < \rho' w > + g \int \rho' v z \, dA_I$, and A^θ and A^S according to Eq. (6.13a)).*

(in Fig. 6.16) by considering its relation with the other terms in the potential energy balance. However, since density transports are in general generated by transports of heat and salt, it may be expected that the buoyancy production is closely linked to its thermal and saline equivalents, via the thermal and saline expansivities. Figure 6.19 shows that this holds when the buoyancy production in the whole World Ocean is considered. However, the comparison between A ($= g < \rho' w > + g \int \rho' vz \; dA_I$), and A^θ and A^S in Eq. (6.13a) breaks up when the Atlantic is considered, and lateral interocean fluxes must be taken into account. This mismatch may be partly caused by the fact that the background stratification $\overline{\rho}$ not only contains the effect of the pressure dependence, but of the background thermal (and saline) stratification as well. Indeed, the relation between $g < \rho' w >$ and $\rho_0 g < \theta' w >$ and $\rho_0 g < S' w >$, with θ' and S' being anomalies with respect to the (global) background temperature and salinity profiles, is much more convincing (not shown).

In summary, the response of the Atlantic overturning circulation to changes in the source amplitudes is reflected by changes in the kinetic energy balance of the Atlantic: an increase in the viscous dissipation of kinetic energy, resulting from an enhanced overturning circulation, is balanced by an increase in the pressure work. The most important component of this pressure work is the so-called buoyancy production. This is the work done by (internal) buoyancy forces, and converts potential into kinetic energy. In other words, the kinetic energy that is needed to enhance the overturning strength is generated by buoyancy forces within the Atlantic, at the expense of potential energy; the work done by buoyancy forces outside the Atlantic, or by the barotropic pressure field, are relatively small.

6.4 Fast source modification

The strategy of the slow source experiment was to increase the South Atlantic sources very smoothly, in order to avoid large disturbances of the equilibrium. And since the heat and salt sources almost balanced with respect to their effect on density, density anomalies could only develop due to the fact that mixed boundary conditions impose different damping time scales on heat and salt anomalies. Although several interesting relations could be deduced, it gave no clue on how the balances are established, and what the corresponding time scales are. To study this process of adjustment in detail, two switch-on experiments are performed. In these experiments the South Atlantic sources are applied suddenly at full strength, rather than gradually increasing their amplitudes. To avoid destabilisation of the density stratification in the source area, the source configurations are chosen such that they represent negative or neutral density input into the Atlantic. This protects the deeper layers from spurious ventilation, allowing only the shallower layers to be affected by the heat and salt sources.

Both experiments are started from the solution of the slow source experiment at 2 kyr, where both the heat and salt sources have an amplitude of 2. Although the flow may not have reached a perfect thermohaline equilibrium during the preceding 500 years in which the source amplitudes was constant, we assume that the equilibrium is sufficiently restored to justify its use as starting point for the adjustment

experiments of this section. However, this solution still displays an oscillation that obscures the signal of the adjustment processes. To reduce the influence of this oscillation, the two runs are compared with a reference run in which the source amplitudes are not changed. The response in the adjustment experiments appears to modify the frequency of this oscillation, causing a phase-shift between the oscillation in the adjustment runs and in the reference run. In the first 100 years of the runs, the oscillation is sufficiently suppressed to allow for studying the adjustment processes.

In the first experiment only the salinity field is perturbed by suddenly reducing the salt source amplitude from 2 to 1. This is equivalent to applying an instantaneous source of freshwater. In the second experiment a sudden heat and salt source is applied by increasing the amplitudes of both the heat and salt sources from 2 to 3.

6.4.1 Dispersion of the perturbation

Figure 6.20 shows the dispersion of the freshwater anomalies that are created in the source region in the freshwater source experiment. Once created in the source region, the freshwater anomaly is picked up by the (model-equivalent of the) North Brazil Current, and enters the interior of the North Atlantic through the Gulf Stream and the North Atlantic Current. It takes about 30 years for the freshwater anomaly to reach the northern part of the North Atlantic. This is in agreement with the advective time-scale, since it takes about 30 years to advect an anomaly over a distance of 10^7m by a velocity of 10^{-2}m s^{-1}, which is characteristic for the wind-driven gyres.

Figure 6.21 shows that a density anomaly reaches the North Atlantic much faster. In the first year the density anomaly develops in the South Atlantic, and reaches the Brazilian coast in the second year. In the third year the density anomaly crosses the Atlantic, and propagates poleward in both the North and South Atlantic Oceans. In this year, it travels as far as the latitudes of 35°N and 35°S, propagating with a speed of more than 0.12 m/s. In the subsequent years the propagation slows down to about 0.05 m/s at the higher latitudes, and the disturbance reaches the northern North Atlantic in year 6. On its way poleward, the density disturbance radiates Rossby wave-like features into the interior of the basins.

The wave-like propagation of density anomalies resembles the adjustment process described by Hirschi et al. (1999), who applied a freshwater perturbation at 72.5°S in a rectangular-basin model of the Atlantic. In their model, it takes 10 years for the density anomaly to reach 30°S (travelling along the western side of the basin), whereas it reaches 30°S and 30°N on the eastern side of the basin in the single year that follows. North of 30°N the propagation slows down again. As in Hirschi et al. (1999), the signal in Fig. 6.21 shares characteristics with baroclinic Kelvin waves (e.g., Gill 1982; Hsieh et al. 1983; Wajsowicz and Gill 1986; Döscher et al. 1994): it causes vertical displacement of isopycnals and propagates with the coastal boundary on the right (left) in the northern (southern) hemisphere. The slower wave propagation at higher latitudes reflects the fact that the stratification weakens towards higher latitudes (Levitus 1982; Hirschi et al. 1999), thus reducing the phase speed of internal gravity waves.

However, Gill (1982, p. 379) estimated that in the ocean the phase-velocity of this

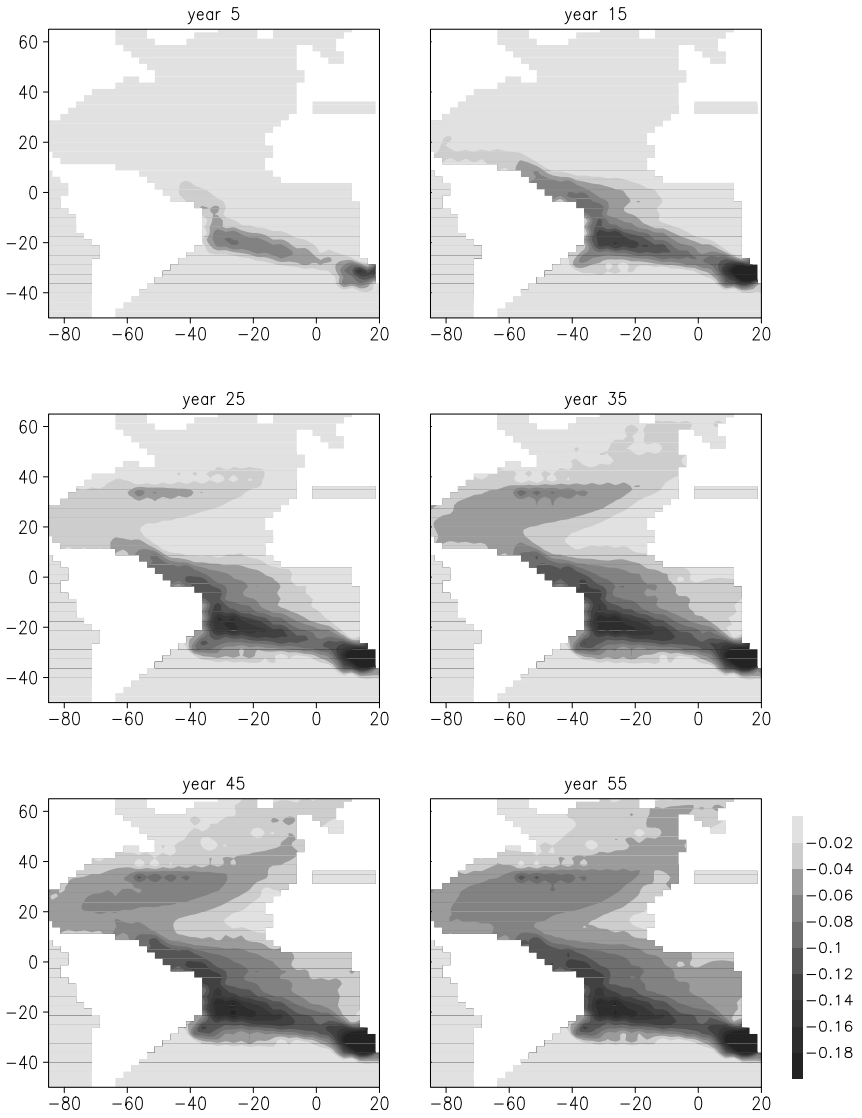

Figure 6.20: *Six snapshots of the annually averaged salinity anomaly ($\Delta S = S_{source} - S_{main}$ in psu) at 250 m depth in the freshwater source experiment. The freshwater source, turned on in year 1, creates a negative salinity anomaly that is slowly advected northward along the east coast of the American continents. It reaches the northern North Atlantic within 30 years.*

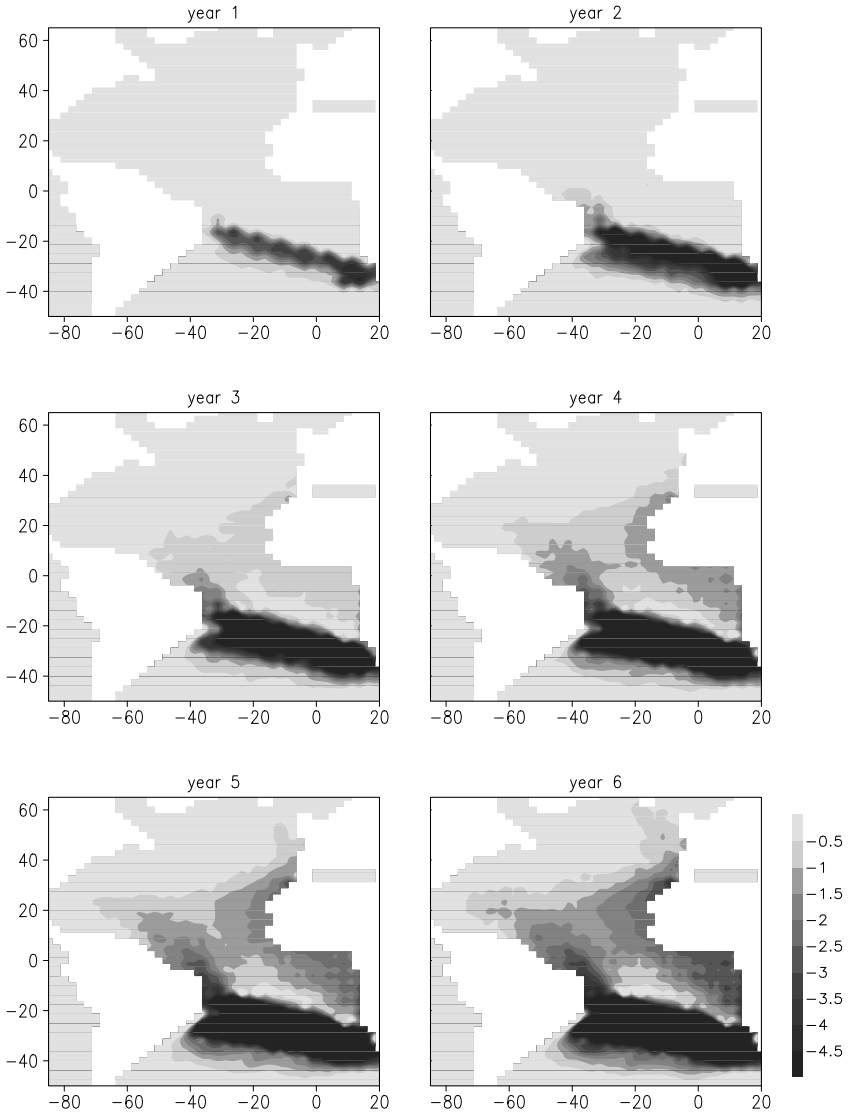

Figure 6.21: *Six snapshots of the annually averaged density anomaly ($\Delta\rho = \rho_{source} - \rho_{main}$ in $10^{-3} kg\ m^{-3}$) at 450 m depth in the freshwater source experiment. The freshwater source, turned on in year 1, generates a negative density anomaly that radiates a wave-like signal. This signal reaches the equator already in year 2, and crosses the Atlantic via the equatorial wave guide between year 2 and 3. From there, the signal propagates rapidly north and southward, with the continent on the right, respectively left. This behaviour is characteristic for (the numerical equivalents of) Kelvin waves. The resulting coast-bound anomalies radiate westward into the interior of the Atlantic.*

kind of waves is in the order of 3 m/s at mid-latitudes. This estimate is at least one order of magnitude higher than the propagation speeds found here. The most probable reason for the slow wave propagation is the bad numerical representation of these waves. Hsieh et al. (1983) argued that baroclinic Kelvin waves are badly represented in low-resolution numerical models. This is due to the large horizontal viscosity in these models, and to the fact that the resolution is in general insufficient to resolve these features. They furthermore showed that the numerical representation of these waves, and thus their phase velocity, depends on the discretisation scheme that is used. For both B- and C-grids they derive analytical expressions for the phase velocity as function of the grid-spacing and lateral viscosity. For both grids, the phase speed decreases up to an order of magnitude (with respect to the phase velocity in the continuous system) when lateral viscosity becomes important. When the spatial resolution decreases, the phase velocity in the B-grid is reduced even further, whereas it approaches the value of the continuous system in the C-grid. Unfortunately, wave propagation on E-grids was not explicitly addressed by Hsieh et al. (1983). Nevertheless, a similar slowing effect of viscosity on the propagation speed may be expected. If we assume that in our model the wave propagation is an order of magnitude too small, than the density anomaly would reach the northern North Atlantic within a year.

6.4.2 Overturning response

Figure 6.22 (upper panel) shows the response of the NADW production and NADW outflow across 30°S upon introducing the freshwater source in the South Atlantic. Clearly, there is an immediate and steady decrease in the NADW outflow. The NADW production, on the other hand, increases initially, and starts to decrease only after about 25 years. At this time, the meridional pressure difference in the upper 1500 m has changes sign, as well (Fig. 6.22, lower panel).

The evolution of the anomalous overturning streamfunction (Fig. 6.23) shows that the freshwater source initially generates a convergence at depth, since it lowers the hydrostatic pressure. This convergence raises the sea level and increases the associated barotropic component of the pressure, forcing a divergence at shallower levels. This explains both the reduced southward export of NADW and the initial increase in the overturning strength. In the course of time, the fresh anomaly disperses northward (Fig. 6.20) and a density anomaly builds up in the northern part of the basin. This weakens the anomalous baroclinic pressure gradient, and the enhancement of the overturning circulation disappears. Why the overturning circulation starts to decrease in strength while the anomalous density gradient in the upper layers is reduced is not completely clear at this moment. When the fresh anomaly has reached the northern North Atlantic, there is a slight reduction in the convective activity, but it is not clear whether this reduces the pressure gradient at depth enough to explain the reduction in the overturning strength. Alternatively, the anomalous deep inflow across 30°S and the anomalous upwelling in the source area result in a cooling of the subsurface subtropical South Atlantic. This reduces the meridional pressure gradient at depth, and may explain the reduction of the overturning circulation. However, the most

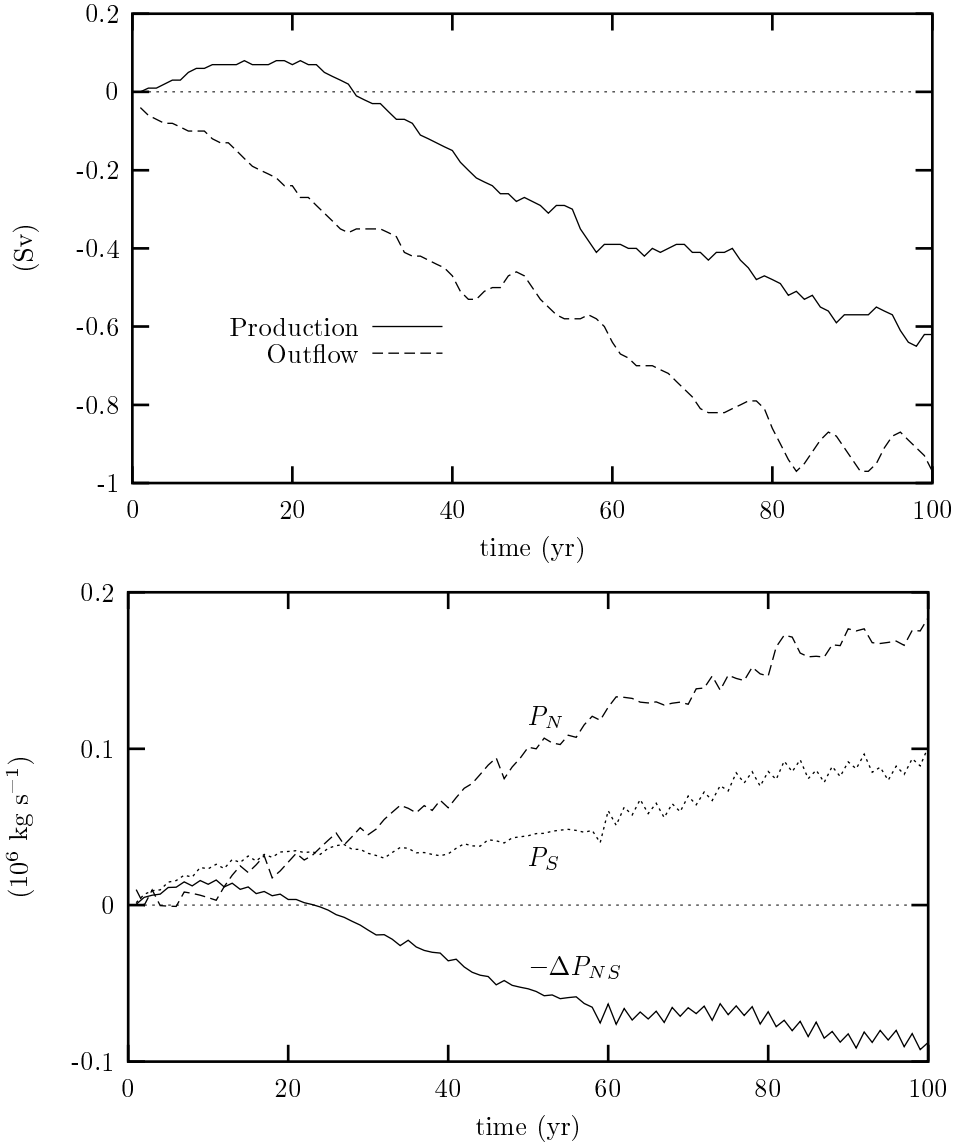

Figure 6.22: *Upper panel: Anomalous NADW formation and NADW outflow across 30°S (with respect to the reference run) in the first adjustment experiment. In this experiment a freshwater source is switched on in the South Atlantic in year 1. Lower panel: Evolution of the (negative) meridional pressure difference (-ΔP_{NS}) and the vertically integrated pressure in the north ($P_N = P(53°N)$) and in the south ($P_S = P(15°S)$). Note that the latitude of P_S is chosen north of the anomalous upwelling region at 25°S (Fig. 6.23).*

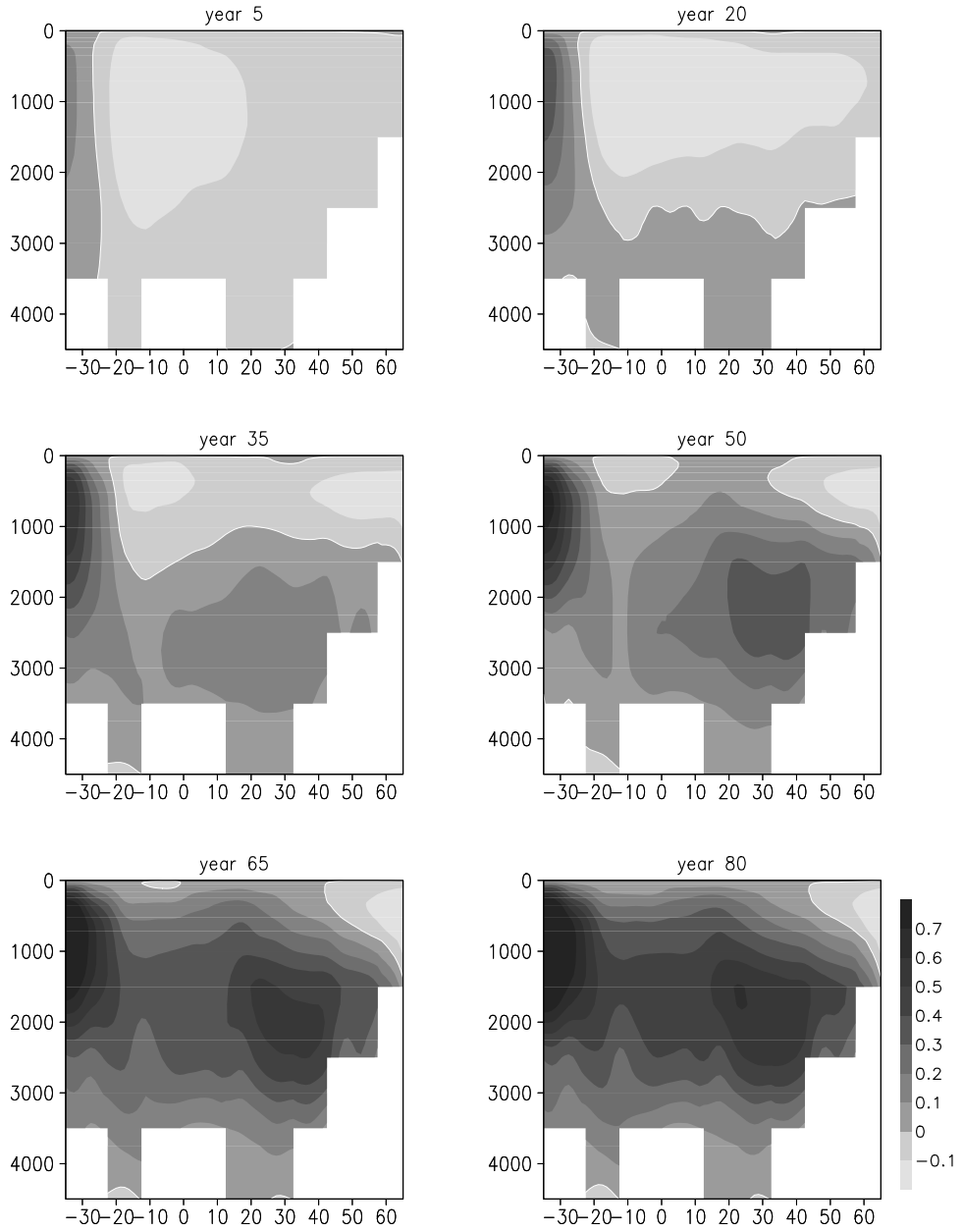

Figure 6.23: *Six snapshots of the streamfunction anomaly (with respect to the reference run) for the freshwater source experiment. A positive anomaly denotes anomalous anti-clockwise circulation.*

probable explanation for the steady reduction in the overturning strength and NADW outflow is that the freshwater anomaly reduces the density difference between the outflowing NADW and the deep waters in the ACC. This would emphasize the global character of the thermohaline circulation, and the importance of Atlantic/Southern Ocean interocean exchange in driving the Atlantic overturning circulation. A detailed investigation of this interaction must be left for future study.

The North Atlantic overturning circulation responds within two years to density disturbances in the South Atlantic (Fig. 6.22, upper panel). According to Fig. 6.20, it takes between 20 and 30 years for a disturbance to reach the North Atlantic by advection. Baroclinic Kelvin waves take 5 or 6 years to reach the northern North Atlantic in this model (Fig. 6.21). The signal generated in the South Atlantic must have reached the North Atlantic through (the numerical equivalents of) barotropic Kelvin waves, since no other mechanism is able to cross the whole Atlantic in less than two years.

In the heat and salt source experiment, the response of the NADW production and outflow rate (Fig. 6.24) differs markedly from that of the freshwater source experiment. Now the change in the NADW production leads the change in the outflow by more than a decade. The difference between the response of the circulation to application of the freshwater source and the combined heat and salt sources is mainly caused by a different evolution of the anomalous density field (Fig. 6.25). In the freshwater source experiment, the largest density anomaly develops in the South Atlantic. It is attenuated on its way north, although the meridional density gradient reduces considerably in the course of time. In the heat and salt source experiment, on the other hand, the density anomaly develops in the north. In the source area, the thermal and saline anomalies almost cancel with respect to their effect on density, and no density anomaly is generated in the first stages of the experiment. When the anomalies are advected northward, the thermal anomaly is removed by air-sea fluxes, and the density anomaly is amplified. Indeed, a meridional pressure gradient develops on the advective time scale of about 25 years (Fig. 6.24, lower panel), and the strength of the overturning circulation is increased accordingly. As in the slow source experiment, the relation between the anomalous overturning and the meridional pressure difference is linear (Fig. 6.26).

6.5 Summary and discussion

6.5.1 Summary

In this chapter it has been studied how Agulhas Leakage influences the strength of the Atlantic overturning circulation. To this end, experiments were performed with the low-resolution OGCM LSG. Since this model does not resolve Agulhas Leakage, its heat and salt exchange were parametrised by sources of heat and salt in the South Atlantic Ocean. The model's overturning circulation turned out to be very sensitive to these sources of heat and salt. Part of the response is linear and related to changes in the north-south pressure difference. There was also a non-linear response, when the overturning suddely increases in response to abrupt changes in the convective

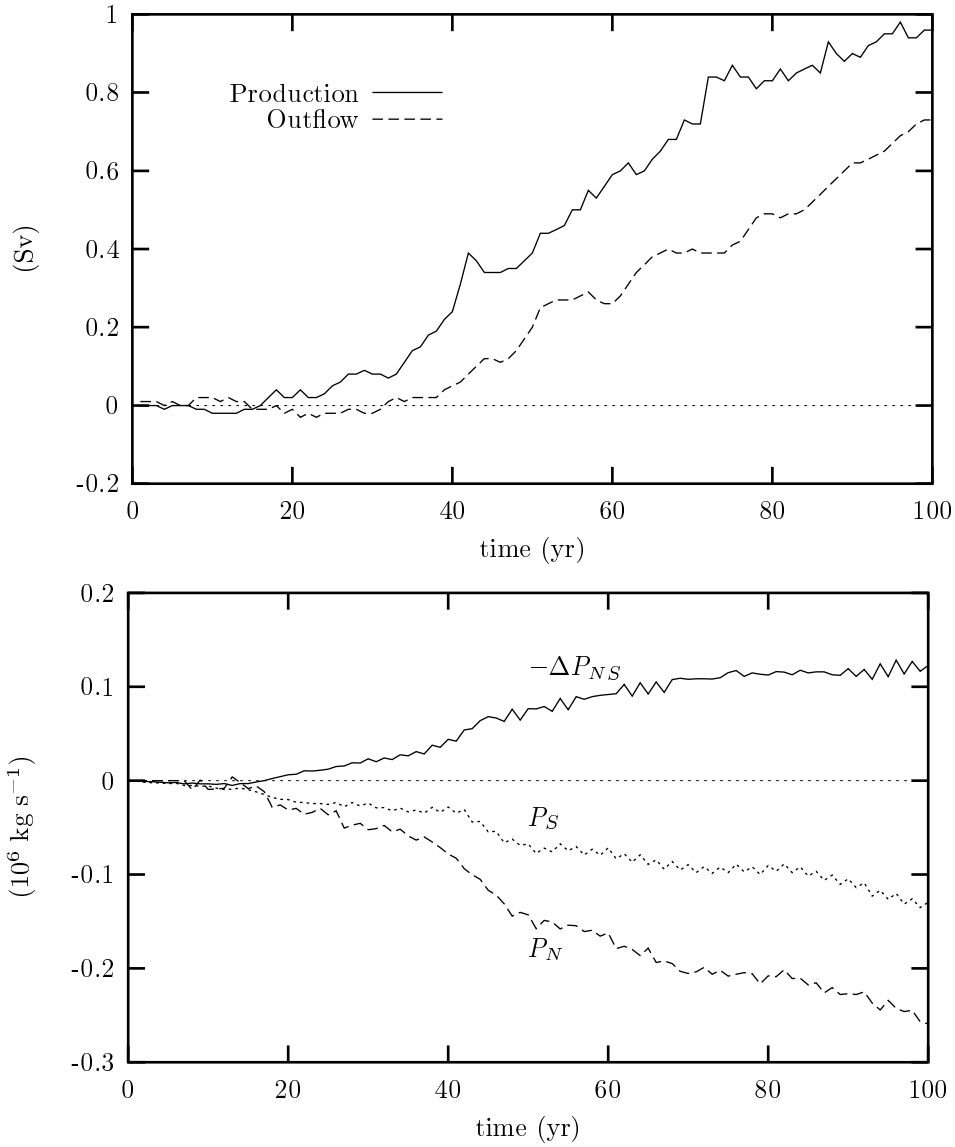

Figure 6.24: *Same as Fig. 6.22, but now for the experiment in which a heat and salt source is switched on in the South Atlantic in year 1.*

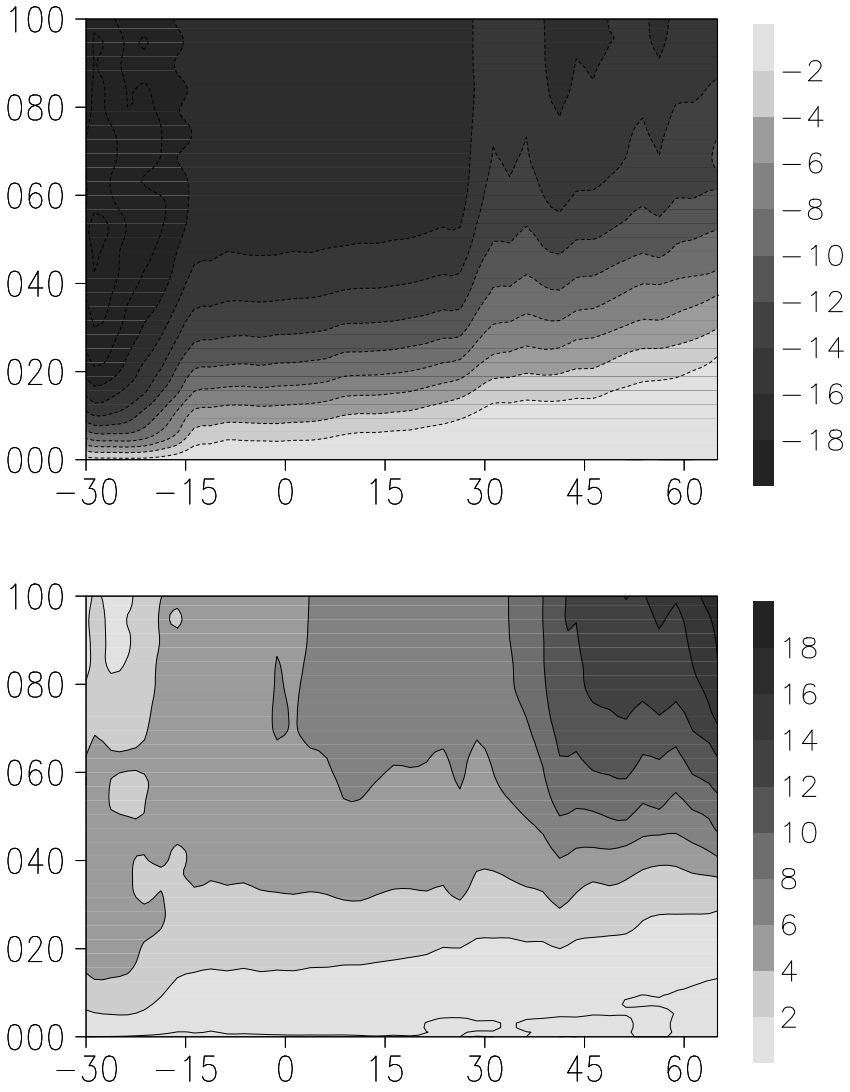

Figure 6.25: *Density anomaly (in $10^{-3}kg\ m^{-3}$), zonally averaged over the Atlantic and over the upper 1000 m, as function of time (vertical axis) and latitude. The upper panel concerns the freshwater source experiment, showing that the maximum anomaly develops in the source area, and decreases northward. The lower panel shows the heat and salt source experiment, where the density anomaly increases northward, when the thermal anomaly is attenuated by atmospheric heat loss, while the salt anomaly retains its strength.*

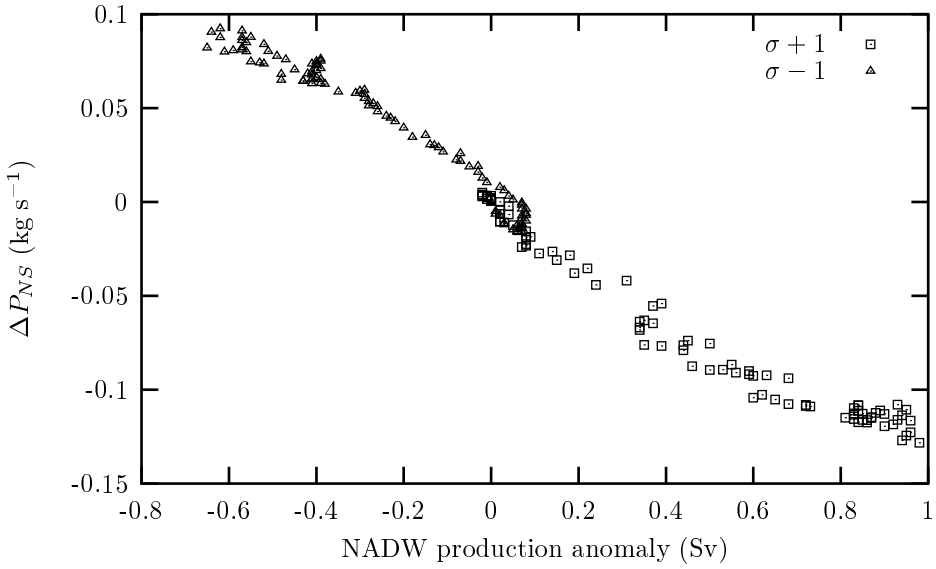

Figure 6.26: *ΔP_{NS} set out against the NADW production rate anomalies for both the freshwater source experiment ($\Delta\sigma = -1$) and the heat and salt source experiment ($\Delta\sigma = +1$). The linear relation between the meridional pressure gradient and the overturning strength, as found in the slow source experiment (Fig. 6.7), holds for the adjustment experiments as well.*

activity in the northern North Atlantic. Two additional experiments illustrated the adjustment of the overturning circulation upon sudden introduction of heat and salt sources in the South Atlantic. The north Atlantic overturning circulation responded within a few years after the sources were switched on, due to barotropic and baroclinic waves reaching the northern North Atlantic. The advection of the anomalies took 3 decades to reach the northern North Atlantic. However, it is likely that the response time scales found in this model are not robust with respect to the numerical model that is used. Hsieh et al. (1983) have shown that the bad numerical representation of especially baroclinic Kelvin waves in low-resolution models may retard their propagation speed by an order of magnitude.

6.5.2 Response of the overturning circulation

Our results suggest that the physical mechanism proposed by Gordon et al. (1992) is not responsible for the linear part of the response of the overturning strength to Agulhas Leakage. In their hypothesis, Agulhas salt input would precondition the Atlantic thermocline waters for deep convection, and thereby stimulate the production rate of NADW. In our experiments, however, there is no gradual increase in convective activity when the amplitude of the Agulhas sources is increased. Moreover, the ad-

justment experiments show that the overturning strength is related to the large-scale meridional difference in sea-surface height (i.e., the barotropic pressure field), with the overturning circulation responding before a thermohaline anomaly has reached the convective areas.

Although changes in convective activity may not be responsible for the linear increase in overturning strength, they do play a role in the non-linear changes. Sudden changes in the overturning strength coincided with a sudden intensification of the convective activity, and a westward expansion of the convective centers. This behaviour points to a scenario in which the original equilibrium becomes unstable, and the solution attains another equilibrium. Hysteresis behaviour of the convective activity occurred with respect to the source strength parameter σ. However, with the switches occurring at an overturning strength of 23 Sv in both the upgoing and the downgoing branches of the experiment, it is not clear whether they have been triggered by an advective feedback, related to an increasing overturning advecting more salt, or by the North Atlantic salinity exceeding a certain threshold. The latter would support the hypothesis of Gordon et al. (1992). This could be tested if the Atlantic overturning strength could be increased to the critical value of 23 Sv without the help of the Agulhas sources. This is left for future study.

Since the multiple equilibria are characterised by different convective areas and hence differ on grid scale (Lenderink and Haarsma 1994), it is unlikely that details of these shifts in equilibria are robust with respect to grid-size, surface forcing, convective adjustment algorithm, etc. (Vellinga 1998). However, it is likely that such shifts do occur in the real ocean. It has, for instance, been observed that during the 90's the convective intensity in the Labrador Sea strongly increased (Dickson et al. 1996; Marshall and Schott 1999).

The 2D models that were applied in Chapters 4 and 5 featured a quadratic relation between the buoyancy work and the overturning strength (ψ_{max}). This relation arose from the balance between buoyancy production and viscous dissipation of kinetic energy (D). With the circulation being confined to the meridional plane, the relation $\psi_{max} \propto D^{1/2}$ followed from a simple scaling argument (Dijkstra and Molemaker 1997). In 3D thermohaline flow, the relation between viscous dissipation and the meridional overturning strength is more complex. Nevertheless, Te Raa and Dijkstra (1999) found the same quadratic relation between buoyancy work and overturning strength in a 3D model simulating thermohaline and wind-driven flow in a single-hemispheric ocean basin. Evidently, changes in the buoyancy work in their model were mainly applied to drive the meridional overturning circulation. Surprisingly, the relation between viscous dissipation and the overturning strength was found to be linear in this model (Fig. 6.14). It may be that the flow was studied in a regime where the presumed parabolic relation is almost linear. Exploring the behaviour of the model for negative values of σ, i.e., by applying heat and salt sinks instead of sources, might reconcile this question, but this is left for future study. Anyhow, this unexpected linear relation yields the overturning strength to be linearly related to the buoyancy work, rather than quadratically as in the 2D case.

Analysis of the kinetic energy balance of the Atlantic showed that the buoyancy work provides the kinetic energy that is needed to change the overturning strength

during the main experiment. We have not been able to determine whether the changes in the buoyancy work *forced* the changes in the overturning strength, as turned out to be the case in the 2D model studies. The non-linear equation of state hindered a transparant analysis of the density balance of the Atlantic, and the potential energy balance could not be closed by considering the conventional transport processes only.

The experiments have shown a clear linear relation between the overturning strength and the meridional pressure gradient. This points to a scenario where the Agulhas heat and salt sources modify the overturning circulation by influencing the meridional pressure gradients. A linear relation between the overturning strength and characteristics of the the meridional pressure gradient has been found before in global ocean models (Hughes and Weaver 1994; Rahmstorf 1996). It contrasts with the third-power relation that is found by classical scaling theory (e.g., Welander 1971; Te Raa and Dijkstra 1999). These scaling relations relate a characteristic density scale via thermocline depth and vertical velocity to the overturning strength, and are generally applied to closed, single-hemispheric basins. Rahmstorf (1996) already noted that in his model most of the upwelling occurred outside the Atlantic. The same behaviour is found in this model (Fig. 6.10). It implies that the Atlantic thermocline depth is *in*dependent of the overturning strength, and that the classical scaling arguments do not hold in these global models.

6.5.3 Comparison with freshwater studies

The study performed here is to some extent related to studies addressing the impact of changes in the freshwater balance on the Atlantic overturning circulation. In fact, the $\sigma = 1$ salt source corresponds to a freshwater loss of about 0.07 Sv, but it is extracted from the entire water column, rather than from the surface. Rahmstorf (1996) examined the response of the overturning circulation in an OGCM to changes in the Atlantic hydrological cycle. In several regions of the Atlantic, two of which were situated in the South Atlantic (his areas C and D), he slowly changed the surface freshwater input. He found a quadratic relation between the freshwater perturbation and the overturning strength, with an increased overturning when more freshwater was extracted from the surface. On the increasing branch of his parabola (corresponding to increased freshwater loss) his overturning increased 7 Sv upon a 0.25 Sv freshwater loss (a sensitivity of 28 Sv/Sv). In comparison, the $\sigma = 5$ salt source at the end of our main experiment corresponds to 0.35 Sv freshwater loss and having a 9 Sv increase in overturning strength; the resulting 25 Sv/Sv sensitivity is in surprising agreement with the findings of Rahmstorf (1996). Although the relation between overturning strength and source amplitudes turned out to be linear in our model, it cannot be ruled out that it corresponds to the flat part of Rahmstorf's parabola.

Nevertheless, it is interesting to see that perturbations in the surface freshwater balance and those brought about by interocean transport have a similar effect on the overturning circulation. The similarity furthermore shows that these effects are robust with respect to the model set-up (surface freshwater extraction vs. internal salt source), model design (GFDL MOM code vs. Hamburg LSG code), thermal surface forcing (atmospheric energy balance model (Rahmstorf and Willebrand 1995) vs.

relaxation to fixed atmospheric temperature) and the presence of the heat source in the present model.

6.5.4 The source/sink parametrisation of Agulhas Leakage

In this model, the heat and salt exchange brought about by Agulhas Leakage was parametrised by sources of heat and salt in the South Atlantic Ocean, and equally large sinks in the south-west Indian Ocean. However, the concept of heat and salt sources implies the physical replacement of two water masses with different temperature and salinity. For instance, leakage of Indian Ocean water into the Atlantic does not really cool the retroflecting waters in the south-west Indian Ocean, unless it is immediately and in-situ compensated by colder water. Therefore, parametrizing Agulhas Leakage by heat and salt sources assumes that all Agulhas Leakage water is compensated by South Atlantic Current water in the Retroflection area, and thus is consistent mainly with the super-gyre scenario (De Ruijter 1982). The scenario in which Agulhas Leakage water is picked up by the overturning circulation and leaves the Atlantic as NADW, is in fact much harder to represent consistently. Observations (e.g., Gordon et al. 1987; Fine et al. 1988) indicate that in the real ocean a considerable amount of NADW leaves the Atlantic in the Retroflection area. This would allow for considering both the input by Agulhas Leakage, as well as the compensating export of NADW, as subgrid-scale processes. This approach would localise the exchange in the Retroflection area, but it is still not clear how the vertical distribution of the sources should be defined.

The horizontal distribution of the sources in the South Atlantic were chosen to reflect the Agulhas Rings corridor (Byrne et al. 1995; Schouten et al. 1999), i.e., the initial path that is taken by most of the rings before they cross the Walvis Ridge. The source distributions were thus placed diagonally over the South Atlantic. We expect that the spatial characteristics of the source distributions are important for the response of the overturning circulation, since they determine to a large extent the changes in the density and pressure fields. To test this idea, the combined heat and salt source adjustment experiment was repeated with a zonally orientated source distribution. It showed that the adjustment process was modified, indeed. The development of P_S occurred in a similar fashion as in Fig. 6.24 (lower panel), but P_N developed very slowly. The response in the overturning strength was accordingly weak and retarded with respect to the original adjustment experiment. Obviously, the diagonal orientation of the original source distribution, with anomalies developing in the northward flowing Benguela Current, stimulates an efficient northward transport and enhancement of the density anomalies.

The horizontal distribution of the corresponding sinks in the south-west Indian Ocean has been chosen more or less arbitrarily. The largest part of the area is covered by the Agulhas Return Current, and the northern part of the ACC. Although it has not been tested, it is not likely that the details of the heat and salt extraction area are important for the response of the overturning circulation in the Atlantic.

6.5.5 The role of surface forcing

The results of this study suggest that, for Agulhas Leakage to have impact on the Atlantic overturning circulation, it is necessary to have different attenuation timescales of the thermal and saline anomalies (Stommel 1961). Only then may density anomalies develop that modify the pressure distribution in the Atlantic, and impact on the overturning strength. Indeed, thermal anomalies are in general rapidly attenuated by intense heat exchange with the overlying atmosphere (Haney 1971; Rahmstorf et al. 1996). Saline anomalies, on the other hand, do not generate such an interaction, and salt anomalies have been shown to persist for decades (Dickson et al. 1988). Cai and Greatbatch (1995) concluded, from comparing two experiments with and without Agulhas Leakage, that a reduction of Indian Ocean input does not influence the strength of the Atlantic overturning circulation, as the reduction of both the heat and salt input leaves the density structure of the Atlantic unmodified. However, they forced their temperature field with a simple parametrisation of air-sea exchange, called the zero heat capacity model. Rahmstorf et al. (1996) noted that the resulting thermal relaxation is unrealistically weak. This might have caused too little distinction between the evolution of the thermal and saline anomalies for a density anomaly to develop in the model of Cai and Greatbatch (1995).

In this model the circulation was forced with so-called mixed boundary conditions: a freshwater flux was prescribed, and a Newtonian relaxation condition was applied to the sea-surface temperature. However, mixed boundary conditions over-simplify the interaction of the ocean with the atmosphere. They imply that the atmosphere has an infinitely large heat capacity, so that the atmosphere does not respond to changes in the SST. Also the freshwater cycle is kept fixed, so that SST anomalies cannot modify the evaporation rate. It is therefore quite likely that models that include (some of) these feedbacks, as well as fully coupled models, will show a modified sensitivity of the overturning strength to Agulhas sources than has been found here. But as long as they predict distinctively different lifetimes for thermal and saline anomalies, an impact on the overturning circulation can be expected.

6.6 Conclusions

In this chapter it was studied how Agulhas Leakage influences the Atlantic overturning circulation in a General Circulation Model. To this end, the Hamburg LSG model was integrated for 10 kyr. Agulhas Leakage heat and salt exchange were parametrised by prescribing sources of heat and salt in the upper 1000 m of the South Atlantic. This allowed for a systematic investigation of the impact of this thermohaline exchange on the strength of the overturning circulation.

The overturning circulation turned out to respond strongly to the applied sources. The response was largely linear and partly non-linear. The linear response is related to changes in the basin-scale meridional density and pressure gradients, similar to the results of Hughes and Weaver (1994) and Rahmstorf (1996). No gradual change in the convective activity has been observed in response to the Agulhas salt source. Consequently, the hypothesis that Agulhas Leakage would stimulate the thermohaline

circulation by preconditioning the Atlantic surface waters for forming deep water (Gordon et al. 1992), does not hold for the linear response of this model.

The non-linear response resulted from a switch between two equilibria that differed in strength and distribution of the North Atlantic convective activity. If this switch was triggered by North Atlantic salinities exceeding a certain threshold, this would support the hypothesis of Gordon et al. (1992) for the non-linear part of the response. However, no proof of such a threshold was found, and the fact that the switch took place at the same strength of the overturning circulation in the up- and downgoing phases of the experiment suggests an advective feedback as triggering mechanism.

The adjustment experiments revealed that the Atlantic overturning circulation can respond within 2 years on a density perturbation in the South Atlantic. This information must have reached the North Atlantic through barotropic waves. Also internal baroclinic Kelvin waves were radiated, and reached the North Atlantic within 5 or 6 years. It is likely that these time scales are considerably shorter in the real ocean. The strongest response set in when the density anomaly reached the North Atlantic by advection. This took about 3 decades.

The adjustment experiments also emphasised the importance of the different attenuation time scales of thermal and saline anomalies in generating density anomalies. Although Agulhas heat and salt input initially balance with respect to their effect on density, it is due to the strong thermal relaxation that a density anomaly can develop further north. Although it is probable that mixed boundary conditions overestimate this difference, and coupled models will produce more reliable estimates, an impact on the overturning circulation can be expected as long as distinctively different lifetimes for thermal and saline anomalies are predicted.

6.A The components of the pressure work

In this appendix it is shown how the pressure work P is made up of several contributions. First we split the density field into a background density profile $\overline{\rho}(z)$ and a deviation $\rho'(\mathbf{x})$:

$$\rho(\mathbf{x}) = \overline{\rho}(z) + \rho'(\mathbf{x}). \tag{6.A1}$$

In this way the pressure dependence of the density is largely eliminated. The pressure field can now be written as:

$$p(\mathbf{x}) = \rho_0 g\zeta(\mathbf{x_h}) + \int_z^0 \overline{\rho}(z')dz' + \int_z^0 \rho'(\mathbf{x})dz' = p_0(\mathbf{x_h}) + \overline{p}(z) + p'(\mathbf{x}). \tag{6.A2}$$

Since $\overline{p}(z)$ depends on z only, the pressure work reduces to:

$$\begin{aligned}
- < \mathbf{u_h} \cdot \nabla_h p > &= - < \mathbf{u_h} \cdot \nabla_h p_0 > - < \mathbf{u_h} \cdot \nabla_h p' > \\
&= -\rho_0 g < \mathbf{u} \cdot \nabla\zeta > - < \mathbf{u} \cdot \nabla p' > + < w \, \frac{\partial p'}{\partial z} > \\
&= -\rho_0 g \oint \zeta \, \mathbf{u} \cdot \mathbf{n} \, dA - \oint p' \, \mathbf{u} \cdot \mathbf{n} \, dA - g < \rho' w > \\
&= -\rho_0 g \int w\zeta \, dA_S - \rho_0 g \int \zeta \, \mathbf{u} \cdot \mathbf{n} \, dA_I \\
&\quad - \int p' \, \mathbf{u} \cdot \mathbf{n} \, dA_I - g < \rho' w > .
\end{aligned} \tag{6.A3}$$

A_S and A_I denote the ocean's surface and the open boundaries of the domain, respectively, and $\mathbf{n}$ is the outward normal. Our domain of interest is the Atlantic, and the open boundaries are the Bering Strait and the zonal section at 30°S in the Atlantic. For convenience, we will assume here that all exchange takes place across this 30°S section, so that:

$$- \int p' \, \mathbf{u} \cdot \mathbf{n} \, dA_I = \int p'v \, dA_I. \tag{6.A4}$$

In the numerical calculations the exchange through Bering Strait is taken into account as well. Let us introduce V as the integrated meridional transport between level z and the bottom (at $z = -H(\mathbf{x_h})$):

$$V = \int_{-H}^{z} v \, dz', \tag{6.A5}$$

so that $V_z = v$. Now we can rewrite Eq. (6.A4) as follows:

$$\begin{aligned}
\int p'v \, dA_I &= \int (p'V)_z - p'_z V \, dA_I \\
&= \int (p'V)_z - (p'_z Vz)_z + p'_{zz} Vz + p'_z V_z z \, dA_I \\
&= \int (p'V - p'_z Vz)|_{-H}^{0} dx - g \int \rho'_z Vz \, dA_I - g \int \rho' vz \, dA_I.
\end{aligned} \tag{6.A6}$$

Since $V(z = -H)$ is zero by construction, and since $p'(z = 0) = 0$, the stock terms disappear.

6.B Convective adjustment as a density source

Although the process of convective adjustment in LSG is purely heat and salt conserving, it turns out to be a source of density. This can be understood by looking at two water parcels with different temperature, the colder parcel overlying the warmer. Convective adjustment acts as to interchange the parcels: upon moving the colder parcel downward adiabatically, its density increases with $d\rho_1 = dp/c_s^2(\text{cold})$, where c_s is the speed of sound. When the warmer parcel is moved upward, its density decreases with $d\rho_2 = -dp/c_s^2(\text{warm})$. The resulting density change $d\rho_1 + d\rho_2$ amounts to $dp[1/c_s^2(\text{cold}) - 1/c_s^2(\text{warm})]$ and is positive, since c_s increases with temperature (Gill 1982, his table A3.1). It therefore follows that the act of interchanging the two parcels will result in a net compaction and a decrease in the net volume, or, since in this model the volume of the two interchanged parcels is kept constant, an increase of mass.

This process is evidently caused by the non-linearity of the equation of state and the compressibility of sea water. Nevertheless it is not directly related to the process of cabbeling (T. Gerkema, personal communication). Cabbeling (Pickard and Emery 1990) is the process that causes the mixture of two water parcels to be denser than the original parcels, due to the non-linearity of the equation of state. In this process the compressibility does not play a role, as it applies to potential density as well. Furthermore, it results from mixing the water parcels, rather than vertically interchanging them.

Let us denote the mass production due to the convective adjustment procedure by $q^\rho(\mathbf{x})$ with volume integral Q. We can define a vertical mass-redistribution component, say $\tilde{q}^\rho(\mathbf{x}) = q^\rho(\mathbf{x}) - Q/V$, where V is the volume of the domain under consideration. This gives us two contributions to the potential energy balance, $< zq^\rho >=< z\tilde{q}^\rho > + \bar{z}Q$, where $\bar{z}$ is the basin-averaged depth (-1995 m for the Atlantic). It turns out that the net mass input, at levels below 0, is responsible for the potential energy loss brought about by convection (Fig. 6.B1). The contribution of $< z\tilde{q}^\rho >$ is even slightly positive. This might indicate that the upward salt transport (Fig. 6.18) has a slightly larger effect on the density than the upward heat transport (Fig. 6.17) when the vertical redistribution of density is concerned. However, it is not at all clear whether this decomposition has any physical significance, nor why the mass production changes so drastically during the experiment. For a detailed analysis of these processes one has to study the thermodynamics of sea-water in more detail.

The classic idea about convection influencing the strength of the thermohaline circulation is that 'heavy' water is mixed downward, and, as this water contrasts with the 'older' water at depth, zonal density and pressure gradients are set up. It might be interesting to study whether the compaction-effect described here has such a significant effect on the height of the water column that it modifies the meridional pressure gradient.

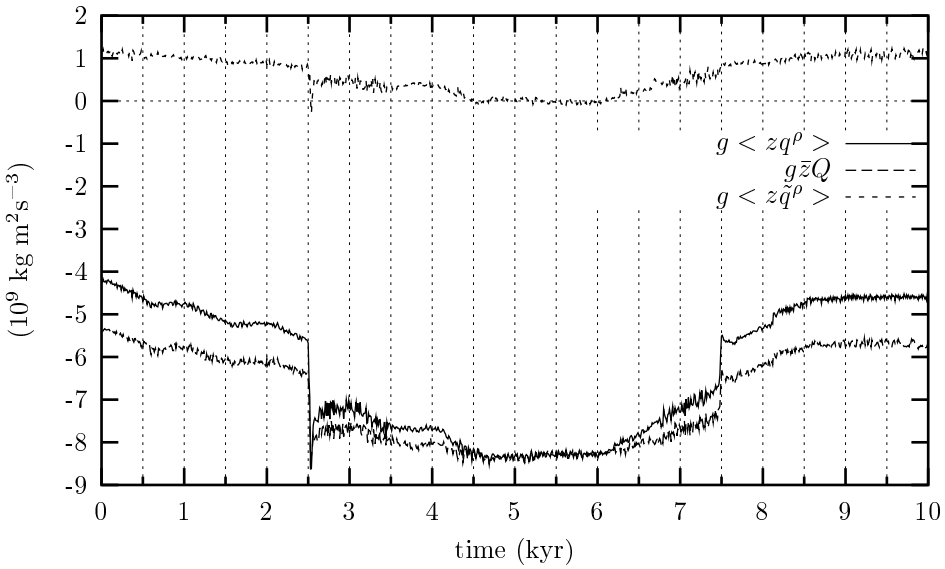

Figure 6.B1: *The contribution of the convective adjustment procedure to the potential energy balance* $g < zq^\rho >$. *The component* $g\bar{z}Q$ *is due to the net mass source, whereas the component* $g < z\tilde{q}^\rho >$ *is due to the vertical redistribution alone.*

Chapter 7

Conclusion

7.1 Discussion

The Atlantic Ocean interacts intensively with the other basins of the World Ocean. Most of the exchange takes place via the Southern Ocean. It is here that the Atlantic issues its North Atlantic Deep Water (NADW) for distribution over the entire World Ocean. And it is here that other water masses are drawn into the Atlantic, as part of the global thermohaline circulation system. This exchange of water masses, each with its own temperature, salinity, and other constituents, makes the Atlantic Ocean a unique and complex blending system, that makes its influence felt worldwide. On the other hand, the thermohaline structure of the Atlantic is largely determined by processes in other parts of the World Ocean.

The interest in the exchange between the Atlantic and the rest of the World Ocean was spurred by a recent debate in the oceanographic literature. This was started by Gordon (1985, 1986), who argued that most of the water supplying the Atlantic for NADW formation is derived from the Pacific and Indian thermoclines. This water enters the Atlantic via a process called Agulhas Leakage, a highly intermittent exchange between the thermoclines of the South Indian and South Atlantic Oceans. Rintoul (1991), on the other hand, argued that most of the water compensating for NADW export is derived from fresh and cold Subantarctic water masses. This water enters the Atlantic sector of the Southern Ocean via Drake Passage, and it finds its way north mainly as so-called Antarctic Intermediate Water (AAIW).

The water masses involved in these two routes for NADW renewal contrast highly with respect to their thermohaline characteristics. Obviously, the ratio with which the two scenarios supply water for NADW formation largely influences the heat and salt balance of the Atlantic. Gordon et al. (1992) suggested that Agulhas Leakage may have a *dynamical* effect on the strength of the Atlantic overturning circulation; its input of salty thermocline water salinifies the Atlantic surface waters, and preconditions them for deep convection in the northern polar region, and associated formation of NADW. This hypothesis has large implications for studies of past and future climate; since the process of Agulhas Leakage probably depends critically on characteristics

of the Indian Ocean wind climatology (De Ruijter et al. 1999), it may be sensitive to relatively small changes in climate. Indeed, paleoceanographic records indicate that Agulhas Leakage may have been strongly reduced or even absent during the major glaciations of the Pleistocene (Howard and Prell 1992; Flores et al. 1999). And it is not known how Agulhas Leakage will react to future climate changes.

The studies presented in this dissertation focussed on the question whether the Atlantic overturning circulation itself is influenced by the heat and salt fluxes brought about by interocean exchange. The results of these studies all suggest that these fluxes do have considerable influence on the Atlantic thermohaline circulation. Especially the heat and salt input by Agulhas Leakage turns out to have a considerable stimulating impact on the strength of the overturning. The results thus support the hypothesis of Gordon et al. (1992). However, the response in our models is not primarily caused by the stimulating effect of enhanced Atlantic surface salinities on the convective activity in the source areas of NADW. The 2D model studies of Chapters 4 and 5, as well as the 3D model study of Chapter 6, show that the heat and salt fluxes influence the stratification and the pressure field of the entire Atlantic to such an extent that it impacts on the strength of the overturning circulation. In fact, the overturning strength in these models turns out to be linearly related to characteristics of the meridional pressure gradient, in line with the results of Hughes and Weaver (1994) and Rahmstorf (1996).

The 2D model studies also show the role of energy conversions in generating the overturning response. The lateral fluxes (Chapter 4) and sources (Chapter 5) of heat and salt, representing the interocean exchange, supply the Atlantic with potential energy. This energy is readily converted into kinetic energy of the flow, establishing a direct connection between the interocean buoyancy fluxes and the overturning strength. In fact, this energy supply turns out to *control* the flow strength; the linear relation between the meridional pressure gradient and the overturning strength is established accordingly. In the real ocean, work must be done outside the Atlantic to make this energy available. If this work is done by buoyancy driven upwelling alone, as is the classical notion about the thermohaline circulation (e.g., Stommels and Arons 1960), then the extra-Atlantic energy loss would cancel the Atlantic energy gain. In this case, the sensitivity of the circulation strength is probably overestimated by the approach of modelling the Atlantic circulation only. However, recent investigations point at the possibility that a part of this work is done by wind-driven upwelling (Toggweiler and Samuels 1993ab; Shriver and Hurlburt 1997; Döös and Coward 1997). This would make this energy really available for the Atlantic overturning circulation (Toggweiler and Samuels 1998). Unfortunately, the importance of the energy balance, as displayed by the 2D models, could not be confirmed in the 3D model context.

The heat and salt fluxes brought about by Agulhas Leakage almost cancel with respect to density, and the resulting buoyancy flux is consequently small. Crucial for generating a response of the overturning strength is a physical mechanism that allows for the development of density anomalies. Only then can the pressure field of the Atlantic be affected, and can a response in the overturning circulation be generated. Indeed, thermal anomalies are in general rapidly attenuated by intense heat exchange with the overlying atmosphere (Haney 1971; Rahmstorf et al. 1996).

Saline anomalies, on the other hand, do not generate such an interaction, and salt anomalies have been shown to persist for decades (Dickson et al. 1988). This difference is to some extent represented by the mixed boundary conditions that were used to force our models. These conditions imply that the surface temperature is strongly restored towards a fixed value, whereas the surface salinity can freely develop under influence of a freshwater flux. However, restoring the sea-surface temperature to a fixed temperature does no justice to the fact that the atmosphere responds to changes in the sea-surface temperature (Rahmstorf and Willebrand 1995). Therefore, mixed boundary conditions are in general thought to overestimate the sensitivity of the circulation to disturbances. It is possible that the sensitivity to Agulhas heat and salt sources is somewhat smaller in ocean models that are coupled to more realistic atmosphere models. But as long as different lifetimes for thermal and saline anomalies are simulated, an impact on the overturning circulation can be expected.

The results found here contrast with the findings of Cai and Greatbatch (1995). They found that the overturning strength in a low-resolution General Circulation Model did not change when Agulhas Leakage was shut off. Rahmstorf et al. (1996) pointed at the unrealistically weak thermal relaxation that was implied by their atmosphere model. This allowed thermal anomalies to develop equally free as saline anomalies. Indeed, despite a general cooling and freshening of the Atlantic, the density field in their model was unaffected when Agulhas Leakage was shut off, leaving the pressure field and the overturning strength unchanged.

7.2 Recommendations

Although this dissertation has shed light on several issues, even more new questions seem to have been raised. Here I will address some of the topics that may become the subject of further study.

Model studies are not more than a theoretical exercise if they are not supported by observations. The validation of (future) climate scenarios is often impossible (and in most cases, undesirable) for obvious reasons. However, a lot can still be learned from paleoceanographic records, containing invaluable information of past climate. Detailed time series of the start-up of the conveyor belt circulation and Agulhas Leakage at the end of the last glacial may provide more information about causal relationships. If it could be determined that the Atlantic surface salinities really changed in response to re-establishing Agulhas Leakage, this would give more support to the hypothesis of Gordon et al. (1992) and the conclusions drawn here.

Presently, Agulhas Leakage seems to be a rather steady process, exhibiting little variability of considerable amplitude. The only event of anomalous Agulhas Leakage that was observed directly took place in the mid-80's (Shannon et al. 1990). It would be interesting to find out what happened to the SSS and SST anomalies that entered into the South Atlantic as a result of this enhanced Agulhas Leakage. Has the dispersion of these anomalies been recorded in hydrographic or remote sensing records? Did these anomalies generate baroclinic waves, and did they in some way influence the net outflow or inflow across 30°S? If these events leave their imprint

on terrestrial climate records (like, for instance, rainfall statistics), then an estimate could be made of the frequency and strength of similar events in the past. It is nevertheless unlikely that these events generate anomalies that are strong enough to influence the overturning strength in the North Atlantic. Therefore, attempts to find correlations between occurrences of anomalous Leakage events and changes in the North Atlantic overturning circulation (e.g., Koltermann et al. 1999; Bersch et al. 1999) must be considered as showing little promise.

In light of the conclusion that the overturning circulation is rather sensitive to Agulhas Leakage, it is important to study the possible response of this Indian-Atlantic exchange in global warming scenarios. Since this exchange depends mainly on the position of the Subtropical Convergence and on the strength of the Agulhas Current, the focus should be laid on those features of the South Indian Ocean wind stress climatology that influence in particular these facets. It would be interesting to examine the suggestion whether feedbacks exist between the amount of Agulhas Leakage and the position of the line of zero wind-stress curl that may explain its relative stability (De Ruijter, personal communication).

The sensitivity estimate of the overturning strength to Agulhas Leakage could be refined by using more sophisticated models. As discussed in the former section, the use of mixed boundary conditions exaggerates the difference in damping time scales of thermal and saline anomalies, and more or less optimises the response of the overturning strength to the applied disturbances. Coupling the ocean model to a more active atmosphere may adjust the estimated sensitivity, probably to a somewhat smaller value. Furthermore, using more sophisticated ocean models, featuring a higher resolution and a better representation of physical processes (like inclusion of momentum advection, lower values of viscosity, or other mixing schemes), may yield an even more reliable estimate of the sensitivity.

Still an open question is how much Agulhas Leakage water ultimately participates in the overturning circulation. A part of this problem could be solved by studying the mixing processes that are involved in the decay of Agulhas Rings. Studying the path of drifters, deployed in newly shed Agulhas Rings, could also help in determining the ultimate fate of Agulhas Leakage water. Theoretical and model studies could help to identify the processes that control the amounts of thermocline and intermediate water that are drawn north for NADW renewal.

Currently, the MARE (Mixing of Agulhas Rings Experiment) project is in progress, aimed at understanding and quantifying the decay processes of Agulhas Rings. This project, a cooperation between the Universities of Utrecht and Cape Town, the Royal Netherlands Meteorological Institute (KNMI) and the Netherlands Institute for Sea Research (NIOZ), combines hydrographic surveys (the same Agulhas Ring will be visited three times), data assimilation techniques, regional and global modelling studies, and paleoceanographic research, to assess the impact of Agulhas Leakage for regional and global climate issues in the present and past. This will contribute to our understanding of the role of Agulhas Leakage in shaping Atlantic and global climate.

References

Arakawa, A., and V. R. Lamb, 1977: Computational design of the basic dynamical processes of the UCLA General Circulation Model. *Methods. Comput. Phys.*, **17**, 173–265.

Barnier, B., P. Marchesiello and A. P. de Miranda, 1996: Modelling the ocean circulation in the South Atlantic: a strategy for dealing with open boundaries. *The South Atlantic: present and past circulation*, G. Wefer et al., Eds., Springer, 289–304.

Baumgartner, A., and E. Reichel, 1975: *The world water balance*, Elsevier, 179 pp.

Bennett, S. L., 1988: *Where three oceans meet: the Agulhas retroflection region.* PhD Dissertation, WHOI and MIT, WHOI-88-51.

Berger, W. H. and G. Wefer, 1996: Expeditions into the past: Paleoceanographic studies in the South Atlantic. *The South Atlantic: present and past circulation*, G. Wefer et al., Eds., Springer, 363–410.

Bersch, M., J. Meincke and A. Sy, 1999. Interannual thermohaline changes in the northern North Atlantic 1991-1996. *Deep-Sea Res.*, **46**, 55–75.

Biastoch, A., 1998: *Zirkulation und Dynamik in der Agulhasregion anhand eines numerischen Modells*, PhD Dissertation, Institut für Meereskunde Kiel, 118 pp.

Biastoch, A., and W. Krauss, 1999: The role of mesoscale eddies in the source regions of the Agulhas Current. *J. Phys. Oceanogr.*, **29**, 2303–2317.

Boddem, J., and R. Schlitzer, 1995: Interocean exchange and meridional mass and heat fluxes in the South Atlantic. *J. Geophys. Res.*, **100**, 15821–15834.

Bonekamp, H., A. Sterl and G. J. Komen, 1999: Interannual variability in the Southern Ocean from an ocean model forced by European Center for Medium-Range Weather Forecasts reanalysis fluxes. *J. Geophys. Res.*, in press.

Broecker, W. S., D. M. Peteet and D. Rind, 1985: Does the ocean-atmosphere system have more than one stable mode of operation? *Nature*, **315**, 21–26.

Broecker, W. S., 1987: The biggest chill. *Nat. Hist. Mag.*, **97**, 74–82.

Broecker, W. S., 1991: The great ocean conveyor. *Oceanogr.*, **4**, 79–89.

Bryan, F., 1986: High-latitude salinity effects and interhemispheric thermohaline circulations. *Nature*, **323**, 301–304.

Bryan, F., 1987: Parameter sensitivity of primitive equation ocean general circulation models. *J. Phys. Oceanogr.*, **17**, 970–985.

Bryden, H. L., 1973: New polynomials for thermal expansion, adiabatic temperatuire gradient, and potential temperature gradient of sea water. *Deep-Sea Res.*, **20**, 401–408.

Bunker, A. F., 1980: Trends of variables and energy fluxes over the Atlantic Ocean from 1948 to 1972. *Mon. Weather Rev.*, **104**, 1122-1140.

Byrne, D. A., A. L. Gordon and W. F. Haxby, 1995: Agulhas eddies: a synoptic view using Geosat ERM data. *J. Phys. Oceanogr.*, **25**, 902–917.

Cai, W., and R. J. Greatbatch, 1995: Compensation for the NADW outflow in a Global Ocean Circulation Model. *J. Phys. Oceanogr.*, **25**, 226–241.

Cessi, P., and W. R. Young, 1992: Multiple equilibria in two-dimensional thermohaline circulation. *J. Fluid Mech.*, **241**, 291–309.

Chandrasekhar, S., 1961: *Hydrodynamic and hydromagnetic stability.* Clarendon Press, 652 pp.

Clement, A. C., and A. L. Gordon, 1995: The absolute velocity field of Agulhas eddies and the Benguela Current. *J. Geophys. Res.*, **100**, 22591–22601.

Coachman, L. K., and K. Aagaard, 1988: Transports through Bering Strait: annual and interannual variability. *J. Geophys. Res.*, **93**, 15535–15539.

Dansgaard, W., H. B. Clausen, N. S. Gundestrup, C. U. Hammer, S. F. Johnsen, P. M. Kristinsdottir and N. Reeh, 1982: A new Greenland deep ice-core. *Science*, **218**, 1273–1277.

Dansgaard, W., S. J Johnsen, H. B. Clausen, D. Dahl-Jensen, N. S. Gundestrup, C. U. Hammer, C. S. Hvidberg, J. P. Steffensen, A. E. Sveinbjörnsdottir, J. Jouzel and G. Bond, 1993: Evidence for general instability of past climate from 250-kyr ice-core record. *Nature*, **364**, 218–220.

De Las Heras, M. M., and R. Schlitzer, 1999: On the importance of intermediate water flows for the global ocean overturning. *J. Geophys. Res.*, **104**, 15515–15536.

De Ruijter, W. P. M., 1982: Asymptotic analysis of the Agulhas and Brazil Current systems. *J. Phys. Oceanogr.*, **12**, 361–373.

De Ruijter, W. P. M., and D. B. Boudra, 1985: The wind-driven circulation in the South Atlantic–Indian Ocean—I. Numerical experiments in a one-layer model. *Deep-Sea Res.*, **32**, 557–574.

De Ruijter, W. P. M., A. Biastoch, S. S. Drijfhout, J. R. E. Lutjeharms, R. P. Matano, T. Pichevin, P. J. van Leeuwen and W. Weijer, 1999: Indian-Atlantic inter-ocean exchange: Dynamics, estimation and impact. *J. Geophys. Res.*, **104**, 20885–20910.

Dickson, R. R., J. Meincke, S. Malmberg and A. J. Lee, 1988: The "Great Salinity Anomaly" in the northern North Atlantic 1968-1982. *Progress in Oceanography*, **20**, 103–151.

Dickson, R. R., J. Lazier, J. Meincke, P. Rhines and J. Swift, 1996: Long-term coordinated changes in the convective activity of the North Atlantic. *Progress in Oceanography*, **38**, 241–295.

Dijkstra, H. A., M. J. Molemaker, A. van der Ploeg and E. F. F. Botta, 1995: An efficient code to compute non-parallel steady flows and their linear stability. *Computers & Fluids*, **24**, 415–434.

Dijkstra, H. A., and M. J. Molemaker, 1997: Symmetry breaking and overturning oscillations in thermohaline driven flows. *J. Fluid Mech.*, **331**, 169–198.

Dijkstra, H. A., and J. D. Neelin, 1999: Imperfections of the thermohaline circulation: latitudinal asymmetry and preferred northern sinking. *J. Climate*, in press.

Dijkstra, H. A., and W. P. M. De Ruijter, 2000: On the physics of the Agulhas Current: steady retroflection regimes. *J. Phys. Oceanogr.*, submitted.

Döös, K., 1995: Interocean exchange of water masses. *J. Geophys. Res.*, **100**, 13499–13514.

Döös, K., and A. Coward, 1997: The Southern Ocean as the major upwelling zone of North Atlantic Deep Water. *International WOCE Newsletter*, **27**, 3–4.

Döscher, R., C.W. Böning and P. Herrmann, 1994: Response of circulation and heat transport in the North Atlantic to changes in thermohaline forcing in northern latitudes: a model study. *J. Phys. Oceanogr.*, **24**, 2306–2320.

Drijfhout, S.S, E. Maier-Reimer and U. Mikolajewicz, 1996a: Tracing the conveyor belt in the Hamburg LSG ocean general circulation model. *J. Geophys. Res.*, **101**, 22563–22575.

Drijfhout, S.S., C. Heinze, M. Latif and E. Maier-Reimer, 1996b: Mean circulation and internal variability in an Ocean Primitive Equation Model. *J. Phys. Oceanogr.*, **26**, 559–580.

Duncombe Rae, C. M., L. V. Shannon and F. A. Shillington, 1989: An Agulhas ring in the South Atlantic Ocean. *South African Journal of Science*, **85**, 747–748.

Duncombe Rae, C. M., F. A. Shillington, J. J. Agenbag, J. Taunton-Clark and M. L. Gründlingh, 1992: An Agulhas ring in the South Atlantic Ocean and its interaction with the Benguela upwelling frontal system. *Deep-Sea Res.*, **39**, 2009–2027.

Duncombe Rae, C. M., S. L. Garzoli and A. L. Gordon, 1996: The eddy field of the southeast Atlantic Ocean: a statistical census from the Benguela sources and Transport project. *J. Geophys. Res.*, **101**, 11949–11964.

Feron, R. C. V., W. P. M de Ruijter and D. Oskam, 1992: Ring shedding in the Agulhas Current system. *J. Geophys. Res.*, **97**, 9467-9477.

Feron, R. C. V., 1994: *Eddies and mean flow in the ocean.* PhD Dissertation, Utrecht University, 126 pp.

Fine, R. A., M. J. Warner and R. F. Weiss, 1988: Water mass modification at the Agulhas Retroflection: chlorofluormethane studies. *Deep-Sea Res.*, **35**, 311–332.

Flierl, G. R., 1981: Particle motions in large-amplitude wave fields. *Geophys. Astrophys. Fluid Dyn.*, **18**, 39–74.

Flores, J.-A., R. Gersonde and F. J. Sierro, 1999: Pleistocene fluctuations in the Agulhas Current Retroflection based on the calcareous plankton record. *Marine Micropaleontology*, **37**, 1–22.

FRAM Group, 1991: An eddy-resolving model of the Southern Ocean. *Eos*, **72**, 169, 174–175.

Fu, L.-L., 1981: The general circulation and meridional heat transport of the subtropical South Atlantic determined by inverse methods. *J. Phys. Oceanogr.*, **11**, 1171-1193.

Garzoli, S. L., and A. L. Gordon, 1996: Origins and variability of the Benguela Current. *J. Geophys. Res.*, **101**, 897–906.

Garzoli, S. L., A. L. Gordon, V. Kamenkovich, D. Pillsbury and C. Duncombe-Rae, 1996: Variability and sources of the southeastern Atlantic circulation. *J. Mar. Res.*, **54**, 1039–1071.

Georgi, D. T., and J. M. Toole, 1982: The Antarctic Circumpolar Current and the oceanic heat and freshwater budgets. *J. Mar. Res.*, **40** (suppl.), 183–197.

Gill, A.E., 1982. Atmosphere-Ocean Dynamics. Academic Press, 666 pp.

Goñi, G. J., S. L. Garzoli, A. J. Roubicek, D. B. Olson and O. B. Brown, 1997: Agulhas ring dynamics from TOPEX/POSEIDON satellite altimeter data. *J. Mar. Res.*, **55**, 861–883.

Gordon, A. L., 1985: Indian-Atlantic transfer of thermocline water at the Agulhas Retroflection. *Science*, **227**, 1030–1033.

Gordon, A. L., 1986: Interocean exchange of thermocline water. *J. Geophys. Res.*, **91**, 5037–5046.

Gordon, A. L., and W. F. Haxby, 1990: Agulhas eddies invade the South Atlantic: evidence from Geosat altimeter and shipboard conductivity-temperature-depth survey. *J. Geophys. Res.*, **95**, 3117–3125.

Gordon, A. L., J. R. E. Lutjeharms and M. L. Gründlingh, 1987: Stratification and circulation at the Agulhas Retroflection. *Deep-Sea Res.*, **34**, 565–599.

Gordon, A. L., R. F. Weiss, W. M. Smethie Jr. and M. J. Warner, 1992: Thermocline and intermediate water communication between the South Atlantic and Indian Oceans. *J. Geophys. Res.*, **97**, 7223–7240.

GRIP (Greenland Ice-core Project) Members, 1993: Climate instability during the last interglacial period recorded in the GRIP ice core. *Nature*, **364**, 203–207.

Gründlingh, M. L., 1995: Tracking eddies in the southeast Atlantic and southwest Indian oceans with TOPEX/POSEIDON. *J. Geophys. Res.*, **100**, 24977–24986.

Haarsma, R. J., and F. M. Selten, 1998: On the mechanism of the Antarctic Circumpolar Wave. *J. Climate*, submitted.

Haney, R. L., 1971: Surface thermal boundary condition for ocean circulation models. *J. Phys. Oceanogr.*, **1**, 241–249.

Harris, T. F. W. and D. van Foreest, 1978: The Agulhas Current in March 1969. *Deep-Sea Res.*, **25**, 549–561.

Hasselmann, K., 1982: An ocean model for climate variability studies. *Progress in Oceanography*, **11**, 69–92.

Hellermann, S., and M. Rosenstein, 1983: Normal monthly wind stress over the World Ocean with error estimates. *J. Phys. Oceanogr.*, **13**, 1093-1104.

Hirschi, J., J. Sander and T. F. Stocker, 1999: Fast interhemispheric teleconnections in an OGCM. *J. Phys. Oceanogr.*, submitted.

Holfort, J., 1994: *Großräumige Zirkulation und meridionale Transporte im Südatlantik (Large-scale circulation and meridional transports in the South Atlantic)*, PhD Dissertation, Institut für Meereskunde Kiel, 96 pp.

Holland, W. R., 1975: Energetics of baroclinic oceans. *Numerical models of the ocean circulation*, National Academy of Sciences, Washington D.C., 168–177.

Howard, W. R., and W. L. Prell, 1992: Late quaternary surface circulation of the southern Indian Ocean and its relationship to orbital variations. *Paleoceanogr.*, **7**, 79–117.

Hsieh, W. W., M. K. Davey and R. C. Wajsowicz, 1983: The free Kelvin wave in finite-difference numerical models. *J. Phys. Oceanogr.*, **13**, 1383–1397.

Huang, R. X., 1998: Mixing and available potential energy in a Boussinesq Ocean. *J. Phys. Oceanogr.*, **28**, 669–678.

Hughes, T. M. C., and A. J. Weaver, 1994: Multiple equilibria of an asymmetric two-basin ocean model. *J. Phys. Oceanogr.*, **24**, 619–637.

Keigwin, L. D., G. A. Jones and S. J. Lehman, 1991: Deglacial meltwater discharge, North Atlantic deep circulation, and abrupt climate change. *J. Geophys. Res.*, **96**, 16811–16826.

Koltermann, K. P., A. V. Sokov, V. P. Tereschenkov, S. A. Dobroliubov, K. Lorbacher and A. Sy, 1999. Decadal changes in the thermohaline circulation of the North Atlantic. *Deep-Sea Res.*, **46**, 109–138.

Lenderink, G., and R. J. Haarsma, 1994: Variability and multiple equilibria of the thermohaline circulation associated with Deep-Water formation. *J. Phys. Oceanogr.*, **24**, 1480–1493.

Levitus, S., 1982: *Climatological Atlas of the World Ocean.* NOAA Prof. Paper No. 13, U.S. Govt. Printing Office, 173 pp.

Levitus, S., and T. P. Boyer, 1994: *World Ocean Atlas 1994, Volume 4, Temperature.* NOAA Atlas NESDIS 4, 117 pp.

Levitus, S., R. Burgett and T. P. Boyer, 1994: *World Ocean Atlas 1994, Volume 3, Salinity.* NOAA Atlas NESDIS 3, 99 pp.

Lutjeharms, J. R. E., 1982: Baroclinic volume transport in the Southern Ocean. *J. Phys. Oceanogr.*, **12**, 3–7.

Lutjeharms, J. R. E., and H. R. Valentine, 1988: Eddies at the Subtropical Convergence south of Africa. *J. Phys. Oceanogr.*, **18**, 761–774.

Lutjeharms, J. R. E., and R. C. van Ballegooyen, 1988: The Retroflection of the Agulhas Current. *J. Phys. Oceanogr.*, **18**, 1571–1583.

Lutjeharms, J. R. E., and D. J. Webb, 1995: Modelling the Agulhas Current system with FRAM (Fine Resolution Antarctic Model). *Deep-Sea Res.*, **42**, 523–551.

Lutjeharms, J. R. E., 1996: The exchange of water between the South Indian and South Atlantic Oceans. *The South Atlantic: present and past circulation*, G. Wefer et al., Eds., Springer, 125–162.

Lutjeharms, J. R. E. and J. Cooper, 1996: Interbasin leakage through Agulhas current filaments. *Deep-Sea Res.*, **43**, 213–238.

Macdonald, A. M., 1993: Property fluxes at 30°S and their implications for the Pacific-Indian throughflow and the global heat budget. *J. Geophys. Res.*, **98**, 6851–6868.

Macdonald, A. M., and C. Wunsch, 1996: An estimate of global ocean circulation and heat fluxes. *Nature*, **382**, 436-439.

Maier-Reimer, E., and U. Mikolajewicz, 1992: *The Hamburg Large-Scale Geostrophic Ocean General Circulation Model (cycle 1).* DKRZ Tech. Rep. No. 2, 34 pp.

Maier-Reimer, E., U. Mikolajewicz, and K. Hasselmann, 1993: Mean circulation of the Hamburg LSG OGCM and its sensitivity to the thermohaline surface forcing. *J. Phys. Oceanogr.*, **23**, 731–757.

Manabe, S., and R. J. Stouffer, 1988: Two stable equilibria of a coupled ocean-atmosphere model. *J. Climate*, **1**, 841–866.

Marchesiello, P., B. Barnier and A. P. de Miranda, 1998: A sigma-coordinate primitive equation model for studying the circulation in the South Atlantic. Part II: Meridional transports and seasonal variability. *Deep-Sea Res.*, **45**, 573–608.

Marotzke, J., and J. Willebrand, 1991: Multiple equilibria of the global thermohaline circulation. *J. Phys. Oceanogr.*, **21**, 1372–1385.

Marshall, J., and F. Schott, 1999: Open-ocean convection: observations, theory, and models. *Rev. Geophys.*, **37**, 1–64.

Matano, R. P., and S. G. H Philander, 1993: Heat and mass balances of the South Atlantic Ocean calculated from a numerical model. *J. Geophys. Res.*, **98**, 977–984.

McCann, M. P., A. J. Semtner Jr. and R. M. Chervin, 1994: Transports and budgets of volume, heat, and salinity from a global eddy-resolving ocean model. *Climate Dyn.*, **10**, 59–80.

McCartney, M. S. and M. E. Woodgate-Jones, 1991: A deep-reaching anticyclonic eddy in the subtropical gyre of the eastern South Atlantic. *Deep-Sea Res.*, **38**, S411–S443.

Mikolajewicz, U., and E. Maier-Reimer, 1990: Internal secular variability in an ocean general circulation model. *Climate Dyn.*, **4**, 145–156.

Nowlin Jr., W. D., and J. M. Klinck, 1986: The physics of the Antarctic Circumpolar Current. *Rev. Geophys.*, **24**, 469–491.

Olbers, D., V. Gouretski, G. Seiß, and J. Schröter, 1992: *Hydrographic Atlas of the Southern Ocean.* AWI, Bremerhaven, xvii pp, 82 plates.

Olson, D. B., and R. H. Evans, 1986: Rings of the Agulhas Current. *Deep-Sea Res.*, **33**, 27–42.

Oort, A. H., 1983: *Global atmospheric circulation statistics, 1985-1973.* NOAA Prof. Paper No. 14, U.S. Govt. Printing Office, 180 pp.

Park, Y-H., and L. Gamberoni, 1997: Cross-frontal exchange of Antarctic Intermediate Water and Antarctic Bottom Water in the Crozet Basin. *Deep-Sea Res.*, **44**, 963–986.

Pickard, G. L., and W. J. Emery, 1990: *Descriptive Physical Oceanography.* Pergamon Press, 320 pp.

Pierce, D. W., T. P. Barnett and U. Mikolajewicz, 1995: Competing roles of heat and freshwater flux in forcing thermohaline circulation. *J. Phys. Oceanogr.*, **25**, 2046-2064.

Piola, A. R., and A. L. Gordon, 1986: On oceanic heat and freshwater fluxes at 30°S. *J. Phys. Oceanogr.*, **16**, 2184–2190.

Quon, C., and M. Ghil, 1992: Multiple equilibria in thermosolutal convection due to salt-flux boundary conditions. *J. Fluid Mech.*, **245**, 449–483.

Quon, C., and M. Ghil, 1995: Multiple equilibria and stable oscillations in thermosolutal convection at small aspect ratio. *J. Fluid Mech.*, **291**, 33–56.

Rahmstorf, S., 1994: Rapid climate transitions in a coupled ocean-atmosphere model. *Nature*, **372**, 82–85.

Rahmstorf, S., 1995: Multiple convection patterns and thermohaline flow in an idealized OGCM. *J. Clim.*, **8**, 3028–3039.

Rahmstorf, S., and J. Willebrand, 1995: The role of temperature feedback in stabilizing the thermohaline circulation. *J. Phys. Oceanogr.*, **25**, 787-805.

Rahmstorf, S., 1996: On the freshwater forcing and transport of the Atlantic thermohaline circulation. *Climate Dyn.*, **12**, 799–811.

Rahmstorf, S., J. Marotzke and J. Willebrand, 1996: Stability of the thermohaline circulation. *The warm water sphere of the North Atlantic*, W. Krauss, Ed., Bornträger, 129–158.

Rahmstorf, S., and M. H. England, 1997: Influence of southern hemisphere winds on North Atlantic Deep Water flow. *J. Phys. Oceanogr.*, **27**, 2040–2054.

Reid, J. L., and R. J. Lynn, 1971: On the influence of the Norwegian-Greenland and Weddell seas upon the bottom waters of the Indian and Pacific Oceans. *Deep-Sea Res.*, **18**, 1063–1088.

Rintoul, S. R., 1991: South Atlantic interbasin exchange. *J. Geophys. Res.*, **96**, 2675–2692.

Sarntheim, M., K. Winn, S. J. A. Jung, J.-C. Duplessy, L. Labeyrie, H. Erlenkeuser and G. Ganssen, 1994: Changes in east Atlantic deepwater circulation over the last 30,000 years: Eight time slice reconstructions. *Paleoceanogr.*, **9**, 209–267.

Saunders, P. M., and S. R. Thompson, 1993: Transport, heat, and freshwater fluxes within a diagnostic numerical model (FRAM). *J. Phys. Oceanogr.*, **23**, 452–464.

Saunders, P. M., A. C. Coward and B. A. de Cuevas, 1999. Circulation of the Pacific Ocean seen in a global ocean model (OCCAM). *J. Geophys. Res.*, in press.

Schlitzer, R., 1993: Determining the mean, large-scale circulation of the Atlantic with the Adjoint Method. *J. Phys. Oceanogr.*, **23**, 1935–1952.

Schlitzer, R., 1996: Mass and heat transports in the South Atlantic derived from historical hydrographic data. *The South Atlantic: present and past circulation*, G. Wefer et al., Eds., Springer, 305–323.

Schmitt, R. W., P. S. Bogden and C. E. Dorman, 1989: Evaporation minus precipitation and density fluxes for the North Atlantic. *J. Phys. Oceanogr.*, **19**, 1208-1221.

Schmitt, R. W., 1994: *The ocean freshwater cycle.* JSC Ocean Observing System Development Panel, Texas A&M University, College Station, TX., 40 pp.

Schmitz Jr., W. J., 1995: On the interbasin-scale thermohaline circulation. *Rev. Geophys.*, **33**, 151–173.

Schouten, M. W., W. P. M. de Ruijter, P. J. van Leeuwen and J. R. E. Lutjeharms, 1999: Translation, decay and splitting of Agulhas rings in the south-eastern Atlantic Ocean. *J. Geophys. Res.*, submitted.

Schröder, M., and E. Fahrbach, 1999: On the structure and the transport of the eastern Weddell Gyre. *Deep-Sea Res.*, **46**, 501–527.

Semtner Jr., A. J., and R. M. Chervin, 1992: Ocean general circulation from a global eddy-resolving model. *J. Geophys. Res.*, **97**, 5493–5550.

Shaffer, G., and J. Bendtsen, 1994: Role of the Bering Strait in controlling North Atlantic ocean circulation and climate. *Nature*, **367**, 354–357.

Shannon, L. V., J. J. Agenbag, N. D. Walker and J. R. E. Lutjeharms, 1990: A major perturbation in the Agulhas retroflection area in 1986. *Deep-Sea Res.*, **37**, 493–512.

Shriver, J. F., and H. E. Hurlburt, 1997: The contribution of the global thermohaline circulation to the Pacific to Indian Ocean throughflow via Indonesia, *J. Geophys. Res.*, **102**, 5491–5511.

Stocker, T. F., and D. G. Wright, 1991a: Rapid transitions of the ocean's deep circulation and climate change. *Nature*, **351**, 729–732.

Stocker, T. F., and D. G. Wright, 1991b: A zonally averaged ocean model for the thermohaline circulation. Part II: Interocean circulation in the Pacific-Atlantic basin system. *J. Phys. Oceanogr.*, **21**, 1725–1739.

Stocker, T. F., and L. A. Mysak, 1992: Climatic fluctuations on the century time scale: A review of high-resolution proxy data and possible mechanisms *Clim. Change*, **20**, 227–250.

Stocker, T. F., D. G. Wright and L. A. Mysak, 1992a: A zonally averaged, coupled ocean-atmosphere model for paleoclimate studies. *J. Clim.*, **5**, 773–797.

Stocker, T. F., D. G. Wright and W. S. Broecker, 1992b: The influence of high-latitude surface forcing on the global thermohaline circulation. *Paleoceanography*, **7**, 529–541.

Stommel, H., 1957: A survey of ocean current theory. *Deep-Sea Res.*, **4**, 149–184.

Stommel, H., and A. B. Arons, 1960: On the abyssal circulation of the world ocean–II. An idealized model of the circulation pattern and amplitude in oceanic basins. *Deep-Sea Res.*, **6**, 217–233.

Stommel, H., 1961: Thermohaline convection with two stable regimes of flow. *Tellus*, **13**, 224–230.

Stommel, H., 1980: Asymmetry of interoceanic fresh-water and heat fluxes. *Proc. Natl. Acad. Sci. USA*, **77**, 2377–2381.

Stramma, L., and R. G. Peterson, 1990: The South Atlantic Current. *J. Phys. Oceanogr.*, **20**, 846–859.

Stramma, L., and J. R. E. Lutjeharms, 1997: The flow field of the subtropical gyre in the South Indian Ocean. *J. Geophys. Res.*, **102**, 5513–5530.

Sverdrup, H. U., M. W. Johnson and R. H. Fleming, 1942: *The Oceans: Their physics, chemistry and general biology* Prentice-Hall, 1087 pp.

Te Raa, L. A., and H. A. Dijkstra, 1999: Coupling of weakly forced wind and thermohaline driven ocean flows. *J. Fluid Mech.*, submitted.

Thompson, S. R., D. P. Stevens and K. Döös, 1997: The importance of interocean exchange south of Africa in a numerical model. *J. Geophys. Res.*, **102**, 3303–3315.

Thual, O., and J. C. McWilliams, 1992: The catastrophe structure of thermohaline convection in a two-dimensional fluid model and a comparison with low-order box models. *Geophys. Astrophys. Fluid Dyn.*, **64**, 67–95.

Toggweiler, J. R., and B. Samuels, 1993a: Is the magnitude of the deep outflow from the Atlantic Ocean actually governed by southern hemisphere winds? *The Global Carbon Cycle, NATO ASI Series, Series I, Global Environmental Change, Vol. 15*, M. Heimann, Ed., 303-331.

Toggweiler, J. R., and B. Samuels, 1993b: New radiocarbon constraints on the upwelling of abyssal water to the ocean's surface, *The Global Carbon Cycle, NATO ASI Series, Series I, Global Environmental Change, Vol. 15*, M. Heimann, Ed., 333-366.

Toggweiler, J. R., and B. Samuels, 1995: Effect of Drake Passage on the global thermohaline circulation. *Deep-Sea Res.*, **42**, 477–500.

Toggweiler, J. R., and B. Samuels, 1998: On the ocean's large-scale circulation near the limit of no vertical mixing. *J. Phys. Oceanogr.*, **28**, 1832–1852.

UNESCO, 1981: *Tenth report of the joint panel on oceanographic tables and standards*. UNESCO Tech. Pap. in Mar. Sci. No. 36. UNESCO, Paris.

Valentine, H. R., J. R. E. Lutjeharms and G. B. Brundrit, 1993: The water masses and volumetry of the southern Agulhas Current region. *Deep-Sea Res.*, **40**, 1285–1305.

Van Ballegooyen, R. C., M. L. Gründlingh and J. R. E. Lutjeharms, 1994: Eddy fluxes of heat and salt from the southwest Indian Ocean into the southeast Atlantic Ocean: a case study. *J. Geophys. Res.*, **99**, 14053-14070.

Van der Schrier, G., and L. Maas, 1998: Chaos in a simple model of the three-dimensional, salt-dominated ocean circulation. *Climate Dyn.*, **14**, 489–502.

Vellinga, M., 1996: Instability of two-dimemsional thermohaline circulation. *J. Phys. Oceanogr.*, **26**, 305–319.

Vellinga, M., 1998: Multiple equilibria in ocean models as a side effect of convective adjustment. *J. Phys. Oceanogr.*, **28**, 621–633.

Wajsowicz, R. C., and A. E. Gill, 1986: Adjustment of the ocean under buoyancy forces. Part I: The role of Kelvin Waves. *J. Phys. Oceanogr.*, **16**, 2097–2114.

Warren, B. A., 1983: Why is no deep water formed in the North Pacific? *J. Mar. Res.*, **41**, 327–347.

Webb, D. J., B. A. de Cuevas and A. C. Coward, 1998: *The first main run of the OCCAM global ocean model*. Internal report of James Renell Division, Southampton Oceanographic Centre, Southampton, 50 pp.

Weijer, W., W. P. M. de Ruijter, H. A. Dijkstra and P. J. van Leeuwen, 1999: Impact of interbasin exchange on the Atlantic overturning circulation. *J. Phys. Oceanogr.*, **29**, 2266–2284.

Weisse, R., U. Mikolajewicz, A. Sterl and S. S. Drijfhout, 1999: Stochastically forced variability in the Antarctic Circumpolar Current. *J. Geophys. Res.*, **104**, 11049–11064.

Welander, P., 1971: The thermocline problem. *Phil. Trans. R. Soc. Lond. A.*, **270**, 415–421.

Welander, P., 1982: A simple heat-salt oscillator. *Dyn. Atmos. Ocean.*, **6**, 233–242.

Wijffels, S. E., R. W. Schmitt, H. L. Bryden and A. Stigebrandt, 1992: Transport of freshwater by the oceans. *J. Phys. Oceanogr.*, **22**, 155–162.

Woodruff, S. D., R. J. Slutz, R. L. Jenne and P. M. Steurer, 1987: A comprehensive ocean-atmosphere data set. *Bull. Amer. Meteor. Soc.*, **68**, 1239–1250.

Wunsch, C., 1978: The North Atlantic general circulation west of 50°W determined by inverse methods. *Reviews of Geophysics and Space Physics*, **16**, 583–620.

Zaucker, F., T. F. Stocker and W. S. Broecker, 1994: Atmospheric freshwater fluxes and their effect on the global thermohaline circulation. *J. Geophys. Res.*, **99**, 12443–12457.

Zhang, X.-H., J.M. Oberhuber, A. Bacher and E. Roeckner, 1998: Interpretation of interbasin exchange in an isopycnal ocean model. *Climate Dyn.*, **14**, 725–740.

Summary

The awareness that anthropogenic activity may change climate has greatly raised the public and scientific interest in the climate system and its components. One of the main issues of present-day climate research is the stability of the global thermohaline ocean circulation. Popularly depicted as a 'conveyor belt', this overturning circulation distributes water, heat and salt world-wide, and is, for instance, responsible for the relatively mild climate in western Europe. Despite its stability during the Holocene, the thermohaline circulation played an essential role in generating the climate fluctuations and switches that characterized the Pleistocene era of ice-ages. The possibility that it attenuates or ceases completely in response to global warming gives rise to concern in view of future climate change scenario's.

The Atlantic plays an essential role in the global overturning circulation. It produces and exports a deep water mass that is known as North Atlantic Deep Water (NADW). NADW is formed by cooling and subduction of surface waters in the Nordic and Labrador Seas, and it is distributed over the entire World Ocean via the Southern Ocean. As compensation, the Atlantic imports upper layer water from the other oceans. This import takes place via two routes of which the relative importance is still a matter of debate. A part of the compensating water enters the Atlantic via the Drake Passage as part of the Antarctic Circumpolar Current ('cold-water route'). This water is cold and relatively fresh. The other part enters the Atlantic south of Africa via a process that is called 'Agulhas Leakage' ('warm-water route'). This intermittent exchange between the Indian and Atlantic oceans is mainly accomplished by large (about 300 km wide) rings that are generated abbout once per two months. Filled with warm and salty Indian Ocean water, these rings influence the stratification in the Atlantic considerably. It has even been suggested that this Indian–Atlantic transfer of salty water stimulates the Atlantic overturning circulation, since it increases the salinity of the Atlantic surface waters and facilitates subduction in the northern North Atlantic. The process of Agulhas Leakage depends strongly on details of the Indian Ocean wind climatology, and may be vulnerable to climate change. Paleoclimatological records suggest that Agulhas Leakage was strongly reduced or even absent during glacial periods. It has been suggested that the re-establishment of Agulhas Leakage at the end of the last ice-age stimulated the restart of the overturning circulation.

In this thesis it is studied how the stability and strength of the Atlantic overturning circulation are affected by the exchange of water between the Atlantic and the rest of the World Ocean. In chapter 2 a summary is given of what is known about interocean

exchange. In chapter 3 an analysis is presented of the interocean exchange in a state-of-the-art Ocean General Circulation Model. The information of these chapters forms the basis of the model studies in chapters 4, 5 and 6. In chapter 4 and 5 a relatively simple model is applied that represents the Atlantic overturning circulation in a 2-dimensional latitude-depth plain. The interocean exchange of heat and salt is represented by lateral fluxes at the southern boundary of the model (chapter 4) and by source/sink distributions (chapter 5). In chapter 6 a more realistic (3-dimensional) global ocean model is used, in which Agulhas Leakage was parametrised by heat and salt sources in the South Atlantic.

The model studies show that the exchange of heat and salt between the Atlantic and the rest of the World Ocean influences the strength of the Atlantic overturning circulation considerably. In particular, the warm and salty input of Indian Ocean water via Agulhas Leakage appears to enhance the overturning strength. Agulhas Leakage also stabilizes the circulation with respect to, e.g., fresh water inflow from the Arctic Ocean (mainly derived from the North Pacific via the Bering Strait). These results indicate that the absence of Agulhas Leakage during the last glacial period may have been partly responsible for the weakness of the glacial overturning state. It may have decreased the stability of the glacial circulation, making it vulnerable to perturbations (like enhanced meltwater events). The re-establishment of Agulhas Leakage at the end of the last ice-age may well have stimulated the restart of the overturning circulation. At present, the variability of Agulhas Leakage is small, so that its direct influence on variations of the western European climate can be neglected. Its importance is that it stabilizes the present-day overturning circulation, and reduces the possibility of catastrophic climate switches.

In both the 2- and 3-dimensional models, the overturning strength is directly related to the north–south pressure difference in the Atlantic. This pressure difference is modified by the buoyancy sources in the South Atlantic. In the 2-dimensional models, however, the buoyancy exchange appears to limit the overturning strength via the energy balance: its supply of potential energy is converted into kinetic energy of the flow, and thus limits the flow strength. Essential for generating response in both 2- and 3-dimensional models is the fact that thermal anomalies are rather rapidly lost to the atmosphere, while saline anomalies are much more persistent. When Indian Ocean water enters the Atlantic, its density anomaly is small, since the effect of the thermal and saline anomalies on the density field almost cancel. However, a density anomaly develops when the water loses its thermal anomaly but retains its anomalous saline anomaly on its way north. The influence of Agulhas Leakage on the density field is therefore largest in the northern North Atlantic. The time-scale on which a change in Agulhas Leakage influences the Atlantic overturning circulation is only a few years. Although it takes about 3 decades for a salinity anomaly to reach the northern North Atlantic, waves modify the North Atlantic density field within a much shorter time.

Samenvatting

Het besef dat menselijk handelen het klimaat zou kunnen veranderen heeft de publieke en wetenschappelijke belangstelling voor het klimaat aanzienlijk vergroot. Een thema van het hedendaagse klimaatonderzoek is de stabiliteit van de thermohaliene oceaancirculatie. Deze omwentelingscirculatie, ook wel aangeduid als 'transport band (conveyor belt)', verdeelt water, warmte en zout over de gehele wereld, en is onder meer verantwoordelijk voor het relatief zachte klimaat in West Europa. Ondanks het feit dat de thermohaliene circulatie momenteel erg stabiel is heeft het een grote rol gespeeld bij de klimaatsfluctuaties en -veranderingen die in grote mate het klimaat van het Pleistoceen hebben bepaald. De mogelijkheid dat de thermohaliene circulatie verzwakt of stil komt te liggen als gevolg van een opwarming van de aarde geeft reden tot bezorgdheid in het licht van scenario's voor klimaatverandering.

De Atlantische Oceaan speelt een belangrijke rol in de mondiale thermohaliene circulatie. In de Noordse en Labrador zeëen wordt namelijk Noord-Atlantisch Diep Water (NADW) gevormd door afkoeling en subductie van oppervlaktewater. Dit NADW wordt verdeeld over de Wereldzee via de Zuidelijke Oceaan. Ter compensatie importeert de Atlantische Oceaan water op ondieper niveau. Deze compensatie kan via twee routes plaats vinden, maar het relatieve belang van deze twee routes is nog niet bekend. Een deel van het water komt de Atlantische Oceaan binnen via de Drake Passage als onderdeel van de Antarctisch Circumpolaire Stroming ('koud-water route'). Het andere deel komt de Atlantische Oceaan binnen ten zuiden van Afrika, via het zogenaamde 'Agulhas Lek'. Deze uitwisseling tussen de Indische en Atlantische Oceaan vindt voornamelijk plaats in de vorm van grote ringen (ongeveer 300 km in doorsnede), waarvan er ongeveer vijf à zes per jaar worden gegenereerd. Deze ringen zijn gevuld met warm en zout Indisch Oceaan water, en hebben een behoorlijke invloed op de stratificatie in de Atlantische Oceaan. Er is gesuggereerd dat deze Indisch–Atlantische zout uitwisseling de omwentelingscirculatie zou stimuleren. Het verzout namelijk de Atlantische oppervlaktewateren, zodat het subductieproces in de Noord Atlantische Oceaan vergemakkelijkt wordt. Agulhas Lekkage is afhankelijk van de windklimatologie van de Indische Oceaan, en is dus gevoelig voor klimaatveranderingen. Paleoklimatologische gegevens laten zien dat Agulhas Lekkage tijdens de laatste ijstijd sterk was afgenomen, of wellicht helemaal afwezig is geweest. Er is gesuggereerd dat het herstel van Agulhas Lekkage aan het eind van de laatste ijstijd de herstart van de omwentelingscirculatie heeft bevorderd.

In dit proefschrift wordt onderzocht hoe de sterkte en stabiliteit van de omwen-

telingscirculatie worden beïnvloed door de uitwisseling tussen de Atlantische Oceaan en de rest van de Wereldzee. In hoofdstuk 2 wordt een samenvatting gegeven van hetgeen bekend is over deze uitwisseling. In hoofdstuk 3 wordt geanalyseerd hoe de uitwisseling plaatsvindt in een modern oceaanmodel. De informatie van deze twee hoofdstukken vormt de basis voor de modelexperimenten in de hoofdstukken 4, 5 en 6. In de hoofdstukken 4 en 5 wordt een relatief eenvoudig model gebruikt, waarin de Atlantische omwentelingscirculatie wordt gemodelleerd in het 2-dimensionale latitude-diepte vlak. De uitwisseling van warmte en zout wordt gerepresenteerd door laterale fluxen (hoofdstuk 4) en bronnen/putten (hoofdstuk 5). In hoofdstuk 6 wordt een realistischer (3-dimensionaal) oceaanmodel gebruikt waarin Agulhas Lekkage wordt gerepresenteerd door warmte- en zoutbronnen in de Zuid-Atlantische Oceaan.

De modelstudies laten zien dat de uitwisseling van warmte en zout tussen de Atlantische Oceaan en de Wereldzee een behoorlijke invloed heeft op de sterkte van de Atlantische omwentelingscirculatie. Met name de warmte- en zouttoevoer door Agulhas Lekkage blijkt de omwentelingscirculatie te versterken. Agulhas Lekkage blijkt ook de omwentelingscirculatie te stabiliseren met betrekking tot bijvoorbeeld een toevoer van zoet water vanuit de Arctische Oceaan (voornamelijk afkomstig van de Stille Oceaan door de Bering Straat). Deze resultaten laten zien dat de afwezigheid van Agulhas lekkage tijdens de laatste ijstijd voor een deel verantwoordelijk is geweest voor de zwakkere glaciale omwentelingscirculatie. Het heeft waarschijnlijk ook de stabiliteit ervan verkleind, zodat het gevoeliger was voor verstoringen (zoals perdiodes van vergroot smeltwater toevoer). Het herstel van Agulhas Lekkage aan het eind van de laatste ijstijd heeft dus wel degelijk de herstart van de omwentelingscirculatie bevorderd. Momenteel is de variabiliteit van Agulhas Lekkage klein, zodat het effect ervan op klimaatfluctuaties in West-Europa te verwaarlozen is. Het feit dat het de hedendaagse circulatie stabiliseert verkleint echter de waarschijnlijkheid van een catastrofale klimaatverandering.

In zowel de 2- en 3-dimensionale modellen is de omwentelingssterkte direct gerelateerd aan het noord–zuid drukverschil in de Atlantische Oceaan. Dit drukverschil wordt beïnvloed door de warmte- en zoutbronnen in de Zuid-Atlantische Oceaan. In de 2-dimensionale modellen speelt warmte- en zoutuitwisseling ook een rol in de energiebalans van het model: het is een bron van potentiële energie die wordt omgezet in kinetische energie van de stroming, en als zodanig de omwentelingssterkte blijkt te limiteren. Essentiëel voor de respons in zowel de 2- als 3-dimensionale modellen is het feit dat een warmteanomalie relatief snel zijn warmte afstaat aan de atmosfeer, terwijl een zoutanomalie veel langer blijft bestaan. Wanneer water via Agulhas Lekkage de Atlantische Oceaan binnenkomt is de ermee samenhangende dichtheidsanomalie klein, aangezien zijn warmte- en zoutanomalie een tegengesteld effect hebben op de dichtheid. Wanneer het water noordwaarts stroomt verdwijnt de warmteanomalie en blijft de zoutanomalie over. Het effect van Agulhas Lekkage op het dichtheidsveld is dus groter naarmate men verder van het brongebied af is. De tijd die een verandering in Agulhas Lekkage nodig heeft om de omwentelingscirculatie te beïnvloeden is slechts een paar jaar. Hoewel het zo'n 30 jaar vergt voordat een zoutanomalie de Noord-Atlantische Oceaan heeft bereikt, doen golven die worden uitgezonden er veel minder lang over om die afstand te overbruggen.

Dankwoord

Velen hebben –direct of indirect– bijgedragen aan het tot stand komen van dit proefschrift. Ik maak graag van de gelegenheid gebruik om hen te bedanken.

Veel dank ben ik verschuldigd aan mijn promotor, Will de Ruijter. Met zijn enthousiasme, interesse en inzicht was hij de grootste stimulerende kracht achter het tot stand komen van dit proefschrift. Zijn geduld en vertrouwen gaven me de vrijheid om mijn eigen(wijze) wegen te bewandelen. Ook wil ik mijn co-promotoren Henk Dijkstra en Peter Jan van Leeuwen bedanken voor hun inspirerende en leerzame begeleiding. De discussies met Henk waren altijd verhelderend. Zijn gevoel voor de grote lijn heeft de inhoud van dit proefschrift in grote mate beïnvloed. Ook de vele discussies met Peter Jan heb ik erg op prijs gesteld. Als kamergenoot fungeerde hij vaak als geduldig en geïnteresseerd klankbord, wat ik zeer heb gewaardeerd.

Gerard van der Schrier en Theo Gerkema wil ik hartelijk bedanken voor hun kameraadschap, en voor de talloze discussies die we hebben gevoerd over van-alles-en-nog-wat. Theo is grotendeels verantwoordelijk voor mijn enthousiasme voor gnuplot. Verder bedank ik al mijn collega's op het IMAU voor hun behulpzaamheid, de goede sfeer, en de vele discussies. Met name de hulp van Paul van der Vaart, Jeroen Molemaker en Mathijs Schouten wordt op prijs gesteld. Piet Jonker, Marcel Portanger en de Facultaire Computergroep (m.n. Henk Mos en Pim van Ingenegeren) wil ik bedanken voor hun ondersteuning op het gebied van computers en printers. Ook de behulpzaamheid van het secretariaat (Eveline, Inge, Marleen, Arianne, Angèle en Ellen) mag niet onvermeld blijven. I thank Guillaume Roullet (LODYC) and Joël Hirschi (University of Bern) for interesting discussions and correspondence. Ook de discussies met Johann Lutjeharms heb ik zeer op prijs gesteld.

Sybren Drijfhout, Andreas Sterl en Hans Bonekamp van het KNMI wil ik bedanken voor het beschikbaar stellen van de LSG code, en voor hun suggesties met betrekking tot hoofdstuk 6. I would like to thank Jürgen Holfort (Institut für Meereskunde, Kiel) for making the data of his inversion available. Beverly de Cuevas and Andrew Coward (Southampton Oceanographic Center) are thanked for providing the output of the OCCAM model. Voor het gebruik van supercomputerfaciliteiten bij het in hoofdstuk 4 en 5 van dit proefschrift beschreven onderzoek is subsidie verleend door de Stichting Nationale Computer Faciliteiten (NCF), met financiële steun van de Nederlandse Organisatie voor Wetenschappelijk Onderzoek (NWO).

Tot slot wil ik mijn vrouw Jolante bedanken voor alles wat ze in de afgelopen jaren voor me betekend heeft.

Curriculum Vitæ

Wilbert Weijer werd op 15 augustus 1971 geboren te Enschede.

1983 – 1989 VWO, Kottenpark College te Enschede

1989 – 1995 Geofysica, Universiteit Utrecht

juni 1990 Propedeutisch examen (met genoegen)

augustus 1995 Doctoraal examen (cum laude)
(doctoraal onderzoek o.l.v. Dr. U. Hansen, *Numerical modeling of the influence of an endothermic phase transition on a depth-dependent-viscosity fluid*)

1990 – 1994 Fysische Oceanografie, Universiteit Utrecht

november 1994 Doctoraal examen (cum laude)
(doctoraal onderzoek o.l.v. Dr. H.A. Dijkstra, *Een phase-tracking model voor oceaan–ijs interactie*)

1995 – 1999 Promotie onderzoek, beschreven in dit proefschrift, Universiteit Utrecht
(in NOP-II projectgroep van Prof. Dr. W.P.M. de Ruijter, *Interbasin exchange, thermocline structure and the global overturning circulation of the (Atlantic) Ocean: remote sensing and modeling*)

1999 – Post-doctoraal onderzoek, Universiteit Utrecht
(in NWO-PIONIER projectgroep van Dr. H.A. Dijkstra, *Stabiliteit en variabiliteit van het klimaatsysteem*)